ARTICLE IN PRESS

Surface Science Reports xxx (xxxx) xxx



Contents lists available at ScienceDirect

Surface Science Reports

journal homepage: www.elsevier.com/locate/surfrep



Synthesis and characterization of 2D transition metal dichalcogenides: Recent progress from a vacuum surface science perspective

Kinga Lasek ^{a, 1}, Jingfeng Li ^{a, 1}, Sadhu Kolekar ^{a, 1}, Paula Mariel Coelho ^{a, 1}, Lu'an Guo ^{a, b, c, 1}, Min Zhang ^b, Zhiming Wang ^c, Matthias Batzill ^{a, *}

- ^a Department of Physics, University of South Florida, Tampa, FL, 33620, USA
- ^b Guangdong Engineering and Technology Research Centre for Advanced Nanomaterials, School of Environment and Civil Engineering, Dongguan University of Technology, Dongguan, 523808, China
- c Institute of Fundamental and Frontier Sciences, University of Electronic Science and Technology of China, Chengdu, 610054, China

ARTICLE INFO

Article history: Received 29 August 2020 Received in revised form 17 February 2021 Accepted 27 February 2021 Available online xxx

Keywords:

Transition metal dichalcogenides van der Waals epitaxy
Scanning tunneling microscopy
Angle resolved photoemission spectroscopy
Charge density waves
Topologically protected states
Monolayer
Heterostructures
Moiré structures
Self-intercalation
Defects
Mirror grain boundaries
Dopants
Molecular adsorption

ABSTRACT

Layered transition metal dichalcogenides (TMDs) are a diverse group of materials whose properties vary from semiconducting to metallic with a variety of many body phenomena, ranging from charge density wave (CDW), superconductivity, to Mott-insulators. Recent interest in topologically protected states revealed also that some TMDs host bulk Dirac- or Wyle-semimetallic states and their corresponding surface states. In this review, we focus on the synthesis of TMDs by vacuum processes, such as molecular beam epitaxy (MBE). After an introduction of these preparation methods and categorize the basic electronic properties of TMDs, we address the characterization of vacuum synthesized materials in their ultrathin limit-mainly as a single monolayer material. Scanning tunneling microscopy and angle resolved photoemission spectroscopy has revealed detailed information on how monolayers differ in their properties from multi-layer and bulk materials. The status of monolayer properties is given for the TMDs, where data are available. Distinct modifications of monolayer properties compared to their bulk counterparts are highlighted. This includes the well-known transition from indirect to direct band gap in semiconducting group VI-B TMDs as the material-thickness is reduced to a single molecular layer. In addition, we discuss the new or modified CDW states in monolayer VSe2 and TiTe2, a Mott-insulating state in monolayer 1T-TaSe2, and the monolayer specific 2D topological insulator 1T'-WTe2, which gives rise to a quantum spin Hall insulator. New structural phases, that do not exist in the bulk, may be synthesized in the monolayer by MBE. These phases have special properties, including the Mott insulator 1T-NbSe₂, the 2D topological insulators of 1T'-MoTe₂, and the CDW material 1T-VTe₂. After discussing the pure TMDs, we report the properties of nanostructured or modified TMDs. Edges and mirror twin grain boundaries (MTBs) in 2D materials are 1D structures. In group VI-B semiconductors, these 1D structures may be metallic and their properties obey Tomonaga Luttinger quantum liquid behavior. Formation of Mo-rich MTBs in Mo-dichalcogenides and self-intercalation in between TMD-layers are discussed as potential compositional variants that may occur during MBE synthesis of TMDs or may be induced intentionally during post-growth modifications. In addition to compositional modifications, phase switching and control, in particular between the 1H and 1T (or 1T') phases, is a recurring theme in TMDs. Methods of phase control by tuning growth conditions or by post-growth modifications, e.g. by electron doping, are discussed. The properties of heterostructures of TMD monolayers are also introduced, with a focus on lateral electronic modifications in the moiré-structures of group VI-B TMDs. The lateral potential induced in the moiré structures forms the basis of the currently debated moiré-excitons. Finally, we review a few cases of molecular adsorption on nanostructured monolayer TMDs. This review is intended to present a comprehensive overview of vacuum studies of fundamental materials' properties of TMDs and should complement the investigations on TMDs prepared by exfoliation or chemical vapor deposition and their applications.

© 2021 Elsevier B.V. All rights reserved.

E-mail address: mbatzill@usf.edu (M. Batzill).

https://doi.org/10.1016/j.surfrep.2021.100523 0167-5729/© 2021 Elsevier B.V. All rights reserved.

Please cite this article as: K. Lasek, J. Li, S. Kolekar *et al.*, Synthesis and characterization of 2D transition metal dichalcogenides: Recent progress from a vacuum surface science perspective, Surface Science Reports, https://doi.org/10.1016/j.surfrep.2021.100523

^{*} Corresponding author.

authors contributed equally.

ARTICLE IN PRESS

K. Lasek, J. Li, S. Kolekar et al. Surface Science Reports xxx (xxxx) xxx

List of acronyms		HER HOMO	hydrogen evolution reaction highest occupied molecular orbital
1H	single layer of transition metal dichalcogenides with	HOPG	highly oriented pyrolytic graphite
	the transition metal in trigonal prismatic	LEED	low energy electron diffraction
	coordination	LUMO	lowest unoccupied molecular orbital
2H	bulk structure of 1H with a 2-layer repeat unit. MoS ₂	MBE	molecular beam epitaxy
	is the prototypical crystal with this structure, and	MI	Mott insulator
	thus the 2H-structure is also sometimes called the	MTB	mirror twin grain boundary
	MoS ₂ -structure	QSHI	quantum spin Hall insulator
1T	transition metal dichalcogenides with the transition	SOC	spin-orbit coupling
	metal in an octahedral coordination. Also called the	STM	scanning tunneling microscopy
	CdI ₂ -structure, because CdI ₂ is the prototypical	STEM	scanning transmission electron microscopy
	crystal with this structure	STS	scanning tunneling spectroscopy
ARPES	angle resolved photoemission spectroscopy	TEM	transmission electron microscopy
BZ	Brillouin zone	TMD	transition metal dichalcogenide
CB	conduction band	TM	transition metal
CBM	conduction band minimum	USPEX	Universal Structure Predictor: Evolutionary
CDW	charge density wave		Xtallography
CCDW	commensurate charge density wave	VB	valence band
CVD	chemical vapor deposition	VBM	valence band maximum
CVT	chemical vapor transport	vdW	van der Waals
DAP	2,3-diaminophenazine	XPD	x-ray photoelectron diffraction
DFT	density functional theory	XPS	x-ray photoemission spectroscopy
FET	field effect transistor		

Contents

1.	Introd	luction	00
1. 2.		ler Waals epitaxy	
۷.		1 3	
	2.1.	Deposition sources	
	2.2.	Growth conditions	
	2.3.	Common substrates for TMD monolayer growth	
		2.3.1. Non-van der Waals semiconductors and insulators	
		2.3.2. Van der Waals substrates	
		2.3.3. Metals-mainly Au(111)	
3.	Gener	ral description of transition metal dichalcogenides	00
	3.1.	Electronic structure	00
	3.2.	Topologically protected electronic states	00
4.	Mono	olayer and surface properties of TMDs	00
	4.1.	Group IV-B TMDs (Ti, Zr, Hf)	00
		4.1.1. Titanium dichalcogenides	00
		4.1.2. Zirconium dichalcogenides	00
		4.1.3. Hafnium dichalcogenides	00
	4.2.	Group V-B TMDs (V, Nb, Ta)	00
		4.2.1. Vanadium dichalcogenides	00
		4.2.2. Niobium dichalcogenides	
		4.2.3. Tantalum dichalcogenides	00
	4.3.	Group VI-B TMDs (Cr. Mo. W)	
		4.3.1. Chromium dichalcogenides	
		4.3.2. Molybdenum dichalcogenides	
		4.3.3. Tungsten dichalcogenides	
	4.4.	Group VII-B TMDs (Mn, Re)	
	4.5.	Group VIII-B (9) (CoTe ₂ and IrTe ₂)	
	4.6.	Group VIII-B (10) TMDs (Ni, Pd, Pt)	
	4.0.	4.6.1. Nickel dichalcogenides	
		4.6.2. Palladium dichalcogenides	
		4.6.3. Platinum dichalcogenides	
	4.7.	Group I—B: AuTe ₂	
_			
5.		fications and nanostructures in TMDs	
	5.1.	One dimensional electronic states: island edges, grain boundaries, and 1D ribbons	
		5.1.1. Edge states	
		5.1.2. Mirror twin grain boundaries	
	5.2.	Compositional variations	00

ARTICLE IN PRESS

K. Lasek, J. Li, S. Kolekar et al. Surface Science Reports xxx (xxxx) xxx

		5.2.1. Excess metal incorporation into the lattice structure	
		5.2.2. Compositional transitions by chalcogen desorption	00
		5.2.3. Self-intercalation	
	5.3.	TMD heterostructures and moiré properties	00
	5.4.	1T to 2H phase control	00
		Molecular and atom adsorption on TMDs	
6.	Concl	sions and outlook	00
	Ackno	vledgment	00
	Refere	nces	00

1. Introduction

Layered materials, in particular the family of transition metal dichalcogenides (TMDs), have fascinated the materials science community for some time [1]. Because of weak, van der Waals (vdW) like interlayer interactions and strong covalent/ionic inplane interactions, their electronic structure is strongly anisotropic with dispersing bands in 2D and only weak, but nonnegligible, dispersion normal to the planes. This quasi-2D electron structure, gives rise to phenomena prevalent in low dimensional materials, such as superconductivity and charge density wave (CDW) instabilities. One obvious question for these materials is: how are these properties modified when the material is reduced from their quasi-2D in the bulk, to a true 2D material in the form of a single layer? First reports of the importance of interlayer interactions in the electronic structure of layered materials did, however, not come from metallic systems but from semiconductor materials. Already in 2001, monolayer growth of WS2 enabled to determine the electronic structure of a single layer by angleresolved photoemission spectroscopy (ARPES) and demonstrate the importance of interlayer interactions in TMDs [2]. The research on monolayer TMDs remained a niche field until 2010s when inexpensive exfoliation methods were developed that enabled to isolate single molecular layers from bulk materials. This opened the door to the study of these materials without the need for expensive growth methods. Furthermore, many of the semiconducting TMDs are chemically stable, and thus could be exfoliated in air. The observation that many of the group VI-B semiconducting TMDs undergo a transition from an indirect to a direct band gap semiconductor when thinned to the monolayer [3] is consistent with the early ARPES studies [2], and made many of these monolayer materials potentially interesting for opto-electronic applications. This further broadened the appeal of these materials also for the semiconductor community. Soon, prototypical semiconductor devices fabricated on exfoliated flakes became a mainstream research endeavor and various aspects of exfoliated semiconducting TMDs have been extensively reviewed [4-13]. This renewed interest in monolayer TMDs, also invigorated efforts in bottom-up growth. Chemical vapor transport (CVT) or chemical vapor deposition (CVD) [14–19] has been successful in growing large single layer flakes for many of the semiconducting TMDs and recent progress in growing on crystalline substrates, e.g. Al₂O₃(0001), also holds promise for epitaxial large-area single crystalline samples. The growth of metallic TMDs, however, still presents challenges for controlling their growth in the monolayer regime and most reports for such materials synthesized by CVD are multilayer flakes. Moreover, sample handling in air or even in a glove box, often causes degradation of the reactive metallic TMDs. Molecular beam epitaxy (MBE) of TMDs, on the other hand, is performed in ultra-high vacuum, thus ensuring the cleanliness of the samples. Moreover, MBE-growth chambers for sample preparation are often combined sophisticated analysis systems with that enable

characterization of fundamental materials properties including electron spectroscopy and atomic scale microscopy tools. This review focuses on materials grown in vacuum by MBE or bulk samples cleaved in vacuum to exhibit pristine surfaces and their characterization by surface sensitive tools, mostly photoemission spectroscopy and scanning probe microscopy. Where appropriate, we make connections to ex-situ (non-vacuum) prepared samples as sometimes vacuum preparation is not an option.

Recent work has demonstrated that most TMDs can be grown by MBE in the monolayer regime. This enabled study of fundamental properties of these materials and address the main question of how monolayers are different from the bulk. These studies revealed some unique monolayer properties for some materials, while others are only modestly modified compared to their bulk. Before we discuss the progress made on studying monolayer TMDs, we briefly discuss the growth methods and the historic background of vdW epitaxy. In Section 3, we lay the foundations to discuss TMDs by describing the basic structural motives of TMDs and their general electronic properties based on their structure and number of delectrons. We also give a brief introduction to topologically protected states as is relevant for TMDs. In Sections 4, we discuss the vacuum synthesis and fundamental properties of all TMDs. We focus on their preparation as monolayers where data is available and their new properties arising from those reduced dimensions. Also, recent developments in TMDs, such as topological states, are emphasized. The goal of this section is to illustrate how the different TMDs can be categorized and how materials properties vary within certain groups of TMDs. It is hoped that this article provides a general introduction to broad properties of TMDs, beyond the mostly studied semiconducting TMDs, and that this article is a resource to find key publications to original research. Section 5 discusses modifications of mostly monolayer TMDs at the nanoscale. This again is a wide field, and we attempt to keep with the theme of this review and concentrate on vacuum processes and characterization. Key ideas of modifying physical properties of TMDs are addressed in this section, such as edge states and line defects, control of the properties of TMDs by phase-engineering, or induced compositional variants, for example, by self-intercalation, and by combining TMDs into heterostructures. We also give a brief summary of work that illustrates how nanostructures in TMDs can modify molecular adsorption. Finally, in section 6, we provide some general conclusions on how vacuum science has been central in recent advances in the understanding of TMDs for the monolayer limit and give an outlook for possible future directions.

2. Van der Waals epitaxy

MBE growth is known for the synthesis of high quality artificial superlattices in closely lattice matched systems. Lattice matching is required to enable atom-to-atom covalent bonding across the interface to maintain perfect crystalline order. For most systems, undesirable interfacial dislocations or other interface defects are

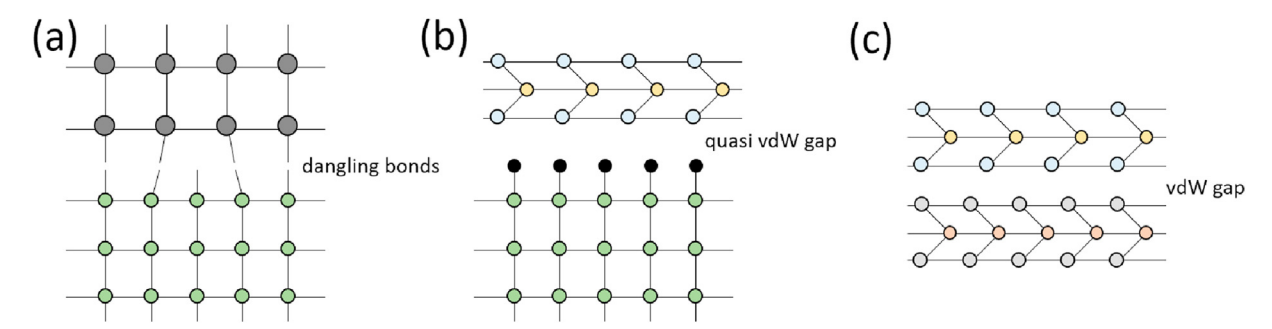


Fig. 1. Schematic of heteroepitaxy for (a) 3D materials, causing interface defects for non-lattice matched materials, and (b) vdW epitaxy of vdW materials on a 3D substrate. Dangling bonds or surface reconstructions of the substrate material remain. (c) vdW heteroepitaxy of two vdW materials. The two materials maintain their layer structure and are separated by a vdW gap. Adapted from Ref. [20] with permission from Elsevier.

needed to accommodate lattice mismatches. Clearly, there are only a few materials systems where the lattice constants are similar enough to grow defect free interfaces, and this limits the kind of heterostructures that can be synthesized with high crystalline quality.

VdW materials have no unsaturated (dangling) bonds at their surfaces, and thus when grown on a substrate will not form interfacial bonds. Consequently, vdW materials may grow defect free even for systems that do not obey lattice matching conditions. In general, this includes both the growth of vdW materials on surfaces of bulk materials (that may have energy lowering surface reconstructions or are modified by a passivation/buffer layer) or on dissimilar vdW substrates (illustrated in Fig. 1 (b) and (c), respectively). Although there is no covalent bonding between the substrate and the grown vdW material, in many cases a preferred rotational alignment between the substrate and the film is observed. This means that if grown on a single crystal substrate, the vdW film also grows as a single crystalline film (although twinning may occur depending on the symmetry of the substrate, which is discussed below). This growth of a rotational aligned vdW materials in the absence of interfacial covalent bonds is known as vdW epitaxy. In vdW epitaxy, the substrate and the vdW material essentially maintain their lattice constants. This causes the formation of lateral moiré superstructures [21], which may cause local lateral electronic modifications. Such electronic modification within a moiré unit cell is especially strong in group VI-B semiconductor heterostructures, and this will be discussed in section

Historically, the concept of vdW epitaxy was developed in the 1980s mainly by Koma et al. [22–30] His group grew TMDs as well as other 2D chalcogenides such as the post-transition metal chalcogenides on various vdW substrates (SnS2, MoS2, mica, highly oriented pyrolytic graphite (HOPG)) as well as on semiconductor surfaces (GaAs, Si) to demonstrate the concepts of rotational alignment. Additional work was done by the Jaegermann group [2,21,31–39], that mainly used photoemission spectroscopy to characterize electronic structure evolution by ARPES and the interface band structure alignment in vdW heterostructures of semiconducting vdW materials [2,21]. All these early studies were motivated by semiconductor physics and the potential use of vdW epitaxy to overcome the limitations of traditional epitaxial growth of semiconductor heterostructures. It should be mentioned that the inverse growth, i.e. the growth of 3D semiconductors on vdW substrates has also been studied extensively for the same idea of avoiding interface defects [40-42]. An interesting aspect in this sense is the event of graphene. Graphene may be transferred onto various substrates, and this may allow for what has been termed 'remote' epitaxy where the stray field of an ionic substrate locks in the epitaxy of the growing film on top of the graphene, while the separation by the graphene avoids the formation of misfit dislocations [43]. However, applications of vdW substrates for growing 3D semiconductors are beyond the scope of this review. Instead, we focus on vdW epitaxy of TMDs mainly on other vdW substrates and in some cases on metal or semiconductor surfaces. The progress for different TMDs for such growth for the known TMDs is discussed in Section 4. First, however, we summarize some general growth techniques for vdW epitaxy, especially the less conventional chalcogen sources and growth substrates employed in some laboratories for fundamental studies of monolayer materials.

2.1. Deposition sources

For MBE growth, the components of the compound material are deposited separately onto the growth substrate where they condense into the film. Controlling the flux may allow to vary the composition of the film. However, the high vapor pressure and the low sticking of chalcogens requires a large overpressure of the chalcogens relative to the transition metals (TM). A chalcogen: TM flux ratio of typically 10:1 and sometimes with a ratio higher than 100:1 is reported for the growth of TMDs. In most cases, the TM are evaporated from an elemental source, which may differ depending on the material and temperature needed to achieve a high enough vapor pressure, and thus deposition rate. For monolayer films, mainly discussed here, simple metal evaporators may be employed, such as direct current heated wires or small metal beads on a direct current heated tungsten wire (the bead is obtained by melting the metal on the tungsten wire). These configurations are enough to grow monolayer films, but the flux and growth rates are often not stable over long periods. Preferred are well temperature-controlled ovens- Knudsen cells, that keep a constant flux over long periods. Materials with very low vapor pressures-such as the refractory metals-may require an e-beam evaporation source. In these sources, electrons emitted from a heated filament are accelerated towards the evaporant by applying a high voltage, and thus achieving a high localized heating power. For the ultrathin films discussed here, a small e-beam source, where the metal is evaporated from an ultrapure wire or rod, is typically used. In addition to elemental MBE growth, metal organic precursors may be dosed onto the surface in vacuum for growing TMDs. For instance, tungsten hexacarbonyl (W(CO)₆) has been reported as a precursor for growing WS_2 films by vdW epitaxy [31]. The advantage of $W(CO)_6$ is that it is easily vaporized and is a well-known precursor for tungsten in particular in electron beam assisted deposition [44]. Molybdenum hexacarbonyl (Mo(Co)₆) should behave similarly, but to the best of our knowledge there are no reports of growing Mo-dichalcogenides with Mo(CO)₆. In general, metalorganic precursors have not been

used in recent work for in-vacuum deposition of TMDs.

The chalcogens have high vapor pressure at modest temperatures with sulfur exhibiting the highest vapor pressure. This makes it challenging to evaporate elemental sulfur in a UHV chamber as it has a melting point of 388 K and would sublimate significantly in vacuum even at room temperature. Solutions to this are valved sources that are available commercially from most MBE component suppliers, where the sulfur is isolated from the rest of the growth chamber by a needle valve that is only opened during deposition. Other methods for growing sulfides are to use sulfur compounds, which evolve sulfur upon heating. For instance, SnS₂ [35,45], FeS₂ (pyrite) [46], or other metal sulfides have been used as sulfur sources. When heated in a Knudsen cell, these sulfur compounds release sulfur that can be used as a molecular beam to grow films. The much higher vapor pressure of sulfur than the metals in this set-up ensures a pure sulfur flux, although very small amounts of metal contamination cannot be excluded. Obviously, metal contaminations can be avoided using source materials that contain the same metal as the film. Others have employed reactive sulfurcontaining gases as sulfur sources. The most common gases are dimethyl disulfide (C₂H₆S₂) or H₂S, which is highly corrosive. Using a precision leak valve, H₂S can be leaked into the vacuum chamber and directed onto the sample through a tube during growth. H₂S is poisonous and care must be taken for handling it. On the surface, H₂S is reacting with the deposited metal to form sulfides and release the hydrogen that is pumped out of the chamber.

In contrast to sulfur, selenium and tellurium have low enough vapor pressures (melting points of 494 K and 722 K for selenium and tellurium, respectively) to be loaded directly into a Knudsen cell for evaporation, and this is the common approach used by most groups for the growth of selenides and tellurides. However, the above described approach for decomposition of metal chalcogenides in a K-cell may also be used for selenides [45].

All the chalcogens tend to evaporate as atom-clusters rather than single atoms. This can be counteracted by using cracker sources that dissociate these clusters. Typical designs are hot-wall cracker sources, where the evaporated chalcogen clusters go through a heated tube, whose temperature is significantly higher

than the source-oven. Atom-clusters evaporated in the oven, dissociate on the hot wall of the tube, and thus form an atom-beam. Such sources are used in MBE systems, but most of the studies on monolayer selenides and tellurides reported here use simple Knudsen cells as chalcogen sources, suggesting that the beam contains sufficient amounts of single atoms or the clusters dissociate on the growth substrate before or during reaction with the TM to form TMDs. Chalcogens react or adsorb on the walls of the UHV chamber and their high vapor pressure results in a constant desorption from the walls. This means that, once chalcogens are deposited in the chamber, it may be difficult to clean the chamber again for the growth of other chalcogenides. Thus, ideally, for every chalcogen a dedicated growth chamber is used.

2.2. Growth conditions

During growth, the elemental chalcogen and metal atoms are co-deposited on a substrate that is mounted on a heated sample manipulator. Growth rates for TMDs for studying monolayer properties are usually very slow in the range of one monolayer in 1 min-30 min. The growth temperature may depend on the grown material and range between 200 °C and 600 °C. Many of the TMDs easily re-evaporate from the surface, thus requiring low growth temperatures. For some materials that we will discuss below, the growth temperature can also affect their structural phase (e.g. NbSe₂ or TaSe₂ has two polymorphs which appear to form preferentially at different growth temperatures) or their composition (e.g. there is evidence that some of the early TM easily form selfintercalation compounds and this may be favored at higher growth temperatures-self-intercalation compounds are discussed in section 5.2.3). The growth morphology is also dependent on the growth conditions. There are only a few systematic studies of the growth as a function of temperature and growth rate. For instance, Rajan et al. [47] has evaluated the surface morphologies of NbSe₂, VSe₂, and TiSe₂ on HOPG substrates as a function of growth temperatures, metal deposition rates, and chalcogen flux to find optimum growth conditions. These studies revealed dependence of the island morphology and sizes on the material, TiSe₂ for instance,

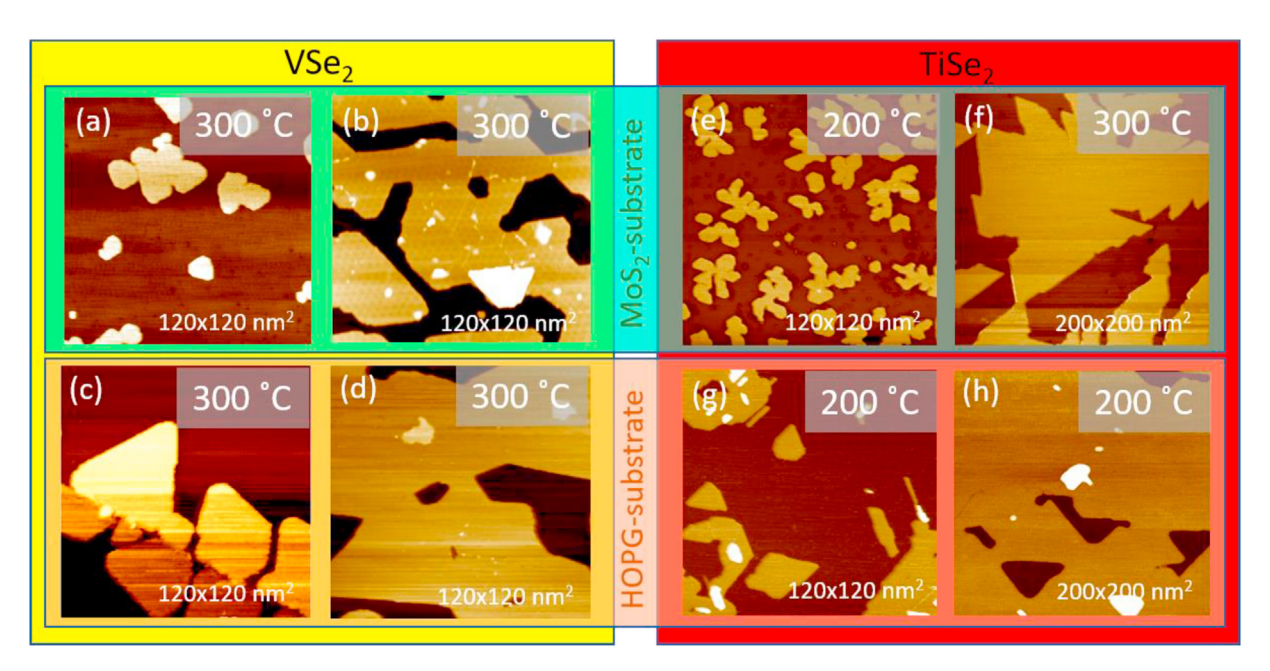


Fig. 2. Comparison of initial growth of monolayer $VSe_2(a)-(d)$ and $TiSe_2(e)-(h)$ on $MoS_2(top-panels)$ and HOPG(bottom-panels) substrates. The growth temperatures are indicated in the STM images.

formed the largest islands of 100s of nm in size while the largest islands for NbSe2 were less than 100 nm in size for optimum growth conditions. Also, island shapes could be tuned from triangular to hexagonal shapes, however, these studies lacked compositional analysis of the islands. Generally, monolayer island sizes in MBE growth are in the 100 nm range, and thus much smaller compared, for example, to CVD processes that use much higher growth temperatures. The surface mobility appears to differ largely for different TMDCs, for VSe2 and TiSe2, for instance, compact islands can be obtained at low growth temperatures of 200-300 °C; note that lower temperatures than 200 °C is usually not accessible because of condensation of elemental Se at the surface. Fig. 2 shows a comparison of the growth of these two materials on MoS₂ and HOPG substrates. A higher nucleation density is observed on MoS₂, most likely related to a higher defect density of MoS₂ substrates than on HOPG leading to heterogeneous nucleation. On HOPG, initial nucleation is often observed at the sparsely distributed step edges as seen in Fig. 2 (c). This suggests a longer diffusion length of adatoms on HOPG than on MoS2 and maybe related to the higher density of heterogeneous nucleation sites on MoS₂ or fundamentally higher diffusion barriers. High defect concentration in MoS₂ makes it difficult to study fundamental growth processes experimentally.

Even at the low growth temperatures, compact islands are observed for VSe₂ after the islands coalesce as shown in Fig. 2(b), suggesting sufficient mobility of the edge atoms to rearrange the island shape. Also, on MoS₂, a moiré structure is clearly discernable (Fig. 2(b)) while on HOPG the moiré is much weaker and cannot be seen in the scanning tunneling microscopy (STM) images in Fig. 2 (c) and (d). For TiSe₂ a lower mobility on MoS₂ than HOPG can be seen from the island shapes at 200 °C growth temperature. On MoS₂, this leads to dendritic growth, as shown in Fig. 2(e), while on HOPG the islands have straight edges. To obtain compact islands, a

temperature of 300 °C is needed on MoS₂ (Fig. 2(f)), while good uniform growth is possible already at 200 °C on HOPG (Fig. 2 (h)). Generally, there are no systematic studies for the synthesis of different TMDs by MBE reported, and a universal understanding of growth conditions and optimizations does not exist. From the few studies available, clear differences in the growth on different vdW substrates and for different TMDs are observed, making it necessary to find optimum conditions for each material system. In the next sub-section, we discuss some common substrates that have been employed for the growth of TMDs.

2.3. Common substrates for TMD monolayer growth

VdW epitaxy studies have been performed on various single crystalline substrates. Interfacing of vdW materials with semiconductors or insulators have been mainly explored for multilayer films of TMDs and the most common substrates are discussed in 2.3.1. Studies of TMDs in the monolayer limit are predominantly performed on vdW substrates and discussed in 2.3.2. Some fundamental research has also been done on single crystal metals, predominantly on Au (111) surfaces, which is discussed in 2.3.3.

2.3.1. Non-van der Waals semiconductors and insulators

Most of the TMDs have a hexagonal crystal structure of their basal plane with 120° rotational symmetry. Given that lattice matching conditions are not relevant in vdW epitaxy, many substrates with hexagonal symmetry have been used for growing single crystal TMD films. Examples of semiconducting/insulator substrates that have been used are GaAs [27,38,48–50], AlN [51–53], InAs [54], Al₂O₃ [55]. Usually, only multilayer vdW films are studied on these substrates and the initial monolayer growth is generally not well characterized. Many of these substrates are known to react with chalcogens and may form complicated surface

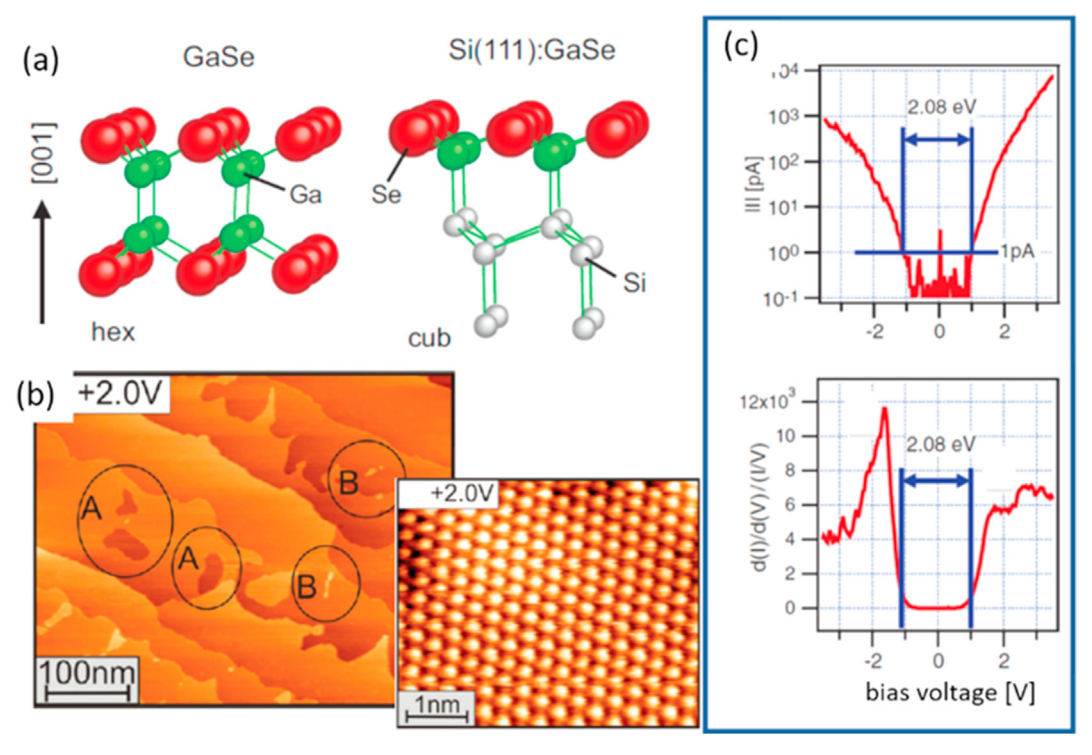


Fig. 3. GaSe passivation of Si(111) surface. The relation of the atomic structure of a monolayer GaSe vdW material with a 'half-layer' covalently adsorbed on Si(111) is schematically shown in (a). In (b) STM images of a GaSe terminated Si(111) surface is shown to exhibit large terraces with the atomic resolution image showing the low defect concentration. 'Holes' and adislands in the film are highlighted by 'A' and 'B', respectively. STS spectra – current vs. bias voltage and dl/dV vs. bias voltage– is shown in (c). The spectra indicate a gap of 2.08 eV in the surface layer. Adapted from Ref. [61].

structures or passivation layers. It is plausible that during MBE growth the interfaces are modified by chalcogens in some of these materials and this requires further studies. Sapphire (Al_2O_3) substrates are particularly interesting as an insulating substrate for studying e.g. transport properties of the grown films. The chemical stability of sapphire makes it a good inert growth substrate. Iwasa's group investigated its use for growing vdW materials and devised growth strategies that result in good vdW films. According to these studies, an initial high substrate temperature followed by growth at a reduced temperature results in best films [55].

An interesting approach for passivating a semiconductor surface for potential subsequent vdW epitaxy was found for Si(111) surfaces. Silicon surfaces are reactive to chalcogens, and thus would be modified during deposition of TMDs. It has been shown, though, that the surface can be terminated by covalently bonding of half of a monochalcogenide vdW material, namely GaSe [56-60]. This is illustrated in Fig. 3(a). The close lattice match between the GaSe and Si(111) enables the covalent bonding across the interface and the surface effectively becomes a vdW termination. Interestingly, photoemission measurements of the electronic structure of such a 'half-GaSe' layer terminated Si(111) surfaces do not exhibit any gap states, and thus the Si surface is similar to that of a hydrogen terminated Si. Moreover, the electronic structure of the covalent bond half-GaSe layer is similar to that of bulk GaSe [61]. Scanning tunneling spectroscopy (STS) determined a surface band gap of 2.08 eV for the GaSe half-layer. While GaSe is obviously not a TMD, the approach of terminating a 3D semiconductor with a vdW layer that does not induce surface or interface states could be used for further vdW epitaxy including TMDs, and thus assist the integration of Si-technology with vdW materials.

2.3.2. Van der Waals substrates

Bulk vdW materials can serve as a substrate for growing dissimilar vdW materials. HOPG has been one of the most common

substrates for vdW epitaxy of TMDs. Its thermal stability in vacuum and its low defect concentrations make HOPG a good substrate. Moreover, good electrical conductivity allows the use of many techniques such as STM or photoemission spectroscopy, without charging effects even at the lowest temperatures. Disadvantages are that, for some TMDs, the nucleation is not uniform across the surface and nucleation and growth at step edges is frequently observed, which can result in non-uniform film growth. The nucleation and growth behavior are, however, very much dependent on the material, for instance, VSe2 tends to nucleate at step edges of the HOPG substrate, shown in Fig. 2 (c), while TiSe2 nucleates more uniformly at HOPG terraces, shown in Fig. 2 (g). Another disadvantage of HOPG is that the samples are polycrystalline, which implies that the grown TMDs are also polycrystalline even if they are aligned with the local crystal structure of the substrate. This makes characterization of the crystallographic anisotropy of the material difficult and requires micro- or nanoprobes to measure crystal symmetry-dependent properties. For this reason, the use of single crystalline substrates is preferred. Famously, graphene can be obtained on SiC wafers with a single orientation [62-66]. Graphene on SiC may be prepared directly in the growth chamber (if it allows annealing to high enough temperatures) or in a separate vacuum chamber. Once formed, the graphene-terminated substrate is stable to be transported through air, if needed. Preparation of graphene on 6H or 4H-SiC(0001), is commonly obtained by flash annealing in vacuum. Note that the (0001) face is the silicon terminated surface, in contrast to the (000–1) surface, which is the C-terminated surface. The growth on the (0001) face can be better controlled while graphenemultilayers (graphite) forms readily on the (000-1) face. A typical graphene synthesis procedure on SiC consists of a prolonged annealing for ~12 h at 600-700 °C, followed by an annealing step at 900 °C for 30 min. Finally, the sample is flashed 3 times to 1400 °C for ~20 min each time. After the final flash, the heater is

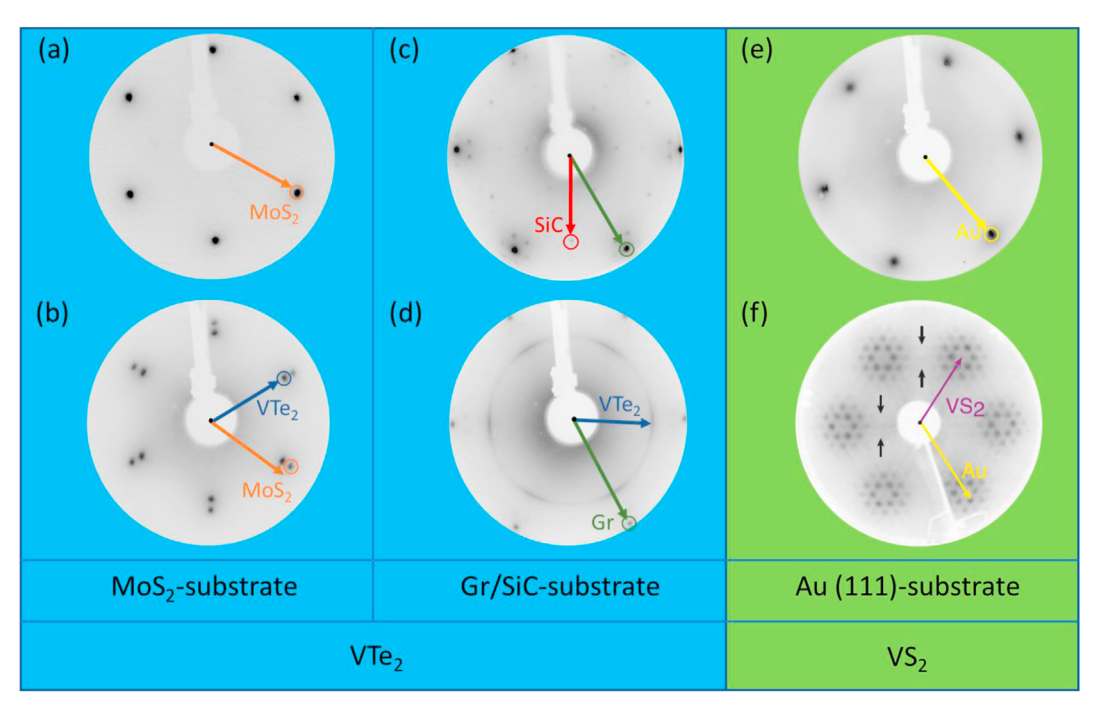


Fig. 4. LEED characterization of common substrates and TMD monolayers grown on these substrates. LEED pattern of the bare MoS₂ and VTe₂ on MoS₂, are shown in (a) and (b), respectively. The MoS₂-substrate and VTe₂ spots align, indicating perfect vdW epitaxy. Graphene/SiC (c) and VTe₂ monolayer grown on that substrate (d). The arc-shape of the VTe₂ diffraction 'spot' indicates a spread of the rotational alignment with respect to the graphene substrate. LEED for Au(111) and VS₂ on Au(111) are shown in (e) and (f). The many diffraction spots for VS₂ on Au indicate the periodicity of a moiré structure. The clear presence of these moiré LEED spots indicates also the strong interaction between Au and TMDs. (e) and (f) are republished with permission of IOP Publishing, Ltd, from Ref. [68]; permission conveyed through Copyright Clearance Center, Inc.

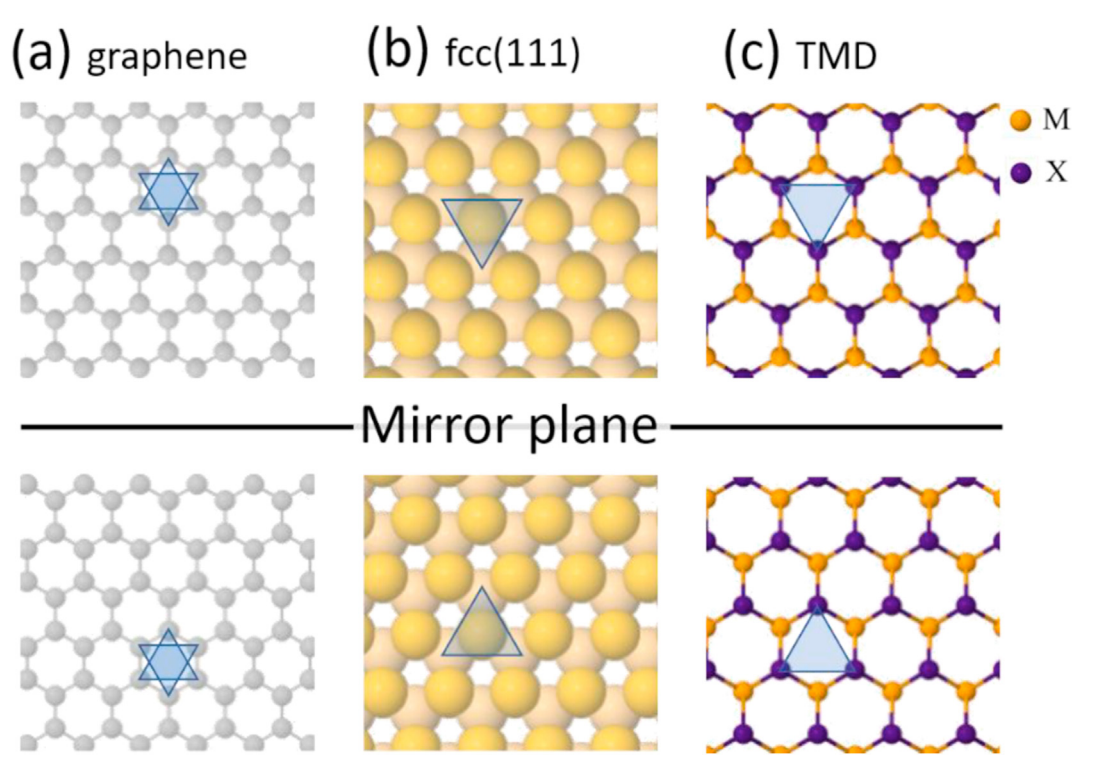


Fig. 5. Illustration of mirror symmetry in graphene/graphite (a) and lack of mirror symmetry in fcc(111) (b) and TMDs (c).

turned off and the sample is cooled back to room temperature. Alternative processes with shorter flash annealing may be employed if a heater is available that allows heating of the SiC with a direct current through the SiC substrate [67], which, however, is usually not the case in an MBE growth chamber. The successful preparation of graphene may be checked by low energy electron diffraction (LEED) [64] that shows a characteristic LEED pattern of the SiC and graphene diffraction spots together with superstructure spots from the moiré pattern formed by the coincidence lattice between graphene and SiC (Fig. 4(c)). Graphene on SiC covers the entire surface, and although step edges from the underlying SiC substrate are present, the graphene layer covers them like a carpet. Depending on the number of graphene layers on SiC, the work function of the surface may vary. This can affect the interface bandalignment between a semiconducting TMD and the substrate causing laterally modified band offsets in the TMD. This has been, for example, studied for WS2 grown on graphene/SiC by micro-ARPES, and this is discussed in section 4.3.3. Inhomogeneities of the substrate of graphene/SiC compared to HOPG may also help with a higher nucleation density and formation of a more uniform TMD coverage in the monolayer regime. LEED of TMD monolayers on graphene/SiC reveals that the TMDs are not always perfectly aligned with the substrate. Fig. 4 (d), for instance, shows LEED of VTe2 grown on graphene/SiC. The diffraction from the VTe2 film does not exhibit a single spot but rather an arc with an arc-length of a few degrees, indicating the spread of misalignments of the grown TMDs with respect to the single crystalline TMDs.

Another source of inhomogeneity for TMDs on graphene are the difference in symmetry. While graphene has a mirror symmetry (or 60° rotational symmetry) as illustrated in Fig. 5 (a), hexagonal TMDs have a 120° rotational symmetry, and thus are not mirror symmetric, illustrated in Fig. 5 (c). The higher symmetry of the substrate implies that two mirror domains of TMDs are equally likely to nucleate on graphene and as consequence mirror twin grains are unavoidable on graphene. Nevertheless, graphene/SiC

has many advantages that made it a popular substrate, especially for studying the electronic properties of monolayer TMDs by ARPES. The strongly dispersing π -band with states at the Fermilevel only at the K-points of its Brillouin zone (BZ) ensures that the substrate bands do not overlap with the bands of interest of the TMD layers, which have a smaller BZ. This allows an undisturbed characterization of the band structure of TMDs, and although there is a rotational spread in the TMD layer, this only causes an acceptable loss of k-space resolution. Below we will discuss some of the ARPES data obtained for TMDs on graphene/SiC.

An alternative single crystalline graphene substrate is graphene grown on single crystalline metal substrates. Graphene has been successfully synthesized on many TM substrates and a review may be found in Ref. [69]. Graphene on Ir(111), is a particularly interesting substrate as the interaction between graphene and the substrate is weak, but graphene can still be obtained as a single crystalline sheet. This graphene/Ir(111) surface has also been used as a substrate for the synthesis of TMDs. A challenge for graphene on metals as growth substrates, is the well-known intercalation of deposited TMs in between the graphene and the metal support [69]. This prevents the direct growth of TMDs on graphene/Ir(111) at elevated temperatures and instead a preparation method consisting of room temperature co-deposition of TM and chalcogen and subsequent annealing in chalcogen atmosphere has been employed to form TMD monolayer islands. These TMD islands exhibit an epitaxial relationship with the graphene substrate, but because of the different symmetry of graphene and TMDs, two mirror orientations of the TMDs are observed, causing formation of mirror twin grain boundaries (MTBs) at the interface of merging islands. In MoS₂, these grain boundaries are metallic and host a 1D Tomonaga Luttinger quantum liquid, this is discussed in section 5.1.

TMD monolayers can also be grown on other TMD substrates. The most popular of these are MoS₂, as it is commercially available as large (\sim 10 × 10 mm) crystals. First experiments for TMD growth on MoS₂ go back to studies by Koma et al. MoS₂ can be obtained as

mineral samples or as synthetically grown samples. Naturally, mineral samples contain impurities that cause local electronic variations and are generally strongly n-type. Synthetically grown samples are much cleaner, however, modulations are still observed in STM, indicating defects and impurities. Moreover, samples still tend to be n-type but less strongly doped than minerals. Another disadvantage of MoS2 and other potential TMD substrates, is their tendency to desorb chalcogens at high growth temperatures. This may limit the growth temperatures at which these substrates can be used at. However, many TMDs grow well at temperatures below 300–400 °C and at these temperatures MoS₂ is sufficiently stable and many TMDs have been successfully grown on MoS₂. Hexagonal TMDs generally exhibit excellent rotational alignment with MoS₂ substrates, as can be seen from the LEED pattern of VTe₂ grown on MoS₂ shown in Fig. 4(b). The sharp spots from the film are aligned with the substrate spots, indicating that the film grows in rotational alignment with the substrate. The diffraction spots do not indicate, however, if the TMD film exhibits mirror grains. For this, more detailed diffraction studies or quantitative LEED I-V analysis are required, which have not yet been reported on films grown on MoS₂ substrates. In general, any TMD can be used as substrate materials and early work has been reported for SnS₂ and MoTe₂ substrates. The main consideration for the use of TMDs would be their thermal stability during growth and, of course, their availability in appropriately sized crystals. For insulating vdW substrates, hex-BN, as well as mica [26], has been used. The former is generally only available as small (mm-sized) crystals and the latter may have many impurities which require prolonged outgassing in UHV. Growth on hex-BN has been mainly performed by CVD [70–72] while MBE growth is rare [73–75]. The insulating character of the substrate is sought for transport measurements in thin films, it prevents, however, the kind of surface studies this review is focusing on. One solution to this is the growth of monolayer hex-BN on transition metal single crystal surfaces such as Ru(0001) [75].

2.3.3. *Metals-mainly Au(111)*

Single crystal metals have also been used for the growth of TMDs. Initial work focused on MoS₂ islands grown on Au(111) [76]. These studies were motivated by gaining a fundamental understanding of MoS2-based catalysts and used gold as a support for surface science studies. Mo was deposited on gold and sulfurized using H₂S. The large immiscibility gap in the Au–Mo phase diagram may also assist in avoiding alloying of Mo with Au substrate. The fcc(111) surface lacks mirror symmetry like the hexagonal TMDs (see Fig. 5 (b)) and this may enable the growth of a single orientation MoS₂, WS₂, and potentially other TMDs without twin domains. Evidence of the absence of twins under the right growth conditions on Au(111) is discussed in section 4.3. Recently, the growth of MoS₂ on Au was also scaled by melting Au on a tungsten substrate to obtain a large Au(111) surface, which then was used to grow single crystal MoS2 wafer by CVD. Such MoS2 layers could subsequently be transferred to other substrates [77]. Semiconductor TMDs on a metal substrate may strongly affect their quasi-particle gap due to efficient electron screening by the metal

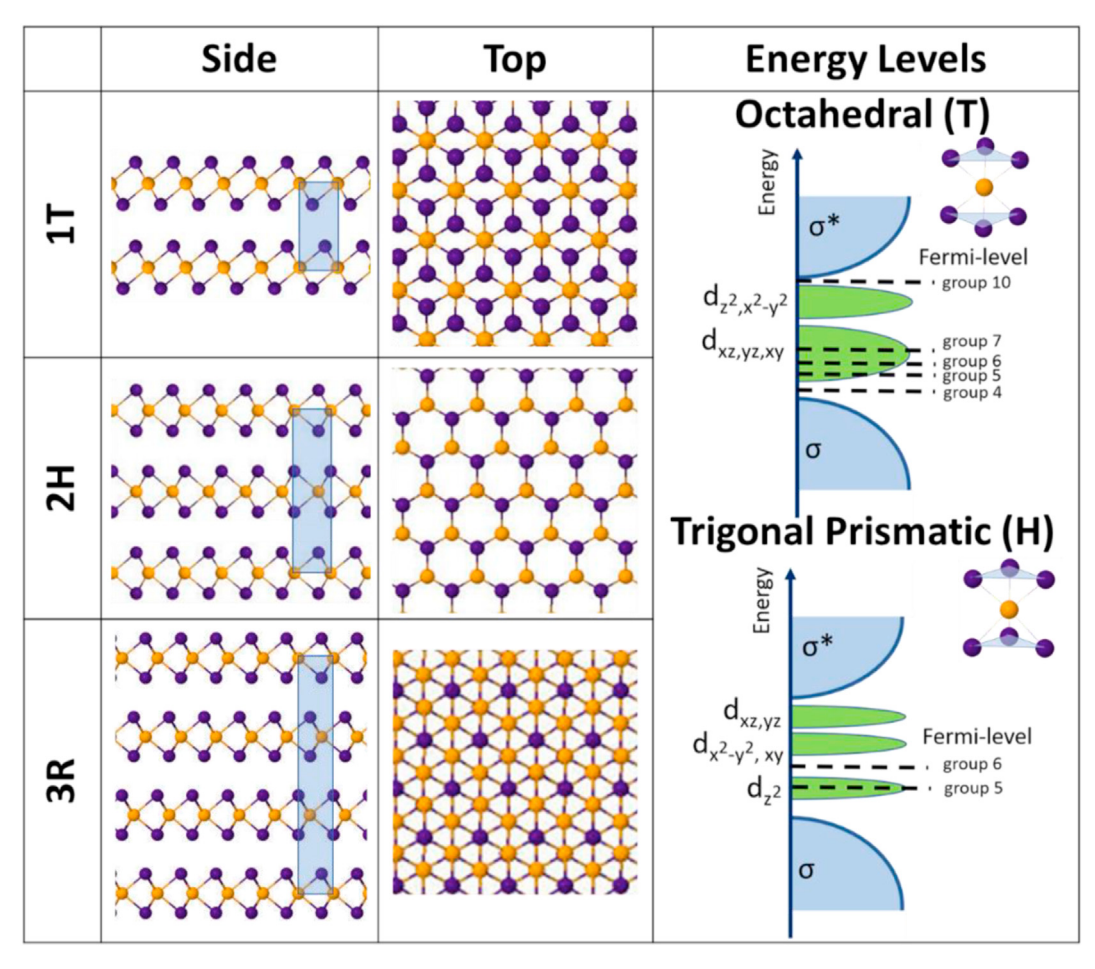


Fig. 6. Schematic of 1T, 2H, and 3R TMDs. The basic electron energy diagram of the octahedral and trigonal prismatic coordinated TMs is also shown. The Fermi-level position depending on the number of d-electron (group in the periodic table) are indicated.

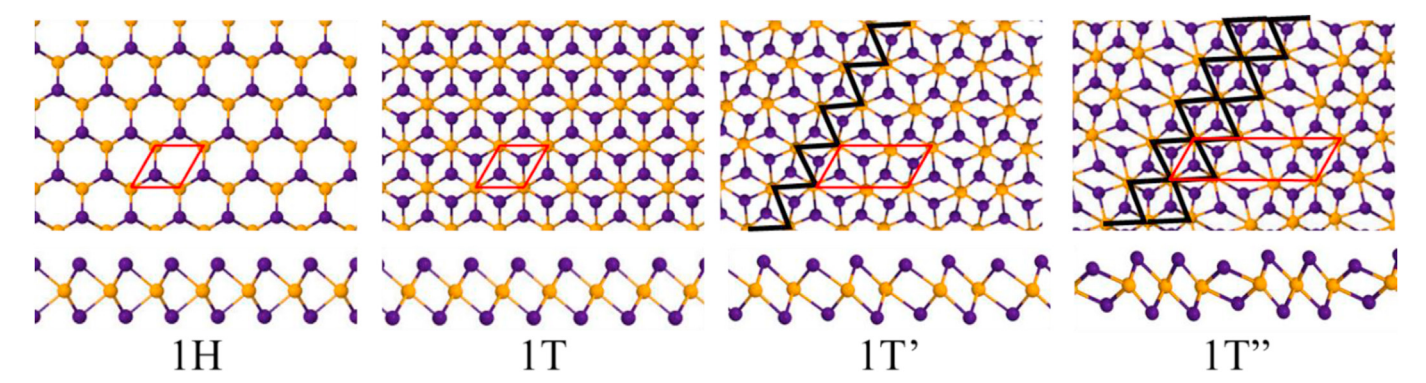


Fig. 7. Comparison of monolayer TMD structures. In addition to the 1H and 1T structures, distorted 1T structures are formed for some TMDs, that are commonly labeled as 1T' or 1T".

and through hybridization of electronic states at the interface. The interaction between the metal substrate and the TMD also often gives rise to pronounced moiré-structures that can be easily discerned in LEED patterns, as shown in Fig. 4(f) for VS₂ grown on Au(111). Substrate induced changes in the TMD properties are discussed for specific cases below in section 4.

3. General description of transition metal dichalcogenides

TMDs are layered materials with vdW gaps between molecular layers. Each molecular layer by itself consists of a layer of TMs sandwiched in between two layers of chalcogens (except for PdSe₂, which is discussed in section 4.6.2). Each TM is coordinated to six chalcogen atoms and there are two main possible coordination of the TM: (i) octahedral (T-phase), or (ii) trigonal prismatic (Hphase). In the bulk the trigonal prismatic coordinated TMs can have different stacking sequences, giving rise to either the 2H or 3R bulk structure (where the letter stands for hexagonal or rhombohedral unit cell and the number describes the number of TMD layers in the repeat unit along the c-axis), while the octahedral structure has only one stacking sequence and is referred to as the 1T structure, indicating a single layer per repeat unit (T stands for trigonal unit cell). Fig. 6 illustrates these three structures. A monolayer of the trigonal prismatic structure is often called the 1H structure, to emphasize that it is a single layer. Compared to the 2H bulk structure, the 1H single layer lacks inversion symmetry, which has consequences for the spin-polarization. In MoS₂, for instance, the spin-orbit split bands at the K-points become spin polarized with reverse spin polarization of the split-bands in alternating K-points causing the formation of two distinct K valleys, often labeled as K and K'. This is discussed further in section 4.3.

3.1. Electronic structure

The electronic structure of TMDs depends on the coordination and the number of d-electrons. From an orbital perspective, the octahedrally coordinated TM exhibit degenerate dz^2 , $x^2.y^2$ and $d_{xy,xz,yz}$ orbitals and the trigonal prismatic coordination causes a splitting of the orbitals in dz^2 , $dx^2.y^2$, xy and dxz, yz energy levels, as schematically shown in Fig. 6. Depending on the number of d-electrons of the TM, different d-orbitals are occupied indicated by the Fermi-level position in Fig. 6. This basic energy level diagram can be modified by quantum confinement effects and interlayer interactions. For instance, 1T- PtSe₂ transform from a semi-conductor in the monolayer limit, in accordance to the energy diagram in Fig. 6, to become metallic for multilayers and bulk materials (see section 4.6.3). In addition, many TMDs in the

octahedral 1T-coordination undergo further structural distortions, known as 1T' or 1T", schematically shown in Fig. 7. These lattice distortions may be discussed in the context of in-plane metal coordination due to d-orbital hybridization [78]. The 1T' structure, or zig-zag structure, has a 2×1 supercell in the basal plane with respect to the 1T structure, while the 1T", or ribbon structure, has a 3×1 supercell. The t2g orbitals in the octahedral 1T structure are split by the lattice distortion in the 1T' and 1T" structures and cause a decrease in the energy of the occupied d_{xz} and d_{xy} bonding orbitals. This is possible if the bonding orbitals are each occupied by two electrons (i.e. a total of four). In the ribbon structure, the bonding orbitals are being shared among three TMs, thus requiring an electron count of 4/3 d-electrons per TM atom [79]. In contrast, a zigzag 1T' structure would share these orbitals between two TMs, and thus requiring an electron count of 2 d electrons per atom for its formation.

Some TMDs may exist in both polymorphs, i.e. either with an octahedral or a trigonal prismatic coordination. For group VI-B TMDs, this implies a semiconducting to metallic transition if the coordination is changed from the H-structure to a T-structure, as suggested by the energy diagram in Fig. 6. In MoS₂, the transition from its semiconducting 2H phase to a metallic 1T phase is well known to occur if the material is electron doped, for instance by alkali atom intercalation. More recently, this has also been applied to monolayer materials and proposed to be a process for making metallic contacts to semiconducting TMDs by locally transforming the phase [80,81]. Excitingly, monolayer materials may also be switched by external stimuli like an applied electric field in a fieldeffect device [82]. Other materials occur naturally in different polymorphs or exhibit structural transitions as a function of temperature. MoTe₂, for instance, has a high temperature metallic 1T' phase while the 2H phase is the ground state at lower temperatures. The transition temperature may be tuned by stoichiometric variations and metallization of 2H-MoTe₂ flakes was obtained, for instance, by local laser heating and transformation into 1T' phase [83]. Also, efforts have succeeded in obtaining 1T' or H-phases of MoTe₂ by controlling growth methods. For a more detailed discussion on phase change in TMDs, see section 5.4.

For some group V—B TMDs, namely vanadium dichalcogenides, density functional theory (DFT) calculations have predicted that the monolayer should form a 1H ground state despite bulk materials generally forming a 1T phase. This may indicate that the formation energies of these two polymorphs are very similar. However, as we will discuss in section 4.2.1, experimentally, monolayer materials grown by MBE always exhibit the 1T structure and the 1H structure has never been observed.

Structural similarities between TMDs, but largely different

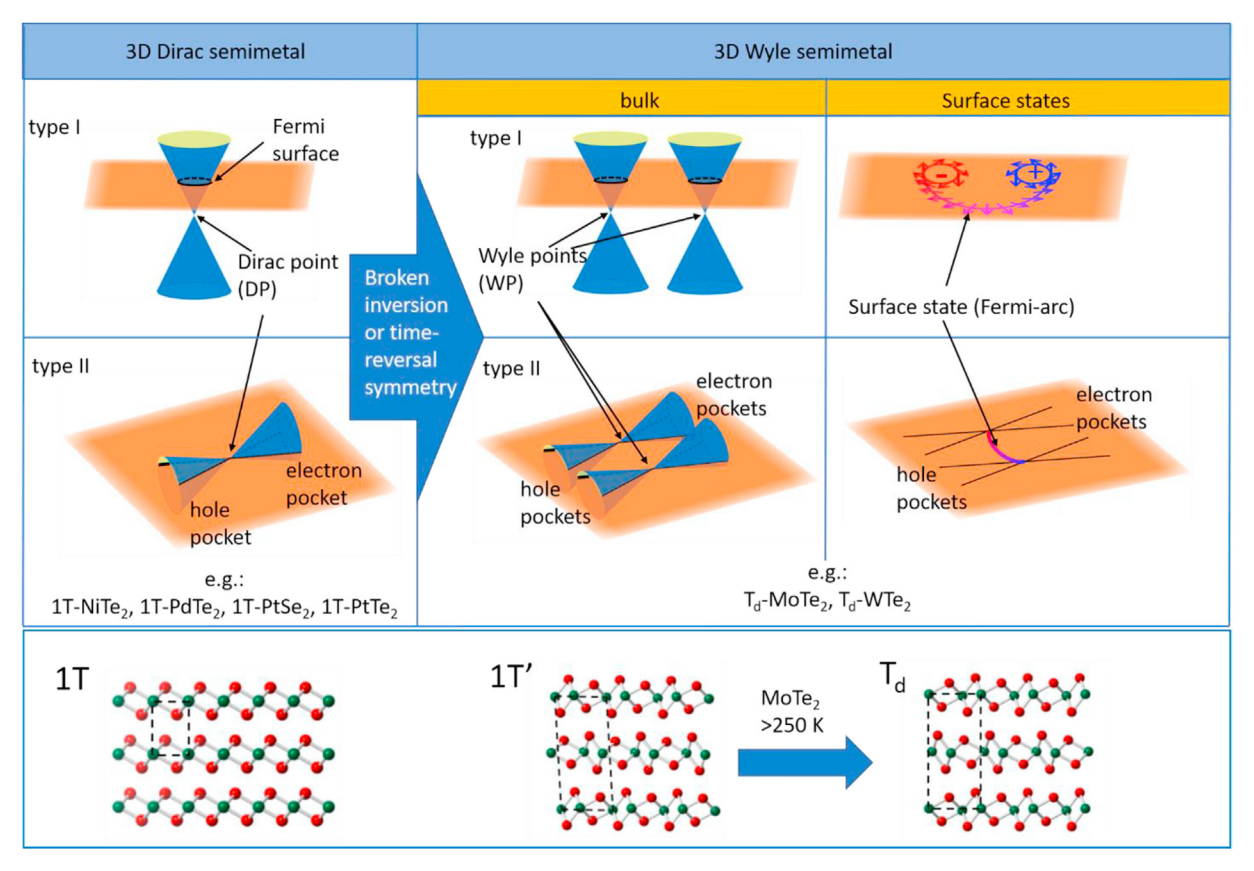


Fig. 8. Categorization of 3D topological materials. The type I and II 3D Dirac semimetals become a 3D Wyle semimetal if the crystal has broken inversion or broken time-reversal symmetry. The Wyle semimetals exhibit Fermi-arc surface states that connect the Dirac cones with opposite chiral spin texture. The typical crystal structures are also illustrated, in particular the relation of the 1T^r structure with the T_d structure.

electronic structure due to different numbers of d-electrons or TM coordination make TMDs highly versatile. The ability to synthesize these materials as truly single layer materials holds the promise of better understanding and controlling the many quantum phenomena different TMDs exhibit. The synthesis and properties of monolayer TMDs by MBE are discussed in section 4.

3.2. Topologically protected electronic states

The concept of topology only recently entered the mainstream of condensed matter research. The field of topological materials and their theoretical description, as well as experimental realization, has been recently reviewed, see e.g. Refs. [84–87]. Here we only briefly describe the main experimental observations as it is relevant in the context of TMDs and their surface characterization.

Topological insulators arise from the inversion of usual band ordering in conduction band (CB) and valence band (VB) through strong spin-orbit coupling (SOC). Such a topological insulator exhibits topological protected metallic surface states with a Diraccone like dispersion. By now, many topological insulators have been discovered, the most well-known one probably is the layered material, Bi₂Se₃, but none of the TMDs are 3D-topological insulators with topologically protected surface states. The concept of topological states can, however, be extended to a 3D band structure where topological states are protected by crystal symmetry. There are two kinds of 3D Dirac semimetals, as illustrated in Fig. 8. In type I 3D Dirac semimetals, the Dirac cone is normal (or at a small tilt angle) to the Fermi-surface, while in type II the Dirac cone is (over) tilted and breaks Lorentz invariance. In a type II Dirac semimetal, a hole-pocket and electron-pocket touch at the Dirac point. Such 3D

Dirac semimetals have been observed for the 1T noble-metal TMDs, NiTe₂, PdTe₂, PtSe₂, and PtTe₂, which we will discuss below in section 4.6.

If, in addition, the time-reversal- or inversion-symmetry is also broken in the crystal structure of a 3D Dirac semimetal, the Dirac point splits into two so-called Wyle points forming a Wyle semimetal (see Fig. 8). Again, type I or type II Wyle semimetals can be observed depending on the tilting of the Dirac cones. The Wyle points always appear as pairs of opposite chirality. At the surface of Wyle semimetals, a surface state exists at the Fermi-level that tangentially connects the pair of Dirac cones. Unlike other Fermisurfaces that form closed pockets, the surface states of Wyle semimetals connect two points in the BZ, and thus does not close; these are the so-called Fermi-arcs of the Wyle semimetal. Identification of these Fermi-arcs in ARPES measurements gives strong evidence for the existence of a Wyle semimetal. For TMDs, the T_d phases of WTe2 and MoTe2 have been predicted to be type II Wyle semimetals [88]. For WTe₂, the splitting between the Wyle points is only 0.7% of the BZ, making an observation of Fermi-arcs in ARPES challenging. For T_d-MoTe₂, the splitting is much larger, and the Wyle points lie only 6 meV above the Fermi-level. DFT calculations indicate that T_d-MoTe₂ has either 2 or 4 pairs of Wyle points depending on very small changes in the lattice constant. These points are connected by Fermi-arcs along the $k_z = 0$ plane [89,90]. Several ARPES [91-93] and STM/STS studies of the quasiparticle interference [94] have been conducted to demonstrate the existence of these Fermi-arcs, and thus the existence of the type II Wyle semimetal. The T_d phase has an orthorhombic structure, as shown in Fig. 8, and has the required broken inversion symmetry. At room temperature, MoTe₂ exhibits the 1T' phase and only undergoes a

phase transition to the Wyle semimetal T_d phase below 250 K WTe₂, on the other hand, prefers the T_d phase at ambient conditions. Doping of MoTe₂ with a few percent of W has also demonstrated to stabilize the T_d phase [95].

In terms of the focus of this review on ultrathin TMDs grown by MBE, monolayer topological insulator phases are most relevant. In the monolayer, 2D topological phases are observed for 1T' WTe₂, 1T' WSe₂, and 1T' MoTe₂ (note that the T_d and 1T' structure are equivalent for the monolayer). The band inversion in the distorted 1T' monolayer structure and the strong SOC of the d-orbitals have been shown to cause a band gap opening [96,97]. It has also been suggested that this gap can be tuned by strain or electric fields. Consequently, it was proposed that these 1T' TMD monolayers are potential candidates for topological field effect transistors [96]. ARPES and STM/STS studies on epitaxially grown monolayer WTe₂ confirmed the band inversion and band gap opening in 1T'-WTe₂ and 1T'-WSe₂ and we will discuss these results in section 4.3 [98]. The gap of the inverted bands is closed at island edges of the monolayer, and thus forming conducting edge states. The hosting of conducting edge channels is the hallmark of a 2D topological insulator. In this edge state, the spin is locked to the momentum, and thus prohibiting elastic backscattering at zero magnetic fields resulting in a quantum spin Hall insulator (QSHI). The zero magnetic field contrasts with a conventional integer quantum Hall system, where an insulating bulk state is induced by a sufficiently strong magnetic field with electrons pinned to quantized small radii orbits that form the conducting and dissipationless chiral edge state by skipping orbits. The 2D topological insulator, on the other hand, displays two counterpropagating, spin polarized edge states due to spin-orbit locking. This produces a QSHI for which an external field is not necessary anymore to produce quantized conductance of ~e [2]/h per edge state. Such conductance was observed for monolayer 1T'-WTe₂ [99,100]. Interestingly it was also shown that electron doping by a field effect can induce superconductivity in monolayer 1T'-WTe₂ [101]. This opens new applications for monolayer TMDs such a superconducting nano devices and fundamental questions of the interplay of superconductivity and topology. To study these 2D topological insulators, as well as to utilize them in devices, MBE growth of monolayers plays an important role. Also developing other materials beyond 1T'-WTe2 may require control of the growth of different TMDs to obtained 2D topological insulators that has been highlighted by the successful synthesis of 1T'-WSe2 monolayers, that contrast the topologically trivial 1T-WSe₂. This is discussed in section 4.3.

4. Monolayer and surface properties of TMDs

In the following, we summarize the work done for the different TMDs grown in vacuum with a focus on the monolayer limit (where available). In addition, we include recent progress in studying topological properties of bulk TMD surfaces-especially for the noble metal dichalcogenides. As shown in Fig. 6, the electronic structure roughly depends on the TM coordination and the d-electron count. Thus we organize the paper by the number of d-electrons, i.e. the group number in the periodic table, and discuss different TM coordination.

4.1. Group IV-B TMDs (Ti, Zr, Hf)

All group IV-B TMDs exhibit the 1T structure. Nominally, the TM have a valency of 4+, and thus the group IV-B TMDs have no dvalence electrons. Thus the Fermi-level lies in between the filled chalcogen derived σ -band and the empty d-bands with semiconducting behavior (except for TiSe2 and the tellurides, which are all semimetallic). The VB consists of a strongly dispersing chalcogen

p-orbital derived bands with the valence band maximum (VBM) at the Γ -point. The CB is derived from the empty TM d-orbitals with the conduction band maximum (CBM) for bulk materials lying at the L-point of the 3D BZ and a second minimum at the M-point, thus forming an indirect band gap semiconductor. For monolayers, it is expected that the minimum is at the M-point of the 2D BZ (some representative band structure measurements are shown below). Generally, the group IV-B TMDs are strong n-type semiconductors with the Fermi-level close to or even above the d-band CBM, forming a degenerate semiconductor. The origin of the n-type behavior is likely a consequence of chalcogen deficiencies or TM excess. Because of the strong doping with an occupation of d-states, ARPES measurements may be used to determine the band gap of these materials. Note that for bulk and multilayers, the true band gap may be smaller because the L-point of the CBM is more difficult to access by ARPES. The filling of the d-band can also be achieved in these materials by alkali metal doping. Alkali atoms are strong electron donors and can be either intercalated in the bulk or vapor deposited on the surface. The alkali atoms then donate their electron to the d-band of the TMD. The filling of the d-band and formation of an electron pocket around the M-point are clearly observed in ARPES [102,103] (see e.g. measurements below for TiSe₂ and ZrS₂). The band gap for the group IV-B TMDs varies with the chalcogen and TM. For a specific TM, the band gap decreases with decreasing electronegativity of the chalcogen, i.e. sulfides always have the largest band gaps followed by selenides. The tellurides form semi-metals, i.e. the chalcogen derived VB overlaps with the d-band. Moreover, the band gap for the sulfides and selenides increases in the order $E_g(Ti) < E_g(Zr) < E_g(Hf)$. Zr and Hf sulfides and selenides have been suggested as possible semiconductor materials for device structures. It has been pointed out that their modest band gaps and potentially high electron mobility make them suitable materials for devices and heterostructures (see section 5.3 for calculations of band gaps and band edge energies for heterostructure band alignments). Theoretically calculated acoustic phonon limited electron mobility [104] indicates a higher mobility for group IV-B TMD-semiconductors than for the more frequently studied group VI-B TMD-semiconductors. However, other scattering mechanisms in 2D materials may also affect charge carrier mobilities [105,106] and a mobility advantage still must be demonstrated. For practical purposes, the formation of a native high κ-dielectric layer (i.e. ZrO₂ or HfO₂) further contributes to the potential of group IV-B TMDs as device semiconductors [107].

4.1.1. Titanium dichalcogenides

 TiS_2 is a semiconductor with a band gap of around 0.5 ± 0.1 eV [108]. Interestingly, it was found by STS measurements, that this band gap is not strongly changed by as much as 10% excess Ti intercalated in the vdW gap, but only the Fermi-level is shifted into the CB, i.e. making it a degenerate semiconductor. This may be important, as during MBE growth the self-intercalation of TM, especially for the early TMs, may be quite common. Self-intercalation in TMDs is discussed in section 5.2.3. While there are some STM studies of bulk surfaces and intercalation studies of alkali-metals or Sn in bulk single crystals [109], to the best of our knowledge, there have not been any experimental studies on monolayer materials. In general, there are fewer studies of MBE growth of sulfides than the other two chalcogenides. This is likely related with challenges of having suitable and inexpensive sulfur sources for MBE growth.

TiSe₂ is a semi-metal in bulk materials that has been extensively studied because it exhibits an unconventional $2 \times 2 \times 2$ CDW. In contrast to most other CDW materials, there is no nesting vector for the Fermi surface that could give rise to a Peierls like instability. Instead, different alternatives for the CDW were discussed

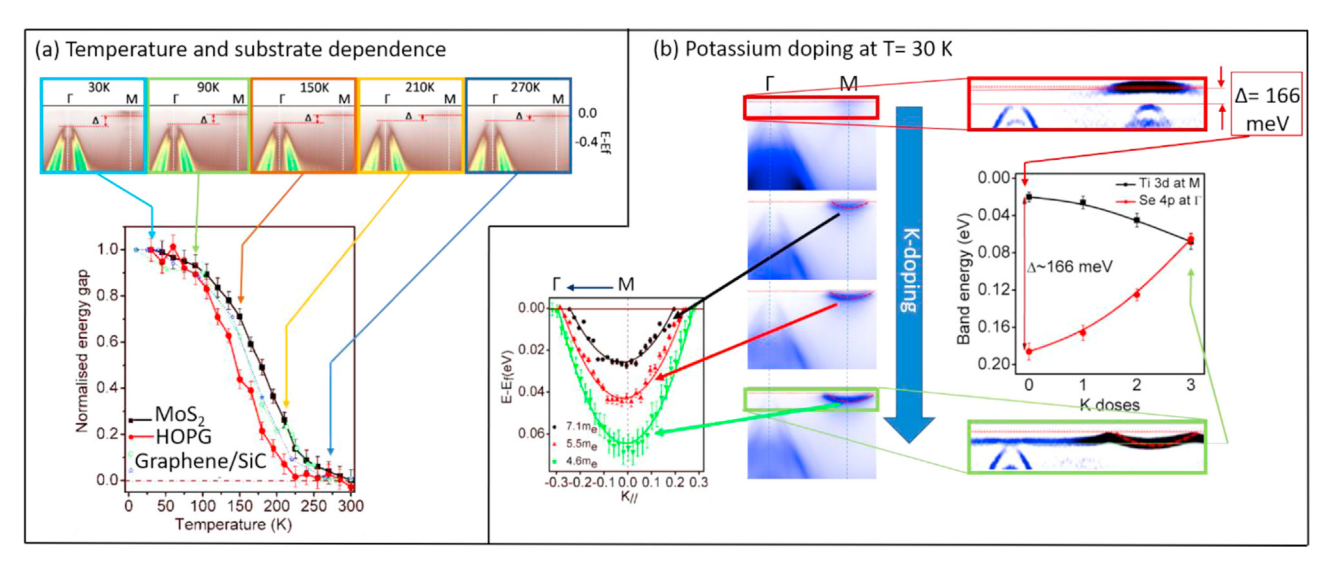


Fig. 9. CDW in monolayer $TiSe_2$. The CDW can be identified in ARPES by a faint replica Se-p band at the M-point and by an opening of a gap between the Se-4p band at Γ and the Ti-3d band at M. In (a) this gap as a function of temperature is plotted for 3 different substrates, MoS_2 , graphene, and HoPG. It can be seen that the transition temperature shifts ~50K to higher temperature for MoS_2 substrates compared to HoPG. Deposition of potassium suppresses the CDW in monolayer $TiSe_2$ as shown in (b). Potassium doping fills the Ti-3d band at M and closes the gap. Reproduced with permission from Ref. [133], Copyright © 2018 Wiley-VCH GmbH.

including a Jahn-Teller like crystal distortion [110-112] and an excitonic insulator transition [113-118]. Recent DFT phonon dispersion simulations for monolayers indicate imaginary phonon modes with a minimum at M-point suggesting that a 2×2 CDW may be explained by a phonon instability [119]. Interestingly, it was suggested that the CDW in bulk TiSe2 undergoes a second phase transition from an achiral to chiral charge order [120-122]. In STM, the supposed chiral nature is observed by domains of clockwise or anticlockwise rotation of three intensity peaks of the tunneling current contributions [120]. Such spiral order may be understood from the three charge density components that are shifted in phase relative to each other and as a consequence the charge order state is rotated as one goes from one TiSe2 layer to the next. It has been further proposed that such a helical configuration of the scalar electron density can be understood by the coupling of electron density, orbital configuration and lattice distortion [123]. However, the existence of a chiral CDW in TiSe2 is controversial [124] and recent STM studies, using symmetry at defects and in adjacent terraces, find an achiral CDW [125]. Regardless of the chiralcharacter of the CDW in bulk TiSe2, no chirality should exist in strictly two-dimensional monolayer materials and a comparison of STM in monolayer and bulk materials may enable further insight in the existence or absence of a chiral CDW. However, to the best of our knowledge a comprehensive comparison of STM work in mono and bulk materials have yet to be reported. TiSe₂ has also attracted interest because it was demonstrated that it could become superconducting if doped with Cu [126]. The interplay between CDW and superconducting phases was also recently probed by ion-liquid gating of exfoliated TiSe₂ flakes [127]. These studies allowed a field effect tuning of the CDW and superconducting transition. Moreover, these studies implied that the superconductivity was supported by a 2D texturing of the CDW in incommensurate states [128]. STM studies on Cu-intercalated TiSe₂ crystals also showed the formation of commensurate-incommensurate domain boundaries [129].

Monolayer TiSe₂ was grown by MBE on graphene/SiC [130,131], HOPG, and MoS₂ substrates [132,133]. The CDW persists for the monolayer on all these substrates exhibiting a 2×2 periodicity as seen from STM studies, as well as from replica bands in ARPES measurements. Temperature dependent ARPES studies show a large opening of the gap between Se- σ band around Γ and the Ti-3d band around M-point. The Ti-3d band is almost empty, but some

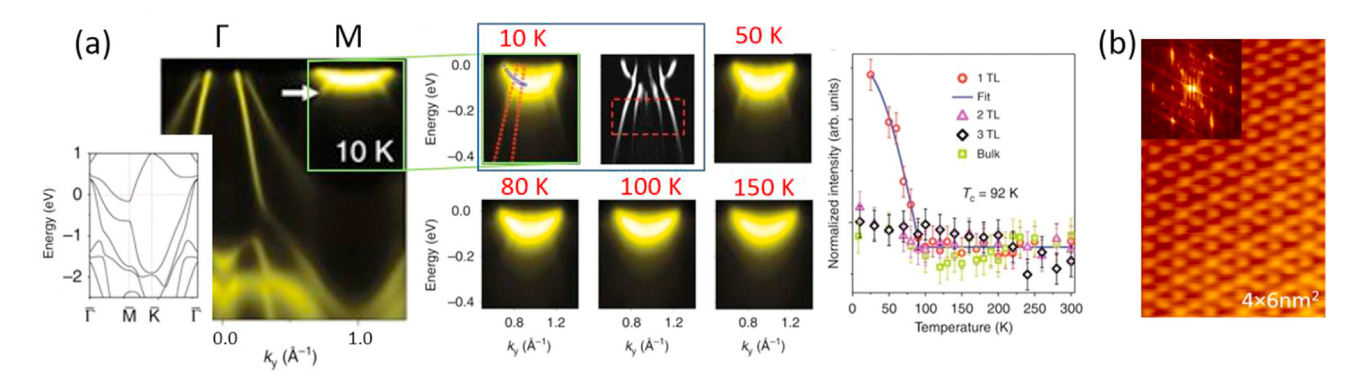


Fig. 10. CDW in monolayer TiTe₂. ARPES measurements show that TiTe₂ monolayer is semimetallic (like the bulk) with band overlap of Te-4p and Ti-3d states. At low temperatures, a replica band is visible at the M-point (white arrow). This replica band disappears at elevated temperature and plotting of the intensity of the replica band as a function of temperature indicates a transition temperature of ~92K. No replica bands are observed for multilayer samples. LT (20 K) STM images shown in (b) also shows a 2 × 2 lattice distortion. Reproduced with permission; (a) from Ref. [135], Copyright © 2017, Springer Nature, and (b) from Ref. [136], Copyright © 2020 American Chemical Society.

residual intensity may be attributed to unintentional doping form defects or substrate effects. Fig. 9 (a) shows that the closing of the gap can be plotted as a function of temperature and fit by a mean field theory temperature dependence to obtain T_{CDW} [130,133]. A dependence of the transition temperature on the substrate has been found [133], with the transition temperature varying between ~200K and ~250 K for TiSe₂ grown on HOPG – or MoS₂-substrates, respectively. The origin of this variation has not been fully resolved; it could be related to environmental screening of the charge carriers by the dielectric properties of the substrate or related to substrate induced charge transfer doping.

Electron doping by alkali (potassium) deposition on monolayers has a pronounced effect on the CDW, as shown in Fig. 9(b). With potassium deposition, the Ti-3d electron pocket around the Mpoint is being filled with electrons. Simultaneously, this results in a suppression of the CDW state as can be observed from the closing of the CDW-gap between Se- σ band the Ti-3d states. Occupation of the Ti-3d bands has also been associated with a transition to the superconducting state in bulk materials [134]. It has, however, not yet been demonstrated that electron doping by alkali atoms can induce superconductivity in monolayers.

TiTe₂ is a semi-metal with the Te- σ band at Γ overlapping with the Ti-3d bands at M. In other words, the overlap of the chalcogen σ band with the Ti-3d bands increases from the sulfide with a semiconducting gap, to selenide with very little or no overlap of the bands, to the telluride with a strong band-overlap. TiTe₂ is not known to exhibit a CDW for bulk materials.

TiTe₂ grows very well as monolayers by MBE. It has been synthesized on graphene/SiC [135], MoS₂, and HOPG [136]. Unexpectedly, Chen et al. reported the formation of a 2×2 CDW in

monolayer TiTe₂. Because of the significant band overlap between Te-4p and Ti-3d, no gap opening could be observed in ARPES (see Fig. 10), but the 2×2 lattice distortion gives rise to replica bands of Te-4p bands at the M-point of the 1×1 BZ, similar to what is observed in TiSe₂. Also, LT STM studies reveal a 2×2 periodicity (Fig. 10 (b)). Using the intensity of the replica band as a function of temperature a transition temperature for this monolayer-CDW has been determined of $T_{CDW} = 92 \text{ K}$. The similarities to the CDW of TiSe₂ suggest a similar origin for the CDW and DFT calculations suggesting a phonon mediated instability to be responsible [137]. Interestingly though, the lack of a gap opening in TiTe2 seems to imply that the gap opening in TiSe2 may not be the driving mechanism but rather a consequence of the CDW. Recently, a 2×2 reconstruction was also observed for multilayer TiTe2 films grown by MBE and it was suggested that it may also be related to a CDW [54]. However, no transition temperature to a normal phase was observed and one may need to consider alternative explanation to that of a CDW, for instance the formation of periodic intercalation compound may give the same periodicity. Such self-intercalation compounds are discussed below in section 5.2.3.

4.1.2. Zirconium dichalcogenides

All Zr-dichalcogenides in their stable 1T phase are indirect band semiconductors. The band gap for ZrS_2 and $ZrSe_2$, are reported as 1.7 eV and 0.9–1.1 eV [107], respectively, while $ZrTe_2$ is semimetallic. Fig. 11 shows a comparison of ARPES studies of $ZrSe_2$ and $ZrTe_2$. Also, a control of the band gap in a $ZrTe_{2(1-x)}Se_{2x}$ has been reported between ~1.1 eV and -0.4 eV (where the minus sign indicates the band overlap in the semimetallic $ZrTe_2$) [138]. Non-stoichiometry, alkali-doping, and pressure can change their

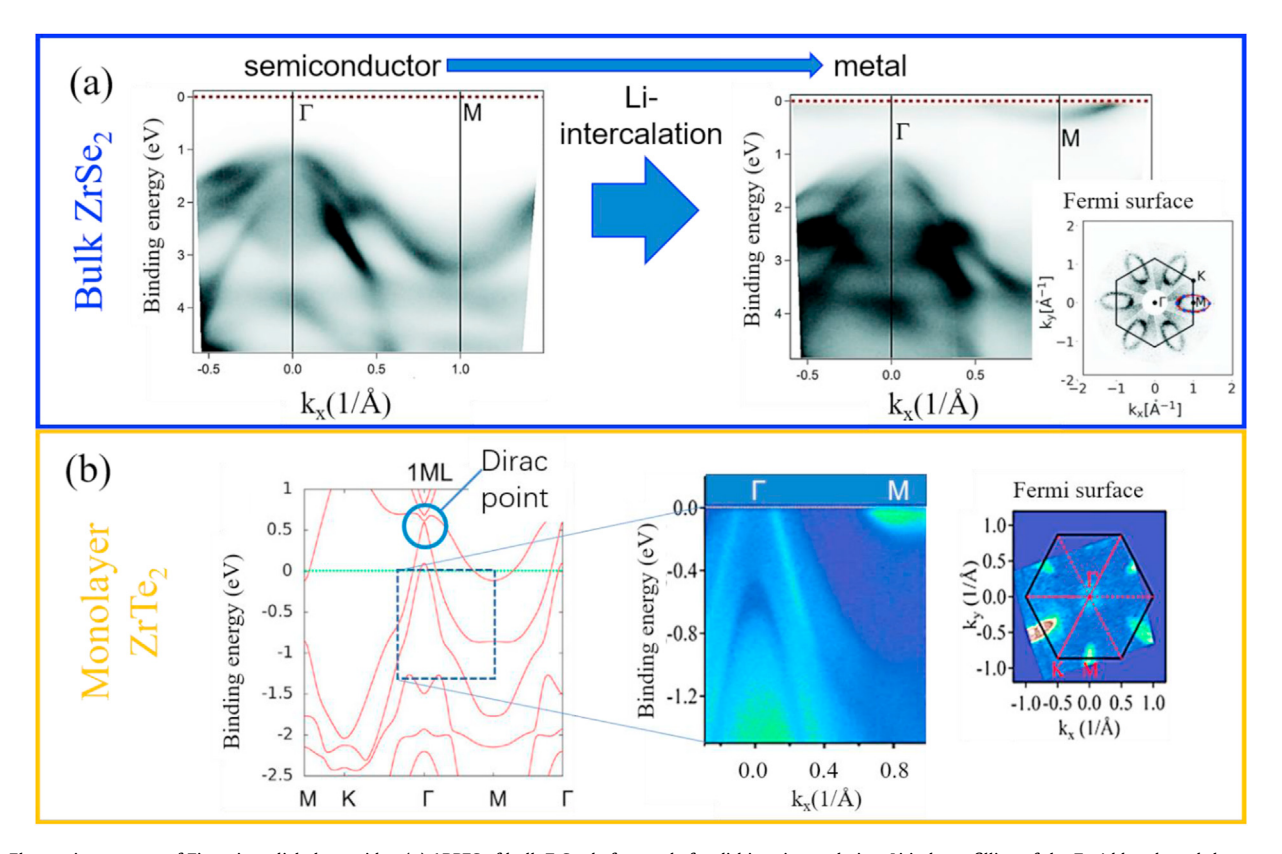


Fig. 11. Electronic structure of Zirconium dichalcogenides. (a) ARPES of bulk ZrSe₂ before and after lithium intercalation. Li induces filling of the Zr-4d bands and thus a transition from semiconductor to metal. (b) band structure calculations for monolayer ZrTe₂ and corresponding ARPES measurements, showing the semimetallic nature of ZrTe₂. (a) is republished with permission of Royal Society of Chemistry, from Ref. [102]; permission conveyed through Copyright Clearance Center, Inc. and (b) is adapted with permission from Ref. [138], Copyright © 2020 American Chemical Society and from Ref. [144] Copyright © 2018 American Chemical Society.

physical properties significantly. For instance, Zr-vacancies in ZrSe₂ has been reported to induce superconductivity [139]. Alkali and copper doping/intercalation have been shown to induce semiconducting to metal transitions [102,140], see Fig. 11 (a). Interestingly, ferromagnetic ordering was also reported for Cu-doped ZrSe₂ [141]. Despite the potential of Zr-dichalcogenides, there have been relatively few direct growth studies by either CVD or MBE. One challenge in the growth of these materials is the presence of many different compositions in Zr-chalcogen phase diagrams. However, successful growth of mono-to few-layer ZrS2 by CVD on hex-BN substrates has been reported [142]. ZrSe2 was grown by MBE and vdW heterostructures of MBE grown ZrSe2/MoSe2 were studied by photoemission to determine the interlayer band alignment [143]. Mono to few layers of ZrTe₂ were grown by MBE on InAs(111) substrates and it was suggested that the σ -band exhibits a Dirac cone [144]. Transport measurements on ZrTe₂ films grown by pulsed laser deposition were also reported to be consistent with a topological Dirac material [145].

4.1.3. Hafnium dichalcogenides

Like the other group IV-B TMDs, the HfS_2 and $HfSe_2$ are indirect band gap semiconductors with band gaps reported as 2.2 eV [102,146] and 1.1–1.3 eV [107], respectively. $HfTe_2$, like the other tellurides in group IV-B, is a semimetal. In 2003, HfS_2 was grown epitaxially on WSe_2 from a monolayer to few layers and studied by ARPES [147]. Naturally, some variation of the k_z dispersion was observed with layer thickness, but no change in the band gap was observed as a function of the number of layers. There are no recent layer-dependent ARPES studies and a repeat of such experiments with modern detectors may be useful for a more accurate determination of layer dependent electronic properties. Recently, few-layer $HfSe_2$ has been successfully grown by MBE on HOPG and MoS_2 substrates [148]. $HfTe_2$ has also been grown by MBE. ARPES studies suggested it to be a topological Dirac semimetal similar to $ZrTe_2$ [52].

4.2. Group V-B TMDs (V, Nb, Ta)

The group V–B TMDs nominally have one d-electron and are metallic. Many of them have CDW instabilities, and some exhibit superconductivity or Mott-insulator (MI) states. Moreover, Nb and Ta disulfides and diselenides can condense in both the 1T- or 2H-structures. In the bulk, the group V–B ditellurides form the distorted 1T" structure (see Fig. 7); only VTe₂ also shows a phase transition to the 1T structure at elevated temperatures (above 480 K). All the group V–B TMDs, with the exception of NbTe₂ and TaTe₂, have been grown by MBE as monolayers on various substrates and some exhibit new properties compared to their bulk. These are discussed in the following.

4.2.1. Vanadium dichalcogenides

Vanadium disulfide and diselenide condense in a 1T structure and exhibit a 4×4 CDW order on their basal planes for bulk surfaces [149], while VTe₂ exhibits a 3×1 reconstruction consistent with the 1T" structure. However, recent studies on bulk VTe₂ surfaces also revealed two different phases that suggest a complex interplay between spin, charge and lattice waves [150]. Interest in monolayer vanadium dichalcogenides was sparked by DFT calculations that predicted that the 1H structure may be energetically favored over the known 1T structure in the monolayer [151–156]. Moreover, ferromagnetic ordering was predicted for the monolayer in several theoretical works [157–159]. Experimentally, however, neither the 1H nor itinerant ferromagnetism could be verified as we discuss below.

VS₂ has been grown on Au(111) substrates by vapor deposition

of V and annealing in H_2S directly dosed onto the surface [68]. LEED, STM, and x-ray photoelectron diffraction (XPD) showed the formation of a single crystalline 1T-VS₂ film. Appearance of moiré-superstructure diffraction spots in LEED (see also Fig. 4(f)) indicates strong site dependent interactions between the metal substrate and VS₂. Vacuum annealing of the monolayer resulted in sulfur loss from the surface and the formation of several ordered VS_{2-x} phases.

VSe₂ has attracted interest because of the above-mentioned theoretical predictions for monolayers of V-dichalcogenides to be an itinerant ferromagnet. DFT calculations consistently predict strongly spin-split bands in VSe₂, which suggest ferromagnetism with a high Curie temperature. Though, a note of caution is that most DFT simulations also suggest VSe₂ in the bulk to be a band magnet with a similar but smaller splitting of majority and minority bands. It is, however, well known that bulk VSe₂ is paramagnetic down to low temperatures and does not show any ferromagnetic ordering.

VSe₂ has been grown by MBE on different vdW substrates, including graphene/SiC, HOPG, and MoS₂ [160–163]. Interestingly, magnetometry (vibrating sample magnetometry or SQUID) by several groups indicate ferromagnetic hysteresis loops [160,162]. Recent studies, shown in Fig. 12, also show that the magnetism in these films strongly depends on the growth temperature or a postgrowth annealing. Importantly, XMCD measurements on VSe2 monolayer films indicate the absence of any magnetic moments on the V-atoms [163,164]. This indicates that the magnetic moments measured in magnetometry cannot originate from the pristine VSe₂ monolayer, and as of now, the origin of the magnetic hysteresis in magnetometry measurements is unresolved. Although pristine VSe₂ is non-magnetic, interfacing it with a ferromagnet by vapor deposition of Fe [165] or Co [166] showed that magnetism can be induced into VSe2 with an antiferromagnetic coupling between VSe₂ and the moments on Fe or Co. Also, very recent XMCD studies showed that vacuum annealing induced Se-deficiency resulted in weak magnetic ordering [167]. This indicates that VSe₂ may be very close to be a ferromagnet, and impurities or structural variations may cause ferromagnetic ordering in this material.

Further evidence for the absence of itinerant magnetic ordering in pristine VSe₂ monolayers comes from ARPES measurements [162–168]. The measured band structure clearly demonstrates that all VSe₂ monolayers grown on vdW substrates are 1T, and the H-structure was never experimentally observed. Importantly, no band splitting into spin polarized majority or minority bands as predicted by DFT calculations has been observed, and thus ARPES is consistent with XMCD studies in that VSe₂ monolayers are not itinerant magnets.

 VSe_2 in the bulk undergoes a CDW transition to a $4 \times 4 \times 3$ lattice distortion with a T_{CDW} of 110/80 K for the incommensurate/ commensurate transition. The CDW has been suggested to be driven by a weak electron phonon coupling in Peierls-like transition that causes a small gap-opening of $2\Delta = (24 \pm 6)$ meV [149]. It was suggested that the electron phonon coupling in bulk VSe₂ can be described by a 3D nesting vector [169,170]. Through nonnegligible interlayer interaction, the Fermi-surface of VSe2 is warped in the kz direction resulting in a nesting vector that has a component normal to the basal plane. For monolayer VSe₂, the CDW instability persists but is significantly modified. The T_c is increased compared to the bulk with values of 220 K [171] or 140 K [163] reported. ARPES measurements report band gap openings for the entire Fermi-surface with values of $\Delta = 100 \text{ meV}$ [171] or $\Delta = 64 \pm 5$ meV [163] for the V d-band along the zone boundary (M-K direction) and a smaller gap of $\Delta = 30 \pm 5$ meV [163] along Γ-K direction. LEED and STM have shown that the monolayer also undergoes a different lattice distortion compared to bulk surfaces. Interestingly, the monolayer exhibits an unusual symmetry

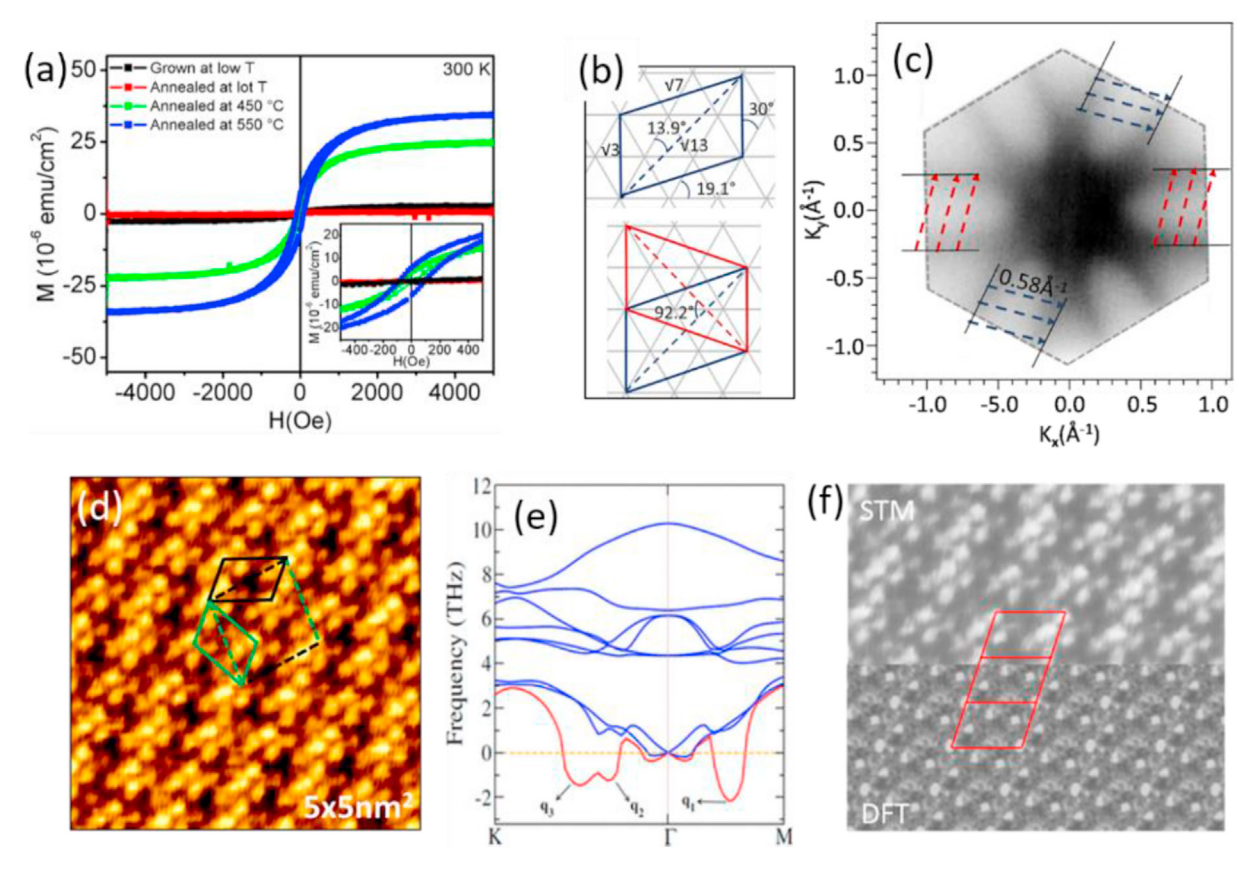


Fig. 12. Characterization of monolayer VSe₂. (a) Magnetometry measurements show that VSe₂ grown at low temperatures exhibit no magnetic moment only post-growth annealing leads to a strong ferromagnetic hysteresis. The origin of this magnetism is unclear but may be related to defects or intercalation. (b) Schematic unit cell of the CDW in monolayer VSe₂ where the diagonal of the unit cell corresponds to a nesting vector in reciprocal space of the d-electron pockets. The nesting vector is illustrated in the experimental Fermi-surface shown in (c). (d) STM image at 20 K of the CDW distortion with the unit cells indicated. (e) Phonon dispersion calculation for a 1T VSe₂ monolayer show several imaginary modes, where q₃ corresponds to the experimentally observed CDW. (f) Simulated STM image of an energy minimized lattice distorted structure found from structure search with the USPEX code is in good agreement with the experimentally measured STM image. Sub-figures (b)—(f) are reprinted with permission from Ref. [168], Copyright © 2019 American Chemical Society.

breaking CDW with a $\sqrt{3} \times \sqrt{7}$ lattice distortion [162–168]. Domain boundaries [168] or a $\sqrt{3} \times 2$ structures may also co-exist [172]. The CDW periodicity can be explained by imaginary phonon modes in DFT phonon dispersion calculations. Also, the observed periodicity of the CDW is consistent with a Fermi-nesting condition of the 2D Fermi-surface (see Fig. 12). Obviously, the monolayer material has a strict 2D Fermi-surface, and thus no 3D Ferminesting, as was suggested for bulk VSe₂, can exist. This difference in the Fermi-surface may thus also explain the different CDW for monolayer and bulk materials [168]. Interestingly, the phonon instability could only be predicted by non-spin polarized DFT calculations, while a ferromagnetic VSe2 would not be expected to show a CDW instability. Thus, the presence of a CDW further supports the absence of an itinerant magnetic state in monolayer VSe₂. Also, the CDW distortion lowers the energy below that of the ferromagnetically ordered ground state. This led to the conclusion that the CDW competes with the ferromagnetic ground state, and this may explain why pristine VSe_2 is not an itinerant magnet [168,173]. On the other hand, this would suggest that suppressing CDW may induce magnetism. Such an interplay between CDW and ferromagnetism still needs to be directly demonstrated.

MBE growth of VSe₂ at elevated temperatures gave rise to a 2×1 periodicity, that resembles a 1T' lattice distortion in STM images [174,175]. However, the distorted 1T structure is not expected for TMDs with a single d-electron, as discussed above. In section 5.2.3, we discuss the possibilities of ordered self-

intercalated compounds that have similar surface corrugations as the 1T' structure and these structures should be considered as an alternative explanation for the observation of 2×1 surface unit cell. Recently, the formation of self-intercalation compounds was also shown for MBE grown multilayers V_5Se_8 [176]. These MBE grown films have shown ferromagnetic properties even though the equivalent intercalation bulk compounds are known to be antiferromagnets [177]. It is tempting to suggest that self-intercalation may also play a role in explaining the observed magnetism in MBE grown monolayers, but to date, this has not been established.

VTe2 has been grown on vdW substrates as monolayers. In the bulk, VTe₂ exhibits a 1T" distorted structure below 480 K [150,178]. For monolayers, it was found, however, that it exhibits an undistorted 1T structure for all temperatures [179–182]. This structural transition from the bulk to the monolayer may be associated with strong interlayer contacts in tellurides [183]. It has been suggested that such contacts cause charge transfer from the Te-5p states into the TM d-orbitals. According to the d-electron count model for the structural distortion of the 1T phase, discussed above, a higher delectron count favors the in-plane lattice distortion [78]. Consequently, for the monolayer, these distortions may be lifted, because of the lack of interlayer contact induced electron transfer to the dorbitals. Currently, there is no clear experimental evidence for this, though. One problem lies in the challenge of growing multilayer VTe₂ by MBE. As we will discuss in section 5.2.3, multilayers are likely forming self-intercalation compounds when grown by MBE

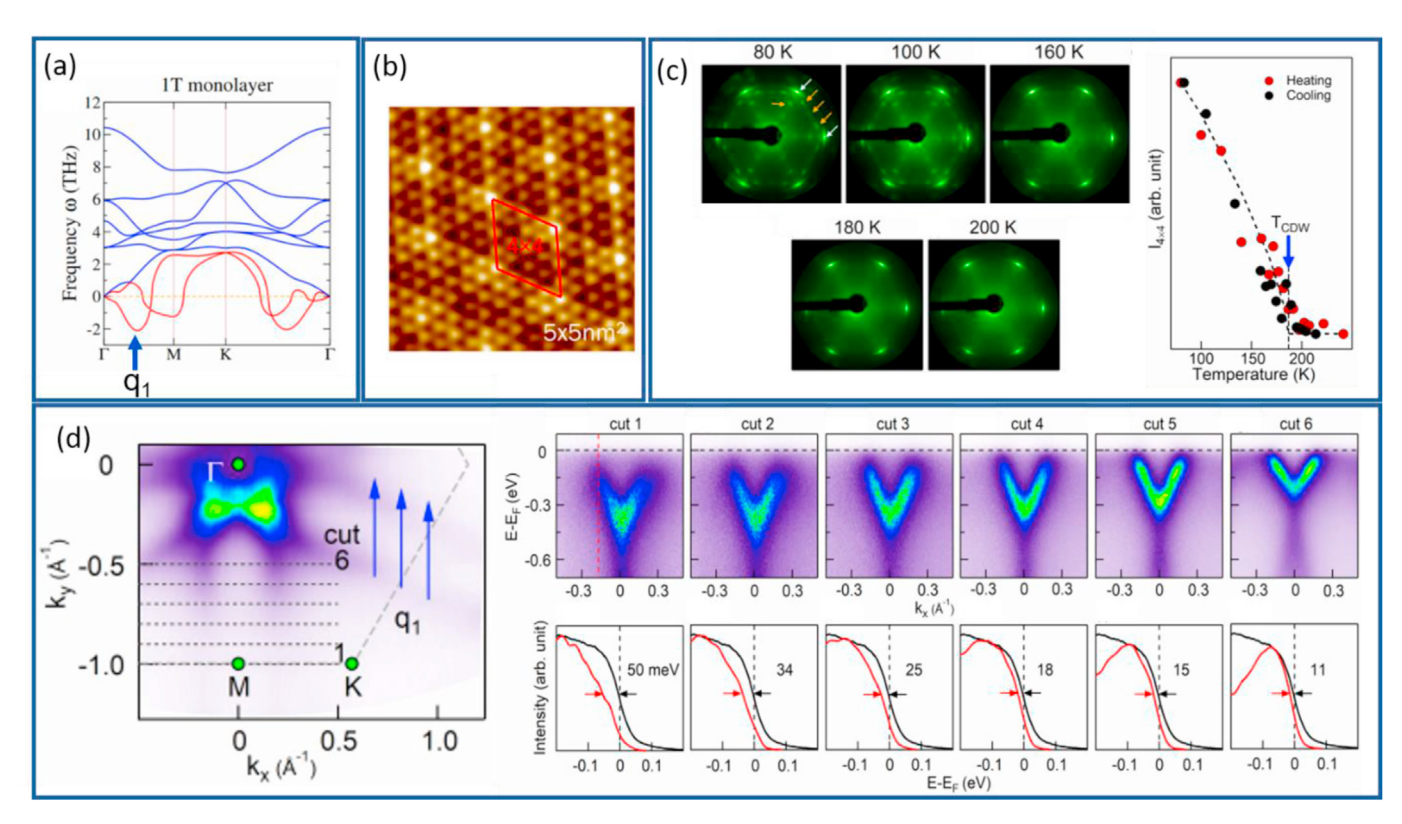


Fig. 13. CDW in monolayer VTe₂. (a) DFT simulations of phonon modes for monolayer 1T VTe₂ indicate imaginary phonon modes, with q₁ corresponding to a 4 × 4 CDW. (b) LT-STM (20 K) indicates a 4 × 4 periodic lattice distortion. Temperature dependent LEED (c) shows a disappearance of 4 × 4 superstructure spots ~190 K. ARPES at 80 K (d) shows a partial opening of a gap in the Fermi-surface around the M-point. The nesting vector q1 is also indicated in the Fermi-surface, as well as the measured gap along the 6 energy distribution cuts in the BZ parallel to the K-M direction. (a) and (b) are adapted with permission from Ref. [179], Copyright © 2019 American Chemical Society. (c) and (d) are reprinted figures with permission from Ref. [182], Copyright © 2020 by the American Physical Society.

and this makes a direct comparison of MBE grown monolayer and multilayer VTe_2 difficult.

Since the monolayer exhibits a 1T structure, it is isostructural to VS₂ and VSe₂ with similar electronic properties. In the bulk, VS₂ and VSe₂ exhibit a 4×4 periodic lattice distortion on the basal planes for their CDW. LT STM and LEED indeed showed that monolayer 1T-VTe₂ also undergoes a 4×4 lattice distortion, as shown in Fig. 13 [179–182]. From the disappearance of the LEED superstructure spots, a T_c of 186–192 K was found [181,182]. Moreover, temperature dependent ARPES shows a partial gap opening [182] in the surface for the d-bands around the BZ boundary, as shown in Fig. 13 (d). This indicates that the CDW can be ascribed to a similar weak electron phonon coupling and Fermi surface nesting as for the other V-dichalcogenides. Phonon dispersion calculations also confirm imaginary phonon modes halfway between Γ and M, consistent with a 4×4 structure observed in the experiments.

4.2.2. Niobium dichalcogenides

Niobium dichalcogenides have been extensively studied primarily because of its superconductive properties and their interplay with CDW transitions. In 2H–NbSe2, a CDW ($T_{CDW}=33K$) coexists with superconductivity ($T_c=7.1K$). In contrast, bulk 2H–NbS2 only exhibits a superconductive phase with a T_c of ~6 K in the absence of a CDW phase transition. However, it has been proposed that 2H–NbS2 is close to a CDW transition and significant softening of phonon modes has been recently observed [184]. NbTe2 exhibits a distorted 1T" structure and also undergoes a transition to superconductivity at $T_c=0.5-0.7$ K [185]. The 1T" structure in NbTe2 has been suggested to be related to a CDW transition, because the calculations for the hypothetical 1T

structure exhibits imaginary phonon modes consistent with the 3×1 lattice distortion [186]. However, unlike usual CDWs, no transition temperature has been reported and the 3×1 structure of the basal plane is observed even for high temperatures. Naturally, these interesting quantum phenomena in the bulk of Nb-dichalcogenides also motivated the synthesis and characterization of monolayer materials, which are summarized next.

NbS₂, so far, has only been grown on Au(111) substrates [187]. High quality epitaxial NbS₂ monolayer films were obtained by vapor deposition of Nb in a dimethyl disulfide ($C_2H_6S_2$) atmosphere with the substrate at room temperature and subsequent annealing at 450 °C for 30 min in the same background. STM and LEED showed the formation of a pronounced moiré pattern, while ARPES measurements showed an electronic structure consistent with a 1H structure of the NbS₂ monolayer. However, a rigid shift of the band structure and other deviations compared to the calculated bands of free-standing NbS₂, suggest charge transfer and hybridization of electronic states of the NbS₂ with the Au(111) substrate.

NbSe₂ monolayers have been grown by several groups by MBE on graphene/SiC substrates [188–191]. The CDW transition temperatures in NbSe₂ has been observed to increase significantly in exfoliated samples from 33 K to 145 K as the number of layers is reduced [192]. These studies were, however, performed in air, which will result in the material contamination and degradation and thus may not be reliable measurements of intrinsic properties. More controlled studies on MBE grown monolayer samples under UHV conditions could not reproduce this large enhancement of the CDW transition temperature demonstrating the importance of controlled environments in the study of these nanomaterials. STM measurements show that the CDW order is the same 3×3

structure as is known for bulk basal planes. Temperature dependent studied showed the disappearance of the CDW at 45 K, only slightly higher than the T_{CDW} reported for bulk NbSe₂ [189]. While the CDW may be enhanced in the monolayer, the superconducting transition is suppressed. Transport measurements to determine superconducting transitions were first performed on MBE grown samples on graphene substrates and with Se-capping layers to prevent degradation from air exposure [193]. In various studies of monolayers, superconducting transition temperatures were found with a T_c of 1.5 K [188], 1.9 K [193] or 2.4 K [190], reduced from 7.2 K in the bulk, ARPES helped to discuss the origin of the CDW in NbSe₂ [188,189]. The simplified band structure of the monolayer with fewer bands crossing the Fermi-level than in bulk materials allowed to effectively rule out Fermi-surface nesting conditions as a possible origin of the CDW in NbSe₂. Thus, it may be concluded that the CDW in NbSe₂ is likely driven by a wave-vector dependent electron phonon coupling, which has been identified experimentally by phonon softening as well as a broad region of imaginary phonon modes in DFT calculations [194].

Interestingly, while in the bulk only the 2H phase of NbSe₂ is known, Nakata et al. [188] demonstrated that by increasing the growth temperature, the 1T phase may be obtained by MBE growth of monolayers. The different phases were identified from ARPES measurements of their distinct band structures. For growth temperatures below 540 °C, the H-phase was primarily obtained while for higher growth temperatures the 1T phase was observed. STM images revealed a $\sqrt{13} \times \sqrt{13}$ periodicity, which was, based on the similarities to the isoelectronic 1T-TaS₂ and 1T-TaSe₂ (discussed below), suggested to be a CDW. In contrast to DFT calculations of the 1T structure, photoemission showed a significant band gap opening in 1T-NbSe₂. Again, in analogy to 1T-TaSe₂/TaSe₂, this was interpreted to be the consequence of the MI state.

NbTe₂ has not yet been reported in the monolayer.

4.2.3. Tantalum dichalcogenides

Tantalum disulfide and diselenide may condense in either the 2H or the 1T structure, while TaTe₂ is known to exhibit the distorted 1T" structure, like the V- and Nb-ditellurides. The 2H-phases of TaS₂ and TaSe₂ exhibit a 3×3 CDW. Also, a superconducting transition is observed at low temperatures. The 1T phase of TaS2 and TaSe2 also exhibit CDW transitions with transition temperatures well above room temperature. Also, 1T-TaS2 has one of the largest lattice distortions in CDW phases that makes it even possible to be observed in transmission electron microscopy (TEM) imaging [195]. The 1Tphase of TaS2 is a well-known MI, while 1T-TaSe2 is not a MI in the bulk. The interplay between CDW, MI state, and superconductivity in the Ta dichalcogenides makes these exciting quantum materials that have been studied extensively in their bulk form. Reducing the system to a monolayer, simplifies the electronic structure and removes the influence of interlayer interactions. Monolayers are also easier modified by changing environments, e.g. by forming heterostructure-interfaces or adsorbates, than bulk materials. This opens potentially new avenues for tuning quantum transition and inducing new properties. Consequently, there have been efforts in a controlled growth of Ta-dichalcogenide monolayers. In the following, we address the different systems separately and put their bulk properties in perspective to surface modifications and their successful monolayer synthesis.

2H–**TaS**₂ is a CDW material with a nearly commensurate [196] 3×3 CDW below 75 K in the bulk [197] and a superconducting transition below $T_c = 1$ K [198]. Layer dependent studies by exfoliation from the bulk suggest an increase in Tc with decreasing layer thickness [199–201]. Monolayer growth of 1H–TaS₂ has been achieved by MBE and their properties vary depending on the substrate. Two main substrates have been employed: (i) metal

substrates, mainly Au(111) [202], or (ii) graphene on either SiC [203] or Ir(111) [204]. On gold substrates, no CDW was found while on graphene, the CDW persisted in the monolayer. The suppression of the CDW of H-TaS₂/Au(111) is likely related to strong S-Au interactions [205]. But DFT simulations also showed that charge transfer doping of TaS₂ removes the phonon instability, and thus may allow tuning and suppression of the CDW transition [206]. On graphene, the substrate interactions are very small because of the large gap of the graphene π -band around Γ and the resulting lack of any band-overlap between the π -band and the bands of TMDs close to the Fermi-level. This results in quasi-free standing TaS2 with only small charge transfers due to work function differences. The quasifree standing TaS2 allowed a detailed characterization of charge doping on monolayer TaS₂ by alkali-atom (Li) deposition [204]. Combined with DFT calculations for phonon instabilities, it was shown that the CDW in TaS_2 can be tuned from a 3×3 CDW for undoped or weakly electron doped sample, to a 2×2 , and eventually to a complete suppression of the CDW with increasing Lideposition (electron doping). These studies thus demonstrate the tunability of the quantum transitions in monolayer TMDs by controlling charge transfer and interface interactions. Interface electrostatic interactions may also be responsible for recently reported room temperature 3×3 CDW on bilayer 2H–TaS₂ grown epitaxially on hex-BN [74].

1T-TaS2 has attracted great interest because of the interplay between its CDW and a MI state. Bulk 1T-TaS2 undergoes several CDW phase transitions from a commensurate CDW to a nearly commensurate phase at 225 K, to an incommensurate CDW at 355 K and a 'normal' phase at 545 K. The CDW has a $\sqrt{13} \times \sqrt{13}$ periodic lattice distortion known as the 'Star of David' CDW. In this lattice distortion, 12 surrounding Ta atoms relax towards a central Ta atom. The MI state is closely linked with this CDW as the MI state of 1T-TaS₂ is not residing by charge correlation on the atomic lattice but on the periodic commensurate CDW. Thus, the MI transition occurs together with the incommensurate to commensurate CDW transition. Since the CDW is susceptible to external perturbations of the electronic structure, this allows a control over the MI transition. Collapse of the MI state was induced by high pressure [207], charge doping [208,209], strain [210], and alloying of TaS2 with TaSe2 [211–214]. The commensurate CDW has a strong quasi-1D dispersion normal to the lattice planes [215], suggesting that CDW in strict monolayer materials may be modified and interlayer electronic ordering may play an important role in the observed metalinsulator transitions in 1T-TaS2 [216]. This asks for a detailed characterization of the behavior in the absence of 3D crystals to better understand the importance of interlayer interactions and 3D-ordering.

Encapsulated, exfoliated 1T-TaS2 flakes enabled study of thin 1T-TaS₂ by transport measurements and demonstrated current driven switching between commensurate and incommensurate CDW [217]. However, up to now there are only a few reports of MBE growth of monolayer 1T-TaS2 on graphene/SiC [218,219]. In contrast to the H-phase, the 1T phase was obtained by growing at high substrate temperatures of 650 °C. In low temperature STM, a commensurate $\sqrt{13} \times \sqrt{13}$ CDW was observed, like in the bulk. STS indicated a 0.45 eV energy gap and with features like those reported for bulk surfaces, suggesting the formation of a MI state also for ML 1T-TaS₂. Certainly, more studies of true monolayer 1T-TaS₂ by transport and ARPES measurements are desirable. The response of the monolayer to external stimuli such as charge doping also would be desirable in order to investigate the tunability of the phases. Effects of charge doping by alkali metal deposition, have, for instance, been observed on surfaces of bulk TaS2 that indicated a metallization of the surface while the CDW persisted [220]. Similar studies would be interesting to be performed on truly 2D

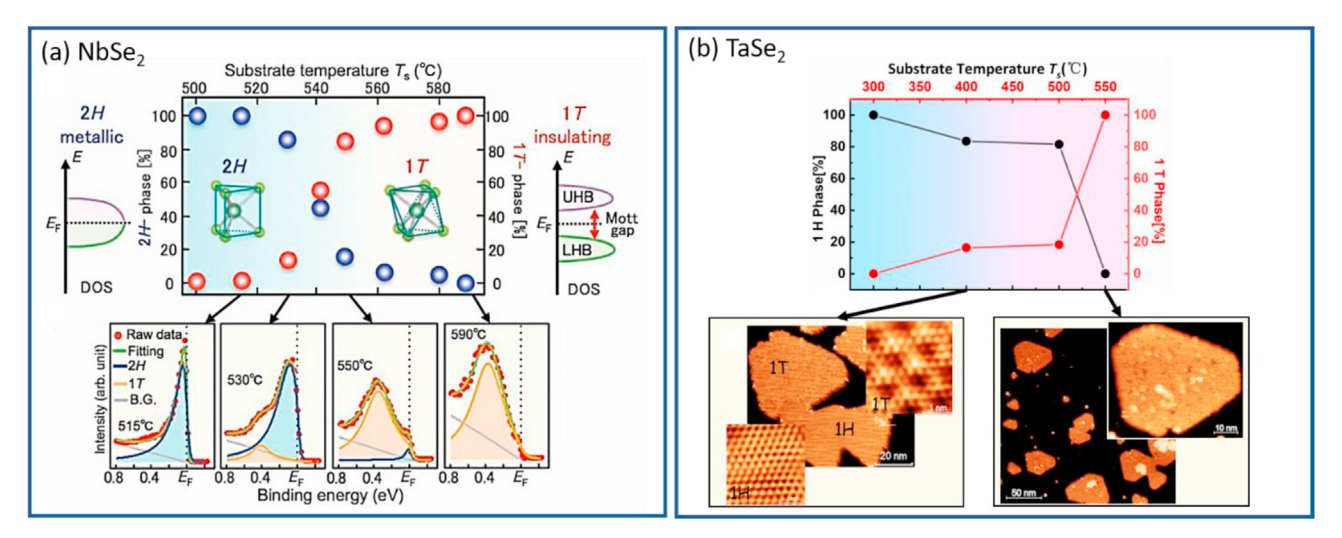


Fig. 14. Controlling 1T and 1H phase in MBE grown monolayers by substrate temperature for (a) NbSe₂ and (b) TaSe₂. Photoemission was used to determine the fraction of 1T and 1H phases as a function of growth temperature by fitting energy distribution curves close to E_F with two Lorentzians assigned to the 1T and 1H phase. The 1T phase exhibits a gap, which was attributed to a Mott-Hubbard band gap. (b) shows phase dependence for TaSe₂ grown by MBE and characterized by room temperature STM. Only the 1T-TaSe₂ phase exhibits a room temperature CDW, which enables the distinction between the 1T and 1H phase in STM. Statistical analysis of STM images shows that at 300 °C only 1H phase is present and at above 550 °C, only the 1T phase is grown. In between 300 °C -550 °C a phase mixture is observed. Figure (a) has been reproduced from Ref. [188], Copyright © 2018, Springer Nature.

monolayers.

2H–**TaSe**₂, like 2H–NbSe₂, exhibits a 3×3 CDW. It undergoes a transition from a normal phase to an incommensurate CDW at ~122 K and a second transition to a commensurate CDW at ~90K. A superconducting phase can only be detected at very low temperatures of ~0.2 K [221]. Monolayer 1H-TaSe2 was grown by MBE on graphene/SiC and characterized by low temperature STM and ARPES measurements [222]. Only a very small increase in the CDW transition temperature was determined from the temperature dependent gap opening in ARPES to T_{CDW}~ 130 K for the monolayer compared to bulk materials. Also, only a slightly larger gap of around 100 meV at 15 K was observed compared to reported gaps between 12 and 80 meV for bulk materials [223-225]. These relatively small changes of the CDW properties compared to bulk materials may be surprising considering relatively strong changes in the electronic structure, such as the number of bands crossing the Fermi-surface. This may suggest that the origin of the CDW must originate from electron-phonon coupling, similar conclusions were reached for the iso-electronic 1H-NbSe₂ [189].

1T-TaSe₂, in contrast to TaS₂, is not a MI in the bulk. However, some reports claim that the surface of bulk TaSe₂ may exhibit a MI state [226,227], suggesting the importance of interlayer interactions in tuning the electron correlation properties and potentially inducing MI in monolayers. MBE growth of TaSe2 was already reported in 1992 and a preferential growth of the 1T- or 2H phase was observed by tuning the substrate temperature [228]. These early reports suggest that at low growth temperatures (300-340 °C) the 2H phase was obtained, while at high temperatures (420-650 °C), the 1T phase can be grown. Recent ARPES characterization of monolayers grown on graphene/SiC at different growth temperatures also showed a transition from H to T-phase [229]. In addition to ARPES, there are differences in the CDW with 1T exhibiting a $\sqrt{13} \times \sqrt{13}$ CDW even at RT, while the 3 × 3 CDW of the H-phase is only observed at LT. This allows to easily distinguish between the phases in RT STM, as shown in Fig. 14 (b). In these STM studies, for samples grown below 300 °C the 2H phase was obtained and above 550 °C, the 1T phase; at intermediate temperatures a phase mixture is observed.

For the 1T phase, an opening of 0.2 eV gap at the Γ -point was

measured in ARPES studies, which is in contrast to DFT simulations of the band structure. Because of the similarities to 1T-TaS₂, the gap has been interpreted to be a Mott-Hubbard transition, and thus the flat-band observed in ARPES to be the lower Hubbard band. Such a MI transition was also concluded from a combined STM and ARPES study [230]. STM/STS indicated an unusual orbital texture in the CDW of the monolayer that is weakened by interlayer interactions in multilayer regions. Moreover, the energy gap is reduced for biand tri-layer regions, suggesting a quenching of the MI through interlayer interactions in 1T-TaSe₂. This indicates that monolayer 1T-TaSe₂ is a strong electron correlated system with distinct properties compared to bulk TaSe₂.

TaTe₂ exhibits a distorted 1T" structure in the bulk with a 3×1 periodicity of its basal plane (with respect to a hexagonal 1T structure, see Fig. 7). Recent LT-STM studies have revealed that this surface undergoes a CDW-like transition that modulates the 3×1 row structure and forms a 3×3 lattice modulation [231]. To the best of our knowledge, there have not been any monolayer studies of this material. With evidence for VTe₂ to undergo a layer dependent structural transition to a 1T structure for the monolayer, an investigation of monolayer TaTe₂ would be interesting to confirm a general trend for these group V-B ditellurides.

4.3. Group VI-B TMDs (Cr, Mo, W)

The group VI-B TMDs can exhibit either the H or 1T' structure. For instance, MoTe $_2$ undergoes a phase transition from H to 1T' as a function of temperature. Moreover, the metastable 1T' phase will transition to the T_d phase (see Fig. 8) and become a type II Wyle semimetal. In other TMDs, a phase transition from semiconducting H-phase to metallic T-phase may be induced by electron doping. This is best documented for MoS_2 and is discussed in section 5.4. These variabilities in their bulk properties, paired with monolayer properties, such as the 2D topological phases of 1T' -WTe $_2$ and -MoTe $_2$, as well as the layer dependent band gaps of the semiconducting H-TMDs, make the group VI-B TMDs interesting from many aspects and consequently are the best studied TMDs.

Mo and W dichalcogenides are among the most widely studied TMDs. Their 2H phases are semiconducting, and thus have been

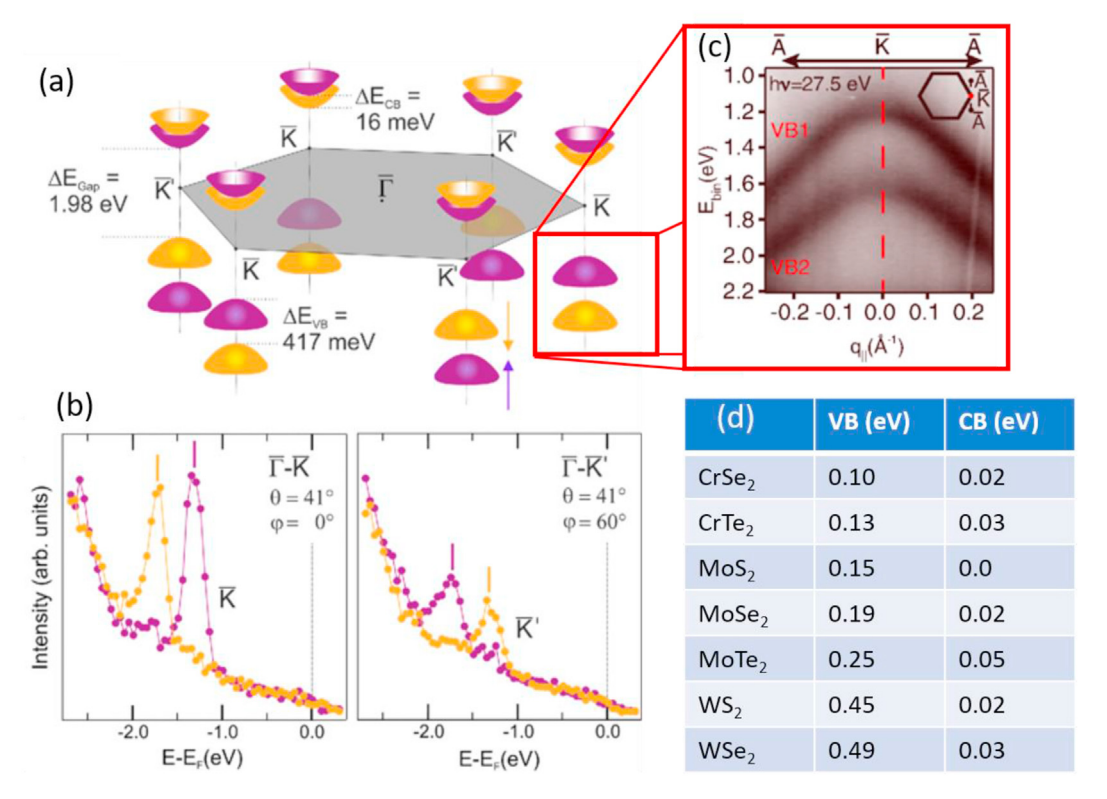


Fig. 15. Spin polarization at the K-points due to SOC and broken inversion symmetry in monolayer 2H Mo- and W- dichalcogenides. (a) schematic of the spin polarized bands at the valleys with alternating spin polarization at the K and K' point and spin and angle resolved photoemission measurements shown in (b) for WS₂. (c) shows the experimental ARPES measurements for the splitting of the bands at K and (d) summarizes theoretical values for the SOC induced band splitting for the VB and CB at the K points. The theoretical values are taken from Ref. [235]. (a) and (b) are reprinted figures with permission from Ref. [236], Copyright © 2018 by the American Physical Society and (c) from Ref. [237], Copyright © 2015 by the American Physical Society.

used in prototypical semiconducting devices. The band gaps and work functions for monolayer group VI-B-TMDs have been calculated [232] (see also section 5.3 for calculated band alignment for various TMD heterostructures). From these calculations, a trend of decreasing electron affinity from sulfides to selenides and tellurides is observed for both Mo- and W- dichalcogenides (note that H–WTe₂ does not exist but WTe₂ rather forms the 1T' phase). All the 2H group VI-B TMDs undergo an indirect to direct band gap transition as they are thinned to the monolayer. Moreover, the valleys at the K-point that are derived from the TM d-orbitals are split due to strong SOC and become spin polarized due to inversion symmetry breaking in the monolayer. Alternating valleys have opposite spin polarization, and thus the valleys are labeled as K and K', as illustrated in Fig. 15. The splitting is much larger in the VB than the CB and increases for the heavier elements. The table in Fig. 15 gives theoretically calculated values for the splitting, which are in good agreement with experimental available data [233-235].

Based on DFT calculations, the energy differences between the 1T (or 1T') phase and the 2H phase is very small, thus enabling phase changes [238], which will be discussed in section 5.4. According to these DFT calculations, only WTe₂ is more stable in the 1T' phase (among the Mo-, W-dichalcogenides) than the 2H phase, but as we will discuss, some materials, namely MoTe₂ and WSe₂ can also be grown as 1T' by MBE. Other materials like e.g. MoS₂ is well known to switch into the 1T phase by Li-intercalation or by other electron doping schemes (see section 5.4). The distorted 1T' phases of WSe₂, WTe₂, and MoTe₂ have also attracted significant interest because of their topological protected electronic states and formation of a QSHI in the monolayer limit. In contrast to 4d and 5d

TM, the 3d TM dichalcogenides, namely CrSe₂ and CrTe₂, have not been studied extensively because they are not stable, and thus not widely available. In the 1T structure, Cr-dichalcogenides are proposed to have itinerant d-electrons and 1T-CrTe₂ exhibits ferromagnetic ordering which could make it an interesting candidate for sought 2D ferromagnets. As in previous sub-sections, we discuss the dichalcogenides of the different TM one-by-one with a focus on MBE grown monolayers and thin films.

4.3.1. Chromium dichalcogenides

The Cr-chalcogenides usually condense in the stable NiAsstructure with periodic Cr-vacancies. These structures may also be viewed as TMD-layers with self-intercalated Cr (see section 5.2.3). The Cr-dichalcogenides (CrSe₂ and CrTe₂) are only metastable. The synthesis of these dichalcogenides in the bulk has been only achieved by synthesizing an alkali-intercalation compound first, that stabilizes the TMD-layers. Subsequently, the alkali atoms can be extracted at a low temperature by chemical means [239,240]. It has been recently reported that bulk 1T-CrTe2 prepared by such means is ferromagnetic with a relatively high Curie temperature of 310 K [240,241]. This would make this material potentially interesting as a layered ferromagnet, such materials are sought for spintronics applications. 1T-CrSe₂, on the other hand, has been suggested to exhibit antiferromagnetic ordering [242]. A challenge for these materials is their low thermal stability. For CrSe₂, a decomposition into Cr₂Se₃ and Se is reported at 600 K [239], while CrTe₂ has an even lower stability, and decomposition temperature of only 330 K has been reported [240]. Monolayer CrSe₂ or CrTe₂ have not yet been exfoliated from these bulk crystals, and so far only multilayer flakes have been reported by exfoliation

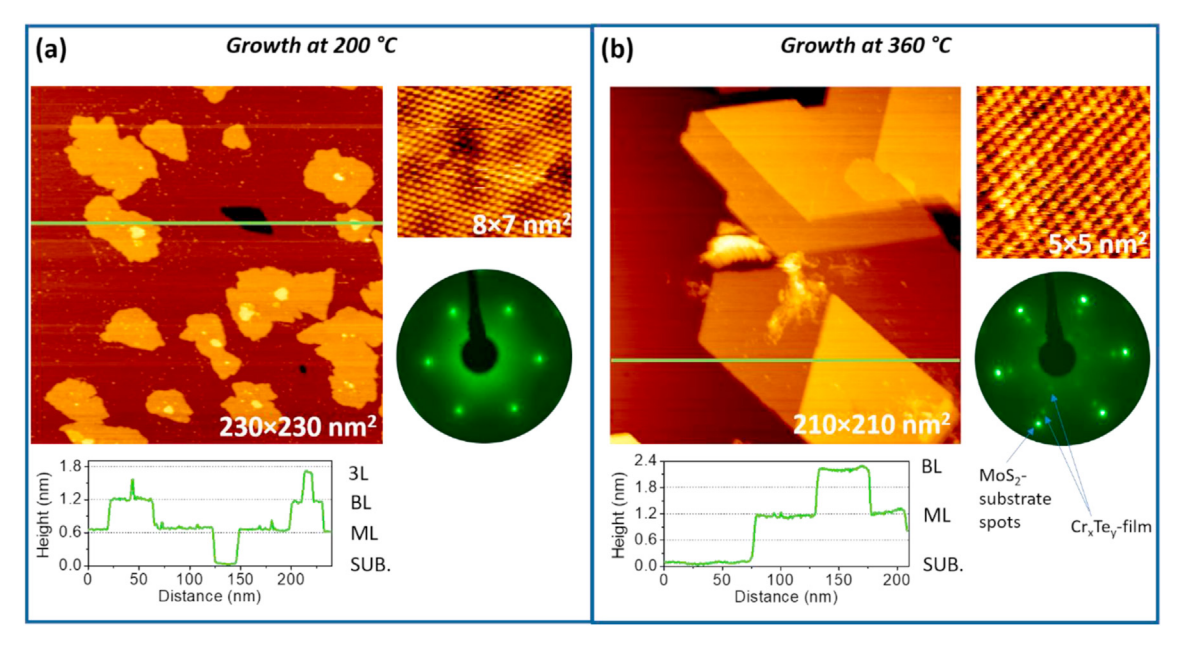


Fig. 16. MBE growth of Cr telluride (on MoS_2 substrate). (a) growth at low temperatures ($\sim 200\,^{\circ}$ C) results in a layer-by-layer growth with the first layer likely to be CrTe₂. High resolution STM images indicate a weak moiré-superstructure and the LEED pattern is consistent with CrTe₂. (b) growth at slightly higher temperatures ($360\,^{\circ}$ C) causes formation of multilayer islands with the bare MoS2 substrate exposed for ultrathin films. Consequently, the LEED pattern shows strong substrate diffraction spots in addition to the diffraction spots of the film. The film exhibits 2×1 superstructure spots, which is consistent with the STM images that show also a 2×1 superstructure. This likely suggests the formation of a self-intercalation compound at higher growth temperatures.

[241].

While the 1T-CrSe₂ and 1T-CrTe₂ have been synthesized, DFT calculations suggest that the 2H phase of Cr-dichalcogenides should be energetically favored [235-244]. One possible explanation for this discrepancy may be the preparation methods for the bulk samples. Bulk samples are obtained by extraction of intercalated alkali atoms, and it is known for other group VI-B TMDs that alkali intercalation can favor the formation of 1T phases over the 2H phase. After extraction of the alkali atoms, the structure may remain in the 1T phase because of kinetic barriers that prevent transitioning into the 2H ground state. This has been observed e.g. for MoS₂ and is discussed in section 5.4. However, until a 2H Crdichalcogenide can be synthesized, it remains an open question of what the true ground state configuration of CrSe2 and CrTe2 is. While the 1T phases are metallic, the 2H phases are expected to be semiconducting with calculated band gaps by LDA (LDA@G₀W₀) of 0.70 eV (1.21 eV) and 0.45 eV (0.77 eV) for CrSe2-and CrTe2-monolayers, respectively [235]. Also, similar to the Mo- and W-

dichalcogenides in the 2H structure, SOC causes a splitting of the dbands in the K-valleys [235,245]. Calculated values for the splitting can be found in Fig. 15. If CrTe₂ can be obtained in the 1T phase, then calculations suggest that it exhibits a phonon instability that should give rise to a CDW [246]. Interestingly, this CDW could stabilize ferromagnetic ordering in the monolayer.

Clearly, experimental verification of the theoretical predictions regarding the structure and properties of Cr-dichalcogenides is needed, especially in the monolayer limit. MBE growth may be an opportunity for the synthesis of this material, however, the metastability of the dichalcogenides and the preference to form intercalation compounds (see also section 5.2.3 for compositional control and formation of self-intercalated compounds) make it challenging. We have recently reported that $CrTe_2$ can be grown as a monolayer on MoS_2 or HOPG at growth temperatures below $250\,^{\circ}C$ [136]. For higher growth temperatures only bi-or multi-layer structures are observed with most likely self-intercalated Cr in between the TMDC layers forming Cr_3Te_4 or related compounds.

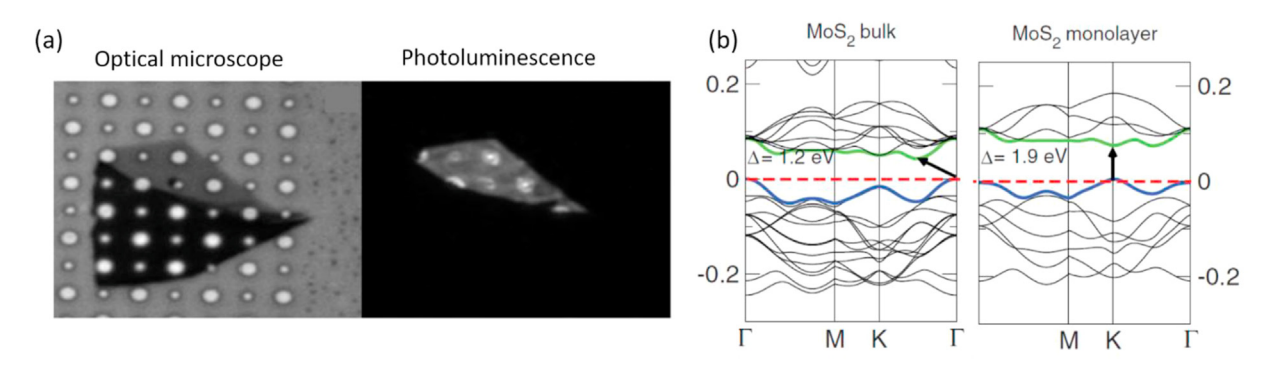


Fig. 17. Indirect-to direct-band gap transition for monolayer MoS₂. (a) optical microscopy image of a MoS₂ flake on a TEM grid. The dark region are multilayers, while the gray region is monolayer MoS₂. In photoluminescence the monolayer region is much brighter, indicating the transition to a direct band gap material. (b) DFT simulations show the indirect to direct band gap transition from bulk to monolayer materials. Both the CBM and VBM shift to the K-point in the monolayer making it a direct band gap. Reproduced with permission: (a) from Ref. [3]], Copyright © 2010 by the American Physical Society, and (b) from Ref. [253], Copyright © 2011 by the American Physical Society.

The sensitive dependence of the structure of MBE grown chromium telluride is illustrated in Fig. 16. At low growth temperatures ~200 °C, a monolayer film that is attributed to CrTe2 is obtained. This film has a hexagonal LEED pattern. It has, however, not yet been establish if the monolayer has a 1T or 1H phase. Recent MBE work claim a 1T phase with antiferromagnetic ordering revealed by spin-polarized STM [247], but challenges in the accurate determination of the presence of intercalated Cr make an unambiguous determination of the composition challenging. Thus, more work is required to determining the structural phase of this monolayer material. For growth at higher temperatures, e.g. 360 °C shown in Fig. 16 (b), the film does not grow as uniform layers but instead form multilayer islands as indicated by the cross-section of the STM image. Moreover, the LEED indicates additional diffraction spots consistent with 2×1 domains and the formation of Cr_3Te_4 (see section 5.2.3).

4.3.2. Molybdenum dichalcogenides

MoS₂ was the first TMD that was exfoliated to a single molecular layer. Famously, it was first demonstrated on MoS2 that when isolated as a single layer the band gap increases and importantly transitions from an indirect gap in the bulk to a direct band gap, as shown in Fig. 17 [3,248]. Subsequently, it was shown that such a transition from indirect to direct band gap is common for all the Mo-dichalcogenides [249-252]. This layer dependent behavior can be explained by two effects [253,254]. Quantum confinement effects and charge carrier screening are largely responsible for the increased band gap in the monolayer, while the transition from indirect to direct band gap is a consequence of interlayer orbital interactions. In the bulk, the VBM is located at the Γ -point of the hexagonal BZ while the weakly dispersing CBM is located between Γ and K. For monolayers both the CBM and VBM are at K. The strong change of the VB can be attributed to the interlayer interactions of orbitals at the Γ -point. For multilayers, frontier orbitals from different layers overlap, pushing them up higher in energy (to lower binding energy), and thus making the Γ -point the VBM. Without these interlayer interactions in the monolayer, the orbitals at Γ -point have a higher binding energy and the VBM shifts to the K-point. A concurrent shift of the CBM to the K-point makes the monolayer a direct gap material. DFT calculations of the band structure for monolayer and bulk MoS₂ are shown in Fig. 17 (b). The change in the VB structure of the TMD as a function of layers was also observed in angle resolved photoemission in a photoemission electron microscope (PEEM) on exfoliated flakes of MoS₂ [255]. From an MBE growth perspective, the evolution of the band structure as a function of layers was probed on MoSe₂ [256], demonstrating the shift of the band maximum from K to Γ with an increasing number of layers. Moreover, the direct band gap of monolayer MoSe₂ was shown by potassium deposition and shifting of the Fermi-level into the CB to show that the CBM is also at the Kpoint. Finally, the difference between the true quasiparticle band gap and the optical band gap due to the large exciton binding energies in monolayer TMDs was demonstrated by measuring monolayer band gaps by STS and comparing it to optical absorption spectra [257]. This also enabled to estimate the exciton binding energy in these materials as the difference between the gap measured by STS and the gap measured by optical absorption

MoS₂ and MoSe₂ have been grown by MBE as monolayer samples on various substrates in their stable H phase, while MoTe₂ can be obtained in either the H or 1T' phase and achieving phase specific growth conditions has been a focus for MBE growth. In the following, we summarize some of these studies and key findings on substrate dependence.

MoS₂ monolayers have been synthesized by vacuum processes

and Au(111) substrates [258–262], or graphene either on SiC [263] or Ir(111) [264]. The 1H monolayer, in contrast to bilayer and bulk 2H, has a broken inversion symmetry and, as a consequence, the valleys at the K-point are inequivalent, as shown in Fig. 15. Strong spin orbit interactions in the Mo and W dichalcogenides causes a significant splitting of the d-band at K [265], which is larger for the heavier W. In the monolayer, with broken inversion symmetry, these split bands become spin polarized and this has been probed for instance with circularly polarized light that allows to address specific valleys [266–268]. In order to exploit the valley polarization, the monolayers should not have any twinning, because the twins have opposite valleys, and thus the overall polarization of the film is lost. As discussed in section 2.3, graphene has a higher symmetry than TMDs, and thus the formation of two twin orientations of TMDs on graphene substrates is unavoidable. This is, for example, shown by the grain orientation for submonolayer MoS₂ grown on graphene/Ir(111) where triangular islands with both orientations are observed [269]. When these islands merge, they cannot 'stitch' together perfectly but must form a twin grain boundary. These twin boundaries in MoS2 are metallic and will be discussed in more detail in section 5.1. In contrast to graphene, on Au(111) (or other fcc metals) the two twin-orientations are inequivalent with respect to the substrate. It was shown that under optimized growth conditions, one twin orientation can be favored over the other, as demonstrated by detailed XPD studies [270].

The choice of substrates also affects the properties of the MoS₂ monolayer. On graphene, the interaction between the TMD and the substrate is weak, although on the reverse system of graphene on MoS_2 , gap opening in graphene was observed where the π -band crosses MoS₂ bands with out of-plane orbital character [271]. Small MoS₂ islands on graphene/Ir(111) can be easily moved by an STM tip illustrating the weak interactions with the substrate [264]. Also, a band gap in MoS₂ of 2.55 eV is measured by STS indicating that the screening from the substrate does not reduce the band gap, compared to free standing MoS₂ monolayers. This is different on Au(111), where significant interactions between the substrate and MoS₂ are observed. These interactions may assist in the growth of single orientation MoS₂, but they modify the electronic structure of the monolayer [258]. STS shows a smaller band gap of ~1.74 eV and ARPES measurements suggest a hybridization of the S-3pz states with the gold substrates at the Γ -point, while the VBM at the Kpoint is not interacting with the substrate. Detailed STM/STS studies also showed a local variation within the moiré structure that forms on Au(111), suggesting variation of the local bonding between the MoS₂ and the Au substrate [261]. Interestingly, sometimes Au-vacancies can cluster underneath of the MoS2 monolayer to form small regions for which the MoS2-layer is suspended over such a vacancy nanopatch, thus forming small areas of quasi-freestanding MoS₂ [262]. Another report showed that 1T' MoS₂ may be possible to be synthesized on Au(111) by growing at high temperatures and low sulfur chemical potential followed by a rapid quenching [272]. These studies suggest that the relatively stronger substrate interactions allow to modify the obtained

MoSe₂ growth by vdW epitaxy was first explored by Koma et al., in 1991 [29]. Recent work includes growth on various vdW substrates, such as graphene/SiC [256,257], HOPG [273,274], MoS₂ [275], hex-BN [73], as well as on non-vdW substrates such as GaAs(111) [276], CaF₂ [277], and Au(111) [278]. On all these substrates, MoSe₂ grows in its 1H/2H structure. Only on Au(111) it was reported that in addition to the 1H structure, the growth could be tuned to obtain a 1T' phase [278]. The 1T' was formed preferentially if the substrate was pre-treated with Se that forms a chemisorbed selenide layer on Au. For the other substrates, the interaction between MoSe₂ and the substrates is weak, mainly preserving the

electronic structure. For MoSe₂ on MoS₂, interactions of the Se porbitals with those of the substrate have been suggested to raise the binding energy of the VB at the Γ point, although, the VBM at Γ was still at higher binding energy than the VBM at K, and thus maintaining a direct band gap for the monolayer [275]. Formation of quasi-1D MoSe₂ ribbons by MBE growth on HOPG substrates was also reported under finely tuned growth conditions [279,280].

MBE growth of defect free MoSe₂ (and H-MoTe₂, which is discussed next) may face some challenges for controlling its stoichiometry. Generally, competing phases and stoichiometry control in MBE growth can be challenging to achieve. For MoSe₂ (and H-MoTe₂) there is a different kind of non-stoichiometry to be considered that leads to crystal modifications with line defects. Most microscopy studies, either by STM or TEM, of MBE grown MoSe₂ on weakly interacting vdW substrates, report a high density of MTBs [273-283]. Such dense networks of MTBs cannot be explained by just coalescence of mirror grains during growth. Instead, it has been shown that these MTBs are preferred crystal modifications that may form under low Se chemical potential instead of high density of Se-vacancies [284]. These give rise to MTBs that are enriched in Mo and have a composition of MoSe; other possible configurations of MTBs are not observed in MBE grown MoSe₂ [285]. The properties of such MTBs and their formation processes are discussed in more detail in section 5.1 and 5.2.1, respectively.

MoTe₂ has attracted interest because the metallic 1T' phase is

very close in formation energy to the semiconducting 2H-phase, and thus both phases are accessible and may be switchable by thermal processes [83] or electrostatic doping [83]. Moreover, the 1T' phase undergoes a reversible phase transition into the T_d phase in the bulk at 250 K. The breaking of inversion symmetry in the bulk makes the Td phase a type II Wyle semi-metal that has been studied extensively, as we discussed in section 3.2.

Controlling the phase in thin film growth of MoTe₂ is of obvious importance. Some success in obtaining 1T' or 2H phase MoTe₂ has been reported in CVD growth [286–288]. The situation in MBE growth is less clear, though. In general, the H-phase seems to be favored over the 1T' phase in MBE growth of MoTe₂ [289]. The formation of the 1T' phase has been reported generally at higher growth temperatures or by a transformation of a 2H-phase by high temperature annealing in a Te-atmosphere [290,291]. However, Tang et al. reported the formation of monolayer 1T' on graphene/SiC for a low growth temperature of 280 °C with post-growth annealing at the same temperature [292]. In some cases, the coexistence of 1T' and H phases are reported for monolayers, which allowed the characterization of the lateral contacts between these phases [293].

STM characterization of mono-to few-layer H-phase grown by MBE shows that the material is prone to the formation of MTB networks [293,294]. This may also be the reason for observed transport properties that suggest localized charge carrier states [295]. Section 5 will describe the structure and properties of MoTe₂

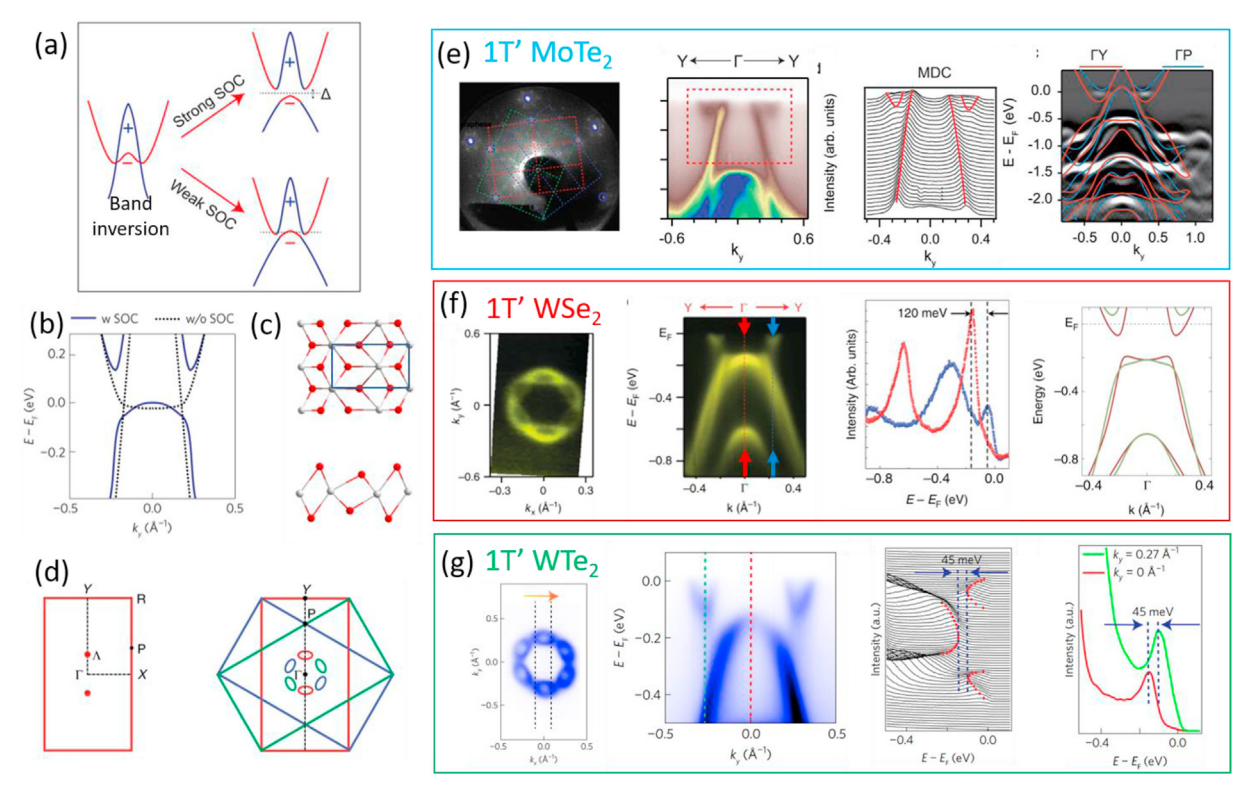


Fig. 18. Comparison of the potential 2D topological insulators: 1T'-MoTe₂, 1T'-WSe₂, and 1T'-WTe₂. (a) schematic illustration of the band inversion in the 1T' phase and how SOC opens a gap for strong interaction to form a topological insulator. (b) DFT simulations for 1T'-WTe₂ with (solid lines) and without (dotted lines) SOC, showing the opening of the gap. (c) unit cell of 1T' TMD and (d) the corresponding BZ. For samples grown by MBE on graphene, three equivalent domains form which are observed simultaneously in space averaging ARPES measurements, causing an overlap of bands along the Γ -Y direction of one domain with the bands along Γ -P (P') of the other two domains. The superpositioning of the Fermi-surface showing the electron pockets of three domains is also illustrated in (d) for strong n-doping and shown experimentally for 1T'-WSe₂ in (f) where n-doping has been achieved via alkali atom deposition. (e) Shows characterization of 1T'-MoTe₂. The LEED pattern shows the orientation of the three domains with respect to the graphene/SiC substrate. The ARPES measurement along Γ -Y (Γ -P) shows that SOC is weak and no gap is opened. (f) ARPES for 1T'-WSe₂, indicates a gap of ~120 meV, which can be seen from the energy distribution cut along the VBM and CBM. DFT simulations are in good agreement with the experiment. (g) AREPS characterization of 1T'-WTe₂ shows the Fermi-surface of the three equivalent domains indicated in (d). A gap opening of 45 meV is measured in ARPES. (a) and (e) are reproduced with permission from Ref. [292], licensed under a Creative Commons Attribution (CC BY) license. (b) and (g) are reprinted by permission from Springer Nature Customer Service Centre GmbH, ref. [98] Copyright © 2018, Springer Nature. (d) and (f) are reprinted with permission from Ref. [297], Copyright © 2018, Springer Nature.

surfaces modified by these MTBs.

The monolayer 1T'-MoTe₂ has been suggested to be a QSHI, but most of the fundamental studies of 2D topological insulators have been conducted on the isostructural 1T'-WTe₂ monolayer and this is discussed in more detail below. ARPES measurements on 1T'-MoTe₂ grown on graphene/SiC show the inverted bands and a SOC induced breaking of the band degeneracy at the crossing of the VB and CB is observed, but the SOC seams too weak to open a band gap [292]. Thus 1T' MoTe₂ does not exhibit a topological insulating gap like 1T'-WSe₂ [296,297] or 1T'-WTe₂ [98]. The ARPES results for these three TMD monolayers are summarized in Fig. 18. All three materials have been grown on graphene/SiC and more details about the tungsten dichalcogenides are given in the next section.

4.3.3. Tungsten dichalcogenides

WS₂ condenses in the 2H phase, and thus is a semiconductor. It exhibits an indirect to direct band gap transition as it is thinned to the monolayer, like the other group VI-B TMDs in the 2H structure. While the 2H phase is also energetically favored for WSe₂, it may be obtained as the metastable 1T' metallic phase [298]. WTe₂ on the other hand is most stable in the 1T' phase. The monolayer 1T' phases have topologically protected edge states that bridge the gap that is opening within the monolayer due to band inversion and SOC [98]. These edge states feature a quantum spin Hall state that exhibit quantized conductance in the absence of magnetic fields, as we discussed in section 3.2. Therefore, there has been significant interest in growing both the semiconducting 2H and the semimetallic 1T' phases by MBE, which is discussed in the following.

WS₂ was grown by MBE on sulfur terminated GaAs(111) by Koma et al. already in 1990 [27], and on HOPG substrates by using metal organic W(CO)₆ precursors and sulfur from decomposition of SnS₂ in UHV by Jaegermann et al., in 1994 [31]. Recently, it was synthesized as monolayers on Au(111) [237,299] or Ag (111) [300] by vapor deposition of W in an H₂S atmosphere and subsequent annealing. Like MoS₂ on Au, strong metal TMD interactions are observed, with sulfur 2p derived states around the Γ point hybridizing with the substrate atoms. The interaction with Ag appears to be even stronger and states at the Fermi-level are induced by the substrate making WS₂ on Ag metallic. These hybridizations can be removed by intercalating bismuth in between the WS2 and the Ag(111) substrate, and thus obtain quasi-free standing WS₂ [301]. While there are hybridization of states around Γ , the mainly inplane d-orbital derived states at the K-points are not affected by the substrate and a strong spin orbit splitting of the states is observed with a splitting of 417 meV measured in ARPES. The strong interaction with the Au substrate enables the growth of single crystal orientation of WS2 (i.e. avoid the formation of twin domains) [299]. This allowed to measure the spin structure and distinction of the K and K' points in the BZ by (spin resolved) ARPES, which determined the opposite spin-polarization in the K and K' points, as has been shown in Fig. 15 [236]. Moreover, time resolved ARPES showed that valley selective photoexcitation with circularly polarized light can result in more than 80% of spin polarized free charge carriers in these samples [302].

CVD grown WS₂ on graphene/SiC was investigated by nano-ARPES (with 500 nm spatial resolution) [303]. Different numbers of graphene layers on SiC exhibit variations of the substrates work function. Consequently, a WS₂ monolayer on such a structured substrate will experience laterally modified band offsets. In a Schottky contact-model, the larger work function of the bilayer graphene compared to single layer graphene on SiC causes a band offset in WS₂ supported on these two substrates of ~0.3 eV. This illustrates the possibility to design lateral built-in biases into 2D TMDs by supporting them on pre-patterned substrates and possibly even designing p-n junctions and other opto-electronic device

structures [304].

WSe₂ has been grown by MBE as mono-to few-layer samples on graphene/SiC [305,306] or HOPG [307]. ARPES identifies the spin orbit splitting at the K-point to 475 meV for the monolayer, and thus is the largest of the TMDs. Also, ARPES studies show the VBM lies at the K-point not just for the monolayer but also for the bilayer, suggesting that the transition from direct to indirect band gap may occur for the tri-layer thick samples [306]. The question if WSe₂ is a direct band gap material for the monolayer is, however, still controversial. Detailed STS studies suggest that the CBM may not be at the K-point which would make the monolayer still an indirect band gap material [305,307].

The effect of air exposure of MBE grown WSe₂ on HOPG was also probed by STM. It was found that even after exposure to air for weeks the terraces of WSe₂ were not significantly affected and STS measured the same band gap as for freshly grown samples. Step edges, on the other hand, reacted with the ambient air and oxidized [308]. STS measurements showed that these oxidized edges may be metallic due to the formation of the metallic sub-oxide WO_{2.7} [309].

Increasing the grain size in MBE grown WSe₂ could be achieved by lowering the W flux in a high Se background and maximizing the growth temperature. These studies were performed on HOPG, cplane (0001) sapphire, and MBE grown Bi₂Se₃ substrates, and the growth temperature was systematically varied between 350 °C and 550 °C [310]. The growth of WSe2 (and other TMDs) on sapphire substrates for multilayer films was optimized by the Iwasa group [55]. Their growth protocol consists of a high Se to W ratio of 200:1 keeping the Se source on throughout the deposition and annealing process. First, W is deposited for a short time at low temperature while the substrate temperature is ramped up to 900 °C, which results in a WSe₂ buffer layer. The growth temperature is then lowered ~450 °C and W-deposition is continued. RHEED oscillations were observed, indicating a layer-by-layer growth. After W deposition is interrupted, the sample is annealed to 900 °C again, all under Se flux.

As pointed out above, the synthesis of 1T' WSe $_2$ has also been achieved on graphene/SiC [296,297]. This is surprising since the 1T' phase is not known to exist in bulk WSe $_2$. It appears that 1T' phase prefers to form at low growth temperatures between $130\,^{\circ}\text{C}$ to $280\,^{\circ}\text{C}$, but a phase mixture with a 1H phase may be obtained. As shown in Fig. 18 (f), the 1T' phase exhibits SOC-induced gap opening of ~120 meV, in the inverted bands, and thus is a 2D topological insulator. Edge states have been observed in STS studies not only at the edges of the 1T' islands but also along 1T'-2H domain boundaries in the monolayer [297].

WTe₂ has been synthesized by MBE as a monolayer in its thermodynamically stable 1T' phase and characterized by STM and ARPES. As shown in Fig. 18 (g), 1T'-WTe₂ is a QSHI and the metallic edge states have been confirmed by STS [98,311,312].

Multilayer 1T'-WTe₂ growth was achieved by beam-interrupted MBE on a variety of vdW substrates [313]. Alloying of the selenide with the telluride was also investigated by MBE growth to form $WSe_{(2-x)}Te_x$ alloys [314]. It was found that for up to 14% Te concentration, the 2H phase was stable, and for Te concentration above 79%, the 1T' phase is preferred. In between, a miscibility gap was found for the growth temperature of 250 °C.

4.4. Group VII-B TMDs (Mn, Re)

The group VII-B layered TMDs are mostly limited to ReS₂ and ReSe₂, which are semiconducting and exhibit a strongly distorted 1T structure. ReTe₂ does not form a layered vdW structure. Technetium (Tc) dichalcogenides are layered TMDs [315], but the rarity and instability of Tc makes the Tc-dichalcogenides without technological importance and have not been studied. For Mn-

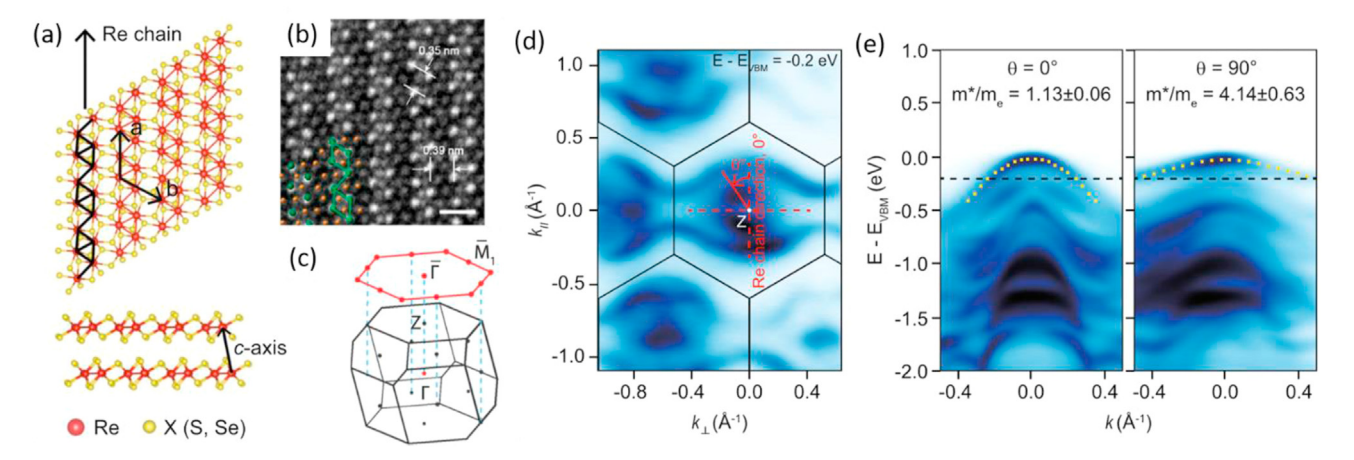


Fig. 19. Anisotropic properties of ReSe₂. (a) Ball-and-stick model of ReSe₂ (ReS₂) with the diamond rows indicated. (b) ADF-STEM images of exfoliated monolayer ReSe₂. (c) bulk BZ and surface projected BZ. (d) Fermi-surface close to VBM at the Z-point. (e) VB along the Re-chain and perpendicular to the Re-chain direction, showing the strong anisotropy of the effective hole-masses. (a) and (b) is reproduced with permission from Ref. [319]; further permissions related to this material excerpted should be directed to the ACS. (a), (d) and (e) are reproduced with permission from Ref. [324], Copyright © 2019, Springer Nature.

dichalcogenides, the non-layered pyrite structure is preferred. Nevertheless, DFT simulations showed that 1T TMD may be a metastable monolayer structure [316]. Moreover, it is predicted to be ferromagnetic with a large magnetic moment and a predicted Curie temperature of ~225 K and 250 K for MnS₂ and MnSe₂, respectively [317]. Experimentally, MBE growth of manganese selenide on GaSe substrates has been suggested to form a monolayer MnSe₂ at the interface before continuing to grow as rocksalt-MnSe. Room temperature ferromagnetic properties were measured for this structure. Since neither the substrate nor rocksalt-MnSe is ferromagnetic, the magnetism was associated with an interface MnSe₂ layer [318]. Clearly more work on this system is desirable to clarify the origin of this magnetism. In the following, we focus on the semiconducting Re-dichalcogenides.

ReS₂ and **ReSe₂** exhibit a strongly distorted 1T structure, as shown in Fig. 19 (a). Fig. 19 (b) shows a high-resolution scanning transmission electron microscopy (STEM) image of an exfoliated monolayer [319]. In-plane bonding of rhenium atoms causes Re to cluster in a diamond-shape with 4 Re-atoms per cluster. These diamond shaped clusters form rows. The atoms within a diamond are coplanar, but each 'diamond' is canted by 1.43° from the basal plane. The diamond-shaped Re-clusters also give rise to a slight difference in the chalcogen heights above the basal plane depending on their position inside or outside of the 'diamond'.

The structural anisotropic of ReS₂ and ReSe₂ in 'diamond'-rows give the material's strong anisotropic conductance and optical properties in the bulk or in few-layer materials [320–322]. Recent ARPES studies on bulk samples demonstrated the anisotropic electronic structure of ReS₂ and ReSe₂ [323–327]. It was found that the hole effective mass is four times heavier across the row structure than along. Also, the dispersion along k_z was found to be larger for ReS₂ (120 meV) than for ReSe₂ (20 meV), suggesting weaker interlayer interactions for ReSe₂. The location of the VBM for ReS₂ is not at the BZ center but at the Z-point on the BZ face for 3D crystals. In the case of ReSe₂ the exact location of the VBM on the BZ face is controversial, while some ARPES work reports the VBM to be at the Z-point [324], others report that it is slightly off at a non-low symmetry direction [325,326].

ReS₂ and ReSe₂ have attracted interest for optoelectronic applications. Strong optical absorption is making them promising materials for light harvesting applications. Moreover, favorable energy level alignments make them possible materials for photoand electro-catalysis [328]. Compared to the group VI-B

semiconducting dichalcogenides, the rhenium based dichalcogenides exhibit much weaker layer dependence [329], which could be an advantage for more uniform materials, and thus device structures. Re-dichalcogenides have a close to direct band gap in the bulk as well as for the monolayer that gives rise to strong photoluminescence. Although layer dependent changes in Redichalcogenides are less pronounced, still a blue shift of the optical band gap from 1.47 eV in the bulk to 1.61 eV in the monolayer of ReS₂ was reported [330]. Surprisingly, this optical band gap is larger than the band gap reported for bulk ReS₂ by STS (1.35 eV) [331] or ARPES (1.2 eV) [327]. The latter has been achieved by electron doping of the CB by Rb-deposition on a bulk crystal to move the Fermi-level into the CB. Nano-ARPES studies of exfoliated monoand multi-layer films, combined with DFT simulations, however, suggest that there is a weak layer dependent variation [332]. In these studies, a transition from an indirect band gap in the bulk, with the CBM slightly away from Γ , to a direct band gap in monoand bi-layer ReS₂ has been observed. Also, the VBM becomes flat in the monolayer suggesting heavier holes in the monolayer than in the bulk.

Mono- and few layer ReS₂ and ReSe₂ have been synthesized by CVD, but to the best of our knowledge, there have not been any MBE or related in-vacuum growth attempts of rhenium dichalcogenides. Surface studies have, however, been performed on cleaved single crystals. Early STM studies date back to 1990s which showed atomic resolution and most of the discussion in these early days of STM focused on what atoms are imaged in STM [333,334]. Recent STM/STS studies focused on the position of sulfur vacancies and their electronic structure in ReS₂ [331]. In these studies, it was found that sulfur vacancies appear to be preferred in the subsurface chalcogen layer.

4.5. Group VIII-B (9) (CoTe2 and IrTe2)

The group 9 TM are not well known for the formation of layered TMDs. However, the tellurides of cobalt and iridium have been reported to form structures related to the 1T phase, although interlayer Te—Te contacts are strong.

CoTe₂ is found as the orthorhombic marcasite-like mineral, as well as in the 1T-like layered structure. However, a strong interlayer Te—Te interaction causes a relatively small layer separation and a small c/a ratio of 1.38–1.41 [335]. Strong interlayer interactions imply larger cleavage energies, and thus CoTe₂ may not be easily

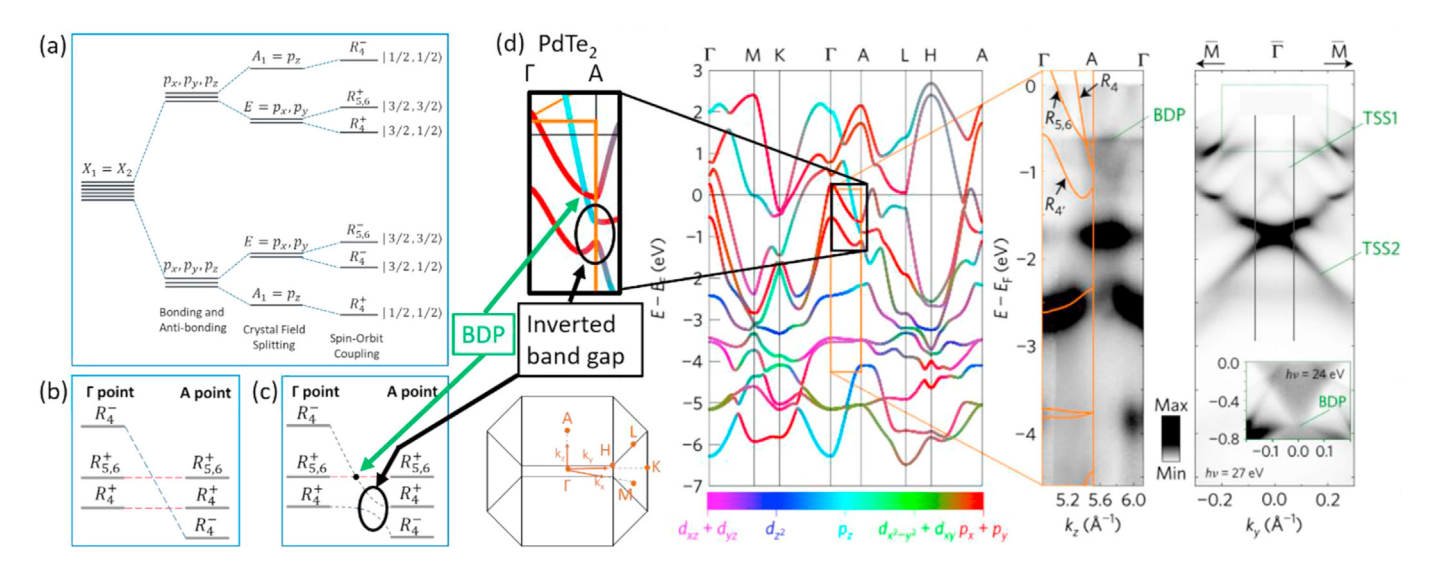


Fig. 20. Emergence of topologically protected states in 1T-TMDs of group VIII-B (10) TM. (a) splitting of p-orbitals due to bonding (BA), crystal field symmetry (CFS), and SOC. (b) and (c) simplified k_z dispersion with negligible dispersion for $p_x p_y$ in-plane orbitals and strong dispersion for bands with p_z -orbital character. In (c) anti crossing gap is indicated in case the bands share the same symmetry and angular momentum. (d) shows band structure calculations (the orbital character of the bands is indicated by the color code) and experimental ARPES measurements for PdTe₂. A bulk Dirac point (BDP) and an inverted band gap are observed consistent with the model in (c). Topological surface states in the inverted band gap are observed in the surface BZ indicated as TSS1 and TSS2 in the ARPES data. Adapted by permission from Springer Nature Customer Service Centre GmbH, ref. [355], Copyright © 2017. (For interpretation of the references to color in this figure legend, the reader is referred to the Web version of this article.)

exfoliated. The structure has been synthesized by CVD growth as few layer thick flakes [336] but to our knowledge has not been synthesized by vacuum techniques or as monolayer materials. Strong interlayer interactions also suggest layer dependence in their properties. The CVD grown multilayer samples exhibited metallic behavior.

IrTe₂ is the only layered dichalcogenide for iridium. IrS₂ and IrSe₂, on the other hand, prefer to condense in the 3D-pyrite structure. However, it has been shown that alloying IrS₂ or IrSe₂ with NbS₂, NbSe₂ [337], TiSe₂ [338] or V(Ta)Se₂ [339], the 1T structure may be obtained, suggesting that these other two Irdichalcogenides are close to form layered compounds.

IrTe2 is a complex material with multiple charge order and superconducting transitions and the bulk surfaces have been studied by ARPES [340-344] and STM/STS [345-349]. It has been suggested that these ordering transitions are strongly affected by interlayer interactions, or Te-Te polymerization at the interlayer contacts, as well as a 3D ordering [350–352]. Thus, one may expect variations of the material properties if reduced to a single layer. Exfoliation to thin flakes already has shown dramatic changes in superconducting transitions [353]. However, to date, there are no reports to our knowledge on exfoliated or monolayer IrTe2 on weakly interacting substrates. A recent report shows the synthesis of IrTe2 monolayers by tellurization of an Ir(111) crystal [354]. DFT simulations, however, suggest strong interaction between IrTe2 and the Ir-surface, which may affect the properties of the monolayer. A synthesis and characterization of quasi free-standing monolayer materials on weakly interacting substrates are required to better understand the role of interlayer interactions for the properties of IrTe2, and thus the synthesis of IrTe2 by e.g. MBE may be a fruitful future endeavor.

4.6. Group VIII-B (10) TMDs (Ni, Pd, Pt)

The group VIII-B (10) dichalcogenides are mostly present as the 1T structure, with the exception of PdS₂ and PdSe₂ that form a unique structure described below. Many of the group 10 1T-TMDs exhibit bulk Dirac cones, both of type I and type II (see section 3.2),

as well as topological band gaps that give rise to topologically protected surface states. Bahramy et al. proposed a unifying scheme for the observed topological states in these TMDs based on the band crossing of the chalcogen derived p-orbitals [355]. Here, we follow Bahramy et al.'s argumentation. The splitting of the p-orbitals in 1T-TMDs due to bonding (BA), crystal field (CF), and SOC is schematically shown in Fig. 20 (a). Bonding and antibonding cause triple degenerate energy levels that split by the trigonal crystal field into double degenerate E level (px, py derived) and a single A1 level (pz derived). SOC transforms the A1 level into a double representation $R_{\overline{d}}^{\pm}(|J=1/2; |m_I|=1/2>)$ and the E manifold splits further into $R_{56}^{\pm}(|I=3/2;|m_I|=3/2>)$ and $R_{4}^{\pm}(|I=3/2;|m_I|=1/2>)$, where the + and – indicates the parity of each level. The bands derived from inplane p_xp_y orbitals have very little interlayer interactions and, therefore, weak dispersion along the k_z direction, i.e. the Γ -A direction in the 3D BZ. This is indicated in Fig. 20 (b) and (c) as flat bands. In contrast, the p_z derived bands disperse strongly in the Γ -A direction, and thus the A1 derived bands may cross the E-bands. This suggests a set of k_z dependent band inversions that are solely based on the p-orbital derived states. Anti-crossing gaps can open, as shown in Fig. 20 (c), if both bands share the same symmetry and angular momentum. Their opposite parity leads to an inverted band gap with topological order. These bulk gaps can lead to topological surface states as has been e.g. observed for PdTe₂ [355,356], shown in Fig. 20 (d).

Strong interlayer interactions that gives rise to k_z dispersion for p_z derived orbitals are required for the existence of these topological states. Interlayer interactions also imply layer dependent properties as these materials are reduced to the monolayer. Indeed, strong variations are observed in some of these materials in the monolayer compared to the bulk. The most notable are the metal to semiconductor transitions in the Pt-family of TMDs, as the number of layers is reduced to the monolayer limit [357,358]. Some of the fundamental properties and applications in gas sensing, electronic devices, and electro- or photo-catalysis of the Pt and Pd families of chalcogenides have been recently reviewed [359–361]. Here we discuss efforts in synthesizing and characterizing different group 10 TMDs as monolayers and thin films by vacuum methods.

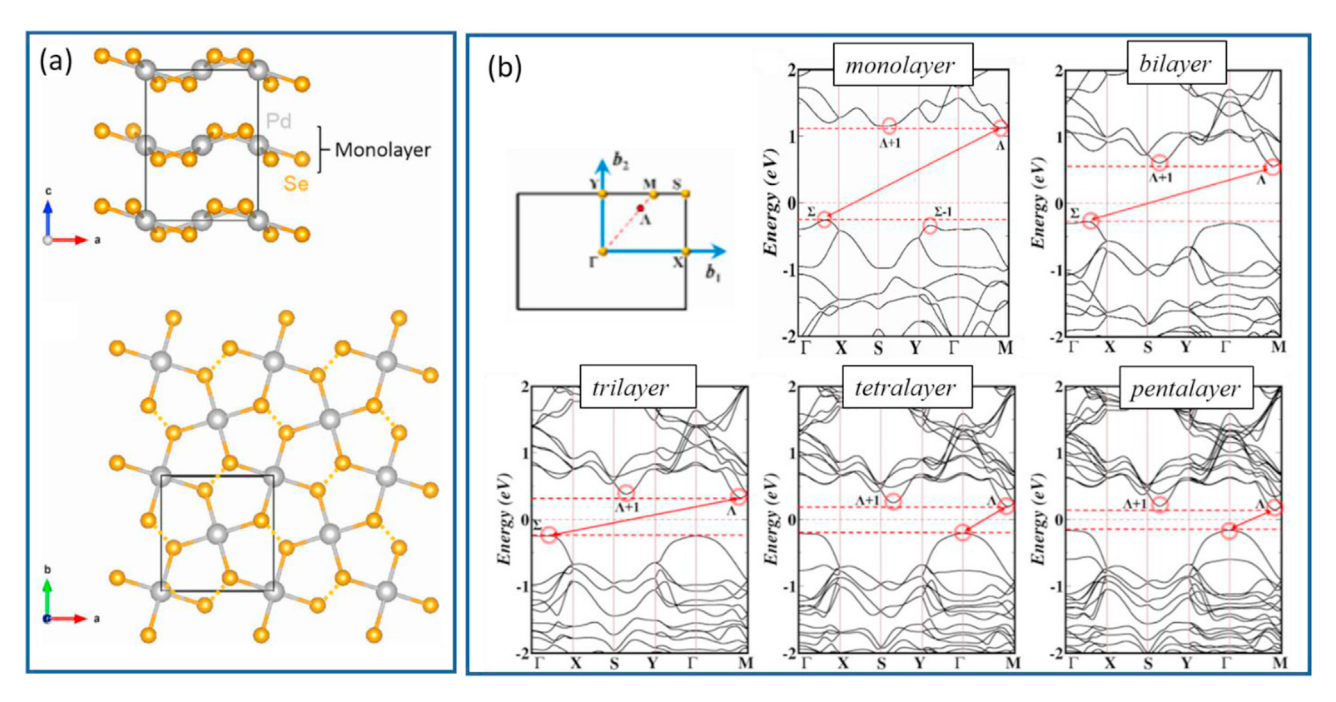


Fig. 21. Properties of PdSe₂. (a) shows the side and top-view of PdSe₂ crystal structure in a ball-and-stick model. Every Pd-atom is coordinated to 4 Se atoms that form a planar-square configuration. The Se-dimers are indicated by dashed lines. The electronic structure of PdSe₂ is strongly dependent on the number of layers. (b) shows DFT calculations of the band structure as a function of layers. A large band gap is opening for the monolayer and the VBM and CBM are off the low symmetry points in the BZ. (a) is reprinted from Ref. [374], with the permission of AIP Publishing (b) is reproduced with permission from Ref. [378]].; further permissions related to this material excerpted should be directed to the ACS.

4.6.1. Nickel dichalcogenides

NiSe $_2$ and NiTe $_2$ are known to form layered vdW materials with the 1T structures. Nickel disulfide only exists in non-layered structures, such as the pyrite crystal structure. NiSe $_2$ has been synthesized as a monolayer material by selenization of metallic nickel foil [362] or Ni(111) single crystal [363]. On Ni(111), NiSe $_2$ was obtained by depositing elemental Se onto the substrate and by subsequent annealing in vacuum at 320 °C for 30 min. A $\sqrt{3} \times \sqrt{3}$ supercell is observed in LEED and STM, which is considered to be a consequence of NiSe $_2$ forming a coincidence lattice with a $\sqrt{7} \times \sqrt{7}$ supercell of the Ni(111) substrate. Formation of such a coincidence lattice suggests strong interactions between the NiSe $_2$ layer and the Ni(111) substrate.

Bulk NiTe₂ has been shown to have topologically protected type II Dirac cones and topologically protected surface states. These topological states have been identified in ARPES studies of single crystal surfaces [364,365]. Compared to other group 10 TMDs (PdTe₂, PtSe₂, and PtTe₂) that have similar topologically protected states, NiTe₂ is special because the Dirac nodes are close to the Fermi-level, which may enable the observation of these topological properties also in transport measurements [366]. However, so far, no signature of topological states could be found in Hall effect measurements [367].

To the best of our knowledge, there have not been any vacuum synthesis or studies of monolayer NiTe₂. The successful growth of multilayer films by CVD has been reported, though [368,369].

4.6.2. Palladium dichalcogenides

 PdS_2 and $PdSe_2$ exhibit an unusual puckered pentagonal crystal structure, unlike any of the other TMDs. In these structures, the layers are configured of Pd-atoms coordinated to four Se or S atoms, with these five atoms lying in one plane. This is the consequence of the d [8] configuration of Pd^{2+} complexes that prefer a planar-square configuration. These 5-atoms building blocks are twisted

and tilted in the layer, with every chalcogen-atom shared between 2 Pd atoms and bound to one other Se-atom, forming Se-dimers within the layers. The unit cell is slightly rectangular for the 2D structure. Fig. 21 (a) shows the unit cell of the monolayer. Stacking these layers on top of each other forms the bulk structure. The unit cell in the bulk consists of two layers, i.e. the third layer repeats the first layer and forms a centrosymmetric structure. Consequently, only two-layer thick films, are non-centrosymmetric. While the puckered pentagonal structure for PdS₂ and PdSe₂ is the energetically favored structure, the 1T structures are metastable and may form under high pressure. A transition from the Pd²⁺ charge state of the puckered pentagonal structure to a Pd⁴⁺ state at high pressures may indicate such a transition to the 1T-structure [370]. For PdTe₂, only the 1T structure is observed.

PdS₂, to the best of our knowledge, has not been studied as ultrathin films and have not been grown by MBE. Bulk PdS_2 is an indirect band semiconductor with an experimental band of 0.7 eV determined from resistivity measurements [371]. This is also in good agreement with DFT simulations, that suggest an increase of the band gap to 1.0 eV [359] to 1.6 eV [372] for the monolayer. Computational studies also suggest that application of biaxial strain can close the band gap and make it a semi-metal under larger than 8% strain [373]. This suggests that both bulk and monolayers are semiconducting. In contrast, the 1T polymorph, if it can be stabilized, is expected to undergo a semi-metal (for the bulk) to semiconductor transition (for the monolayer) [359].

PdSe₂ has been more extensively studied experimentally compared to PdS₂. There has been initial controversy regarding the band gap of bulk PdSe₂. Some initial experimental and DFT studies suggested that the bulk may be (semi)metallic or only have a very small gap [374,375]. This may have been related to the general underestimation of the band gap and inappropriate description of interlayer interactions using PBE functionals in the DFT simulations, and defect induced gap states in the experiments. However, there is

better consensus now that bulk PdSe2 (in its puckered pentagonal structure) is a semiconductor and the gap increase significantly with a reduction of layers towards the monolayer limit [359]. Already in 1965, Hulliger [371] reported that bulk PdSe₂ has a gap of ~0.4 eV. Recently Zhang et al. [376] estimated the gap for bulk PdSe₂ to 0.5 eV and showed that the gap increases to 1.37 eV in the monolayer. The value for the monolayer quasi-particle band gap also seems reasonable when compared to measurements of the optical band gap for mono- and few layer flakes of 1.0-1.2 eV [375]. Recent DFT simulations using hybrid functionals agree with the significant increase of the band gap from bulk to monolayer but suggest that the true band gaps are even larger, with predictions for the variation from the bulk-gap of 0.96 eV-~1.9 eV for the bilayer to ~2.2 eV for the monolayer [359,377]. The significantly larger band gaps predicted by DFT compared to the experiments in these calculations are surprising. Screening different DFT functionals to match experimental lattice constants Sun et al. [378] obtained band structure calculations that appear in better agreement with experiments. They report band gaps of 1.38 eV for the monolayer, 0.83 eV for bilayer and 0.31 eV for five layers. These results are shown in Fig. 21 (b). These calculations also show that the VBM and CBM are slightly off from low symmetry points in the BZ, while the VBM is located at the Γ point for multilayers.

Band gap values measured experimentally by optical absorption show that the layer dependent change of the band gap spreads over 16 to 20 layers. This gives this material a high tunability by controlling the layer numbers.

Most work on few layer materials has been performed on exfoliated flakes. Recently, some CVD growth of few layer PdSe₂ have also been reported, demonstrating that this material can be synthesized by thin film growth methods [379]. PdSe₂ was also grown by MBE on graphene/SiC [380]. Only bilayer PdSe₂ could be obtained, possibly as a consequence of the strong interlayer interaction. The band gap of these bilayers was measured with STS to

 1.15 ± 0.07 eV, which matches the optical absorption data, and thus challenging the notion of strong exciton binding energy in PdSe₂. Also, interface band alignment effects were observed, with the Fermi-level shifting by 0.2 eV depending on the support of the PdSe₂ bilayer on mono- or bilayer graphene. This may be similar to the effects reported above in Nano-ARPES measurements of WS₂ supported in graphene/SiC, reported above.

Passivation of Se-vacancies, as well as modifications are important for practical applications of the material in optoelectronic devices or as a catalyst in chemical transformation reactions. PdSe₂ is touted as an air-stable material, and thus does not easily oxidize [375]. Ozone treatment at 60 °C has, however, shown to induce oxygen in the surface by replacing Se atoms [381]. Such modified materials improved device performances and increased electrochemical hydrogen evolution reaction.

PdTe₂ condenses in the 1T-structure and exhibits type II Dirac fermions and topological surface states [355-382]. These topological properties paired with its superconducting behavior below 1.7 K, makes it an exciting material for fundamental condensed matter explorations. MBE growth of PdTe2 has been studied on Bi₂Te₃ [383] and graphene/SiC [384]. In the first case, a superconducting transition of 1.4 K was observed consistent with the formation of PdTe₂. The growth on graphene/SiC was carried out at a low growth temperature of 510 K, but no uniform monolayer growth was obtained. Careful characterization by STM, XPS, LEED, Raman, and ARPES demonstrated that PdTe2 was indeed obtained. ARPES measurements on 6-layer thick films indicated the presence of the type II Dirac cones. In another study, PdTe₂ was grown by MBE on a SrTiO₃(001) substrate from the monolayer to multi-layers and was characterized by STM/STS and transport measurements [385]. The monolayer exhibited a semiconducting gap while multilayers were metallic and all exhibited superconducting transitions, with Tc increasing with layer thickness up to 1.8 K for bulk like samples.

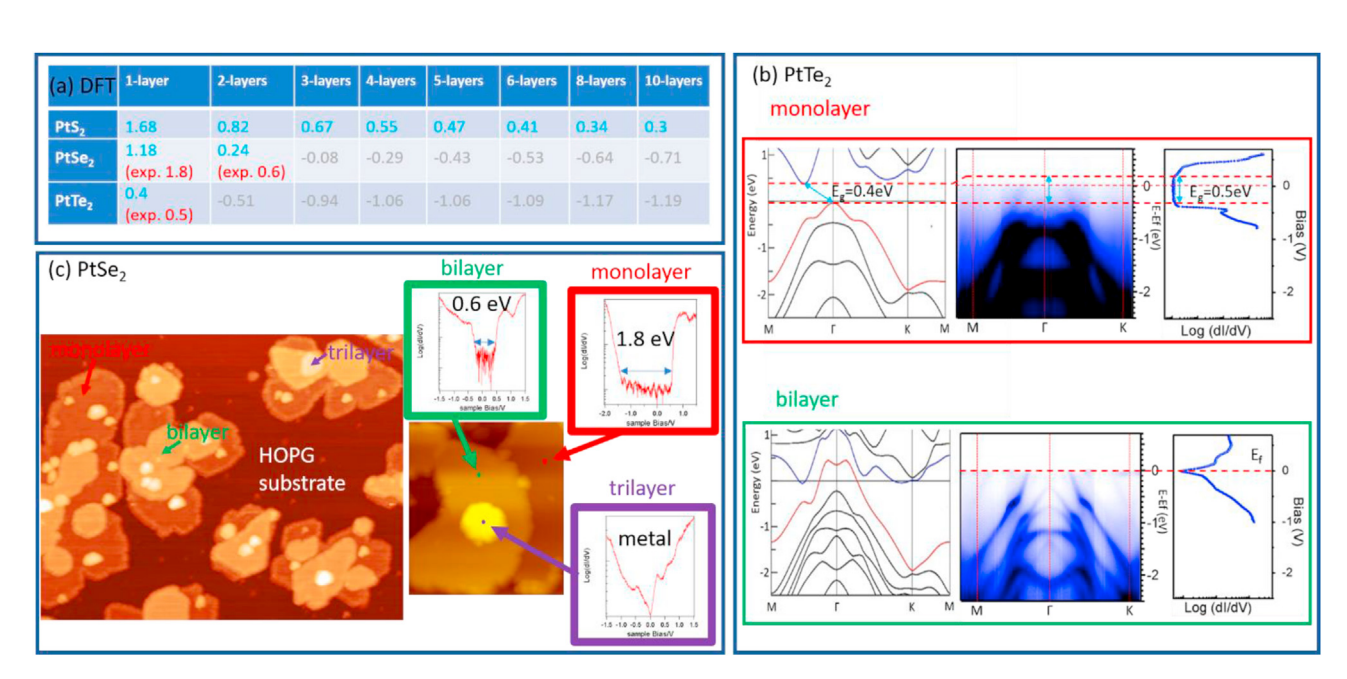


Fig. 22. Layer dependent band gap determination of Pt-dichalcogenides. (a) shows DFT calculated band gaps as a function of layers. Experimental values are shown in red (see (b) and (c)). Gray values are negative values, which indicate band overlaps in semimetals. (b) DFT band structure calculations and experimental ARPES and STS data for mono- and bilayer PtTe₂. Note that the monolayer samples contained 10–20% of bilayer regions (determined by STM), which gives rise to the bands close to the Fermi-level in the 'monolayer' ARPES data. (c) STM and STS characterization of PtSe₂ islands grown on HOPG. Islands with mono-to tri-layer height enables local band gap measurements by STS and the measured band gaps are indicated. DFT band structures and band gap values are adapted from Ref. [357], and STM/STS and ARPES has been adapted from Ref. [395]. (For interpretation of the references to color in this figure legend, the reader is referred to the Web version of this article.)

4.6.3. Platinum dichalcogenides

The three Pt dichalcogenides preferentially condense in the 1T structure. Topological type II Dirac fermions have been first reported by ARPES for bulk 1T-PtTe2 [386] and are also observed in 1T-PtSe₂ [387–389], but not in PtS₂. For non-bulk materials, the Ptdichalcogenides have attracted attention for their strong interlayer interaction induced layer dependent properties. In particular, the tunability of their band gaps as a function of layers has been reported [358-392]. In the bulk, 1T-PtSe₂ and 1T-PtTe₂ are semimetals with the chalcogen p-derived electron pockets at the Γ point and hole pockets at the K-point. A more detailed Fermisurface sampling also showed a hole pocket at non-symmetry points in the 3D BZ within the Γ -M-L-A plane for 1T-PtSe₂ [393]. PtS₂, on the other hand, already possesses a band gap in the bulk. Decreased interlayer interactions in few and monolayer materials increase the separation between VB and CB. Thinning of the material causes opening or widening of the gap. DFT-data of the band gaps in Pt-dichalcogenides [357] with the 1T structure are shown in the table in Fig. 22 (a). From this table, it is apparent that 1T-PtTe₂ remains a semi-metal down to the bilayer and semiconducting properties are only predicted for the monolayer. In MBE growth it appears challenging to obtain single layer 1T-PtTe2 and even for low coverage bi-layer islands seem to form preferentially. This may explain why most ARPES data are only reported for PtTe2-bilayers and thicker [394]. We have found, however, that by reducing the growth temperatures, monolayers can be obtained and Fig. 22 (b) shows PtTe2 ARPES for mono- and bilayers on graphene/SiC and corresponding STS for PtTe2-islands grown on HOPG [395]. Similar ARPES studies have also been reported by others for mono-to fewlayer films on graphene/SiC [396]. These measurements confirm the semiconducting gap for monolayers and a band gap of ~0.5 eV is measured by STS, i.e. slightly larger than the DFT prediction, while bilayers are clearly metallic. 1T-PtSe2 has been grown on HOPG with various island heights on the same sample [395]. This enabled determination of the band gap as a function of number of lavers by STS, as shown in Fig. 22 (c). Band gaps of 1.8 eV and 0.6 eV were found for mono- and bi-layer islands, respectively. Again, these experimental values indicate larger gaps than the DFT values. Trilayer islands have been found to be metallic. Layer dependent modifications of the band structure have also been measured by ARPES for PtSe2 [397]. Moreover, spin resolved ARPES revealed a helical spin texture for monolayers to bulk samples [398]. Preparation of monolayer PtSe₂ was also achieved by selenization of a Pt(111) single crystal surface, by room temperature deposition of elemental Se onto the platinum surface followed by annealing to 270 °C [399]. In contrast to 1T-PtSe₂ and 1T-PtTe₂, that have been synthesized in the mono-to few-layer samples by vacuum processes, 1T-PtS₂ has not yet been grown in vacuum. However, it has been grown by CVD as few layer samples [400]. CVD growth of PtSe₂ on alumina substrates has also reported to result in 2H–PtSe₂ flakes [401]. The formation of 2H–PtSe₂ is surprising, considering the much higher formation energy of the 2H phase compared to the 1T phase [359]. The phase stability and tuning for these materials should be studied in more detail.

Defects in PtSe₂ were characterized by atomic scale STM for PtSe₂ grown on mica by CVT [402]. Combined STM imaging and DFT

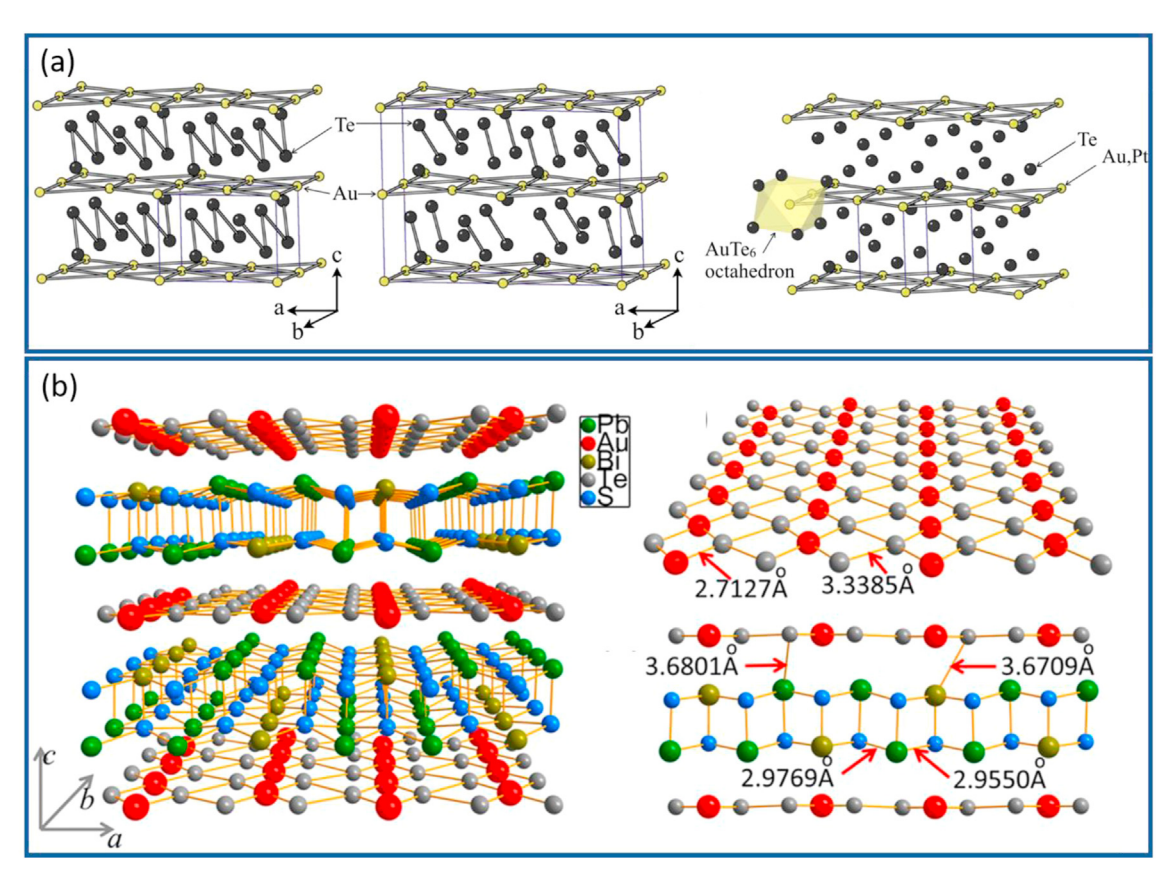


Fig. 23. Crystal structure of AuTe₂. (a) crystal structure of the mineral calaverite. This structure is closely related to the 1T-structure but strong Te—Te interlayer dimerization occurs. For a non-modulated structure, a zig-zag bonding is expected (shown on the left), but an incommensurate structure favors the dimer formation for interlayer tellurium (middle). If doped with Pt, the 1T-like structure is obtained as shown on the right. (b) shows the misfit compound, consisting of Pb₂BiS₃ and AuTe₂ vdW layers. The AuTe₂ layers form planar structures, with Au-chains. (a) is reproduced with permission from Ref. [413], Copyright © 2013 The Physical Society of Japan. (b) is reprinted with permission from Ref. [414], Copyright © 2015 American Chemical Society.

simulations identified Pt- and Se-vacancies as well as Pt and Se antisites (i.e. Pt in Se lattice sites or vice versa). Under the Se-rich growth conditions in CVT, the Se-antisites were the most abundant defects in the studied sample. Recently, exciting magnetic properties were revealed in multilayer exfoliated PtSe₂ samples by magneto transport measurements [403]. These studies suggested that surface defects may magnetically couple across the PtSe₂ layers, and thus induce magnetic properties in this material. Thus, controlling defects in these materials may allow to induce new functionalities in these materials. The Pt dichalcogenides have also attracted interest for their potential electrocatalytic properties [404], with PtSe₂ and PtTe₂ reported to exhibit high activity for hydrogen evolution reaction or oxygen reduction reaction that rivals that of elemental Pt [404-408]. Layer-dependence, defects, and step edges are likely contributing to these chemical activities and MBE grown samples may be an exciting tool for investigating these properties.

4.7. Group I-B: AuTe₂

The group I–B chalcogenides are not known for layered structures. Only $AuTe_2$ is closely related to the 1T-structure. $AuTe_2$ is a known naturally occurring mineral, called calaverite. However, Teatoms in the layers form interlayer dimers, which causes a strong distortion monoclinic structure and an incommensurate layer stacking, illustrated in Fig. 23 (a) [409–411]. Multivalent Au was suggested for $AuTe_2$, but XPS studies have shown that Au is only present in a single Au^{1+} valency [412]. Interestingly, it was found that by Pt incorporation, i.e. formation of $Au_{1-x}Pt_xTe_2$, a 1T structure with broken interlayer Te-dimers is formed for Pt concentration of larger than x=0.2 [413]. This breaking of the interlayer dimers induced superconductivity with a Tc of 4.0 K.

Another structure of a vdW layer of AuTe₂ was found in the misfit compound [Pb₂BiS₃][AuTe₂], which consists of alternating vdW layers of Pb₂BiS₃ and AuTe₂ [414]. In this case, AuTe₂ is a planar structure consisting of AuTe₂ chains, illustrated in Fig. 23 (b).

To the best of our knowledge there have not been any attempts of growing AuTe₂ by MBE or other thin film growth methods. Reducing the layer thickness to the monolayer regime is a natural approach for breaking the interlayer Te-dimerization for the 1T-related structure, and thus may enable to induce superconductivity in the monolayer. On the other hand, the 1T structure may compete with the formation of planar AuTe₂, which is expected to be a strongly anisotropic material, with close 1D atomic chain structures. Thus, the successful synthesis of this material in the monolayer may also reveal new properties.

5. Modifications and nanostructures in TMDs

In the previous section we focused on the properties of extended TMDs in mono- or few-layer form. Naturally, defects and lattice-discontinuities are present in grown films and these can exhibit exciting properties or even induce new functionalities to the material. While defects can form inadvertently, other properties may be controlled and can be tuned on purpose. TMD monolayers and thin films are particularly promising materials to be modified, because the lack of a bulk implies that methods that usually would only affect the surface or an interface of a material, does alter the entire monolayer. In this section, we explore how mono-to few-layer materials can be modified by changing their structure and/or composition, interfacing them with other materials, or by exciting them with an external stimulus. This may lead to locally modified nanostructures or novel materials.

Growth of monolayers will result in lattice-discontinuities, such as grain edges and grain boundaries. In 2D-materials, such an

interruption of the 2D lattice are one-dimensional structures, and thus may exhibit properties characteristic to such reduced dimensions. Further control of the growth by using templated substrates or self-organized growth may lead to nanostructured materials with large aspect ratios, unique grain structures, or novel materials compositions. Properties of 1D-defects and on-surface synthesis of wires and ribbons are discussed in section 5.1.

All thin films are grown on substrates and the substrate interactions may influence the materials properties, as we have discussed above. While the concept of vdW epitaxy relies on negligible bonding between the substrate and the grown vdW materials, long range coincidence lattices or moiré structures will form. This implies variations of the relative positions of the atoms in the monolayer with respect to the substrate, and this may lead to local variations of the electronic properties within the moiré-unit cell. In materials systems where interlayer interactions give rise to strong variations between monolayers and bulk such interlayer interactions should also be expected in TMD heterostructures but with additional modulations due to the moiré superstructures. This is the case for group VI-B semiconductors and moiré superstructures may be achieved by the formation of monolayer heterostructures, or by twisting of layers of the same material relative to each other using exfoliation and re-stacking. Recently, moiré structures in group VI-B semiconducting TMDs have been studied for excitonic lattices enabled by the modifications of the local electronic structure. In addition, other potential applications as templated surfaces may be future applications of such moiré structures in surface science. Properties of TMD heterostructures and their moiré-periodicity are discussed in section 5.2.

Compositional control and modifications of TMDs can give rise to new phases. Some TMDs easily lose chalcogens upon heating and this may cause transformation into other phases. Other methods like ion sputtering can also assist in compositional variations. Different vacuum processes may lead to materials with varying composition or defect structures that accommodate stoichiometric variations. These stoichiometric variations may occur during growth or can be accessed by post-growth modifications of samples with a few TMD layers. Understanding and controlling these modification-mechanisms can result in the design of new materials. Some aspects of modifying TMDs to form compositional variants are discussed in section 5.3.

Some TMDs exist in different structural phases and controlling them is important, especially if they can be switched. We have already seen in section 4 that some TMDs can be grown directly in either the 1T or H phase. In section 5.4, the phase control of some TMDs is investigated further. For some TMDs that exhibit only small differences in the formation energies between different phases, it has been demonstrated that adsorption, intercalation, and stimuli by STM tips, among others, can induce phase switching. Finally, in section 5.5, we will review general studies of molecular and atomic adsorption on TMDs. Especially for monolayers, such adsorption may change the properties of the TMD through bonding or charge transfer.

5.1. One dimensional electronic states: island edges, grain boundaries, and 1D ribbons

5.1.1. Edge states

Edges of monolayer TMDs may exhibit unique properties. Above, we discussed topologically protected edge states of 1T′ WTe₂ and WSe₂ monolayers that give rise to the QSHI. Topologically trivial edge states have been known for group VIB semiconducting TMDs for some time. For MoS₂, islands grown by sulfidation of vacuum deposited Mo on Au(111) have been studied [415]. These studies revealed that step edges of MoS₂ islands are

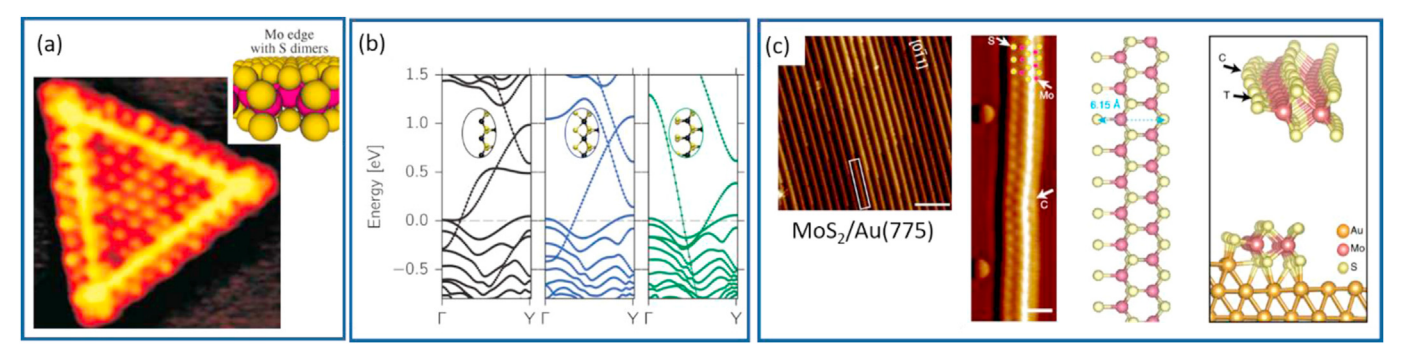


Fig. 24. Zig-zag edge termination of MoS₂. (a) triangular MoS₂ nanoisland grown on Au(111) terminated by sulfur-decorated Mo-zig-zag edges. The bright contrast of the edges in STM indicates their metallic nature. (b) DFT simulations of the electronic structure of Mo-zig-zag edges with three terminations; (i) bare (black), (ii) one sulfur atom (blue), (iii) two sulfur atoms (green) per Mo edge atom. (c) MoS₂ nanoribbon array grown on a vicinal Au surface (Au(775)) by decoration of Au edges. a) presents reprinted figures with permission from Ref. [415], Copyright © 2001 by the American Physical Society. (b) is reprinted with permission from Ref. [418], Copyright © 2015 American Chemical Society. (c) is reprinted with permission from Ref. [426], Copyright © 2016, Springer Nature. (For interpretation of the references to color in this figure legend, the reader is referred to the Web version of this article.)

metallic. In STM images, this gives rise to bright contrast due to electronic imaging effects (see Fig. 24 (a)). In H-TMDs, the zig-zag edges are more stable than armchair terminations. However, from the crystal symmetry, there are two kinds of zig-zag edges, which are either a S- zig-zag or the Mo- zig-zag edge. Under most growth conditions, triangular islands are observed (opposed to hexagonal islands), which indicates the preference for one kind of zig-zag termination. For MoS₂ islands on Au(111), the Mo-zig-zag edge was observed, however, this Mo-edge was terminated with two additional sulfur atoms per Mo-edge atom [415,416]. This sulfur passivation of the edges was also proposed to make them more stable against oxidation [417]. Ab-initio calculations also confirmed that different terminations of the Mo-zigzag edges are metallic (see Fig. 24(b)) [415,418]. The metallic edge state pins the Fermi-level at the edges in the analogy of Fermi-level pinning by surface states in bulk semiconductors. The Fermi-level at the edge was found ~1.2 eV above the VBM [419]. The Fermi-level of the basal plane for monolayer islands on HOPG was obtained at ~5 nm distance away from the edge, indicating a short depletion 'strip' along the edges. Ab-initio thermodynamics calculations also demonstrated that such extra sulfur atoms along the edges have a lower formation energy compared to bare Mo-termination [420]. In the same report, similar chalcogen rich termination has been predicted for the TM-zigzag edges for MoSe2, WS2, and WSe2. Experimental work on WSe2 supports the termination of W-edges with Se and their metallic nature [421]. Surprisingly, HR-TEM studies of nano-porous MoS₂ grown by MBE on SiO₂/Si did not show additional sulfur at the Mozig-zag edge, although it was the dominant edge orientation [422]. The sulfur zig-zag edges were found in three different edge structures. The unrestructured sulfur zig-zag edge termination was a minority and two different Mo-rich restructurings of the edges were identified to be more common. Interestingly, ferromagnetic properties were observed in these nanoporous films up to 400 °C. DFT simulations suggested that these magnetic properties were induced by spin polarized metallic edge states [422-424]. Formation of straight Mo zig-zag edges without sulfur termination could be obtained in MoS₂ ribbons by annealing to 800 °C in a TEM [425]. Growth of MoS₂ nanoribbons with the ultimate width of a single unit cell was obtained by edge decoration of a vicinal Au(775) substrate (Fig. 24(c)) [426]. These nanoribbons were, however, modulated due to strong interaction with the metal support. The Mo-zigzag edge was proposed to be terminated by a single sulfur atom per Mo-edge atom, so that the overall stoichiometry of these ribbons is sulfur rich.

The metallic edge state of MoS₂ islands has also been recently

observed in transport measured of MoS₂ monolayers in a FET device. The transport characteristics are consistent with that of a 1D electron gas described by a Tomonaga Luttinger quantum liquid [427]. Most experimental work was done for MoS₂, but there is also an experimental indication for MoSe₂ and MoTe₂ edges to exhibit metallic properties. Interestingly, recent DFT calculations also predicted metallic edge states for zig-zag edges in monolayer 1T- PtS₂ and PtSe₂ [428]. For PtS₂ magnetic properties of the edges were suggest by DFT for Pt-terminated zig-zag edges that become energetically favored for low sulfur chemical potential [429]. Also, STM images of semiconducting monolayer PtSe₂, shown in Fig. 22 (c), exhibit bright edges suggestive of a metallic edge state. Such predictions and experimental observations warrant further investigations of edge properties of other 2D materials.

5.1.2. Mirror twin grain boundaries

Related to the metallic properties of step edges in Modichalcogenides are the properties of MTBs in these materials [285]. As pointed out in section 2.3.2, if a TMD is grown on a substrate like graphene, then the formation of mirror grains is unavoidable. If such grains merge, a MTB is formed and this has been, for instance, observed for MoS₂ growth on graphene/Ir(111) [264]. Other mechanisms for the formation of MTBs in MBE growth have been revealed for MoSe₂ and MoTe₂ by the incorporation of excess Mo in the lattice. Such incorporation mechanisms can lead to a high density of MTB networks and these mechanisms will be described below in section 5.2 in more detail.

MTBs can have different configurations that vary in their composition. The compositional variants have formation energies as a function of chalcogen chemical potential and computed structures and their formation energies for MoSe₂ are summarized in Fig. 25 [281]. The dependence of the formation energy on the chemical potential may suggest that the MTB configurations are tunable to some degree by the growth conditions, however, kinetic limitations during growth may be important. Generally, during MBE growth, chalcogen deficiency may be expected, and thus TM rich MTBs are more likely to be observed.

The metallic character of MTBs is observed in STM by their bright contrast and are confirmed by DFT simulations that show a dispersing band intersecting the Fermi-level [430]. This metallic character depends on the MTB configuration and may be hole- or electron-like [269]. STM studies of MTBs in MoS₂ formed by coalescence of mirror grains have identified two different grain boundary configurations. Since these are metallic systems with electrons confined in the one-dimensional grain boundary, the

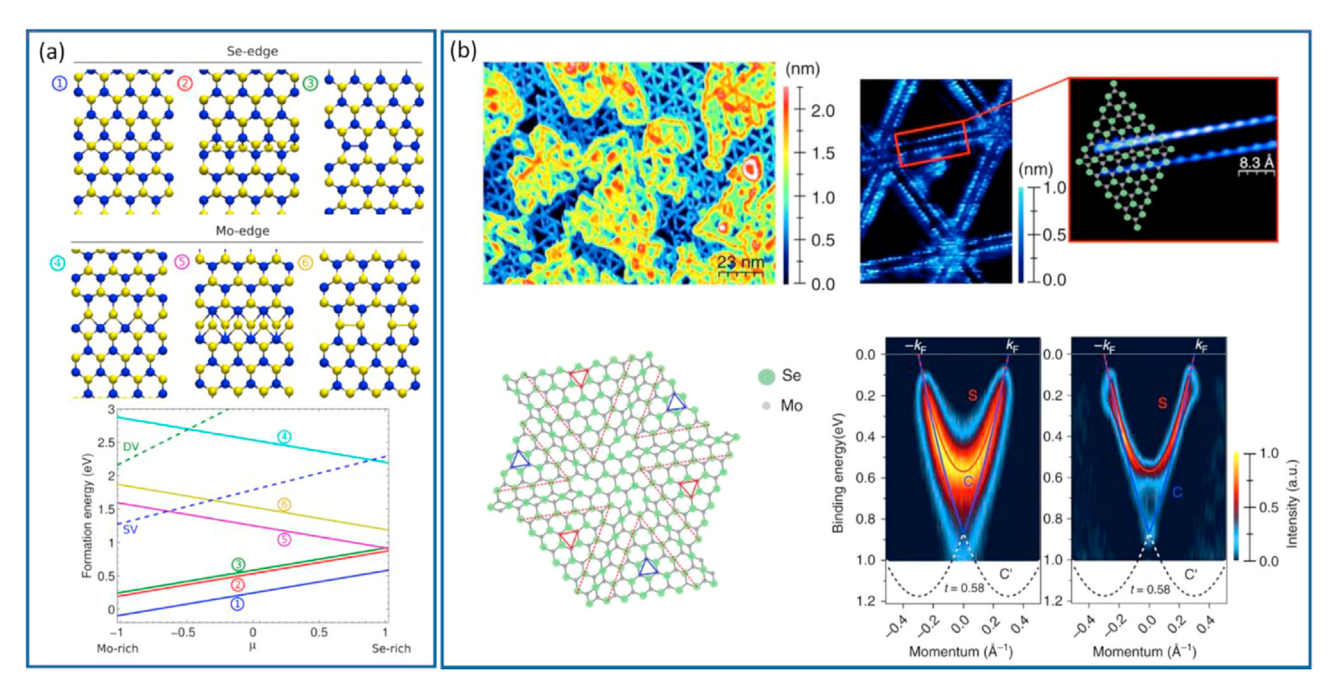


Fig. 25. MTBs in MoSe₂. (a) DFT simulations of different stable configurations of mirror grains joined along the Se-edges (1–3) or Mo-edges (4–6) and their formation energies as a function of Se-chemical potential. For comparison, the Se vacancy formation energies (SV and DV) are also shown. Of all configurations, configuration (1) is the most favored structure. This structure is also observed in MTB networks obtained by MBE growth and shown by STM images in (b). The bright contrast in STM is related to the metallic properties of MTBs and in high resolution STM, they appear as two bright parallel lines. In epitaxial MoSe₂ films on MoS₂ substrates the MTBs are aligned, enabling ARPES studies of the metallic band gap states, also shown in (b). The dispersing band shows two cusps in the second derivative that are consistent with calculated spin (S) and charge (C) excitation bands (shown as red and blue lines) of a 1D Tomonaga Luttinger liquid. (a) is reprinted with permission from Ref. [281], Copyright © 2015 American Chemical Society. (b) is reprinted with permission from Ref. [431], Copyright © 2017, Springer Nature. (For interpretation of the references to color in this figure legend, the reader is referred to the Web version of this article.)

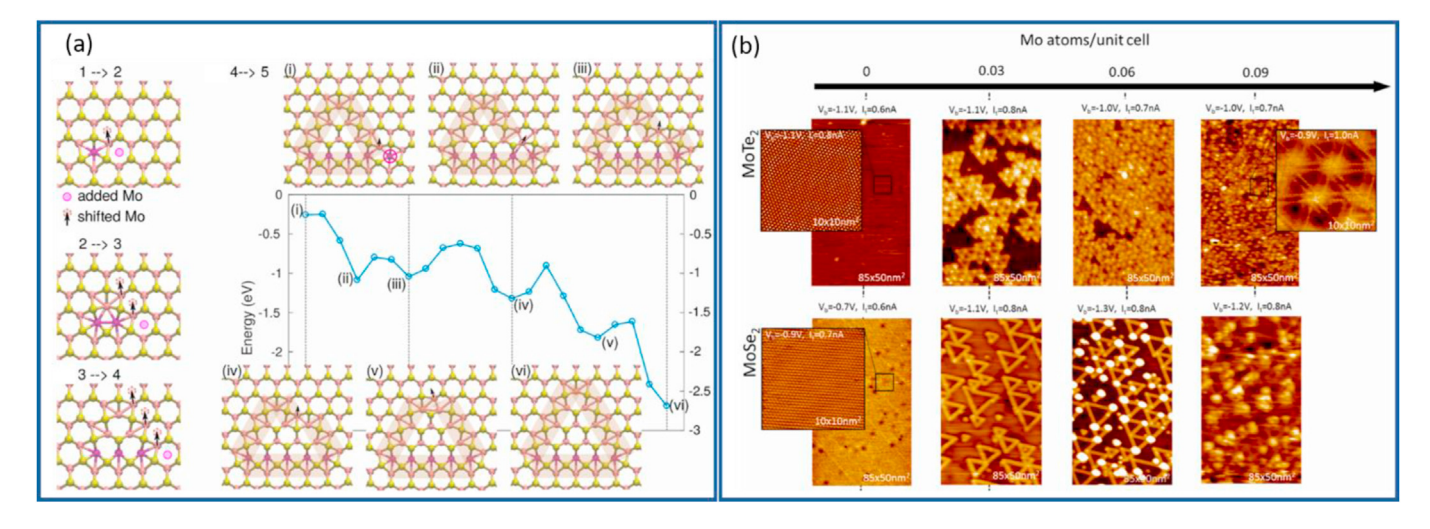


Fig. 26. Formation of MTB-loops in MoSe₂ and MoTe₂ by incorporation of excess Mo. The process of adding Mo-atoms into the interstitial sites of MoSe₂ and proposed rearrangements by adding one atom at a time to grow a closed MTB loop is illustrated in (a). The process of adding a 5th excess Mo atom and the expansion of the MTB loop is shown in detail, indicating that the whole process is energetically downhill. STM studies of the formation of MTB loops and eventually MTB-networks by depositing excess Mo on a single crystal surface of MoTe₂ and MoSe₂ is shown in (b). In MoTe₂ more than 10% of excess Mo can be incorporated to form a dense network of MTBs, while for MoSe₂ MTBs only form initially before Mo-clusters nucleate at the corners of the triangular MTB loops. Reprinted with permission from Ref. [434], Copyright © 2018 American Chemical Society.

electron excitation spectrum should be governed by Tomonaga Luttinger liquid theory. Moreover, since the MTBs synthesized in this study are of limited length due to the size of the MoS_2 islands, the 1D electron system is also confined along the wire, creating a 1D electron-in-a-box system. Careful analysis of dI/dV mapping showed that the electronic modulations along the MTB can be understood as a confined Tomonaga Luttinger system [269].

Similar conclusions of a 1D Tomonaga Luttinger system were

reached from the characterization of MTB networks obtained by MBE growth of MoSe₂ on MoS₂ single crystal substrates, shown in Fig. 25 (b) [431]. The epitaxial relationship of the MoSe₂ with the substrate and a high density of MTBs enabled their characterization by ARPES measurements. These studies revealed Tomonaga Luttinger liquid behavior, such as a power law suppression of the density of states at the Fermi-level and a splitting of the electron excitation spectrum in a spin- and charge-excitation branches.

Reported Peierls' distortion observed in STM with a 3-time periodicity of the atomic lattice [431,432] and band gap opening is still controversial as similar spectroscopic features are expected from the Tomonaga Luttinger liquid-in-a-box model [269].

Measurement of a reduced band gap in the basal plane of MoSe₂ in the vicinity of the MTB suggests that the metallic states in the MTB induce electron screening effects that reduce the band gap [284], similar to screening induced gap narrowing in monolayers on a metallic substrate. Related observations have been made for low angle grain boundaries in WSe₂, which induced localized gap states and modified the band gap of WSe₂ in its vicinity [433].

5.2. Compositional variations

Controlling the composition in MBE growth of chalcogenides is generally challenging because of the high vapor pressure of chalcogens that require a high chalcogen overpressure during growth. In many cases, the TMDs are the preferred crystal structure but are competing with other known (or unknown) compositional phases. Other vacuum processes such as vacuum annealing may also result in loss of chalcogens that then subsequently may transform the film into other compositional phases. Thus, starting with a TMD either as a single crystal or thin film, one may obtain other materials by post-growth annealing. In this sub-section, we review some of the known processes that can lead to a compositional modification of TMDs or a transformation of a TMD into another compositional phase.

5.2.1. Excess metal incorporation into the lattice structure

One intriguing example of compositional variations in MBE growth is the above-mentioned MTB networks in MoSe₂ and MoTe₂ [284,294]. These MTB networks can be very dense with MTBs separated by less than 10 nm (see e.g. Fig. 25(b)). Also, the MTBs observed in these networks are of the number-1 kind shown in Fig. 25 (a) and are thus enriched in Mo compared to the MoSe₂/ MoTe₂ basal planes. Formation of such dense networks by coalescence of mirror-grains is not a conceivable process. Instead, incorporation of excess Mo during growth was proposed, see Fig. 26 [285,434]. Experimentally, it was demonstrated that these MTB networks can be obtained by vapor deposition of Mo onto a freshly cleaved MoSe₂ or MoTe₂ single crystal surface held at 300 °C. The same process was not active for MoS₂ and no MTB networks formed on a MoS₂ single crystal. DFT simulations indicated that it is energetically favorable for excess Mo to be incorporated into the interstitial sites rather than adsorbing as Mo atoms on the surface for MoSe₂ and MoTe₂, but not for MoS₂ [434]. Addition of more Moatoms results in the nucleation of triangular MTB loops that can grow in size by incorporating more Mo-atoms (see Fig. 26 (a)) the energy per excess atom decreases as the size of the loop increases, thus favoring their growth. Eventually, these loops intersect and form the observed MTB network structure. High densities of crystal imperfections that vary the crystal composition are known for examples in oxides, where crystallographic shear planes can alter the composition of the parent material. The formation of MTBs in MoSe₂ and MoTe₂ can be considered linear crystallographic variations that modify the composition of the material. Moreover, the metallic nature of the MTBs, enables an approach to effectively metalize MoSe₂ or MoTe₂ by selective deposition of Mo on the crystal. While the modifications of TMDs with MTB networks has mainly been observed for MoSe2 and MoTe2 a recent report suggests that doping of WSe₂ with Nb may also result in MTB networks [435], and thus doping with heteroatoms may open a new approach for inducing MTBs in materials that do not form MTBs in their pure form.

5.2.2. Compositional transitions by chalcogen desorption

Instead of changing the surface composition of MoTe₂ by adding excess Mo, it was also shown that removal of Te by thermal annealing [289] also results in the formation of MTB networks [436]. This further illustrates that the MTB structures are energetically favored configuration for Te-deficiency or Mo-excess. Interestingly, further annealing and removal of Te causes the surface region of a MoTe₂ crystal to restructure further and eventually quasi 1D vdW crystals are formed consisting of Mo₆Te₆ vdW nanowires [437]. Chalcogens in TMDs may also be desorbed by an electron beam. Thus, it may not be surprising that MTB loops have also been found for MoSe₂ in a TEM [438].

While chalcogen removal in MoTe₂ and MoSe₂ resulted in the formation of a high density of Mo-rich linear defects, there exist many TM chalcogenides with complex compositional phase diagrams with TMDs just as one possible compositional phase. TMDs of such materials systems may transform into another compositional phase upon desorption of chalcogens by, for instance, vacuum annealing. For example, the platinum telluride system contains not just Pt ditelluride (as discussed above) but also Pt monotelluride [439] and various intermediate compositions all as layered materials. Thermal annealing of MBE grown epitaxial PtTe₂ undergoes telluride loss as observed in XPS and formation of a new epitaxial layer [440]. The transition is also clearly observed in ARPES that shows very different electronic structure of the phases. Both phases do exhibit a hexagonal structure. In contrast, thermal annealing of PtSe₂ flakes to 500 °C showed a transition from the layered PtSe2 to a 3D-covalently bonded Pt monoselenide with a cubic structure [441]. This transformation could be followed within a TEM, and thus the transformation mechanism was characterized on an atomic scale. Also, the process resulted in a 3D bonded structures; the resulting flakes were ultrathin. Thus, loss of chalcogens, for instance induced by thermal treatments and subsequent transformation into a different phase, can be an approach for synthesizing new layered materials or ultrathin films. In addition, in the monolayer limit, new compositional phases may form that do not have bulk counterparts. For instance, in VS₂ [68] and VSe₂ [442] monolayers, thermal annealing has been reported to result in significant chalcogen losses and the formation of new ordered structures. In both compounds, STM has shown the formation of linear defects that have been associated with missing chalcogen rows. Exposure to the chalcogen could restore the stoichiometric TMD monolayer structure. As discussed above, the formation of such Sedeficient VSe₂ structures has also been associated with magnetic properties of VSe₂ [167]. Thus, these new phases may also induce functionalities not present in the TMD parent material and, therefore, a full understanding of the compositional control of TMD derived phases is important.

PdSe₂ with its unusual puckered pentagonal structure (see section 4.6.2), also showed some compositional changes induced by electron- or ion-beam desorption. Under the electron beam in a STEM, fusion of a bilayer PdSe2 into a new monolayer structure with a composition of Pd₂Se₃ was observed [443]. Argon plasma treatment of PdSe₂ flakes triggered a transformation of the layered structure into a three-dimensional Pd₁₇Se₁₅ crystal structure [444]. This phase is metallic and it was suggested that this approach is useful for patterning metallic contact patches to PdSe₂ to avoid Schottky barriers. Argon sputtering and annealing procedures were also investigated in a UHV surface science study. Sputtering with 0.2-1 keV Ar ions and subsequent annealing to 200C for 1 h resulted in the transformation of a $PdSe_2$ surface into a new $PdSe_2$ nanoribbon structure [445]. This new PdSe₂ phase forms epitaxially with respect to the underlying PdSe₂ crystal and the weakly bound nanoribbons can be picked up by the STM tip. This allowed measurement of the conductance of these nanoribbons with a ballistic

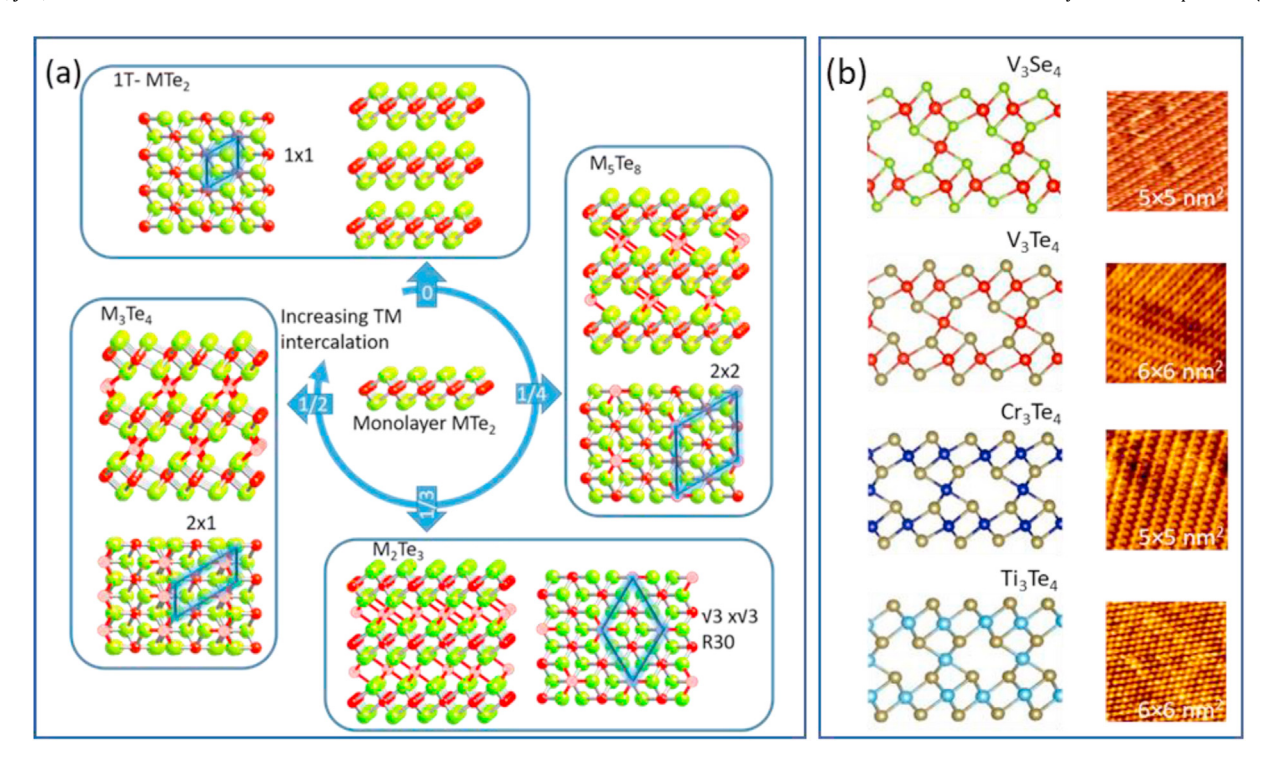


Fig. 27. Self-intercalated TMDs. These crystal structures are also commonly described as NiAs-structure with periodic metal vacancies. (a) schematic ball and stick model of various typical intercalation compound compositions, with the periodicity of the intercalated TM indicated with respect to a 1x1 TMD surface. (b) DFT simulations of bilayer TMDs with a ½ monolayer of TM intercalated between the two TMD layers. Note that the corrugation induced in the TMD layer by the intercalant varies with the TM. STM images of suspected intercalation compounds grown by MBE are also shown. Reprinted with permission from Ref. [136], Copyright © 2020 American Chemical Society.

transport through one conductance channel observed for a length of 20 nm. The metallic nature of the nanoribbons was also confirmed by transferring the nanoribbons to a ${\rm SiO_2}$ substrate to measure transport properties.

5.2.3. Self-intercalation

Above, we have described how, in the case of MoSe₂ and MoTe₂, excess TM are incorporated into the basal plane and form metal rich MTB networks. Another possibility to incorporate excess TM in TMDs is within the vdW gap of multilayer TMDs. Such self-intercalation is particularly likely to occur in TM chalcogenides that have compositional phase diagrams that include ordered 'intercalants'. This is, for instance, the case of the first row TMDs of the early TMs, Ti [446], V [447], and Cr [448–451]. A schematic of possible intercalation compounds with different amounts of self-intercalated TM and its relation to TMDs is illustrated in Fig. 27 (a).

It has been shown that annealing of VSe2 or TiSe2 mono-to bilayer films grown by MBE on HOPG may result in selenium loss and transform the material into an intercalation compound consisting of two layers of TMDs with a single layer of TM in between [452]. Thus this is another example of a post-growth compositional change induced by vacuum annealing. In STM, the intercalated VSe₂ exhibits a corrugated surface with a 2×1 structure with respect to pure VSe₂, which is also confirmed by LEED, suggesting the V₃Se₄ structure (note that the composition of a bilayer TMD with ½ a layer of TM intercalated is V₅Se₈, but we use the composition an extended bulk phase would have). The observed corrugation is reproduced by DFT that demonstrates that an intercalated layer causes significant distortion of the TMD layer. Direct growth of V-, Ti-, and Cr-telluride also reported that the monolayer of these materials can be grown by MBE as TMDs, but multilayer may easily form intercalation compounds, all with the 2×1 structure on the basal plane [136]. The intercalant induced corrugation of the

surface layer is, however, dependent on the material, Fig. 27 (b) shows the simulated corrugation of intercalated bilayers and the reported STM images. It is seen that the Ti_xTe_v intercalation compound exhibits very small corrugation of the TMD layer, which may make it difficult to distinguish from STM alone. It may be important to point out that the intercalant induced distortion of the TMDlayer shows resemblance to the 1T' structure of TMDs. This may lead to some misinterpretation. For example, the formation of 1T' VSe₂ by high temperature MBE growth has been reported in the literature [174,175]. However, as we discussed above the 1T' structure is not expected to form for a TMD with a single d-electron. Since it is challenging to distinguish a true 1T' structure from a selfintercalated VSe2 phase, the latter should be considered as a possible explanation for the composition and structure of MBE grown films with a 2×1 periodicity. Evidence for the formation of intercalation compounds in high temperature MBE grown samples also comes from recent growth studies of V-selenide multilayers on sapphire an its characterization by cross-sectional TEM [176]. Another potential misinterpretation in the literature is for TiTe2 thin films grown by MBE. In these films a CDW with a 2×2 structure was reported that persisted at least to room temperature [54]. In section 4.1.1 we discussed that only monolayer TiTe2 exhibits a CDW with a T_{CDW}~92 K, while bulk TiTe₂ is known for its absence of CDW instabilities. The CDW in thin film TiTe2 was considered to be a consequence of a strain-stabilize phonon instability. However, the detailed characterization of the lattice parameters by synchrotron x-ray diffraction studies would also agree with the expected lattice parameters for a self-intercalation compound. Generally, the possibilities of intercalation compounds should be considered to explain unusual properties in MBE grown films such as magnetism, unexpected CDW distortions, or transition to a 1T' structure in materials known to be stable as 1T.

Mostly the early TMDs are prone to self-intercalation. While

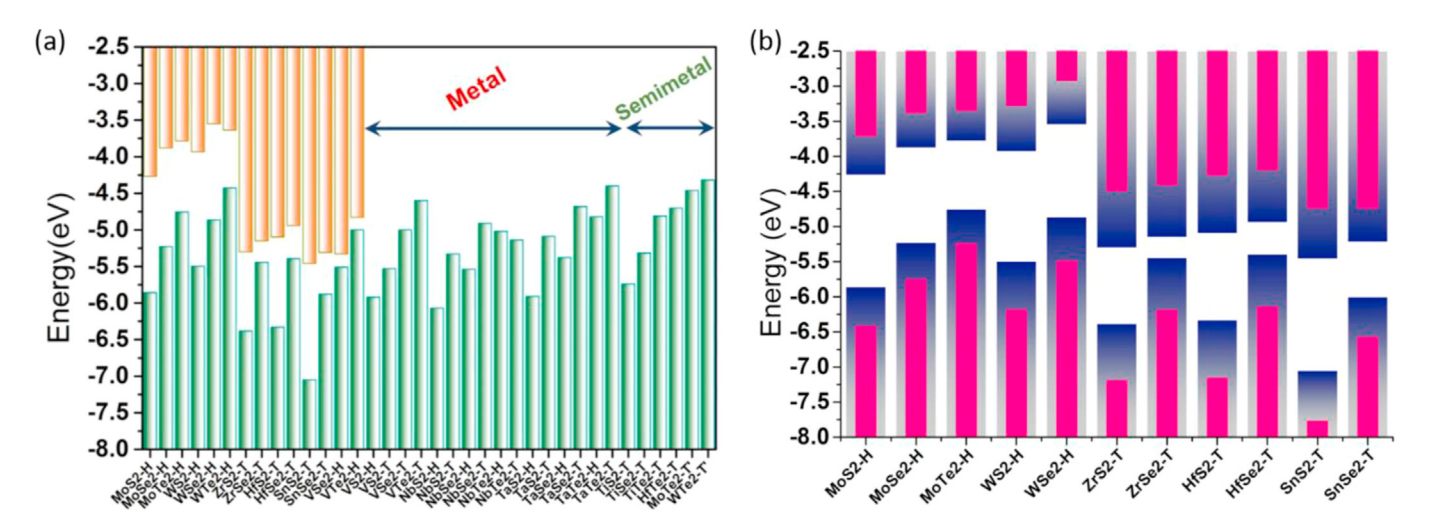


Fig. 28. DFT calculations of band edges of monolayer 2D materials relative to the vacuum level (vacuum level is set to 0 eV). (a) Band edges for semiconducting and metallic TMDs. (b) semiconducting TMDs and tin dichalcogenides. The blue and pink VB and CB edges correspond to calculations using PBE and G_0W_0 functionals, respectively. Republished with permission of IOP Publishing, Ltd, from Ref. [454]; permission conveyed through Copyright Clearance Center, Inc. (For interpretation of the references to color in this figure legend, the reader is referred to the Web version of this article.)

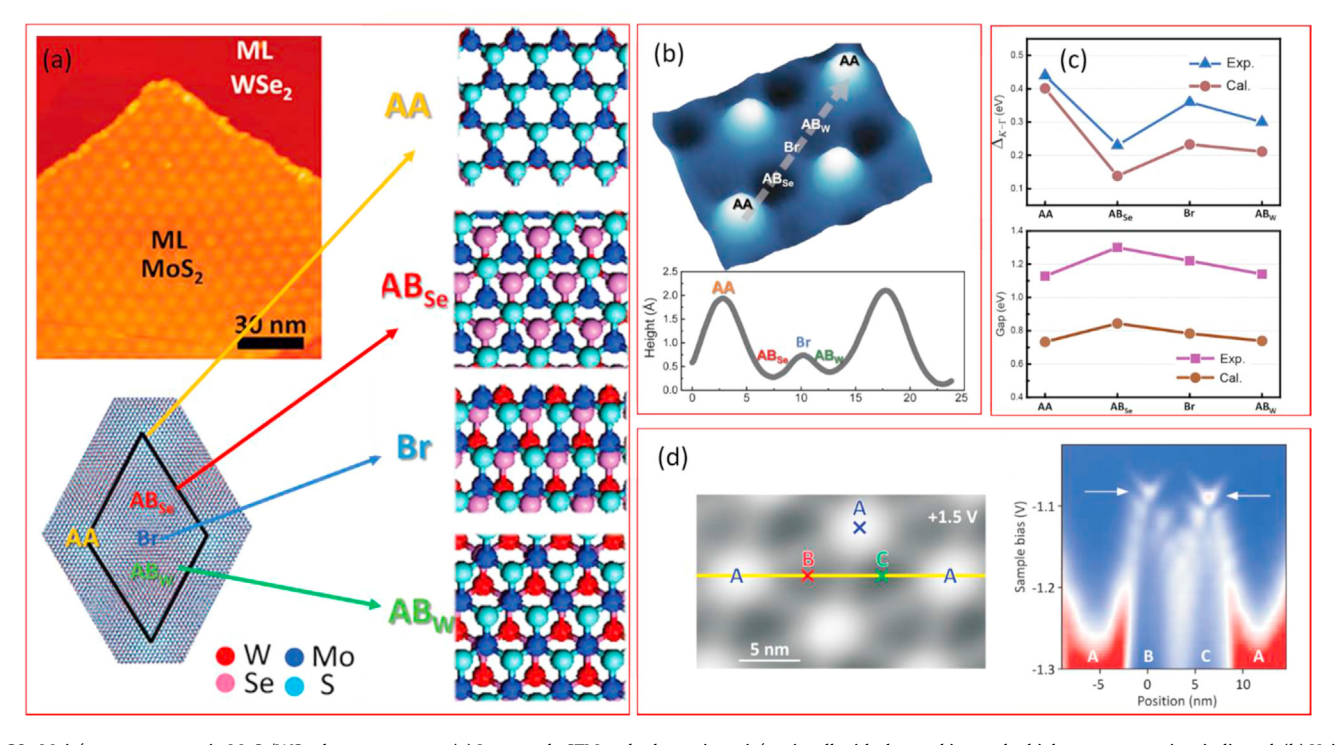


Fig. 29. Moiré superstructure in MoS_2/WSe_2 heterostructure. (a) Large scale STM and schematic moiré-unit cell with the stacking at the high symmetry points indicated. (b) Height variation in STM within the moiré unit cell. (c) Local variation of the electronic structure extracted from STS measurements and DFT calculations. The band edge separation between the K- and Γ-points, and the changes in the overall band gap are shown. (d) measurements at low temperature indicate discrete confined states within the moiré potential. (a-c) are reprinted from Ref. [461] © The Authors, some rights reserved; exclusive licensee American Association for the Advancement of Science. Distributed under a Creative Commons Attribution NonCommercial License 4.0 (CC BY-NC) http://creativecommons.org/licenses/by-nc/4.0/. (d) is reprinted with permission from Ref. [462], Copyright © 2018 American Chemical Society.

during MBE growth self-intercalation of the same TM is possible, the intercalation of a different element may be achieved by a post-growth intercalation into TMDs. For instance, the intercalation of copper from a solid source in between early TMDs was demonstrated recently [453]. Thus, controlled intercalation in MBE grown few layer TMDs by a post-growth process can be another tool for tuning and inducing new properties and this should be studied in more detail in the future.

5.3. TMD heterostructures and moiré properties

Initially, vdW epitaxy was motivated by the ability to combine different materials without restrictions imposed by lattice matching conditions and with the anticipation that the contact between the two materials does not strongly affect the properties of the components. This simple picture assumes that interlayer interactions are mostly negligible, and thus the properties of a vdW

heterostructure may be considered the combination of each individual layer. Thus, the interlayer band alignment in semiconductor vdW heterostructures could be considered just by work function difference and interlayer dipoles. The band edges for many of bilayer TMD heterostructures have been calculated by DFT (see Fig. 28) [454] and these values can be taken as a first approximation for heterostructure formation. Experimental measurements of the band alignment have been done by STM/STS on exfoliated and stacked TMDs [455,456], as well as photoemission on related 2D materials [36,37]. The latter showed the importance of taking interface dipole corrections into account for obtaining the correct band alignment. Particularly for group VI-B TMDs, a band alignment based on electronically non-interacting heterostructures is, however, oversimplified. Based on the experience for group VI-B TMDs that show that the monolayer has distinctly different properties from the bulk material due to their interlayer interactions, one may expect variations in heterostructures, as well. One difference in heterostructures compared to bilayers of the same material is that the layers have different lattice constants, which will give rise to a long-range coincidence lattice, known as a moiré structure. Related moiré structures may also be obtained if two layers of the same material are twisted relative to each other. Such twist structures can be fabricated by exfoliation and re-stacking with defined rotation. The expected moiré-periodicities of two rigid lattices may be calculated from the lattice constants and their relative twist angles [457]. While such moiré structures are generally observed, recent studies showed that group VI-B TMD heterostructures with closely matched lattice constants and small twist angles can also undergo lattice reconstruction forming domains that have H- or Rlike stacking separated by stacking faults [458,459].

In bulk samples of group VI-B semiconducting TMDs, the interlayer interactions of the chalcogen p-orbitals are partially responsible for the strong variation of the band structure from monolayer to bulk. Within the moiré unit cell of a heterostructure, the atoms of the two layers are differently coordinated relative to each other. Consequently, the interlayer orbital interactions are locally modified within the moiré unit cell and a locally modified electronic structures are anticipated [460]. Experimentally, the local electronic structure variation in MoS₂/WSe₂ heterostructures was carefully studied by STS [461,462]. In these studies, MoS₂ is grown on WSe2 by CVD. The layers are rotationally aligned and a moiré structure with a periodicity of ~8.7 nm is observed as can be seen in Fig. 29 (a). The moiré unit cell contains low symmetry stacking configurations with MoS₂ and WSe₂ atoms on top of each other (AA) sulfur atoms of MoS₂ on top of W atoms in WSe₂ (AB_{Se}), a bridge configuration (Br), and Mo-atoms on top of the Se atoms of the WSe₂ (AB_W). These different sites are imaged with significantly different corrugation in STM (Fig. 29 (b)), partially due to differences in the interlayer separation as a consequence of the stacking. STS and DFT simulations are in qualitative agreement that the different stackings give rise to strongly varying interlayer hybridizations that cause local variation in the VBM, particularly the energy separation between the VBM at the Γ - and K-points within the moiré unit cell, as well as a variation of the band gap of ~0.2 eV within the moiré unit cell. Moreover, it has been proposed that the potential variation in the moiré structure gives rise to confined states with discrete energy levels that could be observed at low temperatures (5 K) [462]. Fig. 29 (d) shows a constant height dI/dV map along the yellow line across the moiré unit cell. Discrete confined states appear at the AB_{Se} and AB_W points (labeled B and C in Fig. 29 (d)).

Modifications of exciton binding by the lateral superpotential of the moiré structures in semiconducting group VI-B TMD heterostructures, have recently attracted significant attention [463–467]. Optical properties of TMDs are beyond the scope of this review, and

thus are not further discussed here, but the fundamental electronic modifications demonstrated in the STM/STS studies are foundational for these optical applications.

Most of the work on moiré heterostructures is done by exfoliated samples and the STM work was done on samples synthesized by CVD growth and related methods. MBE synthesis of true heterostructures, i.e. growth of two monolayer TMDs on top of each other, has not vet been reported. One challenge is the above reported formation of MTBs in MoSe₂ and MoTe₂, and the other is the challenge of suitable sulfur sources and the growth sulfides in general. So far, the emphasis for heterostructures has been on the group VI-B TMDs that exhibit strong interlayer interactions that are responsible for the electronic variations in the moiré unit cell. Weaker variations may be expected in group IV-B TMD semiconductors that do not show strong modifications from bulk to monolayer. While the moiré superstructure is exciting for new properties that arise from nanometer scale lateral periodic potential, these modulations are not always desirable for applications, and thus group IV-B semiconductors may be better materials choices if uniform properties are desired. More work should be done to grow heterostructures by MBE and characterize their properties at the nanoscale.

5.4. 1T to 2H phase control

In this sub-section we examine approaches that enable to control or change the structural phase of TMDs without significant compositional change. In TMDs this is typically a switching between the 1T or 1T to the H-phase or vice versa. We have already discussed the controlled growth of monolayers of different phases in MBE in section 4. Here we focus on approaches that can switch one phase into the other by a stimulus like heat or electric field.

Group VI-B TMDS: Controlling the growth to obtain MoTe₂ and WSe₂ in 1T' or H phase has been discussed in section 4.3.2 and 4.3.3, respectively. Also, the phase switching of MoTe₂ from the semiconducting 2H phase to the semi-metallic 1T' phase by localized laser heating has been discussed and may be used to make ohmic contacts to the semiconducting 2H-MoTe₂ [83]. MoTe₂ may be a natural target for exploring phase switching behavior since it does undergo a phase transition from the 2H phase at low temperature to the 1T' phase at 650–900 °C.Error! Bookmark not defined. The large variation of this transition temperature may be related to chalcogen deficiencies in the material. Excitingly, the transition temperature could be tuned to room temperature by applying a tensile strain of 0.2% with an AFM tip [468]. This is consistent with DFT simulations shown in Fig. 30 that indicate that the formation energy of the 1T' phase is the closest to the formation energy of the H-phase for the group VI-B TMDs. Recently, the ability to reversibly switch MoTe₂ from its semiconducting to semimetallic phase was also demonstrated by electrostatic gating [82].

The energy difference between the 1T/1T' phase and the H phase in pristine MoS₂ is significant and a phase change is not easily possible in pristine materials. However, it is well-known that electron doping of MoS₂ or WS₂, for instance by alkali atom intercalation, causes the 2H phase to transform into the 1T or 1T' phase [80,469,470]. Intercalation of ammonium in aqueous solution has also demonstrated to stabilize the 1T phase [471]. Li-intercalation in MoS₂ single crystal and the associated phase transition to the 1T phase was already studied by photoemission in the 1990s [472]. A binding energy shift of ~0.8 eV in the Mo-3d core level allows for a convenient differentiation and assessment of the concentration of the 1T and 2H phases of MoS₂ [473]. Chemically exfoliated monolayer MoS₂ [474] and WS₂ have also been shown to be often heterogeneous and contain 1T, 1T' and H-phases [475–478]. This has been suggested to be a consequence of charge transfer to the TMDs,

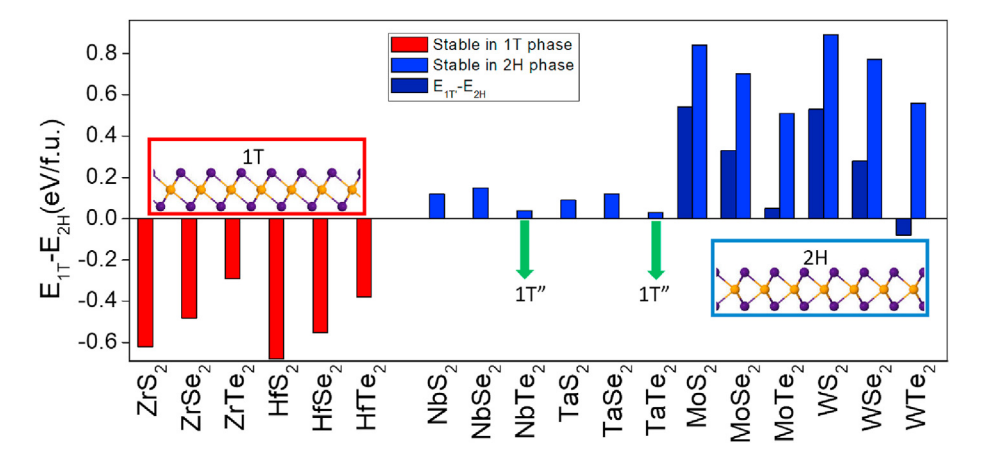


Fig. 30. Calculated formation energies for the H and 1T (1T') phases. 1T phase is preferred for Zr- and Hf-dichalcogenides. For Nb- and Ta- dichalcogenides the 2H phase is only slightly preferred over the 1T phase. For Nb- and Ta—Te₂ the known bulk structure is the distorted 1T" phase, which has not been calculated here. For the group VIB TMDs, only WTe₂ has the 1T' phase as the lowest energy the other materials prefer the 2H phase with 1T'-MoTe₂ being very close in energy to its 2H phase. The data plotted here were taken from DFT calculations presented in references [238,483].

from the organic compounds used for the exfoliation process, typically butyl lithium. However, the 1T phase is retained also when dried and this was attributed to adsorbed ions such as protons and remaining alkali ions that compensate for the negative charge on the 1T-MoS₂ [473,479]. 1T-WS₂ was suggested to be also stable without indication of Li ions [478]. It has been suggested that once the 1T phase is formed for MoS₂ or WS₂, it is metastable with a significant energy barrier of ~ 1eV for reformation of the H-phase [478–481]. However, annealing in vacuum can reform the stable Hphase. This also allows controlled local modification of MoS₂ into 1T (1T') and H patterns, which may be exploited for making metallic contact pads for the semiconducting H-phase [81]. In electrochemical or photocatalytic applications, the 1T phase or a phase mixture is often considered to be beneficial and higher HER has been obtained in 1T MoS2 compared to its H-phase. In monolayer MoTe₂, the phase transition was also monitored at the atomic scale by STEM, which revealed that the transition proceeded via an intermediate phase between the 1T and H-phases and that the transformation into the T-phase can be induced by the electron beam [482].

All in vacuum phase-switching by charge donating molecules on monolayer group VI-B TMDs has not been reported yet and most processes for monolayer materials involve some solution processing. However, phase changes on single crystal surfaces by Li adsorption have been shown some time ago [472], so phase switching for monolayers by vacuum processing is also likely to succeed.

Group V–B TMDs: We have seen that NbSe₂ (section 4.2.2) or TaSe₂ (section 4.2.3) may be grown in either 1T or 1H phase depending on the growth temperatures. The different phases of group V–B TMDs are very close in energy as can be seen in DFT calculations shown in Fig. 30 (b) (note that TaTe₂ and NbTe₂ do not

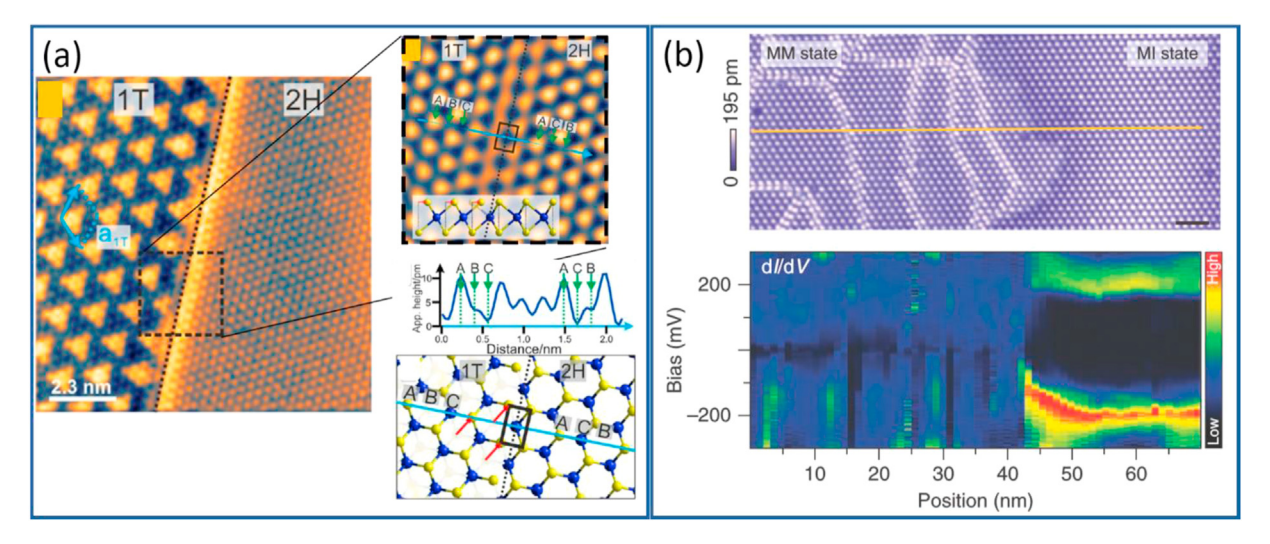


Fig. 31. Surface modifications of group V-B TMDs by voltage pulsing of an STM tip. (a) Local switching of a 2H-NbSe $_2$ into a 1T phase. The new 1T phase exhibits the $\sqrt{13} \times \sqrt{13}$ CDW. The phase boundary between the new 1T and the 2H phase is characterized by atomic resolution STM and the boundary structure is indicated by the ball-and-stick model. (b) Voltage pulsing of 1T-TaS $_2$ does not result in a phase change, but a mosaic structure is observed in the pulsed region. This mosaic structure consists of CCDW domains separated by (brighter) domain boundaries. Note the corrugation of the STM image is that of the CDW, the scale bar in the image is 5 nm dI/dV map along the yellow line, indicates that the region of the mosaic structure is metallic, in contrast to the unaltered region that exhibits MI band gap with the lower and upper Hubbard band resolved in the STS spectra. The breakdown of the MI state in the CCDW of the mosaic domains is believed to be associated with phase shifts relative to the subsurface layer. (a) is reprinted with permission from Ref. [487], Copyright © 2017 American Chemical Society. (b) is reprinted with permission from Ref. [488], Copyright © 2016, Springer Nature. (For interpretation of the references to color in this figure legend, the reader is referred to the Web version of this article.)

form the 'simple' 1T structure but are forming a distorted structure, which we referred to as the 1T" structure). Also, VSe₂ and VS₂, which are not included in Fig. 30 (b) have often been predicted by DFT to be more stable in the H-phase rather than the 1T phase, however, experimentally only the 1T phase has been observed both in the bulk as well as in the monolayer, as was discussed in section 4.2.1. Possibly the CDW phase lowers the energy of the 1T phase sufficiently to stabilize it over the 1H phase, but clearly the formation energy of these two phases must be very close.

According to Fig. 30, the 2H-TaS₂ is the lower energy configuration than its 1T phase and Wang et al. [483] have shown that thermal annealing in vacuum of a 1T crystal may cause the surface layer to transform into a 2H phase. This transformation is verified by the characteristic CDW structures of these materials (see section 4.2.3). Such a transformed 2H-TaS₂ surface layer on the 1T-TaS₂ bulk exhibited an enhanced superconducting transition temperature of 2.1 K, compared to bulk 2H–TaS₂ crystals. Applying voltage pulses with the STM tip allowed to switch the 2H-TaS₂ back to the 1T phase. Such STM tip induced switching has been reported for other group V-B TMDs, but only a switching from the 2H phase to the 1T phase has been observed. The first reports of such switching were for TaSe₂ [484,485] and recently for NbSe₂ [486,487]. Especially the latter is interesting because, as we pointed out in section 4.2.2, the 1T phase of NbSe₂ is not known as a stable phase in the bulk and only was recently synthesized as monolayer materials by MBE. The transformation under the STM tip is induced by voltage pulses of larger than 4V [487] or a raising of the voltage to -1.3Vwhile reducing the tip sample separation [485]. These processes cause a transformation of a patch underneath of the tip of 100's of nanometer in size. The large corrugation of the $\sqrt{13} \times \sqrt{13}$ CDW of the 1T phase allows for a distinction of the transformed region in STM. Fig. 31 (a) shows the phase boundary of the transformed 1T phase within the 2H phase of the NbSe₂ crystal [487]. The mechanism for the transformation is not fully explained, though. While local heating during the tip pulsing could play a role, so could the electron injection, induced strain and strong electric fields during the process.

Pulsing the STM tip on a 1T-TaS₂ sample held at low temperatures does not transform the phase (as pointed out above only phase changes from H to T phase but the inverse is not observed by

STM pulsing of group V-B TMDs), but instead induces a mosaic structure in the $\sqrt{13} \times \sqrt{13}$ CDW structure [488,489]. This mosaic structure is understood to consist of commensurate CDW (CCDW) domains, that are separated by domain walls in which the CDW phase is shifted. As discussed in section 4.2.3, only the CCDW is expected to be a MI. However, STS measurements, shown in Fig. 31 (b), indicate that the whole mosaic patch is metallic, while the surrounding unaltered TaS₂ (without mosaic structure) remains a MI with the lower and upper Hubbard bands resolved in STS measurements. This led to the conclusion that the interlayer stacking is important for the MI state. The tip induced phase shift of the CCDW domains in the surface also implies a shift of the CDWphase with respect to the subsurface layers and this interlayer shift has been proposed to cause the collapse of the MI state. This result suggests that interlayer interactions are important for the MI state in bulk materials. However, this seems to be at odds with results on related monolayer TaSe2 and NbSe2 that suggest that monolayers can be MIs in the absence of adjacent layers. Thus, further studies may be needed to fully understand the role of interlayer interactions for these MIs.

Group VIII-B (10) TMDs. Above in section 5.2, we have already discussed that mild low energy argon sputtering and annealing may transform the PdSe2 surface from its bulk truncation into a novel vdW nanoribbon structure [445]. For the more conventional hexagonal group 10 TMDs, usually, the 1T structure is the most energetically stable phase while the 1H phase has a significantly higher formation energy [359]. Thus, the observation that a 1T PtSe₂ monolayer grown on a Pt(111) crystal could be partially transformed in 1H-phases was unexpected [490]. This transformation was triggered by annealing induced Se-loss. It is proposed that Se-vacancies arrange at the 1T-1H phase boundary and stabilize the 1H-phase. This gives rise to triangular 1H domains within the 1T matrix and eventually an ordered pattern as seen in Fig. 32. The Se-3d core level peak for the 1H phase is shifted by ~0.4 eV to higher binding energy with respect to that of the 1T phase, and thus the relative intensities of the components in XPS also allows for measuring the concentration of the transformed surface. The transformation into the 1H phase is reversible by exposing the surface to Se, further demonstrating the importance of Se-deficiency in the transformation process. Interestingly, the 1H

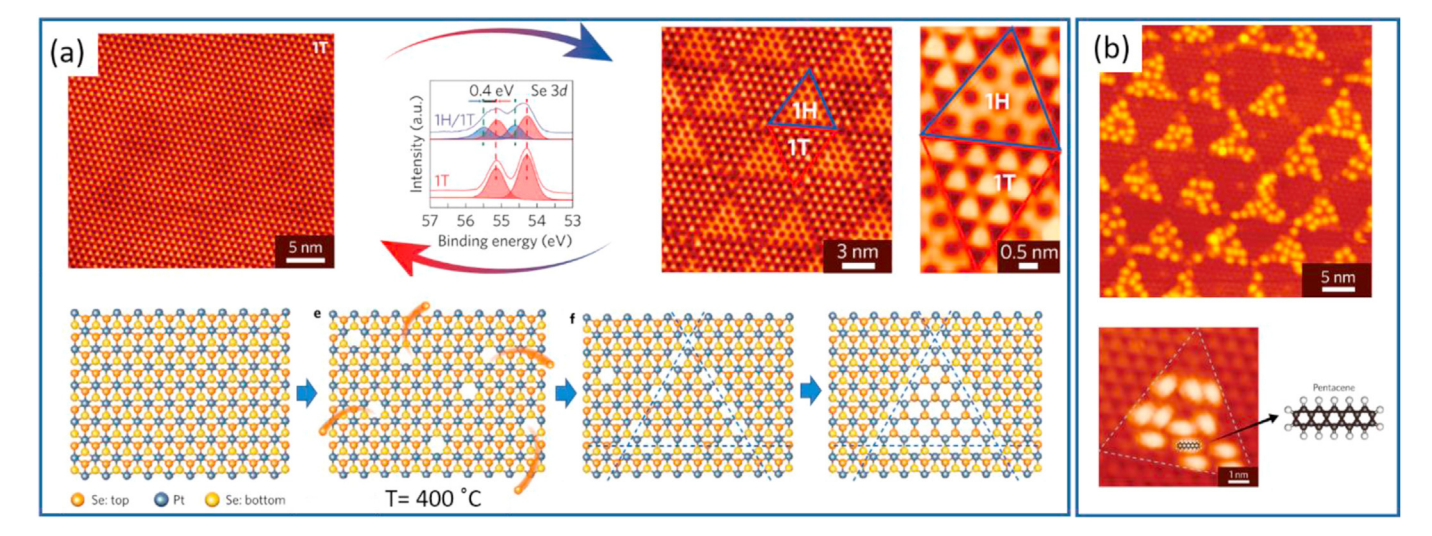


Fig. 32. Nanopatterning of PtSe₂/Pt(111) by vacuum annealing. (a) 1T-PtSe₂ grown on Pt(111) substrates, transform to triangular 1H-domains by vacuum annealing to 400 °C. The proposed process is indicated in the models. Se-loss by annealing results in clustering of vacancies which then stabilizes small domains of 1H phase. The formation of 1H domains is also seen in the Se-3d XPS spectra that shows a 0.4 eV shift to higher binding energy for the 1H phases compared to the 1T phase. (b) the surface patterned with 1T and 1H phases is an adsorption template with pentacene selectively adsorbing on the 1H–PtSe₂ domains. Reprinted by permission from Springer Nature Customer Service Centre GmbH, ref. [490], Copyright © 2017.

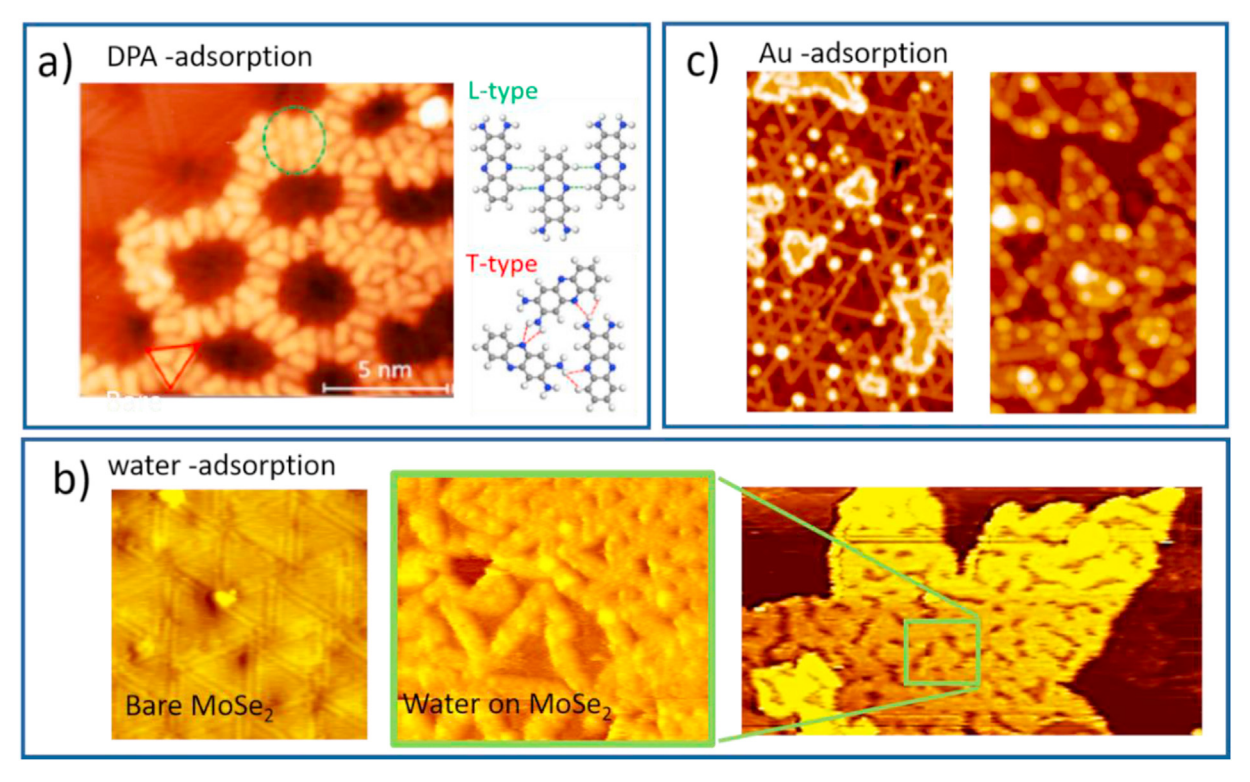


Fig. 33. Adsorption studies on MTB networks in MoSe₂. (a) DAP adsorption shows a preferential alignment of the molecules with the MTBs and variation of L- and T-type coordination, resulting in a nanoporous structure that leaves the vertices of the MTB network free of molecules. (b) water adsorption at 20 K on MTB networks shows the formation of amorphous 2D water islands. Within these islands water exclusively decorates the MTB network, (c) adsorption of Au-atoms results in Au-cluster formation at the vertices of the MTBs. For sub-monolayer MoSe₂ islands on graphite, the edges of the MoSe₂ islands are also decorated with Au. (a) is reprinted with permission from Ref. [493] Copyright © 2019, Springer Nature. (b) has been adapted from Ref. [494], (c) is reprinted with permission from Ref. [284], Copyright © 2017 American Chemical Society.

phase adsorbs pentacene more strongly than the 1T phase, and thus the 1T/1H patterned surface can be used as an adsorption template as shown in Fig. 32 (b). In general, molecular adsorption on monolayer TMDs can be used for their modification and control of properties. This will be discussed in the next section.

5.5. Molecular and atom adsorption on TMDs

Molecular adsorption on monolayer TMDs has been studied mostly on the group VI-B H-phase semiconducting TMDs and among those mostly by solution processes. In these studies, organic components have been used to passivate defects that may otherwise induce charge traps and exciton recombination sites. Moreover, surface passivation has been used for charge transfer doping and charge carrier screening and to enhance photoluminescence or transport properties. In addition, covalently attached organic molecules allow adding variety of functional groups that can provide chemical selectivity for sensing applications or energy conversion. Thus, the organic/TMD interface has potential for enhancing properties and inducing new functionalities to TMDs. Since solution-based functionalization of TMDs [491] as well as vacuum adsorbed molecular layers on TMDs [492] have both been recently reviewed, we point to these articles for detailed description of the progress in these fields.

In extension to these reviewed works, nanopatterns on monolayer TMDs may affect the fundamental adsorption processes. This is, for example, the case on the 1T/1H patterned PtSe₂ surface shown in Fig. 32 for pentacene adsorption. Other patterns we encountered in this review are the MTB networks in MoSe₂ of MBE grown films. MTBs are interesting modifications of the TMD structure since the MTBs themselves are perfect crystal

modifications that are not exposing undersaturated bonds like step edges or vacancies may do. On the other hand, though, the strongly different electronic properties of these line defects may affect molecular adsorption properties, and thus allow these nanoscale structures to be used as templates to direct molecular adsorption. This was found for the adsorption of 2,3-diaminophenazine (DAP), which formed self-assembled porous structures steered by the underlying MTB network in MBE grown MoSe₂ [493], as shown in Fig. 33 (a). This assembly has been attributed to stronger coupling of the MTBs with amino groups in the DAP, and thus causing the assembly of the DAP by alternating T- and L-type aggregation, leaving the vertices of the MTB network free of DAP molecules. A similar decoration of the MTBs was observed for water adsorption, shown in Fig. 33 (b) [494]. Water was adsorbed in UHV with the sample at 20 K. Initial water adsorptions form hexagonal or pentagonal water rings as previously observed for adsorption of other weakly interacting surfaces [495]. These water-rings preferentially adsorb close to the vertices of the MTBs. Further adsorption forms larger disordered or amorphous water islands (like amorphous water found on other inert surfaces [496,497]). Closer inspection of these water islands shows that they are nano-porous water networks. However, in contrast to the DAP the water is decorating the MTBs and their vertices, while leaving the basal plane of the MoSe₂ in between the MTBs free of water. Decoration of MTBs suggests a stronger interaction of the water with the substrate at MTBs, however DFT simulations only find minimal variations of adsorption energies at MTBs compared to defect free basal planes. Substrate induced charge transfer to the MTBs can increase these adsorption energies slightly but alternative mechanisms such as water dissociation and hydrogen adsorption on MTBs may stabilize the water network. There may be other molecules

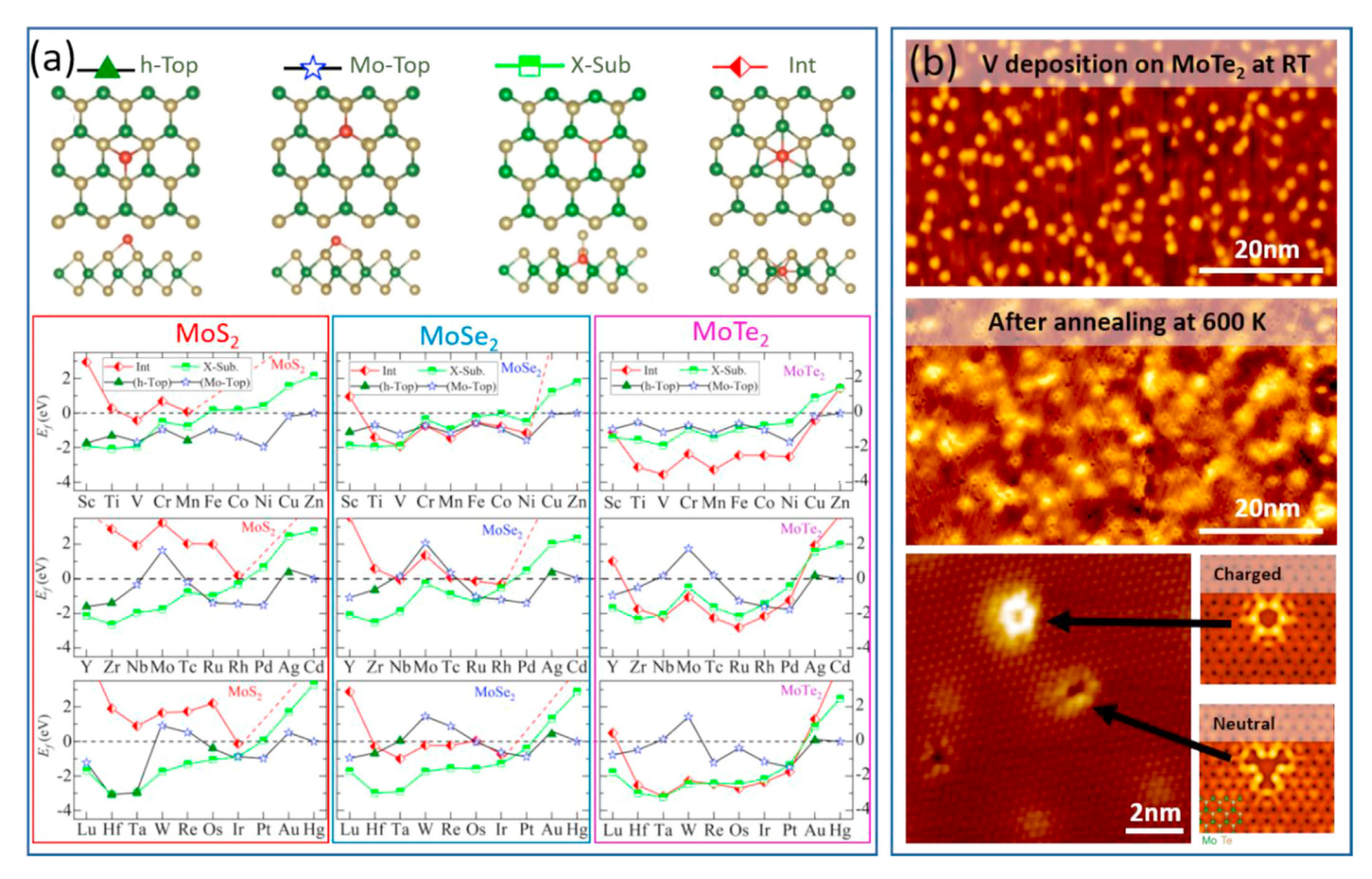


Fig. 34. Incorporation of TM into the H-MoX₂. (a) DFT simulation of formation energies of single TM at two different adsorption sites (h-top and Mo-top), for exchanging sites with a surface chalcogen atom (X-Sub.) and in the interstitial sites (Int). It is seen that many TM gain energy by occupying lattice or interstitial sites, especially for H-MoTe₂. (b) experiments for vapor deposited V on a MoTe₂ surface at room temperature. The V-atoms are dispersed across the surface and no clustering is observed for low V-concentration. Annealing results in the occurrence of two Te-vacancy sites. One site is identified as a neutral vacancy, while brighter contrast is associated with a charged vacancy, which occurs according to DFT calculations if it is associated with a V-atom in the interstitial site. Thus, it is proposed that annealing results in V diffusing into the energetically favored interstitial site and the formation of a Te-vacancy. (a) is reprinted with permission from Ref. [498] Copyright © 2019 American Chemical Society. (b) is reproduced with permission from Ref. [499], Copyright © 2019 Wiley-VCH GmbH.

that even without covalent interactions may exhibit strongly varying interactions with the MTBs versus the basal plane. In first approximation, this may be probed with molecules with suitable HOMO and LUMO levels that enable charge transfer to the MTB induced gap states but not the semiconducting $MoSe_2$ basal planes. Future studies may explore the fundamental adsorption on these line defects further, specifically to use the MTB networks as a template for nanostructured molecular adsorption.

Atomic metal adsorption on TMDs generally results in clustering of the adatoms because of weak interaction with the substrate and strong adhesive energies of metals. Defects in TMDs may act as nucleation sites of such metal clusters, and thus defects induced by annealing or sputtering may affect the nucleation density and the growth of metal clusters. As pointed out above, MTBs are crystal modifications without dangling bonds and may not induce nucleation sites. However, vertices of MTBs are more complex and will contain unsaturated bonds [284]. Au-deposition on MoSe₂-MTB network shows that the gold exclusively nucleates at vertices of MTBs if the surface is completely covered with a MoSe₂ layer, see Fig. 33 (c). For sub-monolayer MoSe₂ on HOPG Au-clusters also form along the edges of the MoSe₂ islands. Thus, such nanopatterned TMDs may be useful for nanocatalyst supports that may prevent sintering of metal clusters.

The formation of MTBs in MoSe₂ and MoTe₂ was explained by the introduction of excess Mo into the lattice (see section 5.4).

Based on this observation, the question if other TMs can also be incorporated into MoX₂ lattices has been addressed. DFT simulations investigated the energies for TMs in interstitial sites, or for exchanging sites with chalcogens [498]. Fig. 34 shows the formation energies for different adsorption configurations of TM on the three H-phase MoX₂. It is apparent that for MoTe₂ the incorporation of many TMs into the TMD matrix is preferred over single atom adsorbing on the surface. This will, however, change once larger atom clusters can form on the surface where the adhesive energies between metal atoms may favor clusters over distributing single atoms. Nevertheless, these results imply that single atoms vapor deposited onto MoTe2, and to a lesser extent on MoSe2 may be incorporated into the lattice. There are few experimental data available for this process. STM studies of V and Ti on MoTe₂ do, however, support such a mechanism [499]. Fig. 34 (b) shows V vapor deposited on MoTe2 at RT. Instead of forming clusters uniformly distributed atomic size protrusions are imaged, which may be associated with V exchanging sites with Te-atoms. After annealing of the surface, these protrusions disappear with two different kinds of Te-vacancies remaining. A regular vacancy that is also observed on the surface without V-doping and Te-vacancies that appear brighter. The latter, based on DFT, has been associated with a charged vacancy due to charge transfer from a V-atom in an adjacent interstitial site, thus forming a defect complex of interstitial plus vacancy. Interestingly, V-doping by this approach

can induce magnetic properties in MoTe₂. There have been a few reports on diluted ferromagnetic TMDs, and detailed characterization of the dopant configurations may help in better understanding these surprising properties. MBE growth of well-defined doped TMDs and their characterization at the atomic scale by STM would provide important information.

As pointed out above, the lack of dangling bonds in TMDs generally results in adatoms to bond weakly to the TMD, and thus causes clustering. However, there are surprising reports in some cases that show dispersion of adatoms on TMDs. For instance, cobalt adatoms on monolayer MoS2 have been reported to form ordered single atom arrays by a sonication induced assembly in solution [500]. It was observed that the adsorbed Co induced a phase transition in MoS₂ to its 1T phase and this may assist in the dispersed adsorption of Co. This single atom array on MoS₂ has been reported to be a superior HER catalyst. Dispersion of single adatoms was also found by vacuum deposition of tin onto 1T"-NbTe₂ surface [501]. In this case the low cohesive energy of Sn may help to prevent clustering. The Sn-atoms adsorb along rows of the 3×1 structure of the distorted 1T" structure. At low coverage, the Sn atoms repel each other as a result of Coulomb repulsion due to charge transfer according to DFT simulations from the substrate to the Sn atom in excess of 0.6 e⁻ per Sn atom. These studies show that adsorption of post-transition metals on TMDs may also be interesting charge transfer dopants and their potential role for tuning the materials properties in monolayer TMDs should be investigated further.

6. Conclusions and outlook

Monolayers of almost all TMDs have been grown by vdW epitaxy and their properties have been characterized in detail by methods like ARPES and STM. These studies have revealed significant modifications of the properties of monolayer materials compared to bulk. Changes occur due to the lack of interlayer interactions that modify electronic structures that have profound effects on band dispersions in semiconductors and cause the transition from indirect to direct band gaps in the H-phase of group VIB TMDs. Reduced charge screening in semiconductors also affects excitons, resulting in large increases in exciton binding energies of TMDs in the 2D limit compared to bulk materials. Changes in metallic TMDs are similarly pronounced as in semiconductors but not always easily understood. Generally, TMDs that exhibit CDW behaviors in the bulk also undergo CDW in the monolayer. Most transitions are even enhanced in the monolayer with an increase in the CDW transition temperatures. Mostly, the periodicity of the lattice distortion in the basal plane remains the same for bulk and monolayers. However, there are notable exceptions, for example for VSe₂, which may be related to the loss of a 3D nesting condition compared to the bulk material. There are also two materials reported that only have a CDW in the monolayer but not in the bulk. VTe2 forms a 1T structure for the monolayer down to low temperatures while in the bulk it exhibits a distorted 1T" structure. This structural variation facilitates a CDW that is like that of the isoelectronic material VSe2 and has been shown to be associated with a Fermi-surface instability. The other material that exhibits a CDW only for the monolayer is TiTe₂. Its CDW may be explained by a phonon instability and this may also help explaining the CDW in its sister compound TiSe2, whose unconventional CDW has been discussed extensively.

Exciting new phenomena may arise through the coupling of CDW with other electronic properties of monolayer materials. A well-known example in the bulk is the coupling of the CDW to the MI states in 1T-TaS₂. It has been shown that a MI state can also be found in monolayer 1T- TaSe₂ (while bulk 1T-TaSe₂ is not a MI).

Moreover, 1T-NbSe2 can be grown as monolayers by MBE (while only the 2H phase exists in bulk form) and this new monolayer material exhibits CDW and MI states, like its 1T Ta-dichalcogenide counterparts. In these materials, the MI state is directly related to their CCDW and it has been shown that modifying the CDW with tip-voltage pulses on bulk 1T-TaS2 surfaces can destroy the MI, giving hints for possible modifications of Mott states also for the monolayers. Monolayer materials, in general, can be more easily modified than bulk surfaces. For instance, charge transfer doping opens new opportunities for tuning materials properties. Alkali metal deposition is a convenient approach for electron doping materials in vacuum, while electron accepting molecules may be used for hole doping. Li-doping of 1T-TaS₂ monolayers, for instance has shown a change of the CDW periodicity from a 3×3 to a 2×2 structure. On TiSe₂, K-doping showed the suppression of CDW with electron doping and the filling of the Ti-3d band. This may also help to induce superconductivity in monolayer TiSe2, like ion-liquid gating has shown for exfoliated flakes. Modifying or inducing new properties in MBE grown TMDs by charge transfer doping appears to be a fruitful future field for gaining a better understanding of quantum phenomena in these materials.

Topologically protected electronic states have become an important aspect of fundamental condensed matter physics. TMDs have made important contributions to this field. Bulk 3D Dirac semimetals have been observed in the group VIII (10) 1T-phases. NiTe₂ is a type I Dirac semimetal while the over-tilted type II Dirac cone has been identified in PtSe₂, PtTe₂, and PdTe₂. Type II Wyle semimetals have been observed in the T_d-phase of MoTe₂ that have indicated the presence of Fermi-arc surface states in ARPES measurements. In context of the main emphasis of this review on monolayer materials, the discovery of the 2D topological insulators of the 1T′-WSe₂ and 1T′-WTe₂ which enables the QSHI, is most noteworthy. Combination of ARPES and STM allowed the identification of the opening of the gap in the inverted bands due to the SOC, while STS allowed a determination of the conducting topologically protected edge states in monolayer islands.

Tuning the properties of TMDs by controlling the growth conditions during MBE is another promising approach for obtaining new materials. This is highlighted by the above-mentioned synthesis of 1T'-WSe2 as a new 2D topological insulator, which has no bulk counterpart as bulk WSe2 only exists in the 1T phase. Other examples of MBE monolayers without bulk counterparts, are the MI 1T-NbSe2 and the CDW-material 1T-VTe2. Others like the semiconducting 1H-CrSe₂ or 1H-CrTe₂ (in contrast to 1T bulk phases) have been theoretically predicted and initial experimental work to synthesize these metastable materials are in progress. Thus, new phases of TMDs may be discovered by controlling growth conditions in their monolayer form. For this to be a more successful approach, guidance from computational screening of potential phases would be desirable. So far, computational predictions, however, have not always been accurate. For instance, a few computational studies suggested that VSe2 should adopt the semiconducting H-structure for monolayers. However, in experiments, the monolayer always shows the same T-structure as known for VSe₂ bulk. This discrepancy may be caused by not taking an energy lowering CDW phase as the ground state into account in the computations. In general, computational predictions must be considered with caution and always require experimental verification. Computation, however, is undoubtedly the approach for accelerating materials discovery and MBE synthesis of chalcogenides is a versatile tool for investigating these predictions.

A challenge in MBE synthesis is that compositional control for chalcogenides cannot just be achieved by controlling the atom flux, because of the low sticking of the chalcogens on the surface. Therefore, compounds that have multiple compositional phases

may require further tuning for obtaining materials with desired compositions. Furthermore, many compositions may be structurally very similar, and thus challenging to distinguish especially for ultrathin films. A common configuration for early TMDs is intercalation compounds, where additional TMs are situated in between TMD lavers. Such intercalation, in between the TMDs can induce new properties in these materials. For instance, Cr₂Te₃ or Cr₃Te₄ are known to exhibit ferromagnetic ordering in their bulk. Therefore, these intercalation compounds are valuable functional materials that can be grown by vdW epitaxy on other vdW substrates. Compounds with different density of ordered intercalants are known, and thus control of the intercalant in the growth process may allow tuning of their properties. Also, the presence of intercalants in between the substrate and the film should be further studied. Another compositional variation in TMDs during MBE growth has been observed for MoSe₂ and MoTe₂ by incorporation of excess Mo not in the vdW gap but directly into 2D lattice by formation of Mo-rich MTB-networks. These form 1D metallic electronic states and it has been shown that these 1D metallic modifications in 2D materials, either as MTBs or island edges, are hosting Tomonaga Luttinger quantum liquids.

In general, while there has been significant progress in the synthesis of mono-to few-layer materials by vdW epitaxy, there has not been any significant work on the growth of heterostructures and superlattices using vdW materials by MBE. The evidence that the materials properties of vdW materials are affected by interlayer interactions and their dielectric environment, suggests that vdW superlattices may be a fruitful avenue for tuning materials properties. In addition to interlayer interactions, that may vary within a moiré structure, charge transfer between layers can cause doping effects that modify the materials properties. Controlling the growth in superlattices is much more challenging than the growth of just monolayers and inhomogeneities will increase with the number of stacks. Vacuum characterization of heterostructures, although not grown by MBE but CVD, has already played an important role in understanding moiré structures. STM and STS of group VI-B semiconductor moirés have demonstrated that the interlayer interactions that are so important to determine the bulk electronic properties of these materials, cause strong local variations within the moiré unit cell. The effect of the moiré structure on the local electronic properties will depend on the TMDs. A first approximation is to expect strong modifications in heterostructures for materials that have strong layer dependent properties. Apart from the group VI-B semiconductors this would also be potentially the case for group 10 noble-metal dichalcogenides, but no heterostructures have yet been reported for these materials.

MBE grown TMDs are also excellent systems to study modifications by interfaces with other materials. This may be either achieved by growing on different substrates or by adsorption of atoms or molecules. Substrate effects are highlighted throughout this review, generally vdW substrates such as HOPG, graphene, or MoS₂, only interact weakly with the grown TMD, and thus these substrates do not affect their properties significantly. Growth on metals (particularly gold), on the other hand, has shown to strongly affect the properties of TMDs. For weakly interacting substrates, modification of the properties of TMDs by adsorption of charge transfer dopants such as alkali-atoms, post-transition metals, or organic molecules can be studied and help us give insight not just of how charge doping may affect many-body physics properties such as CDW and superconductivity, but also structural phase stability and potential for inducing phase changes in these materials. In this review, we also investigate how nanostructures induced in TMDs affect the adsorption of molecules and can be used to control molecular interactions.

Another area in which MBE growth can make contributions is

the controlled doping of layered materials [502]. The flexibility of depositing almost any element in MBE and the relatively low growth temperatures for TMDs, opens opportunities to modify most TMDs with impurities. Doping is most interesting for semiconducting TMDs. For instance, niobium has been suggested as a promising p-type dopant of MoS₂ [503]. However, doping for adjusting the Fermi-level may just be one aspect worthwhile exploring. Recently, several reports suggested that magnetic impurities and intrinsic defects can induce long range magnetic ordering in TMDs [499–507]. Such diluted ferromagnetic materials may offer promise for spintronic applications utilizing the advantages of layered materials and the relatively high Curie temperatures reported in these materials. The origin of the magnetic properties in these materials is, however, still not well understood, and a first step would be to synthesize well defined materials and characterize the dopants and defect-complexes induced by the dopants. In layered materials, dopants may incorporate into the lattice either at TM or chalcogen sites, at interstitial sites, form complex defect structures, or locate in between TMD layers. One study reported that the doping mechanism in monolayers may depend on the growth substrate [508], thus suggesting that the doping and resulting properties are substrate dependent. The magnetic coupling mechanism in diluted layered materials is controversial but MBE grown materials may help in gaining a better understanding. For instance, coupling between magnetic dopants by charge carriers may be probed by controlling the Fermi-level by field-effect of charge transfer doping in MBE grown samples.

In conclusion, initial MBE growth studies of TMDs focused on revealing how properties in TMDs are changed if reduced to the single layer limit. Some materials still await their synthesis and a detailed characterization of their properties as monolayers. This work should be completed and vacuum-vdW epitaxy is a promising approach to prepare monolayer materials and is especially valuable for materials that cannot be easily exfoliated. Future studies will focus more on tuning materials properties for monolayers, synthesize heterostructures, and develop strategies for inducing new functionalities in these materials. The controlled growth that MBE offers, makes it an indispensable tool for advancing the materials research in layered materials.

Acknowledgment

The authors acknowledge financial support from NSF through CHE-1801199 and DMR-1701390.

References

- J.A. Wilson, A.D. Yoffe, The transition metal dichalcogenides discussion and interpretation of the observed optical, electrical and structural properties, Adv. Phys. 18 (1969) 193–335.
- [2] A. Klein, S. Tiefenbacher, V. Eyert, C. Pettenkofer, W. Jaegermann, Electronic band structure of single-crystal and single-layer WS₂: influence of interlayer van der Waals interactions, Phys. Rev. B 64 (2001) 205416.
- [3] K.F. Mak, C. Lee, J. Hone, J. Shan, T.F. Heinz, Atomically thin MoS₂: a new direct-gap semiconductor, Phys. Rev. Lett. 105 (2010) 136805.
- [4] S. Manzeli, D. Ovchinnikov, D. Pasquier, O.V. Yazyev, A. Kis, 2D transition metal dichalcogenides, Nat. Rev. Mater. 2 (2017) 17033.
- [5] C. Huo, Z. Yan, X. Song, H. Zeng, 2D materials via liquid exfoliation: a review on fabrication and applications, Sci. Bull. 60 (2015) 1994–2008.
- [6] G.R. Bhimanapati, Z. Lin, V. Meunier, Y. Jung, J. Cha, S. Das, D. Xiao, Y. Son, M.S. Strano, V.R. Cooper, L. Liang, S.G. Louie, E. Ringe, W. Zhou, S.S. Kim, R.R. Naik, B.G. Sumpter, H. Terrones, F. Xia, Y. Wang, J. Zhu, D. Akinwande, N. Alem, J.A. Schuller, R.E. Schaak, M. Terrones, J.A. Robinson, Recent advances in two-dimensional materials beyond graphene, ACS Nano 9 (2015) 11509—11539.
- [7] N.C.M.A. Islam, J.H. Kim, T.-J. Ko, A. Schropp, L. Hurtado, D. Weitzman, L. Zhai, Y. Jung, Two-dimensional transition metal dichalcogenide hybrid materials for energy applications, Nano Today 19 (2018) 16–40.
- [8] Y.J. Zhang, M. Yoshida, R. Suzuki, Y. Iwasa, 2D crystals of transition metal dichalcogenide and their iontronic functionalities, 2D Mater. 2 (2015) 44004.

- [9] M. Chhowalla, H.S. Shin, G. Eda, L.-J. Li, K.P. Loh, H. Zhang, The chemistry of two-dimensional layered transition metal dichalcogenide nanosheets, Nat. Chem. 5 (2013) 263–275.
- [10] J.R. Brent, N. Savjani, P. O'Brien, Synthetic approaches to two-dimensional transition metal dichalcogenide nanosheets, Prog. Mater. Sci. 89 (2017) 411–478.
- [11] Q. Yun, L. Li, Z. Hu, Q. Lu, B. Chen, H. Zhang, Layered transition metal dichalcogenide-based nanomaterials for electrochemical energy storage, Adv. Mater. 32 (2020) 1903826.
- [12] B.V. Lotsch, Vertical 2D heterostructures, Annu. Rev. Mater. Res. 45 (2015) 85–109.
- [13] C. Tana, H. Zhang, Two-dimensional transition metal dichalcogenide nanosheet-based composites, Chem. Soc. Rev. 44 (2015) 2713–2731.
 [14] Y. Zhang, Y. Yao, M. Getaye, S. Lei, Y.X. Zhan, F. Wang, Z. Wang, J. He, Recent
- [14] Y. Zhang, Y. Yao, M. Getaye, S. Lei, Y.X. Zhan, F. Wang, Z. Wang, J. He, Recent progress in CVD growth of 2D transition metal dichalcogenides and related heterostructures. Adv. Mater. 31 (2019) 1901694.
- [15] X. Duan, C. Wang, A. Pan, R. Yu, X. Duan, Two-dimensional transition metal dichalcogenides as atomically thin semiconductors: opportunities and challenges, Chem. Soc. Rev. 44 (2015) 8859–8876.
- [16] Y. Shi, H. Lib, L.-J. Li, Recent advances in controlled synthesis of twodimensional transition metal dichalcogenides via vapour deposition techniques, Chem. Soc. Rev. 44 (2015) 2744–2756.
- [17] Q. Ji, Y. Zhang, Y. Zhang, Z. Liu, Chemical vapour deposition of group-VIB metal dichalcogenide monolayers: engineered substrates from amorphous to single crystalline, Chem. Soc. Rev. 44 (2015) 2587–2602.
- to single crystalline, Chem. Soc. Rev. 44 (2015) 2587–2602.

 [18] A.G. Rajan, J.H. Warner, D. Blankschtein, M.S. Strano, Generalized mechanistic model for the chemical vapor deposition of 2D transition metal dichalcogenide monolayers. ACS Nano 10 (2016) 4330–4344
- dichalcogenide monolayers, ACS Nano 10 (2016) 4330–4344.

 [19] J.A. Robinson, Growing vertical in the flatland, ACS Nano 10 (2016) 42–45.
- [20] A. Koma, Van der Waals epitaxy for highly lattice-mismatched systems, J. Cryst. Growth 201–202 (1999) 236–241.
- [21] S. Tiefenbacher, C. Pettenkofer, W. Jaegermann, Moiré pattern in LEED obtained by van der Waals epitaxy of lattice mismatched WS₂/MoTe₂(0001) heterointerfaces, Surf. Sci. 450 (2000) 181–190.
- [22] A. Koma, K. Sunouchi, T. Miyajima, Fabrication of ultrathin heterostructures with van der Waals epitaxy, J. Vac. Sci. Technol. B 3 (1985) 724.
- [23] A. Koma, K. Yoshimura, Ultrasharp interfaces grown with van der Waals epitaxy, Surf. Sci. 174 (1986) 556.
- epitaxy, Surr. Sci. 174 (1986) 556. [24] K. Saiki, K. Ueno, T. Shimada, A. Koma, Application of van der Waals epitaxy
- to highly heterogeneous systems, J. Cryst. Growth 95 (1989) 603. [25] A. Koma, K. Saiki, Y. Sato, Heteroepitaxy of a two-dimensional material on a
- three-dimensional material, Appl. Surf. Sci. 41–2 (1989) 451. [26] K. Ueno, K. Saiki, T. Shimada, A. Koma, Epitaxial growth of transition metal
- [26] K. Ueno, K. Saiki, T. Shimada, A. Koma, Epitaxial growth of transition metal dichalcogenides on cleaved faces of mica, J. Vac. Sci. Technol., A 8 (1990) 68.
- [27] K. Ueno, T. Shimada, K. Saiki, A. Koma, Heteroepitaxial growth of layered transition-metal dichalcogenides on sulphur-terminated GaAs (111) surfaces, Appl. Phys. Lett. 56 (1990) 327.
- [28] F.S. Ohuchi, B.A. Parkinson, K. Ueno, A. Koma, Van der Waals epitaxial-growth and characterization of MoSe₂ thin-films on SnS₂, J. Appl. Phys. 68 (1990) 2168.
- [29] F.S. Ohuchi, T. Shimada, B.A. Parkinson, K. Ueno, A. Koma, Growth of MoSe₂ thin films with van der Waals epitaxy, J. Cryst. Growth 111 (1991) 1033–1037.
- [30] A. Koma, Van der Waals epitaxy- a new epitaxial growth method for a highly lattice-mismatched system, Thin Solid Films 216 (1992) 72.
- [31] S. Tiefenbacher, H. Sehnert, C. Pettenkofer, W. Jaegermann, Epitaxial films of WS₂ by metal organic van der Waals epitaxy (MO-VDWE), Surf. Sci. 318 (1994) L1161–L1164.
- [32] R. Schlaf, S. Tiefenbacher, O. Lang, C. Pettenkofer, W. Jaegermann, Van der Waals epitaxy of thin InSe films on MoTe₂, Surf. Sci. 303 (1994) L343–L347.
- [33] O. Lang, R. Schlaf, Y. Tomm, C. Pettenkofer, W. Jaegermann, Single crystalline GaSe/WSe₂ heterointerfaces grown by van der Waals epitaxy: I. Growth conditions, J. Appl. Phys. 75 (1994) 7805.
- [34] R. Schlaf, D. Louder, O. Lang, C. Pettenkofer, W. Jaegermann, K. Nebesny, P. Lee, B.A. Parkinson, N.R. Armstrong, Molecular beam epitaxy growth of thin films of SnS₂ and SnSe₂ on cleaved mica and the basal planes of single-crystal layered semiconductors: reflection high-energy electron diffraction, low-energy electron diffraction, photoemission, and scanning tunneling microscopy/atomic force microscopy characterization, J. Vac. Sci. Technol., A 13 (1995) 1761.
- [35] R. Schlaf, N.R. Armstrong, B.A. Parkinson, C. Pettenkofer, W. Jaegermann, Van der Waals epitaxy of the layered semiconductors SnSe₂ and SnS₂: morphology and growth modes, Surf. Sci. 385 (1997) 1–14.
- [36] R. Schlaf, O. Lang, C. Pettenkofer, W. Jaegermann, Band line-up of layered semiconductor heterointerfaces prepared by van der Waals epitaxy: quantum dipole correction term of the electron affinity rule, J. Appl. Phys. 85 (1999) 2732–2753.
- [37] R. Schlaf, C. Pettenkofer, W. Jaegermann, Band line-up of SnS2/SnSe2/SnS2 semiconductor quantum well prepared by an van der Waals epitaxy, J. Appl. Phys. 85 (1999) 6550–6556.
- [38] R. Rudolph, A. Klein, Y. Tomm, C. Pettenkofer, W. Jaegermann, Van der Waals-Xenotaxy: oriented growth of hexagonal GaSe(0001) on rectangular GaAs(110), Appl. Phys. Lett. 76 (2000) 1101–1103.
- [39] T. Löher, Y. Tomm, C. Pettenkofer, A. Klein, W. Jaegermann, Structural dipoles at interfaces between polar II-VI semiconductors CdS and CdTe and non-

- polar layered transition metal dichalcogenide semiconductors MoTe₂ and WSe₂, Semicond. Sci. Technol. 15 (2000) 514–522.
- [40] M.I.B. Utama, Q. Zhang, J. Zhang, Y. Yuan, F.J. Belarre, J. Arbiol, Q. Xiong, Recent developments and future directions in the growth of nanostructures by van der Waals epitaxy, Nanoscale 5 (2013) 3570–3588.
- [41] J. Kim, C. Bayram, H. Park, C.-W. Cheng, C. Dimitrakopoulos, J.A. Ott, K.B. Reuter, S.W. Bedell, D.K. Sadana, Principle of direct van der Waals epitaxy of single-crystalline films on epitaxial graphene, Nat. Commun. 5 (2014) 4836.
- [42] L. Dai, G. Niu, J. Zhao, H. Zhao, Y. Liu, Y. Wang, Y. Zhang, H. Wu, L. Wang, D. Pfützenreuter, J. Schwarzkopf, C. Dubourdieu, T. Schroeder, Z.-G. Ye, Y.-H. Xief, W. Ren, Toward van der Waals epitaxy of transferable ferroelectric barium titanate films via a graphene monolayer, J. Mater. Chem. C 8 (2020) 3445—3451
- [43] Y. Kim, S.S. Cruz, K. Lee, B.O. Alawode, C. Choi, Y. Song, J.M. Johnson, C. Heidelberger, W. Kong, S. Choi, K. Qiao, I. Almansouri, E.A. Fitzgerald, J. Kong, A.M. Kolpak, J. Hwang, J. Kim, Remote epitaxy through graphene enables two-dimensional material-based layer transfer, Nature 544 (2017) 340–343
- [44] S. Randolph, J. Fowlkes, P. Rack, Focused, nanoscale electron-beam-induced deposition and etching. Crit. Rev. Solid State Mater. Sci. 31 (2006) 55.
- deposition and etching, Crit. Rev. Solid State Mater. Sci. 31 (2006) 55.
 T. Shimada, F.S. Ohuchi, B.A. Parkinson, Thermal decomposition of SnS₂ and SnSe₂: novel molecular-beam epitaxy sources for sulfur and selenium, J. Vac. Sci. Technol. A 10 (1992) 539–542
- Sci. Technol., A 10 (1992) 539–542.

 [46] P. Borna, J. Hall, V. Despoja, I.S. Rakic, M. Petrovic, A. Sohani, C. Busse, T. Michely, M. Kralj, Sulfur structures on bare and graphene-covered Ir(111), J. Phys. Chem. C 124 (2020) 6659–6668.
- [47] A. Rajan, K. Underwood, F. Mazzola, P.D.C. King, Morphology control of epitaxial monolayer transition metal dichalcogenides, Phys. Rev. Mater. 4 (2020) 14003.
- [48] M.-W. Chen, D. Ovchinnikov, S. Lazar, M. Pizzochero, M.B. Whitwick, A. Surrente, M. Baranowski, O.L. Sanchez, P. Gillet, P. Plochocka, O.V. Yazyev, A. Kis, Highly oriented atomically thin ambipolar MoSe₂ grown by molecular beam epitaxy, ACS Nano 11 (2017) 6355–6361.
- [49] A. Ohtake, Y. Sakuma, Effect of substrate orientation on MoSe2/GaAs heteroepitaxy, J. Phys. Chem. C 124 (2020) 5196–5203.
- [50] C.-Z. Xu, X. Wang, P. Chen, D. Flötotto, J.A. Hlevyack, M.-K. Lin, G. Bian, S.-K. Mo, T.-C. Chiang, Experimental and theoretical electronic structure and symmetry effects in ultrathin NbSe₂ films, Phys. Rev. Mater 2 (2018) 64002.
- [51] C.D. Tsoutsou, K.E. Aretouli, P. Tsipas, J. Marquez-Velasco, E. Xenogiannopoulou, N. Kelaidis, S. Aminalragia-Giamini, A. Dimoulas, Epitaxial 2D MoSe₂ (HfSe₂) semiconductor/2D TaSe₂ metal van der Waals heterostructures, ACS Appl. Mater. Interfaces 8 (2016) 1836–1841.
- [52] S. Aminalragia-Giamini, J. Marquez-Velasco, P. Tsipas, D. Tsoutsou, G. Renaud, A. Dimoulas, Molecular beam epitaxy of thin HfTe₂ semimetal films, 2D Mater. 4 (2017) 15001.
- [53] E. Xenogiannopoulou, P. Tsipas, K.E. Aretouli, D. Tsoutsou, S.A. Giamini, C. Bazioti, G.P. Dimitrakopulos, P. Komninou, S. Brems, C. Huyghebaert, I.P. Radu, A. Dimoulas, High-quality, large-area MoSe2 and MoSe2/Bi2Se3 heterostructures on AIN(0001)/Si(111) substrates by molecular beam epitaxy, Nanoscale 7 (2015) 7896–7905.
- 54] S. Fragkos, R. Sant, C. Alvarez, A. Bosak, P. Tsipas, D. Tsoutsou, H. Okuno, G. Renaud, A. Dimoulas, Room temperature commensurate charge density wave in epitaxial strained TiTe₂ multilayer films, Adv. Mater. Interf 6 (2019) 1801850.
- [55] M. Nakano, Y. Wang, Y. Kashiwabara, H. Matsuoka, Y. Iwasa, Layer-by-layer epitaxial growth of scalable WSe₂ on sapphire by molecular beam epitaxy, Nano Lett. 17 (2017) 5595–5599.
- [56] A. Koebel, Y. Zheng, J.F. Petroff, M. Eddrief, L.T. Vinh, C. Sebenne, A transmission electron microscopy structural analysis of GaSe thin films grown on Si(111)substrates, J. Cryst. Growth 154 (1995) 269–274.
- [57] N. Jedrecy, R. Pinchaux, M. Eddrief, Epitaxy of layered compounds: GaSe on Si(111), Phys. Rev. B 56 (1997) 9583–9588.
- [58] R. Rudolph, C. Pettenkofer, A. Klein, W. Jaegermann, Chemical passivation of Si 111 capped by a thin GaSe layer, Appl. Surf. Sci. 167 (2000) 122–124.
- [59] T. Ohta, A. Klust, J.A. Adams, Q. Yu, M.A. Olmstead, F.S. Ohuchi, Atomic structures of defects at GaSe/Si(111) heterointerfaces studied by scanning tunneling microscopy, Phys. Rev. B 69 (2004) 125322.
- [60] S. Meneg, B.R. Schroeder, M.A. Olmstead, Interaction of Se and GaSe with Si(111), Phys. Rev. B 61 (2000) 7215–7218.
- [61] R. Rudolph, C. Pettenkofer, A.A. Bostwick, J.A. Adams, F. Ohuchi, M.A. Olmstead, B. Jaeckel, A. Klein, W. Jaegermann, Electronic structure of the Si(111):GaSe van der Waals-like surface termination, New J. Phys. 7 (2005) 108.
- [62] J. Hass, F. Varchon, J.E. Millan-Otoya, M. Sprinkle, N. Sharma, W.A. de Heer, C. Berger, P.N. First, L. Magaud, E.H. Conrad, Why multilayer graphene on 4H-SiC(000-1) behaves like a single sheet of graphene, Phys. Rev. Lett. 100 (2008) 125504.
- [63] C. Riedl, U. Starke, J. Bernhardt, M. Franke, K. Heinz, Structural properties of the graphene-SiC(0001) interface as a key for the preparation of homogeneous large-terrace graphene surfaces, Phys. Rev. B 76 (2007) 245406.
- [64] C. Riedl, C. Coletti, U. Starke, Structural and electronic properties of epitaxial graphene on SiC(0001): a review of growth, characterization, transfer doping and hydrogen intercalation, J. Phys. D Appl. Phys. 43 (2010) 374009.
- [65] Q. Wang, W. Zhang, L. Wang, K. He, X. Ma, Q. Xue, Large-scale uniform

- bilayer graphene prepared by vacuum graphitization of 6H-SiC(0001) substrates, J. Phys. Condens. Matter 25 (2013) 95002.
- [66] N. Mishra, J. Boeckl, N. Motta, F. Iacopi, Graphene growth on silicon carbide: a review, Phys. Status Solidi 213 (2016) 2277–2289.
- [67] Q. Wang, W. Zhang, L. Wang, K. He, X. Ma, Q. Xue, Large-scale uniform bilayer graphene prepared by vacuum graphitization of 6H-SiC(0001) substrates, J. Phys. Condens, Matter 25 (2013) 95002.
- [68] F. Arnold, R.-M. Stan, S.K. Mahatha, H.E. Lund, D. Curcio, M. Dendzik, H. Bana, E. Travaglia, L. Bignardi, P. Lacovig, D. Lizzit, Z. Li, M. Bianchi, J.A. Miwa, M. Bremholm, S. Lizzit, P. Hofmann, C.E. Sanders, Novel single-layer vanadium sulphide phases, 2D Mater. 5 (2018) 45009.
- [69] M. Batzill, The surface science of graphene: metal interfaces, CVD synthesis, nanoribbons, chemical modifications, and defects, Surf. Sci. Rep. 67 (2012) 83–115.
- [70] S. Wang, X. Wang, J.H. Warner, All chemical vapor deposition growth of MoS₂:h-BN Vvrtical van der Waals heterostructures, ACS Nano 9 (2015) 5246–5254
- [71] A. Yan, J. Velasco Jr., S. Kahn, K. Watanabe, T. Taniguchi, F. Wang, M.F. Crommie, A. Zettl, Direct growth of single- and few-layer MoS2 on h-BN with preferred relative rotation angles, Nano Lett. 15 (2015) 6324–6331.
- [72] M. Zhang, Y. Zhu, X. Wang, Q. Feng, S. Qiao, W. Wen, Y. Chen, M. Cui, J. Zhang, C. Cai, L. Xie, Controlled synthesis of ZrS₂ monolayer and few layers on hexagonal boron nitride, J. Am. Chem. Soc. 137 (2015) 7051–7054.
- [73] S.M. Poh, X. Zhao, S.J.R. Tan, D. Fu, W. Fei, L. Chu, D. Jiadong, W. Zhou, S.J. Pennycook, A.H. Castro Neto, K.P. Loh, Molecular beam epitaxy of highly crystalline MoSe₂ on hexagonal boron nitride, ACS Nano 12 (2018) 7562–7570.
- [74] W. Fu, J. Qiao, X. Zhao, Y. Chen, D. Fu, W. Yu, K. Leng, P. Song, Z. Chen, T. Yu, S.J. Pennycook, S.Y. Quek, K.P. Loh, Room temperature commensurate charge density wave on epitaxially grown bilayer 2H-tantalum sulfide on hexagonal boron nitride, ACS Nano 14 (2020) 3917–3926.
- [75] Q. Zhang, Y. Chen, C. Zhang, C.-R. Pan, M.-Y. Chou, C. Zeng, C.-K. Shih, Bandgap renormalization and work function tuning in MoSe₂/hBN/Ru(0001) heterostructures, Nat. Commun. 7 (2016) 13843.
 [76] A. Tuxen, J. Kibsgaard, H. Gøbel, E. Lægsgaard, H. Topsøe, J.V. Lauritsen,
- [76] A. Tuxen, J. Kibsgaard, H. Gøbel, E. Lægsgaard, H. Topsøe, J.V. Lauritsen, F. Besenbacher, Size threshold in the dibenzothiophene adsorption on MoS₂ nanoclusters, ACS Nano 4 (2010) 4677–4682.
- [77] P. Yang, S. Zhang, S. Pan, B. Tang, Y. Liang, X. Zhao, Z. Zhang, J. Shi, Y. Huan, Y. Shi, S.J. Pennycook, Z. Ren, G. Zhang, Q. Chen, X. Zou, Z. Liu, Y. Zhang, Epitaxial growth of centimeter-scale single-crystal MoS₂ monolayer on Au(111), ACS Nano 14 (2020) 5036–5045.
- [78] M.-H. Whangbo, E. Canadell, Analogies between the concepts of molecular chemistry and solid-state physics concerning structural instabilities. Electronic origin of the structural modulations in layered transition-metal dichalcogenides, J. Am. Chem. Soc. 114 (1992) 9587–9600.
- [79] C. Chen, H.-S. Kim, A.S. Admasu, S.W. Cheong, K. Haule, D. Vanderbilt, W. Wu, Trimer bonding states on the surface of the transition-metal dichalcogenide TaTe₂, Phys. Rev. B 98 (2018) 195423.
- [80] M. Acerce, D. Voiry, M. Chhowalla, Metallic 1T phase MoS₂ nanosheets as supercapacitor electrode materials, Nat. Nanotechnol. 10 (2015) 313.
- [81] R. Kappera, D. Voiry, S.E. Yalcin, W. Jen, M. Acerce, S. Torrel, B. Branch, S. Lei, W. Chen, S. Najmaei, J. Lou, P.M. Ajayan, G. Gupta, A.D. Mohite, M. Chhowalla, Metallic 1T phase source/drain electrodes for field effect transistors from chemical vapor deposited MoS₂, Apl. Mater. 2 (2014) 92516.
- [82] Y. Wang, J. Xiao, H. Zhu, Y. Li, Y. Alsaid, K.Y. Fong, Y. Zhou, S. Wang, W. Shi, Y. Wang, A. Zettl, E.J. Reed, X. Zhang, Structural phase transition in monolayer MoTe₂ driven by electrostatic doping, Nature 550 (2017) 487–491.
- [83] S. Cho, S. Kim, J.H. Kim, J. Zhao, J. Seok, D.H. Keum, J. Baik, D.-H. Choe, K.J. Chang, K. Suenaga, S.W. Kim, Y.H. Lee, H. Yang, Phase patterning for ohmic homojunction contact in MoTe₂, Science 349 (2015) 625–628.
- [84] B. Yan, C. Felser, Topological materials: weyl semimetals annu. Rev. Condens, Matter Phys. 8 (2017) 337–354.
- [85] N. P. Armitage, E. J. Mele, A. Vishwanath, Weyl and Dirac semimetals in threedimensional solids, Rev. Mod. Phys. 90 (2018) 15001.
- [86] J. Ma, K. Deng, L. Zheng, S. Wu, Z. Liu, S. Zhou, D. Sun, Experimental progress on layered topological semimetals, 2D Mater. 6 (2019) 32001.
- [87] S. Jia, S.-Y. Xu, M.Z. Hasan, Weyl semimetals, Fermi arcs and chiral anomalies, Nat. Mater. 15 (2016) 1140–1144.
- [88] A.A. Soluyanov, D. Gresch, Z. Wang, Q.S. Wu, M. Troyer, X. Dai, B.A. Bernevig, Type-II weyl semimetals, Nature 527 (2015) 495–498.
- [89] Z. Wang, D. Gresch, A.A. Soluyanov, W. Xie, S. Kushwaha, X. Dai, M. Troyer, R.J. Cava, B.A. Bernevig, MoTe₂: a Type-II Weyl topological metal, Phys. Rev. Lett. 117 (2016) 56805.
- [90] Y. Sun, S.-C. Wu, M.N. Ali, C. Felser, B. Yan, Prediction of Weyl semimetal in orthorhombic MoTe₂, Phys. Rev. B 92 (2015) 161107(R).
- [91] J. Jiang, Z.K. Liu, Y. Sun, H.F. Yang, C.R. Rajamathi, Y.P. Qi, L.X. Yang, C. Chen, H. Peng, C.-C. Hwang, S.Z. Sun, S.-K. Mo, I. Vobornik, J. Fujii, S.S.P. Parkin, C. Felser, B.H. Yan, Y.L. Chen, Signature of type-II Weyl semimetal phase in MoTe₂, Nat. Commun. 8 (2017) 13973.
- [92] K. Deng, G. Wan, P. Deng, K. Zhang, S. Ding, E. Wang, M. Yan, H. Huang, H. Zhang, Z. Xu, J. Denlinger, A. Fedorov, H. Yang, W. Duan, H. Yao, Y. Wu, S. Fan, H. Zhang, X. Chen, S. Zhou, Experimental observation of topological Fermi arcs in type-II Weyl semimetal MoTe₂, Nat. Phys. 12 (2016) 1105–1110.
- [93] L. Huang, T.M. McCormick, M. Ochi, Z. Zhao, M.-T. Suzuki, R. Arita, Y. Wu,

- D. Mou, H. Cao, J. Yan, N. Trivedi, A. Kaminski, Spectroscopic evidence for a type II Weyl semimetallic state in MoTe₂, Nat. Mater. 15 (2016) 1155–1160.
- [94] D. Iaia, G. Chang, T.-R. Chang, J. Hu, Z. Mao, H. Lin, S. Yan, V. Madhavan, Searching for topological Fermi arcs via quasiparticle interference on a type-II Weyl semimetal MoTe₂, npj Quantum Mater. 3 (2018) 38.
- [95] Y.-Y. Lv, L. Cao, X. Li, B.-B. Zhang, K. Wang, B. Pang, L. Ma, D. Lin, S.-H. Yao, J. Zhou, Y.B. Chen, S.-T. Dong, W. Liu, M.-H. Lu, Y. Chen, Y.-F. Chen, Composition and temperature-dependent phase transition in miscible Mo_{1-x}W_xTe₂ single crystals, Sci. Rep. 7 (2017) 44587.
- [96] X. Qian, J. Liu, L. Fu, J. Li, Quantum spin Hall effect in two-dimensional transition metal dichalcogenides, Science 346 (2014) 1344.
- [97] F. Zheng, C. Cai, S. Ge, X. Zhang, X. Liu, H. Lu, Y. Zhang, J. Qiu, T. Taniguchi, K. Watanabe, S. Jia, J. Qi, J.-H. Chen, D. Sun, J. Feng, On the quantum spin Hall gap of monolayer 1T'-WTe₂, Adv. Mater. 28 (2016) 4845–4851.
- gap of monolayer 1T'-WTe₂, Adv. Mater. 28 (2016) 4845–4851.

 [98] S. Tang, C. Zhang, D. Wong, Z. Pedramrazi, H.-Z. Tsai, C. Jia, B. Moritz, M. Claassen, H. Ryu, S. Kahn, J. Jiang, H. Yan, M. Hashimoto, D. Lu, R.G. Moore, C.-C. Hwang, C. Hwang, Z. Hussain, Y. Chen, M.M. Ugeda, Z. Liu, X. Xie, T.P. Devereaux, M.F. Crommie, S.-K. Mo, Z.-X. Shen, Quantum spin Hall state in monolayer 1T'-WTe₂, Nat. Phys. 13 (2017) 683.
- [99] S. Wu, V. Fatemi, Q.D. Gibson, K. Watanabe, T. Taniguchi, R.J. Cava, P. Jarillo-Herrero, Observation of the quantum spin Hall effect up to 100 Kelvin in a monolayer crystal, Science 359 (2018) 76–79.
- [100] Z. Fei, T. Palomaki, S. Wu, W. Zhao, X. Cai, B. Sun, P. Nguyen, J. Finney, X. Xu, D.H. Cobden, Edge conduction in monolayer WTe₂, Nat. Phys. 13 (2017) 677–682.
- [101] E. Sajadi, T. Palomaki, Z. Fei, W. Zhao, P. Bement, C. Olsen, S. Luescher, X. Xu, J.A. Folk, D.H. Cobden, Gate-induced superconductivity in a monolayer to-pological insulator, Science 362 (2018) 922–925.
- [102] K. Nikonov, N. Ehlen, B. Senkovskiy, N. Saigal, A. Fedorov, A. Nefedov, C. Wöll, G. Di Santo, L. Petaccia, A. Grüneis, Synthesis and spectroscopic characterization of alkali-metal intercalated ZrSe₂, Dalton Trans. 47 (2018) 2986–2991.
- [103] C. Habenicht, J. Simon, M. Richter, R. Schuster, M. Knupfer, B. Büchner, Potassium-intercalated bulk HfS₂ and HfSe₂: phase stability, structure, and electronic structure, Phys. Rev. Mater. 4 (2020) 64002.
- [104] W. Zhang, Z. Huang, W. Zhang, Y. Li, Two-dimensional semiconductors with possible high room temperature mobility, Nano Res. 7 (2014) 1731–1737.
- [105] S. Kim, A. Konar, W.-S. Hwang, J.H. Lee, J. Lee, J. Yang, C. Jung, H. Kim, J.-B. Yoo, J.-Y. Choi, Y.W. Jin, S.Y. Lee, D. Jena, W. Choi, K. Kim, High-mobility and low-power thin-film transistors based on multilayer MoS₂ crystals, Nat. Commun. 3 (2012) 1011.
- [106] X. Li, J.T. Mullen, Z. Jin, K.M. Borysenko, M.B. Nardelli, K.W. Kim, Intrinsic electrical transport properties of monolayer silicon and MoS₂ from first principles, Phys. Rev. B 87 (2013) 115418.
- [107] M.J. Mleczko, C. Zhang, H.R. Lee, H.-H. Kuo, B. Magyari-Köpe, R.G. Moore, Z.-X. Shen, I.R. Fisher, Y. Nishi, E. Pop, HfSe₂ and ZrSe₂: two-dimensional semiconductors with native high-κ oxides, Sci. Adv. 3 (2017) e1700481.
- [108] C. Wang, L. Dotson, M. McKelvy, W. Glaunsinger, Scanning tunneling spectroscopy investigation of charge transfer in model intercalation compounds Ti_{1+x} S₂, J. Phys. Chem. 99 (1995) 8216–8221.
- [109] J. Yuhara, N. Isobe, K. Nishino, Y. Fujii, L.H. Chan, M. Araidai, M. Nakatake, Morphology and electronic structure of Sn-Intercalated TiS₂(0001) layers, J. Phys. Chem. C 123 (2019) 22293–22298.
- [110] A. Zunger, A.J. Freeman, Band structure and lattice instability of TiSe₂, Phys. Rev. B 17 (1978) 1839–1842.
- [111] N. Suzuki, A. Yamamoto, K. Motizuki, Microscopic theory of the CDW state of 1T-TiSe₂, J. Phys. Soc. Jpn. 54 (1985) 4668–4679.
- [112] J. Van Wezel, P. Nahai-Williamson, S.S. Saxena, An alternative interpretation of recent ARPES measurements on TiSe₂, Europhys. Lett. 89 (2010) 47004.
- [113] C. Monney, C. Battaglia, H. Cercellier, P. Aebi, H. Beck, Exciton condensation driving the periodic lattice distortion of 1T —TiSe₂, Phys. Rev. Lett. 106 (2011) 106404.
- [114] H. Cercellier, C. Monney, F. Clerc, C. Battaglia, L. Despont, M.G. Garnier, H. Beck, P. Aebi, L. Patthey, H. Berger, L. Forró, Evidence for an excitonic insulator phase in 1T-TiSe₂, Phys. Rev. Lett. 99 (2007) 146403.
- [115] C. Monney, H. Cercellier, F. Clerc, C. Battaglia, E.F. Schwier, C. Didiot, M.G. Garnier, H. Beck, P. Aebi, H. Berger, L. Forró, L. Patthey, Spontaneous exciton condensation in 1T-TiSe₂: BCS-like approach, Phys. Rev. B 79 (2009) 45116
- [116] E. Möhr-Vorobeva, S.L. Johnson, P. Beaud, U. Staub, R. De Souza, C. Milne, G. Ingold, J. Demsar, H. Schaefer, A. Titov, Nonthermal melting of a charge density wave in TiSe₂, Phys. Rev. Lett. 107 (2011) 36403.
- [117] M.M. May, C. Brabetz, C. Janowitz, R. Manzke, Charge-density-wave phase of 1T-TiSe2: the influence of conduction band population, Phys. Rev. Lett. 107 (2011) 176405.
- [118] T. Rohwer, S. Hellmann, M. Wiesenmayer, C. Sohrt, A. Stange, B. Slomski, A. Carr, Y. Liu, L.M. Avila, M. Kallane, S. Mathias, L. Kipp, K. Rossnagel, M. Bauer, Collapse of long-range order tracked by time-resolved photoemission at high momenta, Nature 471 (2011) 490–493.
- [119] B. Guster, E. Canadell, M. Pruneda, P. Ordejón, First principles analysis of the CDW instability of single-layer 1T-TiSe₂ and its evolution with charge carrier density, 2D Mater. 5 (2018) 25024.
- [120] J. Ishioka, Y.H. Liu, K. Shimatake, T. Kurosawa, K. Ichimura, Y. Toda, M. Oda, S. Tanda, Chiral charge-density waves, Phys. Rev. Lett. 105 (2010) 176401.
- [121] J.-P. Castellan, S. Rosenkranz, R. Osborn, Q. Li, K.E. Gray, X. Luo, U. Welp,

- G. Karapetrov, J.P.C. Ruff, J. van Wezel, Chiral phase transition in charge ordered 1T–TiSe₂, Phys. Rev. Lett. 110 (2013) 196404.
- [122] M. Iavarone, R. Di Capua, X. Zhang, M. Golalikhani, S.A. Moore, G. Karapetrov, Evolution of the charge density wave state in Cu_xTiSe₂, Phys. Rev. B 85 (2012) 155103.
- [123] J. van Wezel, The chiral charge density wave transition in 1T-TiSe₂, J. Phys.: Confer. Series 391 (2012) 12167.
- [124] M.-K. Lin, J.A. Hlevyack, P. Chen, R.-Y. Liu, T.-C. Chiang, Comment on "Chiral phase transition in charge ordered 1T-TiSe₂", Phys. Rev. Lett. 122 (2019) 229701.
- [125] B. Hildebrand, T. Jaouen, M.-L. Mottas, G. Monney, C. Barreteau, E. Giannini, D.R. Bowler, P. Aebi, Local real-space view of the achiral 1T-TiSe $_2$ 2 \times 2 \times 2 charge density wave, Phys. Rev. Lett. 120 (2018) 136404.
- [126] E. Morosan, H.W. Zandbergen, B.S. Dennis, J.W.G. Bos, Y. Onose, T. Klimczuk, A.P. Ramirez, N.P. Ong, R.J. Cava, Superconductivity in Cu_xTiSe₂, Nat. Phys. 2 (2006) 544-550.
- [127] L.J. Li, E.C.T. O'Farrell, K.P. Loh, G. Eda, B. Özyilmaz, A.H. Castro Neto, Controlling many-body states by the electric-field effect in a two-dimensional material, Nature 534 (2016) S21—S22.
- [128] A. Kogar, G. A. de la Pena, S. Lee, Y. Fang, S. X.-L. Sun, D. B. Lioi, G. Karapetrov, K. D. Finkelstein, J. P. C. Ruff, P. Abbamonte, S. Rosenkranz, Observation of a charge density wave incommensuration near the superconducting dome in Cu_xTiSe₂, Phys. Rev. Lett. 118 (2017) 27002.
- [129] S. Yan, D. Iaia, E. Morosan, E. Fradkin, P. Abbamonte, V. Madhavan, Influence of domain walls in the incommensurate charge density wave state of Cu intercalated 1T—TiSe₂, Phys. Rev. Lett. 118 (2017) 106405.
- [130] P. Chen, Y.-H. Chan, X.-Y. Fang, Y. Zhang, M.Y. Chou, S.-K. Mo, Z. Hussain, A.-V. Fedorov, T.-C. Chiang, Charge density wave transition in single-layer titanium disclenide. Nat. Commun. 6 (2015) 8943.
- tanium diselenide, Nat. Commun. 6 (2015) 8943.
 [131] P. Chen, Y.-H. Chan, M.-H. Wong, X.-Y. Fang, M.Y. Chou, S.-K. Mo, Z. Hussain, A.-V. Fedorov, T.-C. Chiang, Dimensional effects on the charge density waves in ultrathin films of TiSe₂, Nano Lett. 16 (2016) 6331–6336.
- [132] S. Kolekar, M. Bonilla, Y. Ma, H.C. Diaz, M. Batzill, Layer-and substrate-dependent charge density wave criticality in 1T–TiSe₂, 2D Mater. 5 (2017) 15006.
- [133] S. Kolekar, M. Bonilla, H.C. Diaz, M. Hashimoto, D. Lu, M. Batzill, Controlling the charge density wave transition in monolayer TiSe₂: substrate and doping effects, Adv. Quantum Technol 1 (2018) 1800070.
- [134] J.F. Zhao, H.W. Ou, G. Wu, B.P. Xie, Y. Zhang, D.W. Shen, J. Wei, L.X. Yang, J.K. Dong, M. Arita, H. Namatame, M. Taniguchi, X.H. Chen, D.L. Feng, Evolution of the electronic structure of 1T-Cu_xTiSe₂, Phys. Rev. Lett. 99 (2007) 146401.
- [135] P. Chen, W.W. Pai, Y.-H. Chan, A. Takayama, C.-Z. Xu, A. Karn, S. Hasegawa, M.Y. Chou, S.-K. Mo, A.-V. Fedorov, T.-C. Chiang, Emergence of charge density waves and a pseudogap in single-layer TiTe₂, Nat. Commun. 8 (2017) 516.
- [136] K. Lasek, P.M. Coelho, K. Zberecki, Y. Xin, S. Kolekar, J. Li, M. Batzill, Molecular beam epitaxy of transition metal (Ti-, V-, and Cr-) tellurides: from monolayer ditellurides to multilayer self-intercalation compounds, ACS Nano 14 (2020) 8473—8484.
- [137] B. Guster, R. Robles, M. Pruneda, E. Canadell, P. Ordejón, 2×2 charge density wave in single-layer TiTe₂, 2D Mater. 6 (2019) 15027.
- [138] Z. Muhammad, B. Zhang, H. Lv, H. Shan, Z. ur Rehman, S. Chen, Z. Sun, X. Wu, A. Zhao, L. Song, Transition from semimetal to semiconductor in ZrTe₂ induced by Se substitution, ACS Nano 14 (2020) 835–841.
- [139] G. Tenorio, L. Bucio, R. Escudero, Filamentary superconductivity in semiconducting policrystalline ZrSe₂ compound with Zr vacancies, J. Supercond. Nov. Magnetism 30 (2017) 2381–2386.
- [140] Z. Muhammad, K. Mu, H. Lv, C. Wu, Z. ur Rehman, M. Habib, Z. Sun, X. Wu, L. Song, Electron doping induced semiconductor to metal transitions in ZrSe₂ layers via copper atomic intercalation, Nano Res. 11 (2018) 4914–4922.
- [141] Z. Muhammad, M.W. Ali, I.A. Mir, Q.U. Khan, L. Zhu, Copper-doped induced ferromagnetic halfmetal zirconium diselenide single crystals, Nanotechnology 31 (2020) 235704.
- [142] M. Zhang, Y. Zhu, X. Wang, Q. Feng, S. Qiao, W. Wen, Y. Chen, M. Cui, J. Zhang, C. Cai, L. Xie, Controlled synthesis of ZrS₂ monolayer and few layers on hexagonal boron nitride, J. Am. Chem. Soc. 137 (2015) 7051–7054.
- [143] P. Tsipas, D. Tsoutsou, J. Marque-Velasco, K.E. Aretoulia, E. Xenogiannopoulou, E. Vassalou, G. Kordas, A. Dimoulas, Epitaxial ZrSe₂/MoSe₂ semiconductor v.d. Waals heterostructures on wide band gap AlN substrates, Microelectron. Eng. 147 (2015) 269–272.
- [144] P. Tsipas, D. Tsoutsou, S. Fragkos, R. Sant, C. Alvarez, H. Okuno, G. Renaud, R. Alcotte, T. Baron, A. Dimoulas, Massless Dirac fermions in ZrTe₂ semimetal grown on InAs(111) by van der Waals epitaxy, ACS Nano 12 (2018) 1696–1703.
- [145] H. Wang, C.H. Chan, C.H. Suen, S.P. Lau, J.-Y. Dai, Magnetotransport properties of layered topological material ZrTe₂ thin film, ACS Nano 13 (2019) 6008–6016.
- [146] M. Traving, T. Seydel, L. Kipp, M. Skibowski, F. Starrost, E.E. Krasovskii, A. Perlov, W. Schattke, Combined photoemission and inverse photoemission study of HfS₂, Phys. Rev. B 63 (2001) 35107.
- [147] C. Kreis, S. Werth, R. Adelung, L. Kipp, M. Skibowski, E.E. Krasovskii, W. Schattke, Valence and conduction band states of HfS₂: from bulk to a single layer, Phys. Rev. B 68 (2003) 235331.
- [148] R. Yue, A.T. Barton, H. Zhu, A. Azcatl, L.F. Pena, J. Wang, X. Peng, N. Lu, L. Cheng, R. Addou, S. McDonnell, L. Colombo, J.W.P. Hsu, J. Kim, M.J. Kim,

- R.M. Wallace, C.L. Hinkle, HfSe₂ thin films: 2D transition metal dichalcogenides grown by molecular beam epitaxy, ACS Nano 9 (2015) 474–480.
- [149] W. Jolie, T. Knispel, N. Ehlen, K. Nikonov, C. Busse, A. Grüneis, T. Michely, Charge density wave phase of VSe₂ revisited, Phys. Rev. B 99 (2019) 115417.
- [150] D. Won, D.H. Kiem, H. Cho, D. Kim, Y. Kim, M.Y. Jeong, C. Seo, J. Kim, J.-G. Park, M.J. Han, H. Yang, S. Cho, Polymorphic spin, charge, and lattice waves in vanadium ditelluride, Adv. Mater. 32 (2020) 1906578.
 [151] A.H.M.A. Wasey, S. Chakrabarty, G.P. Das, Quantum size effects in layered
- [151] A.H.M.A. Wasey, S. Chakrabarty, G.P. Das, Quantum size effects in layered VX₂ (X=S, Se) materials: manifestation of metal to semimetal or semiconductor transition, J. Appl. Phys. 117 (2015) 64313.
- [152] P. Manchanda, R. Skomski, 2D transition-metal diselenides: phase segregation, electronic structure, and magnetism, J. Phys. Condens. Matter 28 (2016) 64002.
- [153] W.-Y. Tong, S.-J. Gong, X. Wan, C.-G. Duan, Concepts of ferrovalley material and anomalous valley Hall effect Nat, Commun. Now. 7 (2016) 13612.
- [154] M. Esters, R.G. Hennig, D.C. Johnson, Dynamic instabilities in strongly correlated VSe₂ monolayers and bilayers, Phys. Rev. B 96 (2017) 235147.
 [155] H.-R. Fuh, C.-R. Chang, Y.-K. Wang, R.F.L. Evans, R.W. Chantrell, H.-T. Jeng,
- [155] H.-R. Fuh, C.-R. Chang, Y.-K. Wang, R.F.L. Evans, R.W. Chantrell, H.-T. Jeng, Newtype single-layer magnetic semiconductor in transition-metal dichalcogenides VX₂ (X = S, Se and Te), Sci. Rep. 6 (2016) 32625.
- [156] F. Li, K. Tu, Z. Chen, Versatile electronic properties of VSe₂ bulk, few-layers, monolayer, nanoribbons, and nanotubes: a computational exploration, J. Phys. Chem. C 118 (2014) 21264–21274.
- [157] Y. Ma, Y. Dai, M. Guo, C. Niu, Y. Zhu, B. Huang, Evidence of the existence of magnetism in pristine VX₂ monolayers (X = S, Se) and their strain-induced tunable magnetic properties, ACS Nano 6 (2012) 1695–1701.
- [158] J. Du, C. Xia, W. Xiong, T. Wang, Y. Jia, J. Li, Two-dimensional transition-metal dichalcogenides-based ferromagnetic van der Waals heterostructures, Nanoscale 9 (2017) 17585–17592.
- [159] W. Chen, J. Zhang, Y. Nie, Q. Xia, G. Guo, Electronic structure and magnetism of MTe₂ (M = Ti, V, Cr, Mn, Fe, Co and Ni) monolayers, J. Magn. Magn Mater. 508 (2020) 166878.
- [160] M. Bonilla, S. Kolekar, Y. Ma, H.C. Diaz, V. Kalappattil, R. Das, T. Eggers, H.R. Gutierrez, M.-H. Phan, M. Batzill, Strong room-temperature ferromagnetism in VSe₂ monolayers on van der Waals substrates, Nat. Nanotechnol. 13 (2018) 289–293.
- [161] Z.-L. Liu, X. Wu, Y. Shao, J. Qi, Y. Cao, L. Huang, C. Liu, J.-O. Wang, Q. Zheng, Z.-L. Zhu, K. Ibrahim, Y.-L. Wang, H.-J. Gao, Epitaxially grown monolayer VSe2: an air-stable magnetic two-dimensional material with low work function at edges, Sci. Bull. 63 (2018) 419–425.
- [162] G. Duvjir, B.K. Choi, I. Jang, S. Ulstrup, S. Kang, T.T. Ly, S. Kim, Y.H. Choi, C. Jozwiak, A. Bostwick, E. Rotenberg, J.-G. Park, R. Sankar, K.-S. Kim, J. Kim, Y.J. Chang, Emergence of a metal—insulator transition and high-temperature charge-density waves in VSe₂ at the monolayer limit, Nano Lett. 18 (2018) 5432—5438.
- [163] J. Feng, D. Biswas, A. Rajan, M.D. Watson, F. Mazzola, O.J. Clark, K. Underwood, I. Marković, M. McLaren, A. Hunter, D.M. Burn, L.B. Duffy, S. Barua, G. Balakrishnan, F. Bertran, P. Le Fèvre, T.K. Kim, G. van der Laan, T. Hesjedal, P. Wahl, P.D.C. King, Electronic structure and enhanced chargedensity wave order of monolayer VSe₂, Nano Lett. 18 (2018) 4493–4499, 7.
- [164] P. Kwan, J. Wong, W. Zhang, F. Bussolotti, X. Yin, T.S. Herng, L. Zhang, Y.L. Huang, G. Vinai, S. Krishnamurthi, D.W. Bukhvalov, Y.J. Zheng, R. Chua, A.T. N'Diaye, S.A. Morton, C.-Y. Yang, K.-H.O. Yang, P. Torelli, W. Chen, K.E.J. Goh, J. Ding, M.-T. Lin, G. Brocks, M.P. de Jong, A.H. Castro Neto, A.T.S. Wee, Evidence of spin frustration in a vanadium diselenide monolayer magnet, Adv. Mater. 31 (2019) 1901185.
- [165] G. Vinai, C. Bigi, A. Rajan, M.D. Watson, T.-L. Lee, F. Mazzola, S. Modesti, S. Barua, M.C. Hatnean, G. Balakrishnan, P.D.C. King, P. Torelli, G. Rossi, G. Panaccione, Proximity-induced ferromagnetism and chemical reactivity in few-layer Heterostructures, Phys. Rev. B 101 (2020) 35404.
- [166] W. Zhang, L. Zhang, P.K.J. Wong, J. Yuan, G. Vinai, P. Torelli, G. van der Laan, Y.P. Feng, A.T.S. Wee, Magnetic transition in monolayer VSe₂ via interface hybridization, ACS Nano 13 (2019) 8997–9004.
- [167] R. Chua, J. Yang, X. He, X. Yu, W. Yu, F. Bussolotti, P.K.J. Wong, K.P. Loh, M.B.H. Breese, K.E.J. Goh, Y.L. Huang, A.T.S. Wee, Can reconstructed Sedeficient line defects in monolayer VSe₂ induce magnetism? Adv. Mater. 32 (2020) 2000693.
- [168] P.M. Coelho, K.N. Cong, M. Bonilla, S. Kolekar, M.-H. Phan, J. Avila, M.C. Asensio, I.I. Oleynik, M. Batzill, Charge density wave state suppresses ferromagnetic ordering in VSe₂ monolayers, J. Phys. Chem. C 123 (2019) 14089—14096.
- [169] K. Terashima, T. Sato, H. Komatsu, T. Takahashi, N. Maeda, K. Hayashi, Charge-density wave transition of 1T–VSe₂ studied by angle-resolved photoemission spectroscopy, Phys. Rev. B 68 (2003) 155108.
- [170] V.N. Strocov, M. Shi, M. Kobayashi, C. Monney, X. Wang, J. Krempasky, T. Schmitt, L. Patthey, H. Berger, P. Blaha, Three-dimensional electron realm in VSe₂ by soft-x-ray photoelectron spectroscopy: origin of charge-density waves, Phys. Rev. Lett. 109 (2012) 86401.
- [171] P. Chen, Woei Wu Pai, Y.-H. Chan, V. Madhavan, M.Y. Chou, S.-K. Mo, A.-V. Fedorov, T.-C. Chiang, Unique gap structure and symmetry of the charge density wave in single-layer VSe₂, Phys. Rev. Lett. 121 (2018) 196402.
- [172] T.T. Ly, G. Duvjir, N.H. Lam, J. Kim, B.K. Choi, Y.J. Chang, $\sqrt{3} \times 2$ and $\sqrt{3} \times \sqrt{7}$ charge density wave driven by lattice distortion in monolayer VSe₂, J. Kor. Phys. Soc. 76 (2020) 412–415.
- [173] A.O. Fumega, M. Gobbi, P. Dreher, W. Wan, C. González-Orellana, M. Peña-

- Díaz, C. Rogero, J. Herrero-Martín, P. Gargiani, M. Ilyn, M.M. Ugeda, Victor Pardo, S. Blanco-Canosa. Absence of ferromagnetism in VSe₂ caused by its charge density wave phase, J. Phys. Chem. C 123 (2019) 27802–27810.
- [174] G. Duvjir, B.K. Choi, T.T. Ly, N.H. Lam, S.-H. Chun, K. Jang, A. Soon, Y.J. Chang, J. Kim, Novel polymorphic phase of two-dimensional VSe₂: the 1T' structure and its lattice dynamics, Nanoscale 11 (2019) 20096–20101.
- [175] G. Chen, S.T. Howard, A.B. Maghirang III, K.N. Cong, K. Cai, S.C. Ganguli, W. Sweich, E. Morosan, I.I. Oleynik, F.-C. Chuang, H. Lin, V. Madhavan, Correlating structural, electronic, and magnetic properties of epitaxial VSe₂ thin films, Phys. Rev. B 102 (2020) 115149.
- [176] M. Nakano, Y. Wang, S. Yoshida, H. Matsuoka, Y. Majima, K. Ikeda, Y. Hirata, Y. Takeda, H. Wadati, Y. Kohama, Y. Ohigashi, M. Sakano, K. Ishizaka, Y. Iwasa, Intrinsic 2D ferromagnetism in V₅Se₈ epitaxial thin films, Nano Lett. 19 (2019) 8806–8810.
- [177] M. Nakanishi, K. Yoshimura, K. Kosuge, T. Goto, T. Fujii, J. Takada, Anomalous field-induced magnetic transitions in V₅X₈ (X=S, Se), J. Magn. Magn Mater. 221 (2000) 301–306.
- [178] K.D. Bronsema, G.W. Bus, G.A. Wiegers, The crystal structure of vanadium ditelluride, V_{1+x}Te₂, J. Solid State Chem. 53 (1984) 415–421.
 [179] P.M. Coelho, K. Lasek, K.N. Cong, J. Li, W. Niu, W. Liu, I.I. Oleynik, M. Batzill,
- [179] P.M. Coelho, K. Lasek, K.N. Cong, J. Li, W. Niu, W. Liu, I.I. Oleynik, M. Batzill, Monolayer modification of VTe₂ and its charge density wave, J. Phys. Chem. Lett. 10 (2019) 4987–4993.
- [180] P.K.J. Wong, W. Zhang, J. Zhou, F. Bussolotti, X. Yin, L. Zhang, A.T. N'Diaye, S.A. Morton, W. Chen, J. Goh, M.P. de Jong, Y.P. Feng, A.T.S. Wee, Metallic 1T phase, 3d¹ electronic configuration and charge density wave order in molecular beam epitaxy grown monolayer vanadium ditelluride, ACS Nano 13 (2019) 12894—12900.
- [181] G. Miao, S. Xue, B. Li, Z. Lin, B. Liu, X. Zhu, W. Wang, J. Guo, Real-space investigation of the charge density wave in VTe₂ monolayer with broken rotational and mirror symmetries. Phys. Rev. B 101 (2020) 35407.
- rotational and mirror symmetries, Phys. Rev. B 101 (2020) 35407.

 [182] Y. Wang, J. Ren, J. Li, Y. Wang, H. Peng, P. Yu, W. Duan, S. Zhou, Evidence of charge density wave with anisotropic gap in monolayer VTe₂ film, Phys. Rev. B 100 (2019) 241404(R).
- [183] E. Canadell, S. Jobic, R. Brec, J. Rouxel, M.-H. Whangbo, Importance of short interlayer Te-Te contacts for the structural distortions and physical properties of Cdl₂-Type layered transition metal ditellurides, J. Solid State Chem. 99 (1992) 99.
- [184] M. Leroux, M. Le Tacon, M. Calandra, L. Cario, M.-A. Measson, P. Diener, E. Borrissenko, A. Bosak, P. Rodiere, Anharmonic suppression of Charge density wave in 2H-NbS₂, Phys. Rev. B 97 (2018) 195140.
- [185] M. van Maaren, G. Schaeffer, Superconductivity in group V^a dichalcogenides, Phys. Lett. 20 (1966) 131.
- [186] C. Battaglia, H. Cercellier, F. Clerc, L. Despont, M.G. Garnier, C. Koitzsch, P. Aebi, H. Berger, L. Forró, C. Ambrosch-Draxl, Fermi-surface-induced lattice distortion in NbTe₂, Phys. Rev. B 72 (2005) 195114.
- [187] R.-M. Stan, S.K. Mahatha, M. Bianchi, C.E. Sanders, D. Curcio, P. Hofmann, J.A. Miwa, Epitaxial single-layer NbS₂ on Au(111): synthesis, structure, and electronic properties, Phys. Rev. Mater. 3 (2019) 44003.
- [188] Y. Nakata, K. Sugawara, S. Ichinokura, Y. Okada, T. Hitosugi, T. Koretsune, K. Ueno, S. Hasegawa, T. Takahashi, T. Sato, Anisotropic band splitting in monolayer NbSe₂: implications for superconductivity and charge density wave, npj 2D Mater. Appl. 2 (2018) 12.
- [189] M.M. Ugeda, A.J. Bradley, Y. Zhang, S. Onishi, Y. Chen, W. Ruan, C. Ojeda Aristizabal, H. Ryu, M.T. Edmonds, H.-Z. Tsai, A. Riss, S.-K. Mo, D. Lee, A. Zettl, Z. Hussain, Z.-X. Shen, M.F. Crommie, Characterization of collective ground states in single-layer NbSe₂, Nat. Phys. 12 (2016) 92–97.
- [190] Y. Xing, K. Zhao, P. Shan, F. Zheng, Y. Zhang, H. Fu, Y. Liu, M. Tian, C. Xi, H. Liu, J. Feng, X. Lin, S. Ji, X. Chen, Q.-K. Xue, J. Wang, Ising superconductivity and quantum phase transition in macrosize monolayer NbSe₂, Nano Lett. 17 (2017) 6802–6807.
- [191] Y. Nakata, K. Sugawara, R. Shimizu, Y. Okada, P. Han, T. Hitosugi, K. Ueno, T. Sato, T. Takahashi, Monolayer 1T-NbSe₂ as a Mott insulator, NPG Asia Mater. 8 (2016) e321.
- [192] X. Xi, L. Zhao, Z. Wang, H. Berger, L. Forró, J. Shan, K.F. Mak, Strongly enhanced charge-density-wave order in monolayer NbSe₂, Nat. Nanotechnol. 10 (2015) 765–769.
- [193] S. Onishi, M.M. Ugeda, Y. Zhang, Y. Chen, C. Ojeda-Aristizabal, H. Ryu, S.-K. Mo, Z. Hussain, Z.-X. Shen, M.F. Crommie, A. Zettl, Selenium capped monolayer NbSe₂ for two-dimensional superconductivity studies, Phys. Stat. Solidi b 253 (2016) 2396–2399.
- [194] F. Weber, S. Rosenkranz, J.-P. Castellan, R. Osborn, R. Hott, R. Heid, K.-P. Bohnen, T. Egami, A.H. Said, D. Reznik, Extended phonon collapse and the origin of the charge-density wave in 2H- NbSe₂, Phys. Rev. Lett. 107 (2011) 107403.
- [195] P.C. Borner, M.K. Kinyanjui, T. Bjorkman, T. Lehnert, A.V. Krasheninnikov, U. Kaiser, Observation of charge density waves in free-standing 1T-TaSe₂ monolayers by transmission electron microscopy, Appl. Phys. Lett. 113 (2018) 173103.
- [196] G.A. Scholz, O. Singh, R.F. Frindt, A.E. Curzon, Charge density wave commensurability in 2H-TaS₂ and Ag_xTaS₂, Solid State Commun. 44 (1982)
- [197] J.P. Tidman, O. Singh, A.E. Curzon, R.F. Frindt, The phase transition in 2H-TaS₂ at 75 K, Philos. Mag. 30 (1974) 1191–1194.
- [198] S. Nagata, T. Aochi, T. Abe, S. Ebisu, T. Hagino, Y. Seki, K. Tsutsumi, Super-conductivity in the layered compound 2H-TaS₂, J. Phys. Chem. Solid. 53

(1992) 1259-1263.

- [199] E. Navarro-Moratalla, J.O. Island, S. Mañas-Valero, E. Pinilla Cienfuegos, A. Castellanos-Gomez, J. Quereda, G. Rubio-Bollinger, L. Chirolli, J.A. Silva-Guillén, N. Agrait, G.A. Steele, F. Guinea, H.S.J. van der Zant, E. Coronado, Enhanced superconductivity in atomically thin TaS₂, Nat. Commun. 7 (2016) 11043.
- [200] Y. Yang, S. Fang, V. Fatemi, J. Ruhman, E. Navarro-Moratalla, K. Watanabe, T. Taniguchi, E. Kaxiras, P. Jarillo-Herrero, Enhanced superconductivity upon weakening of charge density wave transport in 2H-TaS₂ in the two-dimensional limit, Phys. Rev. B 98 (2018) 35203.
- [201] S.C. De La Barrera, M.R. Sinko, D.P. Gopalan, N. Sivadas, K.L. Seyler, K. Watanabe, T. Taniguchi, A.W. Tsen, X. Xu, D. Xiao, B.M. Hunt, Tuning Ising superconductivity with layer and spin orbit coupling in two-dimensional transition-metal bichalcogenides, Nat. Commun. 9 (2018) 1427.
- [202] C.E. Sanders, M. Dendzik, A.S. Ngankeu, A. Eich, A. Bruix, M. Bianchi, J.A. Miwa, B. Hammer, A. Khajetoorians, P. Hofmann, Crystalline and electronic structure of single-layer TaS₂, Phys. Rev. B 94 (2016) 81404.
 [203] H. Lin, W. Huang, K. Zhao, S. Qiao, Z. Liu, J. Wu, X. Chen, S.-H. Ji, Scanning
- [203] H. Lin, W. Huang, K. Zhao, S. Qiao, Z. Liu, J. Wu, X. Chen, S.-H. Ji, Scanning tunneling spectroscopic study of monolayer 1T-TaS₂ and 1T-TaSe₂, Nano Res. 13 (2020) 133–137.
- [204] J. Hall, N. Ehlen, J. Berges, E. van Loon, C. van Efferen, C. Murray, M. Rösner, J. Li, B.V. Senkovskiy, M. Hell, M. Rolf, T. Heider, M.C. Asensio, J. Avila, L. Plucinski, T. Wehling, A. Grüneis, T. Michely, Environmental control of charge density wave order in monolayer 2H-TaS₂, ACS Nano 13 (2019) 10210—10220
- [205] H.M. Lefcochilos-Fogelquist, O.R. Albertini, A.Y. Liu, Substrate-induced suppression of charge density wave phase in monolayer 1H-TaS₂ on Au(111), Phys. Rev. B 99 (2019) 174113.
- [206] O.R. Albertini, A.Y. Liu, M. Calandra, Effect of doping on lattice instabilities of single-layer 1H-TaS₂, Phys. Rev. B 95 (2017) 235121.
- [207] B. Sipos, A.F. Kusmartseva, A. Akrap, H. Berger, L. Forró, E.Tutiš. From Mott state to superconductivity in 1T-TaS₂, Nat. Mater. 7 (2008) 960.
- [208] R. Ang, Y. Tanaka, E. Ieki, K. Nakayama, T. Sato, L.J. Li, W.J. Lu, Y.P. Sun, T. Takahashi, Real-space coexistence of the melted Mott state and super-conductivity in Fe substituted 1T-TaS₂, Phys. Rev. Lett. 109 (2012) 176403.
- [209] Y. Yu, F. Yang, X.F. Lu, Y.J. Yan, Y.-H. Cho, L. Ma, X. Niu, S. Kim, Y.-W. Son, D. Feng, S. Li, S.-W. Cheong, X.H. Chen, Y. Zhang, Gate-tunable phase transitions in thin flakes of 1T-TaSs. Nat. Nanotechnol. 10 (2015) 270.
- sitions in thin flakes of 1T-TaS₂, Nat. Nanotechnol. 10 (2015) 270.

 [210] K. Bu, W. Zhang, Y. Fei, Z. Wu, Y. Zheng, J. Gao, X. Luo, Y.-P. Sun, Y. Yin, Possible strain induced Mott gap collapse in 1T-TaS₂, Commun. Phys. 2 (2019) 146.
- [211] S. Qiao, X. Li, N. Wang, W. Ruan, C. Ye, P. Cai, Z. Hao, H. Yao, X. Chen, J. Wu, Y. Wang, Z. Liu, Mottness collapse in 1T-TaS_{2-x}Se_x transition-metal dichal-cogenide: an interplay between localized and itinerant orbitals, Phys. Rev. X 7 (2017) 41054.
- [212] R. Ang, Y. Miyata, E. Ieki, K. Nakayama, T. Sato, Y. Liu, W.J. Lu, Y.P. Sun, T. Takahashi, Superconductivity and bandwidth-controlled Mott metal-insulator transition in 1T-TaS_{2-x}Se_x, Phys. Rev. B 88 (2013) 115145.
- [213] Y. Liu, R. Ang, W.J. Lu, W.H. Song, L.J. Li, Y.P. Sun, Superconductivity induced by Se-doping in layered charge-density-wave system 1T-TaS_{2-x} Se_x, Appl. Phys. Lett. 102 (2013) 192602.
- [214] R. Ang, Z.C. Wang, C.L. Chen, J. Tang, N. Liu, Y. Liu, W.J. Lu, Y.P. Sun, T. Mori, Y. Ikuhara, Atomistic origin of an ordered superstructure induced superconductivity in layered chalcogenides, Nat. Commun. 6 (2015) 6091.
- [215] A.S. Ngankeu, S.K. Mahatha, K. Guilloy, M. Bianchi, C.E. Sanders, K. Hanff, K. Rossnagel, J.A. Miwa, C.B. Nielsen, M. Bremholm, P. Hofmann, Quasi-one-dimensional metallic band dispersion in the commensurate charge density wave of 1T—TaS₂, Phys. Rev. B 96 (2017) 195147.
- [216] S.-H. Lee, J.S. Goh, D. Cho, Origin of the insulating phase and first-order metal-insulator transition in 1T–TaS₂, Phys. Rev. Lett. 122 (2019) 106404.
- [217] A.W. Tsen, R. Hovden, D. Wang, Y.D. Kim, J. Okamoto, K.A. Spoth, Y. Liu, W. Lu, Y. Sun, J.C. Hone, L.F. Kourkoutis, P. Kim, A.N. Pasupathy, Structure and control of charge density waves in two-dimensional 1T-TaS₂, Proc. Natl. Acad. Sci. Unit. States Am. 112 (2015) 15054–15059.
- [218] H.C. Lin, W.T. Huang, K. Zhao, C.S. Lian, W.H. Duan, X. Chen, S.H. Ji, Growth of atomically thick transition metal sulfide films on graphene/6H-SiC(0001) by molecular beam epitaxy, Nano Res. 11 (2018) 4722–4727.
- [219] H. Lin, W. Huang, K. Zhao, S. Qiao, Z. Liu, J. Wu, X. Chen, J. Shuai-Hua, Scanning tunneling spectroscopic study of monolayer 1T-TaS₂ and 1T-TaSe₂, Nano Res. 13 (2020) 133–137.
- [220] X.-Y. Zhu, S. Wang, Z.-Y. Jia, L. Zhu, Q.-Y. Li, W.-M. Zhao, C.-L. Xue, Y.-J. Xu, Z. Ma, J. Wen, S.-L. Yu, J.-X. Li, S.-C. Li, Realization of a metallic state in 1T-TaS₂ with persisting long-range order of a charge density wave, Phys. Rev. Lett. 123 (2019) 206405.
- [221] T. Kumakura, H. Tan, T. Handa, M. Morishita, H. Fukuyama, Charge density waves and superconductivity in 2H-TaSe₂, Czech. J. Phys. 46 (1996) 2611–2612.
- [222] H. Ryu, Y. Chen, H. Kim, H.-Z. Tsai, S. Tang, J. Jiang, F. Liou, S. Kahn, C. Jia, A.A. Omrani, J.H. Shim, Z. Hussain, Z.-X. Shen, K. Kim, B.I. Min, C. Hwang, M.F. Crommie, S.-K. Mo, Persistent charge-density-wave order in single-layer TaSe₂, Nano Lett. 18 (2018) 689–694.
- [223] S.V. Borisenko, A.A. Kordyuk, A.N. Yaresko, V.B. Zabolotnyy, D.S. Inosov, R. Schuster, B. Büchner, R. Weber, R. Follath, L. Patthey, H. Berger, Pseudogap and charge density waves in two dimensions, Phys. Rev. Lett. 100 (2008) 196402.

- [224] Y. Ge, A.Y. Liu, Effect of dimensionality and spin-orbit coupling on charge-density-wave transition in 2H-TaSe₂, Phys. Rev. B 86 (2012) 104101.
- [225] J. Laverock, D. Newby, E. Abreu, R. Averitt, K.E. Smith, R.P. Singh, G. Balakrishnan, J. Adell, T. Balasubramanian, k-resolved susceptibility function of 2H-TaSe₂ from angle-resolved photoemission, Phys. Rev. B 88 (2013) 35108.
- [226] S. Colonna, F. Ronci, A. Cricenti, L. Perfetti, H. Berger, M. Grioni, Mott phase at the surface of 1T-TaSe₂ observed by scanning tunneling microscopy, Phys. Rev. Lett. 94 (2005) 36405.
- [227] L. Perfetti, A. Georges, S. Florens, S. Biermann, S. Mitrovic, H. Berger, Y. Tomm, H. Höchst, M. Grioni, Spectroscopic signatures of a bandwidthcontrolled Mott transition at the surface of 1T-TaSe₂, Phys. Rev. Lett. 90 (2003) 166401.
- [228] T. Shimada, F.S. Ohuchi, B.A. Parkinson, Epitaxial growth and charge density wave of TaSe₂, Mater. Res. Soc. Symp. Proc. 230 (1992) 231–236.
- [229] Y. Nakata, T. Yoshizawa, K. Sugawara, Y. Umemoto, T. Takahashi, T. Sato, Selective fabrication of Mott-insulating and metallic monolayer TaSe₂, ACS Appl. Nano Mater. 1 (2018) 1456–1460.
- [230] Y. Chen, W. Ruan, M. Wu, S. Tang, H. Ryu, H.-Z. Tsai, R. Lee, S. Kahn, F. Liou, C. Jia, O.R. Albertini, H. Xiong, T. Jia, Z. Liu, J.A. Sobota, A.Y. Liu, J.E. Moore, Z.-X. Shen, S.G. Louie, S.-K. Mo, M.F. Crommie, Strong correlations and orbital texture in single-layer 1T-TaSe₂, Nat. Phys. 16 (2020) 218–224.
- [231] J. Feng, A. Tan, S. Wagner, J. Liu, Z. Mao, X. Ke, P. Zhang, Charge modulation and structural transformation in TaTe₂ studied by scanning tunneling microscopy/spectroscopy, Appl. Phys. Lett. 109 (2016) 21901.
- [232] J. Kang, S. Tongay, J. Zhou, J. Li, J. Wu, Band offsets and heterostructures of two-dimensional semiconductors, Appl. Phys. Lett. 102 (2013) 12111.
- [233] Y.C. Cheng, Z.Y. Zhu, M. Tahir, U. Schwingenschlogl, Spin-orbit—induced spin splittings in polar transition metal dichalcogenide monolayers, Europhys. Lett. 102 (2012) 57001.
- [234] G.B. Liu, W.Y. Shan, Y. Yao, W. Yao, D. Xiao, Three-band tight-binding model for monolayers of group-VIB transition metal dichalcogenides, Phys. Rev. B 88 (2013) 85433.
- [235] F.A. Rasmussen, K.S. Thygesen, Computational 2D materials database: electronic structure of transition-metal dichalcogenides and oxides, J. Phys. Chem. C 119 (2015) 13169–13183.
- [236] P. Eickholt, C. Sanders, M. Dendzik, L. Bignardi, D. Lizzit, S. Lizzit, A. Bruix, P. Hofmann, M. Donath, Spin structure of K valleys in single-layer WS₂ on Au(111), Phys. Rev. Lett. 121 (2018) 136402.
- [237] M. Dendzik, M. Michiardi, C. Sanders, M. Bianchi, J.A. Miwa, S.S. Grønborg, J.V. Lauritsen, P. Hofmann, Growth and electronic structure of epitaxial single-layer WS₂ on Au(111), Phys. Rev. B 92 (2015) 245442.
- [238] K.-A.N. Duerloo, Y. Li, E.J. Reed, Structural phase transitions in twodimensional Mo- and W-dichalcogenide monolayers, Nat. Commun. 5 (2014) 4214.
- [239] C.F. van Bruggen, R.J. Haange, G.A. Wiegers, D.K.G. de Boer, CrSe₂, a new layered dichalcogenide, Phys. B+C 99 (1980) 166–172.
- [240] D.C. Freitas, R. Weht, A. Sulpice, G. Remenyi, P. Strobel, F. Gay, J. Marcus, M. Nunez-Regueiro, Ferromagnetism in layered metastable 1T-CrTe₂, J. Phys. Condens. Matter 27 (2015) 176002.
- [241] A. Purbawati, J. Coraux, J. Vogel, A. Hadj-Azzem, N.J. Wu, N. Bendiab, D. Jegouso, J. Renard, L. Marty, V. Bouchiat, A. Sulpice, L. Aballe, M. Foerster, F. Genuzio, A. Locatelli, T.O. Mentes, Z.V. Han, X. Sun, M. Núñez-Regueiro, N. Rougemaille, In-plane magnetic domains and Néel-like domain walls in thin flakes of the room temperature CrTe₂ van der Waals ferromagnet, ACS Appl. Mater. Interfaces 12 (2020) 30702—30710.
- [242] D.C. Freitas, M. Núñez, P. Strobel, A. Sulpice, R. Weht, A.A. Aligia, M. Núñez-Regueiro, Antiferromagnetism and ferromagnetism in layered 1T-CrSe₂ with V and Ti replacements, Phys. Rev. B 87 (2013) 14420.
- [243] C. Ataca, H. Şahin, S. Ciraci, Stable, single-layer MX₂ transition-metal oxides and dichalcogenides in a honeycomb-like structure, J. Phys. Chem. C 116 (2012) 8983–8999.
- [244] W. Chen, J. Zhang, Y. Nie, Q. Xia, G. Guo, Electronic structure and magnetism of MTe₂ (M= Ti, V, Cr, Mn, Fe, Co and Ni) monolayers, J. Magn. Magn Mater. 508 (2020) 166878.
- [245] C. Lei, Y. Ma, T. Zhang, X. Xu, B. Huang, Y. Dai, Valley polarization in monolayer CrX₂ (X = S,Se) with magnetically doping and proximity coupling, New J. Phys. 22 (2020) 33002.
- [246] A.O. Fumega, J. Phillips, V. Pardo, Controlled 2D ferromagnetism in 1T-CrTe₂. The role of charge density wave and strain, arXiv 2005.00097 (2020).
- [247] J.-J. Xian, C. Wang, R. Li, M. Han, J. Lin, W.-H. Zhang, Z.-Y. Liu, Z.-M. Zhang, J.-H. Nie, W. Ji, Y.-S. Fu, Spin mapping of intralayer antiferromagnetism and spin-flop transition in monolayer CrTe₂, arXiv (2011), 05620v1.
- [248] A. Splendiani, L. Sun, Y. Zhang, T. Li, J. Kim, C.-Y. Chim, G. Galli, F. Wang, Emerging photoluminescence in monolayer MoS₂, Nano Lett. 10 (2010) 1271–1275
- [249] S. Tongay, J. Zhou, C. Ataca, K. Lo, T.S. Matthews, J. Li, J.C. Grossman, J. Wu, Thermally driven crossover from indirect toward direct bandgap in 2D semiconductors: MoSe₂ versus MoS₂, Nano Lett. 12 (2012) 5576–5580.
- [250] C. Ruppert, O.B. Aslan, T.F. Heinz, Optical properties and band gap of singleand few-layer MoTe₂ crystals, Nano Lett. 14 (2014) 6231–6236.
- [251] I.G. Lezama, A. Arora, A. Ubaldini, C. Barreteau, E. Giannini, M. Potemski, A.F. Morpurgo, Indirect-to-direct band gap crossover in few-layer MoTe₂, Nano Lett. 15 (2015) 2336–2342.
- [252] I.G. Lezama, A. Úbaldini, M. Longobardi, E. Giannini, C. Renner,

- A.B. Kuzmenko, A.F. Morpurgo, Surface transport and band gap structure of exfoliated 2H-MoTe₂ crystals, 2D Mater. 1 (2014) 21002.
- [253] A. Kuc, N. Zibouche, T. Heine, Influence of quantum confinement on the electronic structure of the transition metal sulfide TS₂, Phys. Rev. B 83 (2011) 245213.
- [254] J.K. Ellis, M.J. Lucero, G.E. Scuseria, The indirect to direct band gap transition in multilayered MoS₂ as predicted by screened hybrid density functional theory, Appl. Phys. Lett. 99 (2011) 261908.
- [255] W. Jin, P.-C. Yeh, N. Zaki, D. Zhang, J.T. Sadowski, A. Al-Mahboob, A.M. van der Zande, D.A. Chenet, J.I. Dadap, I.P. Herman, P. Sutter, J. Hone, R.M. Osgood Jr., Direct measurement of the thickness-dependent electronic band structure of MoS₂ using angle-resolved photoemission spectroscopy, Phys. Rev. Lett. 111 (2013) 106801.
- [256] Y. Zhang, T.-R. Chang, B. Zhou, Y.-T. Cui, H. Yan, Z. Liu, F. Schmitt, J. Lee, R. Moore, Y. Chen, H. Lin, H.-T. Jeng, S.-K. Mo, Z. Hussain, A. Bansil, Z.-X. Shen, Direct observation of the transition from indirect to direct bandgap in atomically thin epitaxial MoSe₂, Nat. Nanotechnol. 9 (2014) 111–115.
 [257] M.M. Ugeda, A.J. Bradley, S.-F. Shi, F.H. da Jornada, Y. Zhang, D.Y. Qiu,
- [257] M.M. Ugeda, A.J. Bradley, S.-F. Shi, F.H. da Jornada, Y. Zhang, D.Y. Qiu, W. Ruan, S.-K. Mo, Z. Hussain, Z.-X. Shen, F. Wang, S.G. Louie, M.F. Crommie, Giant bandgap renormalization and excitonic effects in a monolayer transition metal dichalcogenide semiconductor, Nat. Mater. 13 (2014) 1091–1095.
- [258] A. Bruix, J.A. Miwa, N. Hauptmann, D. Wegner, S. Ulstrup, S.S. Grønborg, C.E. Sanders, M. Dendzik, A.G. Čabo, M. Bianchi, J.V. Lauritsen, A.A. Khajetoorians, B. Hammer, P. Hofmann, Single-layer MoS₂ on Au(111): band gap renormalization and substrate interaction, Phys. Rev. B 93 (2016) 165422
- [259] S.S. Grønborg, S. Ulstrup, M. Bianchi, M. Dendzik, C.E. Sanders, J.V. Lauritsen, P. Hofmann, J.A. Miwa, Synthesis of epitaxial single-layer MoS₂ on Au(111), Langmuir 31 (2015) 9700–9706.
- [260] F. Tumino, C.S. Casari, M. Passoni, V. Russoa, A.L. Bassia, Pulsed laser deposition of single-layer MoS₂ on Au(111): from nanosized crystals to large-area films, Nanoscale Adv. 1 (2019) 643–655.
- [261] N. Krane, C. Lotze, K.J. Franke, Moiré structure of MoS₂ on Au(111): local structural and electronic properties, Surf. Sci. 678 (2018) 136–142.
- [262] N. Krane, C. Lotze, J.M. Läger, G. Reecht, K.J. Franke. Electronic structure and luminescence of quasi-freestanding MoS₂ nanopatches on Au(111), Nano Lett. 16 (2016) 5163–5168.
- [263] J.A. Miwa, M. Dendzik, S.S. Grønborg, M. Bianchi, J.V. Lauritsen, P. Hofmann, S. Ulstrup, Van der Waals epitaxy of two-dimensional MoS₂ graphene heterostructures in ultrahigh vacuum, ACS Nano 9 (2015) 6502–6510.
- [264] J. Hall, B. Pielić, C. Murray, W. Jolie, T. Wekking, C. Busse, M. Kralj, T. Michely, Molecular beam epitaxy of quasi-freestanding transition metal disulphide monolayers on van der Waals substrates: a growth study, 2D Mater. 5 (2018) 25005
- [265] H.C. Diaz, F. Bertran, C. Chen, J. Avila, J. Rault, P. Le Fèvre, M.C. Asensio, M. Batzill, Band renormalization and spin polarization of MoS₂ in graphene/ MoS₂ heterostructures. Phys, Status Solidi RRL 9 (2015) 701–706.
- [266] H. Zeng, J. Dai, W. Yao, D. Xiao, X. Cui, Valley polarization in MoS₂ monolayers by optical pumping, Nat. Nanotechnol. 7 (2012) 490–493.
- [267] K.F. Mak, K. He, J. Shan, T.F. Heinz, Control of valley polarization in monolayer MoS₂ by optical helicity, Nat. Nanotechnol. 7 (2012) 494–498.
- [268] T. Cao, G. Wang, W. Han, H. Ye, C. Zhu, J. Shi, Q. Niu, P. Tan, E. Wang, B. Liu, J. Feng, Valley-selective circular dichroism of monolayer molybdenum disulphide, Nat. Commun. 3 (2012) 887.
- [269] W. Jolie, C. Murray, P.S. Weiß, J. Hall, F. Portner, N. Atodiresei, A.V. Krasheninnikov, C. Busse, H.-P. Komsa, A. Rosch, T. Michely, Tomonaga-Luttinger liquid in a box: electrons confined within MoS2 mirror-twin boundaries, Phys. Rev. X 9 (2019) 11055.
- [270] H. Bana, E. Travaglia, L. Bignardi, P. Lacovig, C.E. Sanders, M. Dendzik, M. Michiardi, M. Bianchi, D. Lizzit, F. Presel, D. De Angelis, N. Apostol, P.K. Das, J. Fujii, I. Vobornik, R. Larciprete, A. Baraldi, P. Hofmann, S. Lizzit, Epitaxial growth of single-orientation high-quality MoS₂ monolayers, 2D Mater. 5 (2018) 35012.
- [271] H.C. Diaz, J. Avila, C. Chen, R. Addou, M.C. Asensio, M. Batzill, Direct observation of interlayer hybridization and Dirac relativistic carriers in graphene/ MoS₂ van der Waals heterostructures, Nano Lett. 15 (2015) 1135–1140.
- [272] H.X. Dong, H. Yang, B. Fang, C. Zijing, D. Sherman, J.R. Tan, K.P. Loh, Observation of gap opening in 1T' phase MoS₂ nanocrystals, Nano Lett. 18 (2018) 5085–5090.
- [273] H. Liu, L. Jiao, F. Yang, Y. Cai, X. Wu, W. Ho, C. Gao, J. Jia, N. Wang, H. Fan, W. Yao, M. Xie, Dense network of one-dimensional mid-gap metallic modes in monolayer MoSe₂ and their spatial undulations, Phys. Rev. Lett. 113 (2014) 66105.
- [274] L. Jiao, H.J. Liu, J.L. Chen, Y. Yi, W.G. Chen, Y. Cai, J.N. Wang, X.Q. Dai, N. Wang, W.K. Ho, M.H. Xie, Molecular-beam epitaxy of monolayer MoSe₂: growth characteristics and domain boundary formation, New J. Phys. 17 (2015) 53023
- [275] H.C. Diaz, Y. Ma, S. Kolekar, J. Avila, C. Chen, M.C. Asensio, M. Batzill, Substrate dependent electronic structure variations of van der Waals heterostructures of MoSe₂ or MoSe_{2 (1-x)} Te_{2x} grown by van der Waals epitaxy, 2D Mater. 4 (2017) 25094.
- [276] M.-W. Chen, D. Ovchinnikov, S. Lazar, M. Pizzochero, M. Brian, W.A. Surrente, M. Baranowski, O.L. Sanchez, P. Gillet, P. Plochocka, O.V. Yazyev, A. Kis, Highly oriented atomically thin ambipolar MoSe₂ grown by molecular beam

- epitaxy, ACS Nano 11 (2017) 6355-6361.
- [277] S. Vishwanath, X. Liu, S. Rouvimov, P.C. Mende, A. Azcatl, S. McDonnell, R.M. Wallace, R.M. Feenstra, J.K. Furdyna, D. Jena, Comprehensive structural and optical characterization of MBE grown MoSe₂ on graphite, CaF₂ and graphene. 2D Mater. 2 (2015) 24007.
- [278] F. Cheng, Z. Hu, H. Xu, Y. Shao, J. Su, Z. Chen, W. Ji, K.P. Loh, Interface engineering of Au(111) for the growth of 1T'-MoSe₂, ACS Nano 13 (2019) 2316–2323.
- [279] S.M. Poh, S.J.R. Tan, X. Zhao, Z. Chen, I. Abdelwahab, D. Fu, H. Xu, Y. Bao, W. Zhou, K.P. Loh, Large area synthesis of 1D-MoSe₂ using molecular beam epitaxy, Adv. Mater. 29 (2017) 1605641.
- [280] Y. Chen, P. Cui, X. Ren, C. Zhang, C. Jin, Z. Zhang, C.-K. Shih, Fabrication of MoSe₂ nanoribbons via an unusual morphological phase transition, Nat. Commun. 8 (2017) 15135.
- [281] O. Lehtinen, H.-P. Komsa, A. Pulkin, M.B. Whitwick, M.-W. Chen, T. Lehnert, M.J. Mohn, O.V. Yazyev, A. Kis, U. Kaiser, A.V. Krasheninnikov, Atomic scale microstructure and properties of Se-deficient two-dimensional MoSe₂, ACS Nano 9 (2015) 3274–3283.
- [282] X. He, L. Zhang, R. Chua, P.K.J. Wong, A. Arramel, Y.P. Feng, S.J. Wang, D. Chi, M. Yang, Y.L. Huang, A.T.S. Wee, Selective self-assembly of 2,3-diaminophenazine molecules on MoSe₂ mirror twin boundaries, Nat. Commun. 10 (2019) 2847.
- [283] T. Kosmala, H.C. Diaz, H.-P. Komsa, Y. Ma, A.V. Krasheninnikov, M. Batzill, S. Agnoli, Metallic twin boundaries boost the hydrogen evolution reaction on the basal plane of molybdenum selenotellurides, Adv. Energy Mater. 8 (2018) 1800031.
- [284] Y. Ma, S. Kolekar, H.C. Diaz, J. Aprojanz, I. Miccoli, C. Tegenkamp, M. Batzill, Metallic twin grain boundaries embedded in MoSe₂ monolayers grown by molecular beam epitaxy, ACS Nano 11 (2017) 5130-5139.
- [285] M. Batzill, Mirror twin grain boundaries in molybdenum dichalcogenides, J. Phys. Condens. Matter 30 (2018) 493001.
- [286] L. Zhou, A. Zubair, Z. Wang, X. Zhang, F. Ouyang, K. Xu, W. Fang, K. Ueno, J. Li, T. Palacios, J. Kong, M.S. Dresselhaus, Synthesis of high-quality large-area homogenous 1T⁷ MoTe₂ from chemical vapor deposition, Adv. Mater. 28 (2016) 8526–9531.
- [287] L. Zhou, K. Xu, A. Zubair, A.D. Liao, W. Fang, F. Ouyang, Y.-H. Lee, K. Ueno, R. Saito, T. Palacios, J. Kong, M.S. Dresselhaus, Large-area synthesis of high-quality uniform few-layer MoTe₂, J. Am. Chem. Soc. 137 (2015) 11892—11895.
- [288] T.A. Empante, Y. Zhou, V. Klee, A.E. Nguyen, I.-H. Lu, M.D. Valentin, S.A.N. Alvillar, E. Preciado, A.J. Berges, C.S. Merida, M. Gomez, S. Bobek, M. Isarraraz, E.J. Reed, L. Bartels, Chemical vapor deposition growth of few-layer MoTe₂ in the 2H, 1T', and 1T phases: tunable properties of MoTe₂ films, ACS Nano 11 (2017) 900–905.
- [289] H.C. Diaz, R. Chaghi, Y. Ma, M. Batzill, Molecular beam epitaxy of the van der Waals heterostructure MoTe₂ on MoS₂: phase, thermal, and chemical stability, 2D Mater. 2 (2015) 44010.
- [290] S. Vishwanath, A. Sundar, X. Liu, A. Azcatl, E. Lochocki, A.R. Woll, S. Rouvimov, W.S. Hwang, N. Lu, X. Peng, H.-H. Lien, J. Weisenberger, S. McDonnell, M.J. Kim, M. Dobrowolska, J.K. Furdyna, K. Shen, R.M. Wallace, D. Jena, H.G. Xing, MBE growth of few-layer 2H-MoTe₂ on 3D substrates, J. Cryst. Growth 482 (2018) 61–69.
- [291] Q. He, P. Li, Z. Wu, B. Yuan, Z. Luo, W. Yang, J. Liu, G. Cao, W. Zhang, Y. Shen, P. Zhang, S. Liu, G. Shao, Z. Yao, Molecular beam epitaxy scalable growth of wafer-scale continuous semiconducting monolayer MoTe₂ on inert amorphous dielectrics, Adv. Mater. 31 (2019) 1901578.
- [292] S. Tang, C. Zhang, C. Jia, H. Ryu, C. Hwang, M. Hashimoto, D. Lu, Z. Liu, T.P. Devereaux, Z.-X. Shen, S.-K. Mo, Electronic structure of monolayer 1T'-MoTe₂ grown by molecular beam epitaxy, Apl. Mater. 6 (2018) 26601.
 [293] J. Chen, G. Wang, Y. Tang, H. Tian, J. Xu, X. Dai, H. Xu, J. Jia, W. Ho, M. Xie,
- [293] J. Chen, G. Wang, Y. Tang, H. Tian, J. Xu, X. Dai, H. Xu, J. Jia, W. Ho, M. Xie, Quantum effects and phase tuning in epitaxial hexagonal and monoclinic MoTe₂ monolayers, ACS Nano 11 (2017) 3282–3288.
- [294] H.C. Diaz, Y. Ma, R. Chaghi, M. Batzill, High density of (pseudo) periodic twingrain boundaries in molecular beam epitaxy-grown van der Waals heterostructure: MoTe₂/MoS₂, Appl. Phys. Lett. 108 (2016) 191606.
- [295] A. Roy, H.C.P. Movva, B. Satpati, K. Kim, R. Dey, A. Rai, T. Pramanik, S. Guchhait, E. Tutuc, S.K. Banerjee, Structural and electrical properties of MoTe₂ and MoSe₂ grown by molecular beam epitaxy, ACS Appl. Mater. Interfaces 8 (2016) 7396—7402.
- [296] P. Chen, W.W. Pai, Y.-H. Chan, W.-L. Sun, C.-Z. Xu, D.-S. Lin, M.Y. Chou, A.-V. Fedorov, T.-C. Chiang, Large quantum-spin-Hall gap in single-layer 1T' WSe₂, Nat. Commun. 9 (2018) 2003.
- [297] M.M. Ugeda, A. Pulkin, S. Tang, H. Ryu, Q. Wu, Y. Zhang, D. Wong, Z. Pedramrazi, A. Martín-Recio, Y. Chen, F. Wang, Z.-X. Shen, S.-K. Mo, O.V. Yazyev, M.F. Crommie, Observation of topologically protected states at crystalline phase boundaries in single-layer WSe₂, Nat. Commun. 9 (2018) 3401
- [298] M.S. Sokolikova, P.C. Sherrell, P. Palczynski, V.L. Bemmer, C. Mattevi, Direct solution-phase synthesis of 1T WSe₂ nanosheets, Nat. Commun. 10 (2019) 712.
- [299] L. Bignardi, D. Lizzit, H. Bana, E. Travaglia, P. Lacovig, C.E. Sanders, M. Dendzik, M. Michiardi, M. Bianchi, M. Ewert, L. Buß, J. Falta, J.I. Flege, A. Baraldi, R. Larciprete, P. Hofmann, S. Lizzit, Growth and structure of singly oriented single-layer tungsten disulfide on Au(111), Phys. Rev. Materials 3 (2019) 14003.

- [300] M. Dendzik, A. Bruix, M. Michiardi, A.S. Ngankeu, M. Bianchi, J.A. Miwa, B. Hammer, P. Hofmann, C.E. Sanders, Substrate-induced semiconductor-to-metal transition in monolayer WS₂, Phys. Rev. B 96 (2017) 235440.
- [301] S.K. Mahatha, M. Dendzik, C.E. Sanders, M. Michiardi, M. Bianchi, J.A. Miwa, P. Hofmann, Quasi-free-standing single-layer WS₂ achieved by intercalation, Phys. Rev. Mater. 2 (2018) 124001.
- [302] H. Beyer, G. Rohde, A.G. Cabo, A. Stange, T. Jacobsen, L. Bignardi, D. Lizzit, P. Lacovig, C.E. Sanders, S. Lizzit, K. Rossnagel, P. Hofmann, M. Bauer, Larger than 80% valley polarization of free carriers in singly-oriented single layer WS₂ on Au(111), Phys. Rev. Lett. 123 (2019) 236802.
- [303] S. Ulstrup, C.E. Giusca, J.A. Miwa, C.E. Sanders, A. Browning, P. Dudin, C. Cacho, O. Kazakova, D.K. Gaskill, R.L. Myers-Ward, T. Zhang, M. Terrones, P. Hofmann, Nanoscale mapping of quasiparticle band alignment, Nat. Commun. 10 (2019) 3283.
- [304] C.-H. Lee, G.-H. Lee, A.M. van der Zande, W. Chen, Y. Li, M. Han, X. Cui, G. Arefe, C. Nuckolls, T.F. Heinz, J. Guo, J. Hone, P. Kim, Atomically thin p—n junctions with van der Waals heterointerfaces, Nat. Nanotechnol. 9 (2014) 676—681.
- [305] C. Zhang, Y. Chen, A. Johnson, M.-Y. Li, L.-J. Li, P.C. Mende, R.M. Feenstra, C.-K. Shih, Probing critical point energies of transition metal dichalcogenides: surprising indirect gap of single layer WSe₂, Nano Lett. 15 (2015) 6494–6500
- [306] Y. Zhang, M.M. Ugeda, C. Jin, S.-F. Shi, A.J. Bradley, A. Martín-Recio, H. Ryu, J. Kim, S. Tang, Y. Kim, B. Zhou, C. Hwang, Y. Chen, F. Wang, M.F. Crommie, Z. Hussain, Z.-X. Shen, S.-K. Mo, Electronic structure, surface doping, and optical response in epitaxial WSe₂ thin films, Nano Lett. 16 (2016) 2485–2491.
- [307] H.J. Liu, L. Jiao, L. Xie, F. Yang, J.L. Chen, W.K. Ho, C.L. Gao, J.F. Jia, X.D. Cui, M.H. Xie, Molecular-beam epitaxy of monolayer and bilayer WSe₂: a scanning tunneling microscopy/spectroscopy study and deduction of exciton binding energy, 2D Mater. 2 (2015) 34004.
- [308] J.H. Park, S. Vishwanath, X. Liu, H. Zhou, S.M. Eichfeld, S.K. Fullerton-Shirey, J.A. Robinson, R.M. Feenstra, J. Furdyna, D. Jena, H.G. Xing, A.C. Kummel, Scanning tunneling microscopy and spectroscopy of air exposure effects on molecular beam epitaxy grown WSe₂ monolayers and bilayers, ACS Nano 10 (2016) 4258–4267.
- [309] R. Addou, C.M. Smyth, J.-Y. Noh, Y.-C. Lin, Y. Pan, S.M. Eichfeld, S. Fölsch, R.M. Feenstra, J.A. Robinson, K. Cho, R.M. Wallace, One dimensional metallic edges in atomically thin WSe₂ induced by air exposure, 2D Mater. 5 (2018) 25017.
- [310] R. Yue, Y. Nie, L.A. Walsh, R. Addou, C. Liang, N. Lu, A.T. Barton, H. Zhu, Z. Che, D. Barrera, L. Cheng, P.-R. Cha, Y.J. Chabal, J.W.P. Hsu, J. Kim, M.J. Kim, L. Colombo, R.M. Wallace, K. Cho, C.L. Hinkle, Nucleation and growth of WSe₂: enabling large grain transition metal dichalcogenides, 2D Mater. 4 (2017) 45019.
- [311] Z.-Y. Jia, Y.-H. Song, X.-B. Li, K. Ran, P. Lu, H.-J. Zheng, X.-Y. Zhu, Z.-Q. Shi, J. Sun, J. Wen, D. Xing, S.-C. Li, Direct visualization of a two-dimensional topological insulator in the single-layer 1T'-WTe2, Phys. Rev. B 96 (2017), 041108(R).
- [312] Y.-H. Song, Z.-Y. Jia, D. Zhang, X.-Y. Zhu, Z.-Q. Shi, H. Wang, L. Zhu, Q.-Q. Yuan, H. Zhang, D.-Y. Xing, S.-C. Li, Observation of Coulomb gap in the quantum spin Hall candidate single-layer 1T'-WTe₂, Nat. Commun. 9 (2018) 4071.
- [313] L.A. Walsh, R. Yue, Q. Wang, A.T. Barton, R. Addou, C.M. Smyth, H. Zhu, J. Kim, L. Colombo, M.J. Kim, R.M. Wallace, C.L. Hinkle, WTe₂ thin films grown by beam-interrupted molecular beam epitaxy, 2D Mater. 4 (2017) 25044.
- [314] A.T. Barton, R. Yue, L.A. Walsh, G. Zhou, C. Cormier, C.M. Smyth, R. Addou, L. Colombo, R.M. Wallace, C.L. Hinkle, WSe_(2-x)Te_x alloys grown by molecular beam epitaxy, 2D Mater. 6 (2019) 45027.
- [315] J.C. Wildervanckm, F. Jellinek, The Dichalcogenides of technetium and rhenium, J. Less Common. Met. 24 (1971) 73–81.
- [316] C. Ataca, H. Şahin, S. Ciraci, Stable, single-layer MX₂ transition-metal oxides and dichalcogenides in a honeycomb-like structure, J. Phys. Chem. C 116 (2012) 8983–8999.
- [317] M. Kan, S. Adhikari, Q. Sun, Ferromagnetism in MnX₂ (X = S, Se) monolayers, Phys. Chem. Chem. Phys. 16 (2014) 4990–4994.
- [318] D.J. O'Hara, T. Zhu, A.H. Trout, A.S. Ahmed, Y.K. Luo, C.H. Lee, M.R. Brenner, S. Rajan, J.A. Gupta, D.W. McComb, R.K. Kawakami, Room temperature intrinsic ferromagnetism in epitaxial manganese selenide films in the monolayer limit, Nano Lett. 18 (2018) 3125—3131.
- [319] Y.-C. Lin, H.-P. Komsa, C.-H. Yeh, T. Bjorkman, Z.-Y. Liang, C.-H. Ho, Y.-S. Huang, P.-W. Chiu, A.V. Krasheninnikov, K. Suenaga, Single-layer ReS₂: two-dimensional semiconductor with tunable in-plane anisotropy, ACS Nano 9 (2015) 11249—11257.
- [320] C.H. Ho, Y.S. Huang, K.K. Tiong, In-plane anisotropy of the optical and electrical properties of ReS₂ and ReSe₂ layered crystals, J. Alloys Compd. 317–318 (2001) 222–226.
- [321] D. Wolverson, S. Crampin, A.S. Kazemi, A. Ilie, S.J. Bending, Raman spectra of monolayer, few-layer, and bulk ReSe₂: an anisotropic layered semiconductor, ACS Nano 8 (2014) 11154–11164.
- [322] F. Liu, S. Zheng, X. He, A. Chaturvedi, J. He, W.L. Chow, T.R. Mion, X. Wang, J. Zhou, Q. Fu, H.J. Fan, B.K. Tay, L. Song, R.-H. He, C. Kloc, P.M. Ajayan, Z. Liu, Highly sensitive detection of polarized light using anisotropic 2D ReS₂, Adv. Funct. Mater. 26 (2016) 1169–1177.
- [323] J.L. Webb, L.S. Hart, D. Wolverson, C. Chen, J. Avila, M.C. Asensio, Electronic

- band structure of ReS₂ by high-resolution angle-resolved photoemission spectroscopy, Phys. Rev. B 96 (2017) 115205.
- [324] B.S. Kim, W.S. Kyung, J.D. Denlinger, C. Kim, S.R. Park, Strong onedimensional characteristics of hole-carriers in ReS₂ and ReSe₂, Sci. Rep. 9 (2019) 2730.
- [325] L.S. Hart, J.L. Webb, S. Dale, S.J. Bending, M. Mucha-Kruczynski, D. Wolverson, C. Chen, J. Avila, M.C. Asensio, Electronic bandstructure and van der Waals coupling of ReSe₂ revealed by high-resolution angle-resolved photoemission spectroscopy, Sci. Rep. 7 (2017) 5145.
- spectroscopy, Sci. Rep. 7 (2017) 5145.

 [326] P. Eickholt, J. Noky, E.F. Schwier, K. Shimada, K. Miyamoto, T. Okuda, C. Datzer, M. Drüppel, P. Krüger, M. Rohlfing, M. Donath, Location of the valence band maximum in the band structure of anisotropic 1T' -ReSe₂, Phys. Rev. B 97 (2018) 165130.
- [327] D. Biswas, A.M. Ganose, R. Yano, J.M. Riley, L. Bawden, O.J. Clark, J. Feng, L. Collins-Mcintyre, M.T. Sajjad, W. Meevasana, T.K. Kim, M. Hoesch, J.E. Rault, T. Sasagawa, D.O. Scanlon, P.D.C. King, Narrow-band anisotropic electronic structure of ReS₂, Phys. Rev. B 96 (2017) 85205.
 [328] M. Rahman, K. Davey, S.-Z. Qiao, Advent of 2D rhenium disulfide (ReS₂):
- [328] M. Rahman, K. Davey, S.-Z. Qiao, Advent of 2D rhenium disulfide (ReS₂): fundamentals to applications, Adv. Funct. Mater. 27 (2017) 1606129.
- [329] S. Tongay, H. Sahin, C. Ko, A. Luce, W. Fan, K. Liu, J. Zhou, Y.S. Huang, C.H. Ho, J. Yan, D.F. Ogletree, S. Aloni, J. Ji, S. Li, J. Li, F.M. Peeters, J. Wu, Monolayer behavior in bulk ReS₂ due to electronic and vibrational decoupling, Nat. Commun. 5 (2014) 3252.
- [330] O.B. Aslan, D.A. Chenet, A.M. van der Zande, J.C. Hone, T.F. Heinz, Linearly polarized excitons in single- and few-layer ReS₂ crystals, ACS Photonics 3 (2016) 96–101.
- [331] S.J. Jung, T. Jeong, J. Shim, S. Park, J.-h. Park, B.G. Shin, Y.J. Song. Atomic-registry-dependent electronic structures of sulfur vacancies in ReS₂ studied by scanning tunneling microscopy/spectroscopy, Curr. Appl. Phys. 19 (2019) 224–229, 2019.
- [332] M. Gehlmann, I. Aguilera, G. Bihlmayer, S. Nemšák, P. Nagler, P. Gospodaric, G. Zamborlini, M. Eschbach, V. Feyer, F. Kronast, E. Młyńczak, T. Korn, L. Plucinski, C. Schüller, S. Blügel, C.M. Schneider, Direct observation of the band gap transition in atomically thin ReS₂, Nano Lett. 17 (2017) 5187–5192.
- [333] S.P. Kelty, A.F. Ruppert, R.R. Chianelli, J. Ren, M.-H. Whangbo, Scanning probe microscopy study of layered dichalcogenide ReS₂, J. Am. Chem. Soc. 116 (1994) 7857–7863.
- [334] K. Friemelt, S. Akari, M.C. Lux-Steiner, T. Schill, E. Bucher, K. Dransfeld, Scanning tunneling microscopy with atomic resolution on ReS₂ single crystals grown by vapor phase transport, Ann. Phys. 504 (1992) 248–253.
- [335] M. Muhler, W. Bensch, M. Schur, Preparation, crystal structures, experimental and theoretical electronic band structures of cobalt tellurides in the composition range CoTe_{1.3}- Co Te₂, J. Phys. Condens. Matter 10 (1998) 2947.
- [336] H. Ma, W. Dang, X. Yang, B. Li, Z. Zhang, P. Chen, Y. Liu, Z. Wan, Q. Qian, J. Luo, K. Zang, X. Duan, X. Duan, Chemical vapor deposition growth of single crystalline CoTe₂ nanosheets with tunable thickness and electronic properties, Chem. Mater. 30 (2018) 8891–8896.
- [337] M. Shimakawa, K. Kawachi, S. Nishikawa, K. Hayashi, Structural stability of the 1T structure on transition-metal dichalcogenides, J. Solid State Chem. 129 (1997) 242–249.
- [338] M. Shimakawa, K. Hayashi, Phase relations and properties of compounds in TiSe₂-IrSe₂ system, J. Alloys Compd. 259 (1997) 219–224.
- [339] K. Hayashi, Y. Tanino, K. Kawachi, Y. Nakata, K. Inoue, N. Maeda, Homogeneity range of the 1T phase in the systems- IrSe₂- V(Ta) Se₂, J. Alloys Compd. 442 (2007) 117–118.
- [340] M.J. Eom, K. Kim, Y.J. Jo, J.J. Yang, E.S. Choi, B.I. Min, J.-H. Park, S.-W. Cheong, J.S. Kim, Dimerization-induced fermi-surface reconstruction in IrTe₂, Phys. Rev. Lett. 113 (2014) 266406.
- [341] H. Lee, K.-T. Ko, K. Kim, B.-G. Park, J. Yang, S.-W. Cheong, J.-H. Park, Electronic reconstruction on dimerized IrTe₂, Europhys. Lett. 120 (2017) 47003.
- [342] D. Ootsuki, S. Pyon, K. Kudo, M. Nohara, M. Horio, T. Yoshida, A. Fujimori, M. Arita, H. Ansai, H. Namatame, M. Taniguchi, N.L. Saini, T. Mizokawa, Electronic structure reconstruction by orbital symmetry breaking in IrTe₂, J. Phys. Soc. Japan 82 (2013) 93704.
- [343] D. Ootsuki, H. Ishii, K. Kudo, M. Nohara, M. Takahashi, M. Horio, A. Fujimori, T. Yoshida, M. Arita, H. Anzai, H. Namatame, M. Taniguchi, N.L. Saini, T. Mizokawa, A novel one-dimensional electronic state at IrTe₂ surface, J. Phys. Soc. Japan 86 (2017) 123704.
- [344] C. Monney, A. Schuler, T. Jaouen, M.-L. Mottas, T. Wolf, M. Merz, M. Muntwiler, L. Castiglioni, P. Aebi, F. Weber, M. Hengsberger, Robustness of the charge-ordered phases in IrTe₂ against photoexcitation, Phys. Rev. B 97 (2018) 75110
- [345] H.S. Kim, S. Kim, K. Kim, B.I. Min, Y.-H. Cho, L. Wang, S.-W. Cheong, H.W. Yeom, Nanoscale superconducting honeycomb charge order in IrTe₂, Nano Lett. 16 (2016) 4260–4265.
- [346] C. Chen, J. Kim, Y. Yang, G. Cao, R. Jin, E.W. Plummer, Surface phases of the transition-metal dichalcogenide IrTe₂, Phys. Rev. B 95 (2017) 94118.
- [347] H.S. Kim, T.-H. Kim, J. Yang, S.-W. Cheong, H.W. Yeom, Structural versus electronic distortions in IrTe₂ with broken symmetry, Phys. Rev. B 90 (2014) 201103(R)
- [348] Q. Li, W. Lin, J. Yan, X. Chen, A.G. Gianfrancesco, D.J. Singh, D. Mandrus, S.V. Kalinin, M. Pan, Bond competition and phase evolution on the IrTe₂ surface, Nat. Commun. 5 (2014) 5358.
- [349] T. Machida, Y. Fujisawa, K. Igarashi, A. Kaneko, S. Ooi, T. Mochiku, M. Tachiki,

- K. Komori, K. Hirata, H. Sakata, Visualizing the effect of structural supermodulation on electronic structure of IrTe₂ by scanning tunneling spectroscopy, Phys. Rev. B 88 (2013) 245125.
- [350] Y.S. Oh, J.J. Yang, Y. Horibe, S.-W. Cheong, Anionic depolymerization transition in IrTe₂, Phys. Rev. Lett. 110 (2013) 127209.
- [351] J. Dai, K. Haule, J.J. Yang, Y.S. Oh, S.-W. Cheong, W. Wu, Hierarchical stripe phases in IrTe₂ driven by competition between Ir dimerization and Te bonding, Phys. Rev. B 90 (2014) 235121.
- [352] G.L. Pascut, K. Haule, M.J. Gutmann, S.A. Barnett, A. Bombardi, S. Artyukhin, T. Birol, D. Vanderbilt, J.J. Yang, S.-W. Cheong, V. Kiryukhin, Dimerizationinduced cross-layer quasi-two-dimensionality in metallic IrTe₂, Phys. Rev. Lett. 112 (2014) 86402.
- [353] M. Yoshida, K. Kudo, M. Nohara, Y. Iwasa, Metastable superconductivity in two-dimensional IrTe₂ crystals, Nano Lett. 18 (2018) 3113–3117.
 [354] A. Wang, Z. Liu, J. Pan, Q. Li, G. Li, Q. Huan, S. Du, H.-J. Gao, Construction of
- [354] A. Wang, Z. Liu, J. Pan, Q. Li, G. Li, Q. Huan, S. Du, H.-J. Gao, Construction of monolayer IrTe₂ and the structural transition under low temperatures, Chin. Phys. B 29 (2020) 78102.
- [355] M.S. Bahramy, O.J. Clark, B.-J. Yang, J. Feng, L. Bawden, J. M.Riley, I. Marković, F. Mazzola, V. Sunko, D. Biswas, S.P. Cooil, M. Jorge, J.W. Wells, M.Leandersson, T. Balasubramanian, J. Fujii, I. Vobornik, J.E. Rault, T.K. Kim, M. Hoesch, K. Okawa, M. Asakawa, T. .. Sasagawa, T. Eknapakul, W. Meevasana, P.D.C. King, Ubiquitous formation of bulk Dirac cones and topological surface states from a single orbital manifold in transition-metal dichalcogenides, Nat. Mater. 17 (2017) 21–28.
- [356] Y. Liu, J.-Z. Zhao, L. Yu, C.-T. Lin, A.-J. Liang, C. Hu, Y. Ding, Y. Xu, S.-L. He, L. Zhao, G.-D. Liu, X.-L. Dong, J. Zhang, C.-T. Chen, Z.-Y. Xu, H.-M. Weng, X. Dai, Z. Fang, X.-J. Zhou, Identification of topological surface state in PdTe₂ superconductor by angle-resolved photoemission spectroscopy, Chin. Phys. Lett. 32 (2015) 67303.
- [357] R.A.B. Villaos, C.P. Crisostomo, Z.-Q. Huang, S.-M. Huang, A.A.B. Padama, M.A. Albao, H. Lin, F.-C. Chuang, Thickness dependent electronic properties of Pt dichalcogenides, npj 2D Mater. Appl. 3 (2019) 2.
- [358] A. Ciarrocchi, A. Avsar, D. Ovchinnikov, A. Kis, Thickness-modulated metalto-semiconductor transformation in a transition metal dichalcogenide, Nat. Commun. 9 (2018) 919.
- [359] R. Kempt, A. Kuc, T. Heine, in: Angew Chem Int (Ed.), Two-dimensional Noble-Metal Chalcogenides and Phosphochalcogenides, vol. 59, 2020, pp. 9242–9254.
- [360] E. Chen, W. Xu, J. Chen, J.H. Warner, 2D noble metal dichalcogenides (Pt, Pd, Se, S) for electronics and energy applications, Mater. Today Adv. 7 (2020) 100076.
- [361] L. Pi, L. Li, K. Liu, Q. Zhang, H. Li, T. Zhai, Recent progress on 2D noble-transition-metal dichalcogenides, Adv. Funct. Mater. 29 (2019) 1904932.
- [362] H. Sun, Z. Liang, K. Shen, M. Luo, J. Hu, H. Huang, Z. Zhu, Z. Li, Z. Jiang, F. Song, Fabrication of NiSe₂ by direct selenylation of a nickel surface, Appl. Surf. Sci. 428 (2018) 623–629.
- [363] Y. Shao, S. Song, X. Wu, J. Qi, H. Lu, C. Liu, S. Zhu, Z. Liu, J. Wang, D. Shi, S. Du, Y. Wang, H.-J. Gao, Epitaxial fabrication of two-dimensional NiSe₂ on Ni(111) substrate, Appl. Phys. Lett. 111 (2017) 113107.
- [364] S. Mukherjee, S.W. Jung, S.F. Weber, C. Xu, D. Qian, X. Xu, P.K. Biswas, T.K. Kim, L.C. Chapon, M.D. Watson, J.B. Neaton, C. Cacho, Fermi-crossing type-II Dirac fermions and topological surface states in NiTe₂, Sci. Rep. 10 (2020) 12957.
- [365] B. Ghosh, D. Mondal, C.-N. Kuo, C.S. Lue, J. Nayak, J. Fujii, I. Vobornik, A. Politano, A. Agarwal, Observation of bulk states and spin-polarized topological surface states in transition metal dichalcogenide Dirac semimetal candidate NiTe₂, Phys. Rev. B 100 (2019) 195134.
- [366] C. Xu, B. Li, W. Jiao, W. Zhou, B. Qian, R. Sankar, N.D. Zhigadlo, Y. Qi, D. Qian, F.-C. Chou, X. Xu, Topological type-II Dirac fermions approaching the Fermi level in a transition metal dichalcogenide NiTe₂, Chem. Mater. 30 (2018) 4822, 4820.
- [367] Q. Liu, F. Fei, B. Chen, X. Bo, B. Wei, S. Zhang, M. Zhang, F. Xie, M. Naveed, X. Wan, F. Song, B. Wang, Nontopological origin of the planar Hall effect in the type-II Dirac semimetal NiTe₂, Phys. Rev. B 99 (2019) 155119.
- [368] B. Zhao, W. Dang, Y. Liu, B. Li, J. Li, J. Luo, Z. Zhang, R. Wu, H. Ma, G. Sun, Yu Huang, X. Duan, X. Duan, Synthetic control of two-dimensional NiTe₂ single crystals with highly uniform thickness distributions, J. Am. Chem. Soc. 140 (2018) 14217.
- [369] J. Li, X. Yang, Y. Liu, B. Huang, R. Wu, Z. Zhang, B. Zhao, H. Ma, W. Dang, Z. Wei, K. Wang, Z. Lin, X. Yan, M. Sun, B. Li, X. Pan, J. Luo, G. Zhang, Y. Liu, Y. Huang, X. Duan, X. Duan, General synthesis of two-dimensional van der Waals heterostructure arrays, Nature 579 (2020) 368–374.
- [370] E. Selb, T. Götsch, O. Janka, S. Penner, G. Heymann, Crystal structures of the high-pressure palladium dichalcogenides Pd_{0.94(1)}S₂ and Pd_{0.88(1)}Se₂ comprising exceptional Pd^{IV} oxidation states. Z. Anorg, Allg. Chem. 643 (2017) 1415–1423.
- [371] F. Hulliger, Electrical properties of some nickel-group chalcogenides, J. Phys. Chem. Solid. 26 (1965) 638–645.
- [372] Y. Wang, Y. Li, Z. Chen, Not your familiar two dimensional transition metal disulfide: structural and electronic properties of the PdS₂ monolayer, J. Mater. Chem. C 3 (2015) 9603–9608.
- [373] S. Deng, L. Li, Y. Zhang, Strain modulated electronic, mechanical, and optical properties of the monolayer PdS₂, PdSe₂, and PtSe₂ for tunable devices, ACS Appl. Nano Mater. 1 (2018) 1932–1939.
- [374] J. Sun, H. Shi, T. Siegrist, D.J. Singh, Electronic, transport, and optical

- properties of bulk and mono-layer PdSe₂, Appl. Phys. Lett. 107 (2015) 153902
- [375] A.D. Oyedele, S. Yang, L. Liang, A.A. Puretzky, K. Wang, J. Zhang, P. Yu, P.R. Pudasaini, A.W. Ghosh, Z. Liu, C.M. Rouleau, B.G. Sumpter, M.F. Chisholm, W. Zhou, P.D. Rack, D.B. Geohegan, K. Xiao, PdSe₂: pentagonal two-dimensional layers with high air stability for electronics, J. Am. Chem. Soc. 139 (2017) 14090—14097.
- [376] G. Zhang, M. Amani, A. Chaturvedi, C. Tan, J. Bullock, X. Song, H. Kim, D.-H. Lien, M.C. Scott, H. Zhang, A. Javey, Optical and electrical properties of two-dimensional palladium diselenide, Appl. Phys. Lett. 114 (2019) 253102.
- [377] A.V. Kuklin, H. Ågren, Quasiparticle electronic structure and optical spectra of single-layer and bilayer PdSe₂: proximity and defect-induced band gap renormalization, Phys. Rev. B 99 (2019) 245114.
- [378] M. Sun, J.-P. Chou, L. Shi, J. Gao, A. Hu, W. Tang, G. Zhang, Few-layer PdSe₂ sheets: promising thermoelectric materials driven by high valley convergence, ACS Omega 3 (2018) 5971–5979.
- [379] Y. Gu, H. Cai, J. Dong, Y. Yu, A.N. Hoffman, C. Liu, A.D. Oyedele, Y.-C. Lin, Z. Ge, A.A. Puretzky, G. Duscher, M.F. Chisholm, P.D. Rack, C.M. Rouleau, Z. Gai, X. Meng, F. Ding, D.B. Geohegan, K. Xiao, Two-dimensional palladium diselenide with strong in-plane optical anisotropy and high mobility grown by chemical vapor deposition, Adv. Mater. 32 (2020) 1906238.
- [380] E. Li, D. Wang, P. Fan, R. Zhang, Y.-Y. Zhang, G. Li, J. Mao, Y. Wang, X. Lin, S. Du, H.-J. Gao, Construction of bilayer PdSe₂ on epitaxial graphene, Nano Res. 11 (2018) 5858–5865.
- [381] Q. Liang, Q. Zhang, J. Gou, T. Song Arramel, H. Chen, M. Yang, S.X. Lim, Q. Wang, R. Zhu, N. Yakovlev, S.C. Tan, W. Zhang, K.S. Novoselov, A.T.S. Wee, Performance improvement by ozone treatment of 2D PdSe2, ACS Nano 14 (2020) 5668–5677.
- [382] H.-J. Noh, J. Jeong, E.-J. Cho, K. Kim, B.I. Min, B.-G. Park, Experimental realization of type-II Dirac fermions in a PdTe₂ superconductor, Phys. Rev. Lett. 119 (2017) 16401.
- [383] H.Y. Xue, H. Yang, Y.F. Wu, G. Yao, D.D. Guan, S.Y. Wang, H. Zheng, C.H. Liu, Y.Y. Li, J.F. Jia, Molecular beam epitaxy of superconducting PdTe₂ films on topological insulator Bi₂Te₃, Sci. China Phys. Mech. Astron. 62 (2019) 76801.
- [384] E. Li, R.-Z. Zhang, H. Li, C. Liu, G. Li, J.-O. Wang, T. Qian, H. Ding, Y.-Y. Zhang, S.-X. Du, X. Lin, H.-J. Gao, High quality PdTe₂ thin films grown by molecular beam epitaxy, Chin. Phys. B 27 (2018) 86804.
- [385] C. Liu, C.-S. Lian, M.-H. Liao, Y. Wang, Y. Zhong, C. Ding, W. Li, C.-L. Song, K. He, X.-C. Ma, W. Duan, D. Zhang, Y. Xu, L. Wang, Q.-K. Xue, Two-dimensional superconductivity and topological states in PdTe₂ thin films, Phys. Rev. Mater. 2 (2018) 94001.
- [386] M. Yan, H. Huang, K. Zhang, E. Wang, W. Yao, K. Deng, G. Wan, H. Zhang, M. Arita, H. Yang, Z. Sun, H. Yao, Y. Wu, S. Fan, W. Duan, S. Zhou, Lorentz-violating type-II Dirac fermions in transition metal dichalcogenide PtTe₂, Nat. Commun. 8 (2017) 257.
- [387] H. Huang, S. Zhou, W. Duan, Type-II Dirac fermions in the PtSe₂ class of transition metal dichalcogenides, Phys. Rev. B 94 (2016), 121117(R).
- [388] K. Zhang, M. Yan, H. Zhang, H. Huang, M. Arita, Z. Sun, W. Duan, Y. Wu, S. Zhou, Experimental evidence for type-II Dirac semimetal in PtSe₂, Phys. Rev. B 96 (2017) 125102.
- [389] H. Yang, M. Schmidt, V. Süss, M. Chan, F.F. Balakirev, R.D. McDonald, S.S.P. Parkin, C. Felser, B. Yan, P.J.W. Mol, Quantum oscillations in the type-II Dirac semi-metal candidate PtSe₂, New J. Phys. 20 (2018) 43008.
- [390] Y. Zhao, J. Qiao, P. Yu, Z. Hu, Z. Lin, S.P. Lau, Z. Liu, W. Ji, Y. Chai, Extraordinarily strong interlayer interaction in 2D layered PtS₂, Adv. Mater. 28 (2016) 2399–2407.
- [391] Y. Zhao, J. Qiao, Z. Yu, P. Yu, K. Xu, S.P. Lau, W. Zhou, Z. Liu, X. Wang, W. Ji, Y. Chai, High-electron-mobility and air-stable 2D layered PtSe₂ FETs, Adv. Mater. 29 (2017) 1604230.
- [392] L. Ansari, S. Monaghan, N. McEvoy, C.Ó. Coileáin, C.P. Cullen, J. Lin, R. Siris, T. Stimpel-Lindner, K.F. Burke, G. Mirabelli, R. Duffy, E. Caruso, R.E. Nagle, G.S. Duesberg, P.K. Hurley, F. Gity, Quantum confinement-induced semi-metal-to-semiconductor evolution in large-area ultra-thin PtSe₂ films grown at 400°C, npj 2D Mater. Appl. 3 (2019) 1–8.
- [393] O.J. Clark, F. Mazzola, J. Feng, V. Sunko, I. Markovic, L. Bawden, T.K. Kim, P.D.C. King, M.S. Bahramy, Dual quantum confinement and anisotropic spin splitting in the multivalley semimetal PtSe₂, Phys. Rev. B 99 (2019) 45438.
- [394] K. Deng, M. Yan, C.-P. Yu, J. Li, X. Zhou, K. Zhang, Y. Zhao, K. Miyamoto, T. Okuda, W. Duan, Y. Wu, X. Zhong, S. Zhou, Crossover from 2D metal to 3D Dirac semimetal in metallic PtTe₂ films with local Rashba effect, Sci. Bull. 64 (2019) 1044—1048.
- [395] J. Li, S. Kolekar, M. Ghorbani-Asl, T. Lehnert, J. Biskupek, U. Kaiser, A. Krasheninnikov, M. Batzill. Layer Dependent Electronic Properties in Pt-Dichalcogenides Probed by Scanning Tunneling Microscopy. Submitted.
- [396] M.-K. Lin, R.A.B. Villaos, J.A. Hlevyack, P. Chen, R.-Y. Liu, C.-H. Hsu, J. Avila, S.-K. Mo, F.-C. Chuang, T.-C. Chiang, Dimensionality-mediated semimetalsemiconductor transition in ultrathin PtTe₂ films, Phys. Rev. Lett. 124 (2020) 36402.
- [397] M. Yan, E. Wang, X. Zhou, G. Zhang, H. Zhang, K. Zhang, W. Yao, N. Lu, S. Yang, S. Wu, T. Yoshikawa, K. Miyamoto, T. Okuda, Y. Wu, P. Yu, W. Duan, S. Zhou, High quality atomically thin PtSe₂ films grown by molecular beam epitaxy, 2D Mater. 4 (2017) 45015.
- [398] W. Yao, E. Wang, H. Huang, K. Deng, M. Yan, K. Zhang, K. Miyamoto, T. Okuda, L. Li, Y. Wang, H. Gao, C. Liu, W. Duan, S. Zhou, Direct observation of spin-layer locking by local Rashba effect in monolayer semiconducting PtSe₂

- film, Nat. Commun. 8 (2017) 14216.
- [399] Y. Wang, L. Li, W. Yao, S. Song, J.T. Sun, J. Pan, X. Ren, C. Li, E. Okunishi, Y.-Q. Wang, E. Wang, Y. Shao, Y.Y. Zhang, H.-t. Yang, E.F. Schwier, H. Iwasawa, K. Shimada, M. Taniguchi, Z. Cheng, S. Zhou, S. Du, S.J. Pennycook, S.T. Pantelides, H.-J. Gao, Monolayer PtSe₂, a new semiconducting transition-metal dichalcogenide, epitaxially grown by direct selenization of Pt, Nano Lett. 15 (2015) 4013–4018.
- [400] D. Zhao, S. Xie, Y. Wang, H. Zhu, L. Chen, Q. Sun, D.W. Zhang, Synthesis of large-scale few-layer PtS₂ films by chemical vapor deposition, AIP Adv. 9 (2019) 25225.
- [401] Z. Wang, Q. Li, F. Besenbacher, M. Dong, Facile synthesis of single crystal PtSe₂ nanosheets for nanoscale electronics, Adv. Mater. 28 (2016) 10224–10229.
- [402] H. Zheng, Y. Choi, F. Baniasadi, D. Hu, L. Jiao, K. Park, C. Tao, Visualization of point defects in ultrathin layered 1T-PtSe₂, 2D Mater. 6 (2019) 41005.
- [403] A. Avsar, A. Ciarrocchi, M. Pizzochero, D. Unuchek, O.V. Yazyev, A. Kis, Defect induced, layer-modulated magnetism in ultrathin metallic PtSe₂, Nat. Nanotechnol. 14 (2019) 674–678.
- [404] X. Chia, A. Adriano, P. Lazar, Z. Sofer, J. Luxa, M. Pumera, Layered platinum dichalcogenides (PtS₂, PtSe₂, and PtTe₂) electrocatalysis: monotonic dependence on the chalcogen size. Adv. Funct. Mater. 26 (2016) 4306–4318.
- dence on the chalcogen size, Adv. Funct. Mater. 26 (2016) 4306–4318.

 [405] J. Shi, Y. Huan, M. Hong, R. Xu, P. Yang, Z. Zhang, X. Zou, Y. Zhang, Chemical vapor deposition grown large scale atomically thin platinum diselenide with semimetal—semiconductor transition, ACS Nano 13 (2019) 8442–8451.
- [406] N.F. Rosli, C.C. Mayorga-Martinez, N.M. Latiff, N. Rohaizad, Z. Sofer, A.C. Fisher, M. Pumera, Layered PtTe₂ matches electrocatalytic performance of Pt/C for oxygen reduction reaction with significantly lower toxicity, ACS Sustain. Chem. Eng. 6 (2018) 7432–7441.
- [407] H. Huang, X. Fan, D.J. Singh, W. Zheng, Modulation of hydrogen evolution catalytic activity of basal plane in monolayer platinum and palladium dichalcogenides, ACS Omega 3 (2018) 10058–10065.
- [408] S. Lina, Y. Liua, Z. Hub, W. Luc, C.H. Maka, L. Zenga, J. Zhaoa, Y. Lia, F. Yana, Y.H. Tsanga, X. Zhanga, S.P. Lau, Tunable active edge sites in PtSe₂ films towards hydrogen evolution reaction, Nano Energy 42 (2017) 26–33.
- [409] R. Caracas, X. Gonze, Ab initio study of incommensurately modulated crystals, Comput. Mater. Sci. 22 (2001) 112–117.
- [410] A. Janner, B. Dam, The morphology of calaverite (AuTe₂) from data of 1931. A solution of an old problem of rational indices, Acta Crystallogr. Sect. A 45 (1989) 115–123.
- [411] B.C.H. Krutzen, J.E. Inglesfield, First-principles electronic structure calculations for incommensurately modulated calaverite, J. Phys. Condens. Matter 2 (1990) 4829.
- [412] A. van Triest, W. Folkerts, C. Haas, Electronic structure and photoelectron spectra of calaverite, AuTe₂, J. Phys. Condens. Matter 2 (1990) 8733.
- [413] K. Kudo, H. Ishii, M. Takasuga, K. Iba, S. Nakano, J. Kim, A. Fujiwara, M. Nohara, Superconductivity induced by breaking Te₂ dimers of AuTe₂, J. Phys. Soc. Jpn. 82 (2013) 63704.
- [414] L. Fang, J. Im, C.C. Stoumpos, F. Shi, V. Dravid, M. Leroux, A.J. Freeman, W.-K. Kwok, D.Y. Chung, M. Kanatzidis, Two-dimensional mineral [Pb₂BiS₃] [AuTe₂]: high-mobility charge carriers in single-atom-thick layers, J. Am. Chem. Soc. 137 (2015) 2311–2317.
- [415] M.V. Bollinger, J.V. Lauritsen, K.W. Jacobsen, J.K. Nørskov, S. Helveg, F. Besenbacher, One-dimensional metallic edge states in MoS₂, Phys. Rev. Lett. 87 (2001) 196803.
- [416] J.V. Lauritsen, J. Kibsgaard, S. Helveg, H. Topsøe, B.S. Clausen, E. Lægsgaard, F. Besenbacher, Size-dependent structure of MoS₂ nanocrystals, Nat. Nanotechnol. 2 (2007) 53–58.
- [417] S.S. Grønborg, K. Thorarinsdottir, L. Kyhl, J. Rodriguez-Fernández, C.E. Sanders, M. Bianchi, P. Hofmann, J.A. Miwa, S. Ulstrup, J.V. Lauritsen, Basal plane oxygen exchange of epitaxial MoS₂ without edge oxidation, 2D Mater. 6 (2019) 45013.
- [418] M. Gibertini, N. Marzari, Emergence of one-dimensional wires of free carriers in transition metal-dichalcogenide nanostructures, Nano Lett. 15 (2015)
- [419] C. Zhang, A. Johnson, C.-L. Hsu, L.-J. Li, C.-K. Shih, Direct imaging of band profile in single layer MoS₂ on graphite: quasiparticle energy gap, metallic edge states, and edge band bending, Nano Lett. 14 (2014) 2443—2447.
- [420] D. Davelou, G. Kopidakis, E. Kaxiras, I.N. Remediakis, Nanoribbon edges of transition-metal dichalcogenides: stability and electronic properties, Phys. Rev. B 96 (2017) 165436.
- [421] L. Liu, Z. Ge, C. Yan, A.D. Moghadam, M. Weinert, L. Li, Termination-dependent edge states of MBE-grown WSe₂, Phys. Rev. B 98 (2018) 235304.
- [422] X. Zhao, D. Fu, Z. Ding, Y.-Y. Zhang, D. Wan, S.J.R. Tan, Z. Chen, K. Leng, J. Dan, W. Fu, D. Geng, P. Song, Y. Du, T. Venkatesan, S.T. Pantelides, S.J. Pennycook, W. Zhou, K.P. Loh, Mo-terminated edge reconstructions in nanoporous molybdenum disulfide film, Nano Lett. 18 (2018) 482–490.
- [423] A.R. Botello-Mendez, F. Lopez-Urias, M. Terrones, H. Terrones, Metallic and ferromagnetic edges in molybdenum disulfide nanoribbons, Nanotechnology 20 (2009) 325703.
- [424] Y. Li, Z. Zhou, S. Zhang, Z. Chen, MoS₂ nanoribbons; high stability and unusual electronic and magnetic properties, J. Am. Chem. Soc. 130 (2008) 16739–16744.
- [425] Q. Chen, H. Li, W. Xu, S. Wang, H. Sawada, C.S. Allen, A.I. Kirkland, J.C. Grossman, J.H. Warner, Atomically flat zigzag edges in monolayer MoS₂ by thermal annealing, Nano Lett. 17 (2017) 5502–5507.

- [426] H. Xu, S. Liu, Z. Ding, S.J.R. Tan, K.M. Yam, Y. Bao, C.T. Nai, M.-F. Ng, J. Lu, C. Zhang, K.P. Loh, Oscillating edge states in one-dimensional MoS₂ nanowires, Nat. Commun. 7 (2016) 12904.
- [427] G. Yang, Y. Shao, J. Niu, X. Ma, C. Lu, W. Wei, X. Chuai, J. Wang, J. Cao, H. Huang, G. Xu, X. Shi, Z. Ji, N. Lu, D. Geng, J. Qi, Y. Cao, Z. Liu, L. Liu, Y. Huang, L. Liao, W. Dang, Z. Zhang, Y. Liu, X. Duan, J. Chen, Z. Fan, X. Jiang, Y. Wang, L. Li, H.-J. Gao, X. Duan, M. Liu, Possible Luttinger liquid behavior of edge transport in monolayer transition metal dichalcogenide crystals, Nat. Commun. 11 (2020) 659, 2020.
- [428] S. Liu, Z. Liu, Hybridization induced metallic and magnetic edge states in noble transition-metal-dichalcogenides of PtX₂ (X = S, Se) nanoribbons, Phys. Chem. Chem. Phys. 20 (2018) 21441–21446.
- [429] S. Liu, H. Zhu, Z. Liu, G. Zhou, Symmetrical metallic and magnetic edge states of nanoribbon from semiconductive monolayer PtS₂, Phys. Lett. 382 (2018) 776–780.
- [430] X. Zou, Y. Liu, B.I. Yakobson, Predicting dislocations and grain boundaries in two-dimensional metal-disulfides from the first principles, Nano Lett. 13 (2013) 253–258.
- [431] Y. Ma, H.C. Diaz, J. Avila, C. Chen, V. Kalappattil, R. Das, M.-H. Phan, T. Čadež, J.M.P. Carmelo, M.C. Asensio, M. Batzill, Angle resolved photoemission spectroscopy reveals spin charge separation in metallic MoSe₂ grain boundary, Nat. Commun. 8 (2017) 14231.
- [432] S. Barja, S. Wickenburg, Z.-F. Liu, Y. Zhang, H. Ryu, M.M. Ugeda, Z. Hussain, Z.-X. Shen, S.-K. Mo, E. Wong, M.B. Salmeron, F. Wang, M.F. Crommie, D.F. Ogletree, J.B. Neaton, A. Weber-Bargioni, Charge density wave order in 1D mirror twin boundaries of single-layer MoSe₂, Nat. Phys. 12 (2016) 751–756
- [433] Y.L. Huang, Z. Ding, W. Zhang, Y.-H. Chang, Y. Shi, L.-J. Li, Z. Song, Y.J. Zheng, D. Chi, S.Y. Quek, A.T.S. Wee, Gap states at low-angle grain boundaries in monolayer tungsten diselenide, Nano Lett. 16 (2016) 3682–3688.
- [434] P.M. Coelho, H.-P. Komsa, H.C. Diaz, Y. Ma, A.V. Krasheninnikov, M. Batzill, Post-synthesis modifications of two-dimensional MoSe₂ or MoTe₂ by incorporation of excess metal atoms into the crystal structure, ACS Nano 12 (2018) 3975—3984.
- [435] B. Wang, Y. Xia, J. Zhang, H.-P. Komsa, M. Xie, Y. Peng, C. Jin, Niobium doping induced mirror twin boundaries in MBE grown WSe₂ monolayers, Nano Res. 13 (2020) 1889–1896.
- [436] H. Zhu, Q. Wang, L. Cheng, R. Addou, J. Kim, M.J. Kim, R.M. Wallace, Defects and surface structural stability of MoTe₂ under vacuum annealing, ACS Nano 11 (2017) 11005–11014.
- [437] H. Zhu, Q. Wang, C. Zhang, R. Addou, K. Cho, R.M. Wallace, M.J. Kim, New Mo₆Te₆ sub-nanometer-diameter nanowire phase from 2H-MoTe₂, Adv. Mater. 29 (2017) 1606264.
- [438] J. Lin, S.T. Pantelides, W. Zhou, Vacancy-induced formation and growth of inversion domains in transition-metal dichalcogenide monolayer, ACS Nano 9 (2015) 5189–5197.
- [439] Y. Wang, Y. Li, T. Heine, PtTe monolayer: two-dimensional electrocatalyst with high basal plane activity toward oxygen reduction reaction, J. Am. Chem. Soc. 140 (2018) 12732–12735.
- [440] S. Kolekar, K. Lasek, P.M. Coelho, M. Batzill. In Preparation.
- [441] G.H. Ryu, J. Chen, Y. Wen, J.H. Warner, In-situ atomic-scale dynamics of thermally driven phase transition of 2D few-layered 1T PtSe₂ into ultrathin 2D nonlayered PtSe crystals, Chem. Mater. 31 (2019) 9895–9903.
- [442] Z.-L. Liu, B. Lei, Z.-L. Zhu, L. Tao, J. Qi, D.-L. Bao, X. Wu, L. Huang, Y.-Y. Zhang, X. Lin, Y.-L. Wang, S. Du, S.T. Pantelides, H.-J. Gao, Spontaneous formation of 1D pattern in monolayer VSe₂ with dispersive adsorption of Pt atoms for HER catalysis, Nano Lett. 19 (2019) 4897—4903.
- [443] J. Lin, S. Zuluaga, P. Yu, Z. Liu, S.T. Pantelides, K. Suenaga, Novel Pd₂Se₃ two-dimensional phase driven by interlayer fusion in layered PdSe₂, Phys. Rev. Lett. 119 (2017) 16101.
- [444] A.D. Oyedele, S. Yang, T. Feng, A.V. Haglund, Y. Gu, A.A. Puretzky, D. Briggs, C.M. Rouleau, M.F. Chisholm, R.R. Unocic, D. Mandrus, H.M. Meyer, S.T. Pantelides, D.B. Geohegan, K. Xiao, Defect-mediated phase transformation in anisotropic two dimensional PdSe₂ crystals for seamless electrical contacts, J. Am. Chem. Soc. 141 (2019) 8928–8936.
- [445] G.D. Nguyen, A.D. Oyedele, A. Haglund, W. Ko, L. Liang, A.A. Puretzky, D. Mandrus, K. Xiao, A.-P. Li, Atomically precise PdSe₂ pentagonal nanoribbons, ACS Nano 14 (2020) 1951–1957.
- [446] H. Cordes, R. Schmid-Fetzer, Phase equilibria in the Ti-Te system, J. Alloys Compd. 216 (1994) 197–206.
- [447] T. Ohtemi, S. Onoue, M. Nakahira, Phase relationships and properties in the V-Te system, Mater. Res. Bull. 19 (1984) 1367—1375.
- [448] G. Chattopadhyay, The Cr-Te (Chromium-Tellurium) system, J. Phase Equil. 19 (1994) 431–440.
- [449] Y. Ueda, T. Ohtani, Mechanochemical Synthesis, Handbook of Solid State Chemistry, first ed., 2017. R. Dronskowski, S. Kikkawa, A. Stein; Wiley-VCH Verlag GmbH & Co.
- [450] A. Hayashi, Y. Ueda, K. Kosuge, H. Murata, H. Asano, N. Watanabe, F. Izumi, Cation distribution in (M', M)3Se4: II. (V, Ti)₃Se₄ and (Cr, V)₃Se₄, J. Solid State Chem. 71 (1987) 234–237.
- [451] A. Hayashi, K. Imada, K. Inoue, Y. Ueda, K. Kosuge, Phase diagram of $(M_xM^*)_1$ Se $_4$ (0<x<1) (M, M' 3d-transition metal), Bull. Inst. Chem. Res. Kyoto Univ. vol. 64 (1986) 186–206.
- [452] M. Bonilla, S. Kolekar, J. Li, Y. Xin, P.M. Coelho, K. Lasek, K. Zberecki, D. Lizzit, E. Tosi, P. Lacovig, S. Lizzit, M. Batzill, Compositional phase change of early

- transition metal diselenide (VSe₂ and TiSe₂) ultrathin films by post-growth annealing, Adv. Mater. Interf. 15 (2020) 2000497.
- [453] X.-C. Liu, S. Zhao, X. Sun, L. Deng, X. Zou, Y. Hu, Y.-X. Wang, C.-W. Chu, J. Li, J. Wu, F.-S. Ke, P.M. Ajayan, Spontaneous self-intercalation of copper atoms into transition metal dichalcogenides, Sci Adv 6 (2020) eaay4092.
- [454] C. Zhang, C. Gong, Y. Nie, K.-A. Min, C. Liang, Y.J. Oh, H. Zhang, W. Wang, S. Hong, L. Colombo, R.M. Wallace, K. Cho, Systematic study of electronic structure and band alignment of monolayer transition metal dichalcogenides in van der Waals heterostructures. 2D Mater. 4 (2017) 15026.
- [455] H.M. Hill, A.F. Rigosi, K.T. Rim, G.W. Flynn, T.F. Heinz, Band alignment in MoS₂/WS₂ transition metal dichalcogenide heterostructures probed by scanning tunneling microscopy and spectroscopy, Nano Lett. 16 (2016) 4831–4837.
- [456] M.-H. Chiu, C. Zhang, H.-W. Shiu, C.-P. Chuu, C.-H. Chen, C.-Y.S. Chang, C.-H. Chen, M.-Y. Chou, C.-K. Shih, L.-J. Li, Determination of band alignment in the single-layer MoS₂/WSe₂ heterojunction, Nat. Commun. 6 (2015) 7666.
- [457] H. Kumar, D. Er, L. Dong, J. Li, V.B. Shenoy, Elastic deformations in 2D van der Waals heterostructures and their impact on optoelectronic properties: predictions from a multiscale computational approach, Sci. Rep. 5 (2015) 10872.
- [458] M.R. Rosenberger, H.-J. Chuang, M. Phillips, V.P. Oleshko, K.M. McCreary, S.V. Sivaram, C.S. Hellberg, B.T. Jonker, Twist angle-dependent atomic reconstruction and moiré patterns in transition metal dichalcogenide heterostructures, ACS Nano 14 (2020) 4550–4558.
- [459] A. Weston, Y. Zou, V. Enaldiev, A. Summerfield, N. Clark, V. Zolyomi, A. Graham, C. Yelgel, S. Magorrian, M. Zhou, J. Zultak, D. Hopkinson, A. Barinov, T. Bointon, A. Kretinin, N.R. Wilson, P.H. Beton, V.I. Fal'ko, S.J. Haigh, R. Gorbachev, Atomic reconstruction in twisted bilayers of transition metal dichalcogenides, Nat. Nanotechnol. 15 (2020) 592–597.
- [460] J. Kang, J. Li, S.-S. Li, J.-B. Xia, L.-W. Wang, Electronic structural moiré pattern effects on MoS₂/MoSe₂ 2D heterostructures, Nano Lett. 13 (2013) 5485–5490.
- [461] C. Zhang, C.-P. Chuu, X. Ren, M.-Y. Li, L.J. Li, C. Jin, M.Y. Chou, C.-K. Shih, Interlayer couplings, moiré patterns, and 2D electronic superlattices in MoS₂/WSe₂ hetero-bilayers, Sci. Adv. 3 (2017) e1601459.
- [462] Y. Pan, S. Fölsch, Y. Nie, D. Waters, Y.-C. Lin, B. Jariwala, K. Zhang, K. Cho, J.A. Robinson, R.M. Feenstra, Quantum-confined electronic states arising from the moiré pattern of MoS₂—WSe₂ heterobilayers, Nano Lett. 18 (2018) 1849—1855.
- [463] W.-T. Hsu, B.-H. Lin, L.-S. Lu, M.-H. Lee, M.-W. Chu, L.-J. Li, W. Yao, W.-H. Chang, C.-K. Shih, Tailoring excitonic states of van der Waals bilayers through stacking configuration, band alignment, and valley spin, Sci. Adv. 5 (2019) eaax7407.
- [464] H. Yu, G.-B. Liu, J. Tang, X. Xu, W. Yao, Moiré excitons: from programmable quantum emitter arrays to spin-orbit—coupled artificial lattices, Sci. Adv. 3 (2017) e1701696.
- [465] E.M. Alexeev, D.A. Ruiz-Tijerina, M. Danovich, M.J. Hamer, D.J. Terry, P.K. Nayak, S. Ahn, S. Pak, J. Lee, J.I. Sohn, M.R. Molas, M. Koperski, K. Watanabe, T. Taniguchi, K.S. Novoselov, R.V. Gorbachev, H.S. Shin, V.I. Fal'ko, A.I. Tartakovskii, Resonantly hybridized excitons in moiré superlattices in van der Waals heterostructures, Nature 567 (2019) 81–86.
- [466] K. Tran, G. Moody, F. Wu, X. Lu, J. Choi, K. Kim, A. Rai, D.A. Sanchez, J. Quan, A. Singh, J. Embley, A. Zepeda, M. Campbell, T. Autry, T. Taniguchi, K. Watanabe, N. Lu, S.K. Banerjee, K.L. Silverman, S. Kim, E. Tutuc, L. Yang, A.H. MacDonald, X. Li, Evidence for moiré excitons in van der Waals heterostructures, Nature 567 (2019) 71–75.
- [467] K.L. Seyler, P. Rivera, H. Yu, N.P. Wilson, E.L. Ray, D.G. Mandrus, J. Yan, W. Yao, X. Xu, Signatures of moiré-trapped valley excitons in MoSe₂/WSe₂ heterobilayers, Nature 567 (2019) 66–70.
- [468] S. Song, D.H. Keum, S. Cho, D. Perello, Y. Kim, Y.H. Lee, Room temperature semiconductor—metal transition of MoTe₂ thin films engineered by strain, Nano Lett. 16 (2016) 188–193.
- [469] Q. Li, Z. Yao, J. Wu, S. Mitra, S. Hao, T.S. Sahu, Y. Li, C. Wolverton, V.P. Dravid, Intermediate phases in sodium intercalation into MoS₂ nanosheets and their implications for sodium-ion batteries, Nano Energy 38 (2017) 342–349.
- [470] L. Liu, J. Wu, L. Wu, M. Ye, X. Liu, Q. Wang, S. Hou, P. Lu, L. Sun, J. Zheng, L. Xing, L. Gu, X. Jiang, L. Xie, L. Jiao, Phase-selective synthesis of 1T' MoS₂ monolayers and heterophase bilayers, Nat. Mater. 17 (2018) 1108–1114.
- [471] Q. Liu, X. Li, Q. He, A. Khalil, D. Liu, T. Xiang, X. Wu, L. Song, Gram-scale aqueous synthesis of stable few-layered 1T-MoS₂: applications for visiblelight-driven photocatalytic hydrogen evolution, Small 11 (2015) 5556–5564.
- [472] C.A. Papageorgopoulos, W. Jaegermann, Li intercalation across and along the van der Waals surfaces of MoS₂(0001), Surf. Sci. 338 (1995) 83–93.
- [473] G. Eda, H. Yamaguchi, D. Voiry, T. Fujita, M. Chen, M. Chhowalla, Photoluminescence from chemically exfoliated MoS₂, Nano Lett. 11 (2011) 5111–5116.
- [474] P. Joensen, R.F. Frindt, S.R. Morrison, Single-layer MoS₂, Mater. Res. Bull. 21 (1986) 457–461.
- [475] S. Jiménez Sandoval, D. Yang, R.F. Frindt, J.C. Irwin, Raman study and lattice dynamics of single molecular layers of MoS₂, Phys. Rev. B 44 (1991) 3955.
- [476] J. Heising, M.G. Kanatzidis, Structure of restacked MoS2 and WS2 elucidated by electron crystallography, J. Am. Chem. Soc. 121 (1999) 638.
- [477] G. Eda, T. Fujita, H. Yamaguchi, D. Voiry, M. Chen, M. Chhowalla, Coherent atomic and electronic heterostructures of single-layer MoS₂, ACS Nano 6 (2012) 7311–7317.
- [478] D. Voiry, H. Yamaguchi, J. Li, R. Silva, D.C.B. Alves, T. Fujita, M. Chen, T. Asefa,

- V.B. Shenoy, G. Eda, M. Chhowalla, Enhanced catalytic activity in strained chemically exfoliated WS_2 nanosheets for hydrogen evolution, Nat. Mater. 12 (2013) 850–855.
- [479] D. Voiry, M. Salehi, R. Silva, T. Fujita, M. Chen, T. Asefa, V.B. Shenoy, G. Eda, M. Chhowalla, Conducting MoS₂ nanosheets as catalysts for hydrogen evolution reaction, Nano Lett. 13 (2013) 6222–6227, 12.
- [480] F. Wypych, R. Schöllhorn, 1T-MoS₂, a new metallic modification of molybdenum disulfide, J. Chem. Soc., Chem. Commun. (1992) 1386–1388.
- [481] H.-L. Tsai, J. Heising, J.L. Schindler, C.R. Kannewurf, M.G. Kanatzidis, Exfoliated—restacked phase of WS₂, Chem. Mater. 9 (1997) 879—882.
- [482] Y.-C. Lin, D.O. Dumcenco, Y.-S. Huang, K. Suenaga, Atomic mechanism of the semiconducting-to-metallic phase transition in single-layered MoS₂, Nat. Nanotechnol. 9 (2014) 391–396.
- [483] Z. Wang, Y.-Y. Sun, I. Abdelwahab, L. Cao, W. Yu, H. Ju, J. Zhu, W. Fu, L. Chu, H. Xu, K.P. Loh, Surface-limited superconducting phase transition on 1T-TaS₂, ACS Nano 12 (2018) 12619–12628.
- [484] J. Zhang, J. Liu, J. Huang, P. Kim, C.M. Lieber, Creation of nanocrystals via tipinduced solid-solid transformations, Mater. Res. Soc. Symp. Proc. 466 (1997) 89–94
- [485] J. Zhang, J. Liu, J.L. Huang, P. Kim, C.M. Lieber, Creation of nanocrystals through a solid-solid phase transition induced by an STM tip, Science 274 (1996) 757-760.
- [486] H. Wang, J. Lee, M. Dreyer, B.I. Barker, A scanning tunneling microscopy study of a new superstructure around defects created by tip—sample interaction on 2H-NbSe₂, J. Phys. Condens. Matter 21 (2009) 265005.
 [487] F. Bischoff, W. Auwärter, J.V. Barth, A. Schiffrin, M. Fuhrer, B. Weber, Nano-
- [487] F. Bischoff, W. Auwärter, J.V. Barth, A. Schiffrin, M. Fuhrer, B. Weber, Nanoscale phase engineering of niobium diselenide, Chem. Mater. 29 (2017) 9907–9914.
- [488] L. Ma, C. Ye, Y. Yu, X.F. Lu, X. Niu, S. Kim, D. Feng, D. Tomanek, Y.-W. Son, X.H. Chen, Y. Zhang, A metallic mosaic phase and the origin of Mott-insulating state in 1T-TaS₂. Nat, Commun. Now. 7 (2016) 10956.
- [489] D. Cho, S. Cheon, K.-S. Kim, S.-H. Lee, Y.-H. Cho, S.-W. Cheong, H.W. Yeom, Nanoscale manipulation of the Mott insulating state coupled to charge order in 1T-TaS₂, Nat. Commun. 7 (2016) 10453.
- [490] X. Lin, J.C. Lu, Y. Shao, Y.Y. Zhang, X. Wu, J.B. Pan, L. Gao, S.Y. Zhu, K. Qian, Y.F. Zhang, D.L. Bao, L.F. Li, Y.Q. Wang, Z.L. Liu, J.T. Sun, T. Lei, C. Liu, J.O. Wang, K. Ibrahim, D.N. Leonard, W. Zhou, H.M. Guo, Y.L. Wang, S.X. Du, S.T. Pantelides, H.-J. Gao, Intrinsically patterned two-dimensional materials for selective adsorption of molecules and nanoclusters, Nat. Mater. 16 (2017) 717—721.
- [491] S. Bertolazzi, M. Gobbi, Y. Zhao, C. Backes, P. Samorì, Molecular chemistry approaches for tuning the properties of two-dimensional transition metal dichalcogenides, Chem. Soc. Rev. 47 (2018) 6845–6888.
- [492] Y.L. Huang, Y.J. Zheng, Z. Song, D. Chi, A.T.S. Wee, S.Y. Quek, The organic—2D transition metal dichalcogenide heterointerface, Chem. Soc. Rev. 47 (2018) 3241—3264
- [493] X. He, L. Zhang, R. Chua, P.K.J. Wong, A. Arramel, Y.P. Feng, S.J. Wang, D. Chi, M. Yang, Y.L. Huang, A.T.S. Wee, Selective self-assembly of 2,3diaminophenazine molecules on MoSe₂ mirror twin boundaries, Nat. Commun. 10 (2019) 2847.
- [494] J. Li, T. Joseph, M. Ghorbani-Asl, S. Kolekar, A.V. Krasheninnikov, M. Batzill,

- Mirror twin boundaries in MoSe₂ monolayers as one dimensional nanotemplates for selective water adsorption, Nanoscale 13 (2021) 1038–1047.
- [495] A. Dong, L. Yan, L. Sun, S. Yan, X. Shan, Y. Guo, S. Meng, X. Lu, Identifying few-molecule water clusters with high precision on Au(111) surface, ACS Nano 12 (2018) 6452–6457.
- [496] L.R. Merte, R. Bechstein, G. Peng, F. Rieboldt, C.A. Farberow, H. Zeuthen, J. Knudsen, E. Lægsgaard, S. Wendt, M. Mavrikakis, F. Besenbacher, Water clustering on nanostructured iron oxide films, Nat. Commun. 5 (2014) 4193.
- [497] S. Standop, T. Michely, C. Busse, H₂O on graphene/lr(111): a periodic array of frozen droplets, J. Phys. Chem. C 119 (2015) 1418–1423.
- [498] J. Karthikeyan, H.-P. Komsa, M. Batzill, A.V. Krasheninnikov, Which transition metal atoms can be embedded into two-dimensional molybdenum dichalcogenides and add magnetism? Nano Lett. 19 (2019) 4581–4587.
- [499] P.M. Coelho, H.-P. Komsa, K. Lasek, V. Kalappattil, J. Karthikeyan, M.-H. Phan, A.V. Krasheninnikov, M. Batzill, Room-temperature ferromagnetism in MoTe₂ by post-growth incorporation of vanadium impurities, Adv. Electr. Mater 5 (2019) 1900044.
- [500] K. Qi, X. Cui, L. Gu, S. Yu, X. Fan, M. Luo, S. Xu, N. Li, L. Zheng, Q. Zhang, J. Ma, Y. Gong, F. Lv, K. Wang, H. Huang, W. Zhang, S. Guo, W. Zheng, P. Liu, Single-atom cobalt array bound to distorted 1T MoS₂ with ensemble effect for hydrogen evolution catalysis, Nat. Commun. 10 (2019) 5231.
- [501] H. Feng, Z. Xu, J. Zhuang, L. Wang, Y. Liu, X. Xu, L. Song, W. Hao, Y. Du, Role of charge density wave in monatomic assembly in transition metal dichalcogenides, Adv. Funct. Mater. 29 (2019) 1900367.
- [502] A.A. Tedstone, D.J. Lewis, P. O'Brien, Synthesis, properties, and applications of transition metal-doped layered transition metal dichalcogenides, Chem. Mater. 28 (2016) 1965–1974.
- [503] M.R. Laskar, D.N. Nath, L. Ma, E.W. Lee II, C.H. Lee, T. Kent, Z. Yang, R. Mishra, M.A. Roldan, J.-C. Idrobo, S.T. Pantelides, S.J. Pennycook, R.C. Myers, Y. Wu, S. Rajan, P-type doping of MoS₂ thin films using Nb, Appl. Phys. Lett. 104 (2014) 92104.
- [504] Z. Guguchia, A. Kerelsky, D. Edelberg, S. Banerjee, F. von Rohr, D. Scullion, M. Augustin, M. Scully, D.A. Rhodes, Z. Shermadini, H. Luetkens, A. Shengelaya, C. Baines, E. Morenzoni, A. Amato, J.C. Hone, R. Khasanov, S.J.L. Billinge, E. Santos, A.N. Pasupathy, Y.J. Uemura, Magnetism in semi-conducting molybdenum dichalcogenides, Sci. Adv. 4 (2018) eaat3672.
- [505] S. Fu, K. Kang, K. Shayan, A. Yoshimura, S. Dadras, X. Wang, L. Zhang, S. Chen, N. Liu, A. Jindal, X. Li, A.N. Pasupathy, A.N. Vamivakas, V. Meunier, S. Strauf, E.-H. Yang, Enabling room temperature ferromagnetism in monolayer MoS₂ via in situ iron-doping, Nat. Commun. 11 (2020) 2034.
- [506] M.T. Dau, C. Vergnaud, M. Gay, C.J. Alvarez, A. Marty, C. Beigné, D. Jalabert, J.-F. Jacquot, O. Renault, H. Okuno, M. Jamet, Van der Waals epitaxy of Mndoped MoSe₂ on mica, Apl. Mater. 7 (2019) 51111.
- [507] J. Wang, F. Sun, S. Yang, Y. Li, C. Zhao, M. Xu, Y. Zhang, H. Zeng, Robust ferromagnetism in Mn-doped MoS₂ nanostructures, Appl. Phys. Lett. 109 (2016) 92401.
- [508] K. Zhang, S. Feng, J. Wang, A. Azcatl, N. Lu, R. Addou, N. Wang, C. Zhou, J. Lerach, V. Bojan, M.J. Kim, L.-Q. Chen, R.M. Wallace, M. Terrones, J. Zhu, J.A. Robinson, Manganese doping of monolayer MoS₂: the substrate is critical, Nano Lett. 15 (2015) 6586–6591.